Parasites, Hosts and Diseases

Volume 64 • Number 1 • January 2026

CONTENTS

Mini Review

1 Nucleolar organization and divergent transcriptional machinery in *Giardia lamblia*: Structural insights and implications for drug targeting
Carlos Gaona-López

Original Articles

7 Transcriptomic profiling reveals *Trichinella spiralis*-mediated attenuation of respiratory syncytial virus-induced inflammation in mice
Ki Back Chu, Fu-Shi Quan

18 A human case of cercarial dermatitis and molecular characterization of *Trichobilharzia* cercariae from *Radix plicatula* of paddy field in Tokyo, Japan
Azusa Banzai, Hiromu Sugiyama, Kentaro Wada, Hirotaka Katahira, Rei Hirasawa, Ryota Tanabe, Sou Saito, Kunitaka Kobayashi

27 Exploration of *Naegleria*-preferentially secreted proteins for identifying diagnostic candidates to detect *Naegleria fowleri*
Hye-Jeong Jo, Hae-Ahm Lee, Fu-Shi Quan, Hyun-Hee Kong, Eun-Kyung Moon

37 The effect of *Legionella pneumophila* infection on the encystation of *Acanthamoeba castellanii*
Hye-Jeong Jo, Hae-Ahm Lee, Fu-Shi Quan, Hyun-Hee Kong, Eun-Kyung Moon

45 IKK2, calcium, MAP kinase, and PI3 kinase are required for exocytosis and interleukin-8 production in human mast cells stimulated by *Trichomonas vaginalis*-derived secretory products
Shin Hye Park, Young Ah Lee, Myeong Heon Shin

52 Genetic polymorphisms of merozoite surface protein-1 ICB 5–6 in Vietnamese *Plasmodium vivax* isolates
Thu Hằng Nguyễn, Đăng Thùy Dương Nguyễn, Hương Giang Lê, Tuấn Cường Võ, Nguyen Thi Minh Trinh, Minkyoung Cho, Chau Van Khanh, Huynh Hong Quang, Byoung-Kuk Na

62 Genotyping of *Blastocystis* species in hemodialysis patients from Makkah, Saudi Arabia
Hattan S. Gattan, Ebtihal O. Bahwaireth, Majed H. Wakid, Muslimah N. Alsulami, Mohammed A. Al-Matary, Asmaa M. El-Kady

70 Development and validation of a species-specific loop-mediated isothermal amplification assay for rapid detection of *Perkinsus marinus*
S.D.N.K. Bathige, Seung-Hyeon Kim, Donghyun Lee, Hyung-Bae Jeon, Yu Chen, Kyung-Il Park

Brief Communications

82 Identification of maternal antibodies targeting a cystatin-like protein of *Trichinella spiralis* in offspring
Minkyoung Cho, Hak Sun Yu

87 First record of 3 chewing louse species from the Oriental stork (*Ciconia boyciana*) in Korea: Insights into conservation of co-associated species
Jeong Hun Shim, Seongjun Choe, Sukyung Kim, Dongsoo Ha, Soo Hyung Eo

Case Reports

92 Feline heartworm (*Dirofilaria immitis*) infection in stray cats in Ulsan, Korea
Jihyun Kim, Miryeng Kim, Seungjin Lee, Youngmin Yun

98 A fatal case of complex hepatic alveolar echinococcosis
Li Xin, Li Mengmeng, Yu Huixia, Zan Runna, Li Guojun, Shang Rongjian, Yu Jia

http://parahostdis.org

The Korean Society for Parasitology and Tropical Medicine

Parasites, Hosts and Diseases

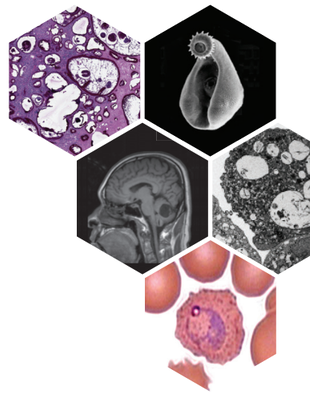

Parasites, Hosts and Diseases

pISSN 2982-5164 eISSN 2982-6799

Volume 64 • Number 1 • January 2026

Volume 64 • Number 1 • January 2026

http://parahostdis.org

The Korean Society for Parasitology and Tropical Medicine

Parasites, Hosts and Diseases

pISSN 2982-5164
eISSN 2982-6799

Volume 64 • Number 1 • January 2026

Parasites, Hosts and Diseases (Parasites Hosts Dis, PHD) is a peer-reviewed, open-access journal published quarterly on the last day of January, April, July, and October. Established in 1963 as *The Korean Journal of Parasitology*, the journal transitioned to an online-only publication starting with Vol. 53 in 2015, and adopted its current title in 2023. As the official publication of The Korean Society for Parasitology and Tropical Medicine, PHD is dedicated to advancing knowledge on human and animal parasites, disease vectors, host-parasite interactions, zoonoses, and tropical medicine. The journal publishes original articles, review articles, case reports, brief communications, letters to the editor, and book reviews.

Abstracting and Indexing Services

A part of articles, metadata, or full text is available from KoreaMed (1963–), CrossRef metadata (1963–), Korea Citation Index (2002–), Science Citation Index Expanded (2008–), MedLine (1993–), PubMed Central (1998–), PubMed (1993–), Scopus (1977–), and EMBASE (2023–).

Publisher The Korean Society for Parasitology and Tropical Medicine
Editor-in-Chief Myeong Heon Shin, MD, PhD

Editorial Office The Korean Society for Parasitology and Tropical Medicine
Department of Tropical Medicine, Yonsei University College of Medicine, Yonsei-ro 50-1, Seodaemun-gu, Seoul 03722 Korea
Tel: +82-2-2228-1844 E-mail: support@parahostdis.org

Publishing Office M2PI
#805, 26 Sangwon 1-gil, Seongdong-gu, Seoul 04779, Korea
Tel: +82-2-6966-4930 Fax: +82-2-6966-4945 E-mail: support@m2-pi.com

This journal was supported by the Korea Association of Health Promotion, National Research Foundation of Korea (NRF) grant and the Korean Federation of Science and Technology Societies (KOFST) grant funded by the Korean Government.

Parasites, Hosts and Diseases

pISSN 2982-5164
eISSN 2982-6799

Volume 64 • Number 1 • January 2026

Editorial Board

Parasites, Hosts and Diseases

pISSN 2982-5164
eISSN 2982-6799

Volume 64 • Number 1 • January 2026

Contents

Mini Review

1 Nucleolar organization and divergent transcriptional machinery in *Giardia lamblia*: Structural insights and implications for drug targeting
Carlos Gaona-López

Original Articles

7 Transcriptomic profiling reveals *Trichinella spiralis*-mediated attenuation of respiratory syncytial virus-induced inflammation in mice
Ki Back Chu, Fu-Shi Quan

18 A human case of cercarial dermatitis and molecular characterization of *Trichobilharzia* cercariae from *Radix plicatula* of paddy field in Tokyo, Japan
Azusa Banzai, Hiromu Sugiyama, Kentaro Wada, Hirotaka Katahira, Rei Hirasawa, Ryota Tanabe, Sou Saito, Kunitaka Kobayashi

27 Exploration of *Naegleria*-preferentially secreted proteins for identifying diagnostic candidates to detect *Naegleria fowleri*
Hye-Jeong Jo, Hae-Ahm Lee, Fu-Shi Quan, Hyun-Hee Kong, Eun-Kyung Moon

37 The effect of *Legionella pneumophila* infection on the encystation of *Acanthamoeba castellanii*
Hye-Jeong Jo, Hae-Ahm Lee, Fu-Shi Quan, Hyun-Hee Kong, Eun-Kyung Moon

45 IKK2, calcium, MAP kinase, and PI3 kinase are required for exocytosis and interleukin-8 production in human mast cells stimulated by *Trichomonas vaginalis*-derived secretory products
Shin Hye Park, Young Ah Lee, Myeong Heon Shin

52 Genetic polymorphisms of merozoite surface protein-1 ICB 5–6 in Vietnamese *Plasmodium vivax* isolates
Thu Hằng Nguyễn, Đăng Thùy Dương Nguyễn, Hương Giang Lê, Tuấn Cường Võ, Nguyen Thi Minh Trinh, Minkyoung Cho, Chau Van Khanh, Huynh Hong Quang, Byoung-Kuk Na

62 Genotyping of *Blastocystis* species in hemodialysis patients from Makkah, Saudi Arabia
Hattan S. Gattan, Ebtihal O. Bahwaireth, Majed H. Wakid, Muslimah N. Alsulami, Mohammed A. Al-Matary, Asmaa M. El-Kady

70 Development and validation of a species-specific loop-mediated isothermal amplification assay for rapid detection of *Perkinsus marinus*
S.D.N.K. Bathige, Seung-Hyeon Kim, Donghyun Lee, Hyung-Bae Jeon, Yu Chen, Kyung-Il Park

Parasites, Hosts and Diseases

pISSN 2982-5164
eISSN 2982-6799

Volume 64 • Number 1 • January 2026

Brief Communications

82 Identification of maternal antibodies targeting a cystatin-like protein of *Trichinella spiralis* in offspring
Minkyoung Cho, Hak Sun Yu

87 First record of 3 chewing louse species from the Oriental stork (*Ciconia boyciana*) in Korea: Insights into conservation of co-associated species
Jeong Hun Shim, Seongjun Choe, Sukyung Kim, Dongsoo Ha, Soo Hyung Eo

Case Reports

92 Feline heartworm (*Dirofilaria immitis*) infection in stray cats in Ulsan, Korea
Jihyun Kim, Miryeng Kim, Seungjin Lee, Youngmin Yun

98 A fatal case of complex hepatic alveolar echinococcosis
Li Xin, Li Mengmeng, Yu Huixia, Zan Runna, Li Guojun, Shang Rongjian, Yu Jia

Mini Review

Parasites Hosts Dis 2026;64(1):1-6
https://doi.org/10.3347/PHD.25093

Parasites, Hosts and Diseases

pISSN 2982–5164 • eISSN 2982–6799

Nucleolar organization and divergent transcriptional machinery in *Giardia lamblia*: Structural insights and implications for drug targeting

Carlos Gaona-López[1,2,*]

[1]*Department of Cell Biology, Faculty of Sciences, National Autonomous University of Mexico, Mexico City, Mexico;* [2]*Laboratory 5, Faculty of Biology (Xalapa), Universidad Veracruzana, Xalapa-Enríquez, Mexico*

Giardia lamblia is a protozoan parasite responsible for Giardiasis, one of the most prevalent intestinal infections worldwide. Despite its medical relevance, the molecular organization of its transcriptional apparatus remains poorly characterized. Here, I present an integrative analysis of the structural and functional features of the *Giardia* nucleolus and its transcription machinery. Treatment with actinomycin D induces nucleolar disorganization, confirming active rRNA transcription and nucleolar stress. Additionally, I highlight the highly divergent TATA-binding protein as a potential therapeutic target, given its essential role in transcription and its low mutation rate. Collectively, these findings provide new insights into the minimalist eukaryotic architecture of *G. lamblia* and identify unique molecular elements that may serve as selective antiparasitic targets.

Keywords: *Giardia lamblia*, nucleolus, transcription, actinomycin D, TATA-binding protein, drug targets

Introduction

Giardia lamblia is a cosmopolitan, single-celled parasite responsible for Giardiasis, one of the most common causes of diarrheal disease globally [1,2]. Despite its public health relevance and status as a neglected tropical disease, the molecular biology of this disease remains underexplored [3]. Insights into its transcriptional machinery and the previously unrecognized presence of a nucleolus have revealed potential therapeutic targets unique to this parasite [4].

G. lamblia is an important eukaryote characterized by a highly reduced cellular architecture. Its simplified nucleolus and transcriptional machinery contain divergent molecular components that differ from those of higher eukaryotes. Understanding these unique features provides fundamental information that can support future development of antiparasitic drugs. This review summarizes current structural and functional evidence to highlight their relevance as potential drug targets.

Global Relevance and Therapeutic Challenges of *G. lamblia*

Giardiasis affects approximately 300 million people annually, with children under 5 being the most vulnerable [1,5]. Although treatable, the drugs currently used—metronidazole, tinidazole, albendazole, mebendazole, and nitazoxanide—often have ad-

Received: September 22, 2025 Accepted: November 28, 2025
*Correspondence: peanuts@ciencias.unam.mx

Citation
Gaona-López C. Nucleolar organization and divergent transcriptional machinery in *Giardia lamblia*: structural insights and implications for drug targeting. Parasites Hosts Dis 2026;64(1):1-6.

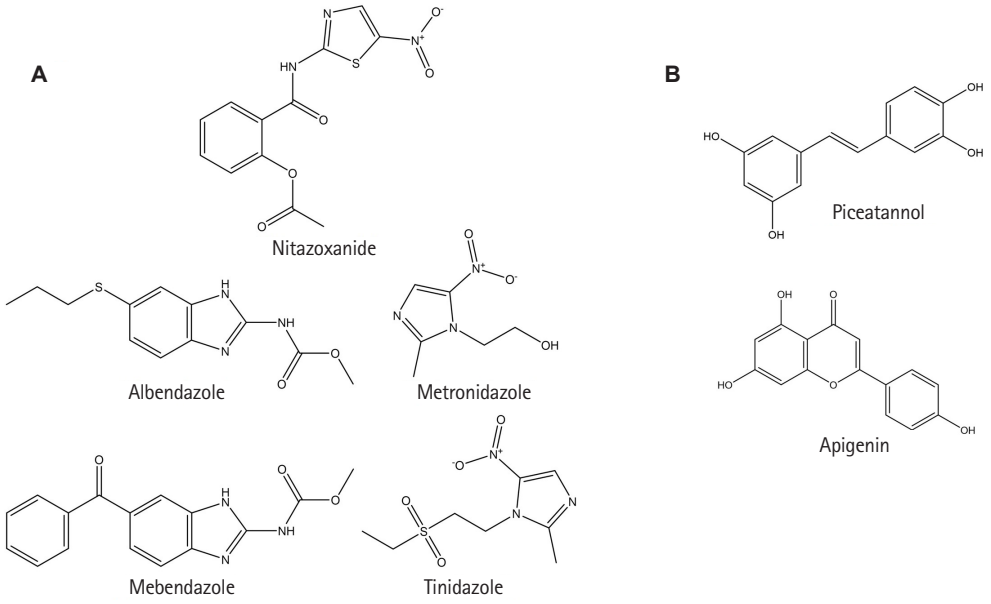

Fig. 1. Chemical compounds related to treating Giardiasis and the potential inhibition of *Giardia lamblia* TATA-binding protein. (A) Chemical structures of the primary drugs currently used to treat Giardiasis: metronidazole, tinidazole, albendazole, mebendazole, and nitazoxanide. (B) Chemical structures of piceatannol and apigenin, 2 compounds identified in a previous study by our group as potential inhibitors of the TATA-binding protein of *G. lamblia*, based on molecular modeling tools.

verse effects and rising reports of drug resistance (Fig. 1A) [6,7]. These challenges underscore the urgent need to identify novel drug targets that exploit the parasite's unique molecular features [8], as shown in Fig. 1B.

Unfortunately, several of these drugs present adverse effects ranging from mild to severe, highlighting that some have been reported as genotoxic and even carcinogenic in animals. However, the potential risk in humans remains a subject of debate [9-11].

Discovery and Structural Characterization of the Nucleolus in *G. lamblia*

G. lamblia challenges traditional views of eukaryotic cell biology due to its minimalist architecture. Long considered an early-diverging eukaryote for lacking canonical organelles such as mitochondria and peroxisomes, and possessing only a rudimentary Golgi complex [12-14]. Recent studies suggest that its simplicity reflects a high specialization for parasitism [14,15]. Originally believed to lack a nucleolus, this idea was based on the homogeneous distribution of rDNA and nucleolar markers such as fibrillarin (involved in 2'-O-methylation and processing of pre-rRNA) [16,17]. However, the discovery of key nucleolar components like KRR1 (small subunit processome component homolog) involved in small ribosomal subunit biogenesis, CBF5 (Cajal body-specific factor 5) a pseudouridine synthase, and a set of at least 20 small nucleolar RNAs including *Gls*R17 (which guide site-specific chemical modifications of rRNA), combined with ultrastructural imaging and in situ hybridization, confirmed the presence of a small but functional nucleolus (Fig. 2A) [4,18-21]. Notably, these proteins exhibit low sequence identity with their human homologs, and several of the small nucleolar RNAs lack clear orthologs in higher eukaryotes, suggesting their potential as selective therapeutic targets. This nucleolus is unusually stable throughout the cell cycle, unlike in higher eukaryotes [20,22]. Its reduced RNA polymerase I machinery includes only a minimal set of components required for rRNA transcription in *Giardia*, reflecting the streamlined nature of its nucleolar organization [23].

Functional Evidence of Nucleolar Activity under Transcriptional Stress

Exposure of *Giardia* trophozoites to actinomycin D—a selective inhibitor of RNA polymerase I—leads to structural reorganization of the nucleolus. This disaggregation of nucleolar material mimics nucleolar stress observed in higher eukaryotes and indicates that *Giardia*'s nucleolus is actively engaged in rRNA transcription (Fig. 2B) [24].

https://doi.org/10.3347/PHD.25093

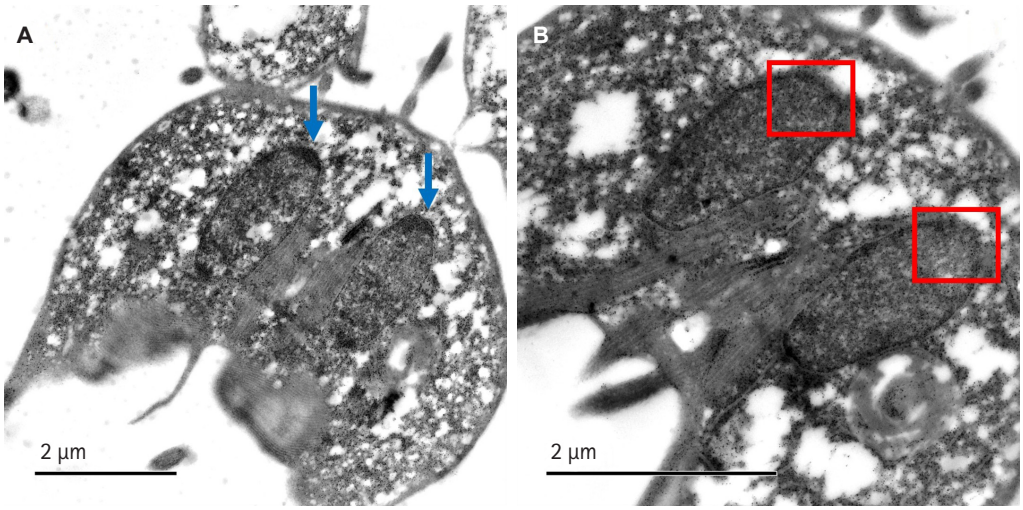

Fig. 2. Ultrastructural analysis of the nucleolus in *Giardia lamblia* trophozoites under control and actinomycin D-treated conditions. (A) Transmission electron microscopy image of untreated *G. lamblia* trophozoites showing intact nucleolar structure within the 2 nuclei; blue arrows indicate the nucleolus. (B) Trophozoites treated with actinomycin D (0.2 μg/ml) exhibit disorganization and dispersion of nucleolar material. This nucleolar disaggregation indicates nucleolar stress and reflects the transcriptional arrest of ribosomal RNA synthesis. The red box indicates the region where the nucleolus would usually be located. These structural changes provide additional evidence supporting the presence of a functional nucleolus in *G. lamblia*.

A Minimalist but Essential Transcriptional Machinery

Compared to higher eukaryotes, *G. lamblia* retains only 4 of the 12 basal transcription initiation factors, specifically Rrn3, A43, BRF, and C34. In addition, *Giardia* encodes a highly divergent TATA-binding protein (TBP) that, although not included in the canonical set of 12 basal factors, remains essential for transcription by all 3 RNA polymerases. This TBP is remarkably unusual: it lacks 3 of the 4 conserved phenylalanine residues required for DNA binding in other eukaryotes, yet it still carries out promoter recognition and transcription initiation, highlighting the extreme structural simplification of the giardial transcription machinery [23]. The nucleolar components discussed in this review, together with the general transcription initiation factors present in *Giardia*, are summarized in Supplementary Table 1.

Additionally, it has been reported that the sequence of the small subunit ribosomal RNA in *G. lamblia* has an unusually high G-C content, close to 75%, and a length of 1,453 nucleotides—both distinctive features of prokaryotic organisms. Moreover, the small subunit ribosomal RNA of *Giardia* retains the Shine-Dalgarno sequence, which is essential for ribosome binding to bacterial mRNA [25]. This G-C richness may also enhance *Giardia's* susceptibility to actinomycin D. This drug intercalates into G-C-rich DNA regions and inhibits transcription by RNA polymerase I, further underscoring the parasite's potential vulnerability due to its streamlined transcriptional machinery [24].

The Divergent TBP as a Potential Selective Drug Target

Given the high divergence reported for the universal transcription factor TBP, and because TBP is essential for transcription by all 3 RNA polymerases, it can be postulated that this protein may be susceptible to selective therapeutic targeting [8]. This idea is supported by comparative analyses showing that TBPs from protozoan parasites exhibit markedly lower conservation than those in higher eukaryotes. As illustrated in Fig. 3, structural comparisons between human and *Giardia* TBP reveal pronounced differences in the surface topology of the protein, further highlighting its evolutionary divergence and potential suitability as a selective drug target [26,27]. Additionally, the different crystal structures of TBPs in complex with other transcription factors reveal that almost all proteins interact with multiple transcription factors. For example, the characteristic folding of the C-terminal domain of the TBP is a saddle-like structure; such a conformation generates 2 surfaces in the TBP. On the one hand, the convex surface interacts with various general transcription factors, which are essential for assembling the pre-initiation complex. On the other hand, the concave surface interacts with the minor groove of the DNA in the gene's promoter region, enabling transcription [27]. Addition-

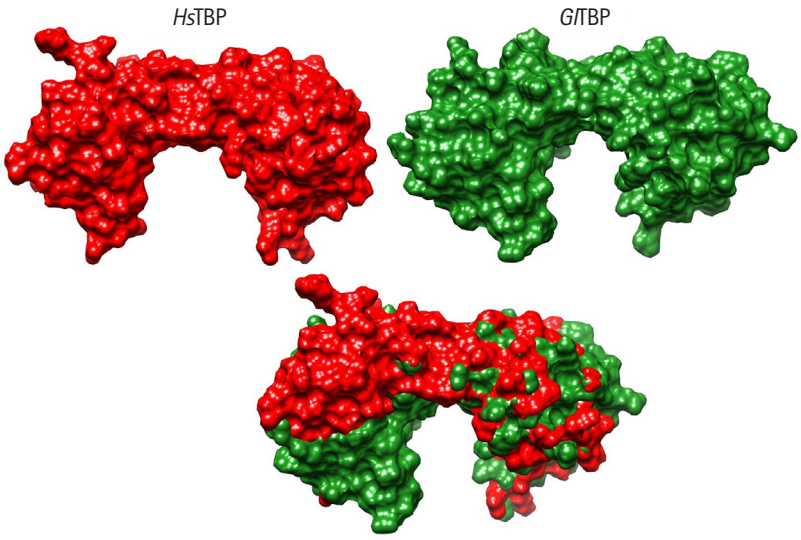

Fig. 3. Structural comparison between *Hs*TBP and *Gl*TBP. Surface representations of *Hs*TBP (red) and *Gl*TBP (green) are shown individually (top) and as a structural alignment (bottom). The human TATA-binding protein (TBP) structure corresponds to the crystallographic model PDB ID: 1JFI, whereas the 3D structure of *Giardia lamblia* TBP was obtained using AlphaFold 3. Both models were visualized and aligned using UCSF ChimeraX. The comparison highlights pronounced differences in surface topology and molecular volume between the 2 proteins. These structural deviations illustrate the high evolutionary divergence of *G. lamblia* TBP relative to its human counterpart, supporting its consideration as a potential selective drug target.

ally, Santiago et al. [28] reported the first systematic structural analysis of TBPs of parasites, finding many differences between the TBPs of parasites and their counterpart in higher eukaryotes, finding that the convex surface is susceptible to the use of drugs that prevent the proper assembly of the pre-initiation complex by steric hindrances, inhibiting transcription. One aspect to highlight concerning other therapeutic targets is that TBP has an extremely low mutation rate; therefore, the problem of developing resistance to drugs that target this protein would be significantly more difficult for the pathogen to achieve [28].

Recently, in silico analyses identified compounds such as apigenin and piceatannol as potential TBP inhibitors, supporting in vitro data showing impaired parasite growth [8] (Fig. 1B).

Conclusion

The study of *G. lamblia*'s nucleolus and transcription factors reveals fundamental aspects of eukaryotic biology and offers unexpected therapeutic opportunities. Targeting its minimalist yet essential molecular machinery could lead to more effective, selective antiparasitic treatments.

Author contributions

Conceptualization: Gaona-López C. Data curation: Gaona-López C. Formal analysis: Gaona-López C. Funding acquisition: Gaona-López C. Investigation: Gaona-López C. Methodology: Gaona-López C. Project administration: Gaona-López C. Resources: Gaona-López C. Software: Gaona-López C. Supervision: Gaona-López C. Validation: Gaona-López C. Visualization: Gaona-López C. Writing – original draft: Gaona-López C. Writing – review & editing: Gaona-López C.

Conflict of interest

The author has no conflicts of interest to declare.

Acknowledgments

Carlos Gaona-López gratefully acknowledges the postdoctoral fellowship awarded by the Dirección General de Asuntos del Personal Académico (DGAPA), Universidad Nacional Autónoma de México (UNAM), during the period 2018–2020. He also expresses his sincere appreciation to the Departamento de Educación Continua of Instituto Nacional de Medicina Genómica (INMEGEN) for granting tuition-free scholarships that enabled his participation in several specialized training courses.

https://doi.org/10.3347/PHD.25093

Supplementary information

Supplementary material is available with this article at https://doi.org/10.3347/PHD.25093.

ORCID

Carlos Gaona-López, https://orcid.org/0000-0001-7953-2875

References

1. Cernikova L, Faso C, Hehl AB. Five facts about *Giardia lamblia*. PLoS Pathog 2018;14:e1007250. https://doi.org/10.1371/journal.ppat.1007250
2. Lanata CF, Fischer-Walker CL, Olascoaga AC, et al. Global causes of diarrheal disease mortality in children < 5 years of age: a systematic review. PLoS One 2013;8:e72788. https://doi.org/10.1371/journal.pone.0072788
3. Savioli L, Smith H, Thompson A. *Giardia* and *Cryptosporidium* join the 'Neglected Diseases Initiative.'. Trends Parasitol 2006;22:203-8. https://doi.org/10.1016/j.pt.2006.02.015
4. Gaona-López C, Martínez-Vázquez AV, Villalobos-Rocha JC, Juárez-Rendón KJ, Rivera G. Analysis of *Giardia lamblia* nucleolus as drug target: a review. Pharmaceuticals (Basel) 2023;16:1168. https://doi.org/10.3390/ph16081168
5. Kotloff KL, Nataro JP, Blackwelder WC, et al. Burden and aetiology of diarrhoeal disease in infants and young children in developing countries (the Global Enteric Multicenter Study, GEMS): a prospective, case-control study. Lancet 2013;382:209-22. https://doi.org/10.1016/S0140-6736(13)60844-2
6. Argüello-García R, Leitsch D, Skinner-Adams T, Ortega-Pierres MG. Drug resistance in *Giardia*: mechanisms and alternative treatments for Giardiasis. Adv Parasitol 2020;17:201-82. https://doi.org/10.1016/bs.apar.2019.11.003
7. Escobedo AA, Cimerman S. Giardiasis: a pharmacotherapy review. Expert Opin Pharmacother 2007;8:1885-902. https://doi.org/10.1517/14656566.8.12.1885
8. Gaona-López C, Méndez-Álvarez D, Moreno-Rodríguez A, et al. TATA-binding protein-based virtual screening of FDA drugs identified new anti-Giardiasis agents. Int J Mol Sci 2024;25:6238. https://doi.org/10.3390/ijms25116238
9. Bendesky A, Menéndez D, Ostrosky-Wegman P. Is metronidazole carcinogenic? Mutat Res 2002;511:133-44. https://doi.org/10.1016/s1383-5742(02)00007-8
10. Dingsdag SA, Hunter N. Metronidazole: an update on metabolism, structure-cytotoxicity and resistance mechanisms. J Antimicrob Chemother 2018;73:265-79. https://doi.org/10.1093/jac/dkx351
11. IARC Working Group on the Evaluation of Carcinogenic Risks to Humans. Ingested nitrate and nitrite, and cyanobacterial peptide toxins. International Agency for Research on Cancer; 2010.
12. Reiner DS, McCaffery M, Gillin FD. Sorting of cyst wall proteins to a regulated secretory pathway during differentiation of the primitive eukaryote, *Giardia lamblia*. Eur J Cell Biol 1990;53:142-53.
13. Marti M, Regös A, Li Y, et al. An ancestral secretory apparatus in the protozoan parasite *Giardia intestinalis*. J Biol Chem 2003;278:24837-48. https://doi.org/10.1074/jbc.M302082200
14. Adam RD. *Giardia duodenalis*: biology and pathogenesis. Clin Microbiol Rev 2021;34:e0002419. https://doi.org/10.1128/CMR.00024-19
15. Morrison HG, McArthur AG, Gillin FD, et al. Genomic minimalism in the early diverging intestinal parasite *Giardia lamblia*. Science 2007;317:1921-6. https://doi.org/10.1126/science.1143837
16. Narcisi EM, Glover CV, Fechheimer M. Fibrillarin, a conserved pre-ribosomal RNA processing protein of *Giardia*. J Eukaryot Microbiol 1998;45:105-11. https://doi.org/10.1111/j.1550-7408.1998.tb05077.x
17. Guo J, Chen Y, Zhou K, Li J. Distribution of rDNA in the nucleus of *Giardia lamblia*: detection by Ag-I silver stain. Biotech Histochem 2005;80:31-4. https://doi.org/10.1080/10520290500050981
18. Xin DD, Wen JF, He D, Lu SQ. Identification of a *Giardia* krr1 homolog gene and the secondarily anucleolate condition of *Giardia lamblia*. Mol Biol Evol 2005;22:391-4. https://doi.org/10.1093/molbev/msi052
19. Saraiya AA, Wang CC. snoRNA, a novel precursor of microRNA in *Giardia lamblia*. PLoS Pathog 2008;4:e1000224. https://doi.org/10.1371/journal.ppat.1000224
20. Jiménez-García LF, Zavala G, Chávez-Munguía B, et al. Identification of nucleoli in the early branching protist *Giardia duodenalis*. Int J Parasitol 2008;38:1297-304. https://doi.org/10.1016/j.ijpara.2008.04.012
21. Tian XF, Yang ZH, Shen H, Adam RD, Lu SQ. Identification of the nucleoli of *Giardia lamblia* with TEM and CFM. Parasitol Res 2010;106:789-93. https://doi.org/10.1007/s00436-009-1715-3
22. Hernandez-Verdun D. Assembly and disassembly of the nucleolus during the cell cycle. Nucleus 2011;2:189-94. https://doi.org/10.4161/nucl.2.3.16246
23. Best AA, Morrison HG, McArthur AG, Sogin ML, Olsen GJ. Evolution of eukaryotic transcription: insights from the genome of *Giardia lamblia*. Genome Res 2004;14:1537-47. https://doi.org/10.1101/gr.2256604
24. Sobell HM. Actinomycin and DNA transcription. Proc Natl Acad Sci U S A 1985;82:5328-31. https://doi.org/10.1073/pnas.82.16.5328
25. Sogin ML, Gunderson JH, Elwood HJ, Alonso RA, Peattie DA. Phylogenetic meaning of the kingdom concept: an unusual ribosomal RNA from *Giardia lamblia*. Science 1989;243:75-7. https://doi.org/10.1126/science.2911720

26. Hernandez N. TBP, a universal eukaryotic transcription factor? Genes Dev 1993;7:1291-308. https://doi.org/10.1101/gad.7.7b.1291
27. Parra-Marín O, López-Pacheco K, Hernández R, López-Villaseñor I. The highly diverse TATA box-binding proteins among protists: a review. Mol Biochem Parasitol 2020;239:111312. https://doi.org/10.1016/j.molbiopara.2020.111312
28. Santiago Á, Razo-Hernández RS, Pastor N. The TATA-binding protein DNA-binding domain of eukaryotic parasites is a potentially druggable target. Chem Biol Drug Des 2020;95:130-49. https://doi.org/10.1111/cbdd.13630

https://doi.org/10.3347/PHD.25093

Original Article

Parasites Hosts Dis 2026;64(1):7-17
https://doi.org/10.3347/PHD.25067

Parasites, Hosts and Diseases

pISSN 2982-5164 • eISSN 2982-6799

Transcriptomic profiling reveals *Trichinella spiralis*-mediated attenuation of respiratory syncytial virus-induced inflammation in mice

Ki Back Chu[1,2], Fu-Shi Quan[3,4,*]

[1]Department of Parasitology, Inje University College of Medicine, Busan, Korea; [2]Department of Infectious Disease and Malaria, Paik Institute of Clinical Research, Inje University, Busan, Korea; [3]Department of Medical Zoology, School of Medicine, Kyung Hee University, Seoul, Korea; [4]Medical Research Center for Bioreaction to Reactive Oxygen Species and Biomedical Science Institute, Core Research Institute (CRI), Kyung Hee University, Seoul, Korea

Helminth-mediated immunomodulation has been extensively studied in animal models, demonstrating its potential as both a prophylactic and therapeutic option for inflammatory lung diseases. However, its role in attenuating respiratory virus-induced inflammation remains largely unexplored. In this study, we examined whether pre-existing infection with the helminth *Trichinella spiralis* confers protection against pulmonary pathology induced by respiratory syncytial virus (RSV) infection in mice. Mice with prior *T. spiralis* infection exhibited reduced pulmonary inflammation and lower viral titers in the lungs compared with RSV-infected controls. Transcriptomic profiling of lung tissue using RNA sequencing identified 407 differentially expressed genes. Among these, enrichment was observed in categories associated with the Gene Ontology (GO) terms "inflammatory response" (GO:0006954) and "defense response to virus" (GO:0051607). Selected genes from these categories were further validated by quantitative real-time PCR. Validation confirmed that co-exposure to *T. spiralis* and RSV resulted in attenuated expression of inflammation-related genes. Collectively, these findings demonstrate that pre-existing *T. spiralis* infection can alleviate virus-induced pulmonary pathology and inflammation, highlighting its potential as a novel therapeutic approach for respiratory inflammatory diseases.

Keywords: Immunomodulation, inflammation, respiratory syncytial viruses, *Trichinella spiralis*

Introduction

Helminths are a diverse group of large multicellular organisms, including nematodes, cestodes, and trematodes, that have co-evolved with humans over millennia. Although many helminths are parasitic and their presence within the human body can be deleterious, these organisms have developed versatile immunomodulatory strategies that enable long-term persistence while minimizing host tissue damage [1]. Globally, an estimated 2 billion individuals, predominantly in impoverished tropical and subtropical regions, are infected with helminths, whereas their prevalence has markedly declined in industrialized nations [2]. However, growing evidence indicates that improvements in sanitation and widespread deworming have been accompanied by unintended consequences, particularly a rise in allergic and inflammatory disorders [3]. One early epidemiological study reported a significantly lower prevalence of allergic diseases in rural communities co-exposed to bacterial, viral, and helminthic pathogens compared with urban populations living under hygienic conditions [4]. These observations

Received: August 19, 2025 Accepted: November 4, 2025
*Correspondence: fsquan@khu.ac.kr

Citation
Chu KB, Quan FS. Transcriptomic profiling reveals *Trichinella spiralis*-mediated attenuation of respiratory syncytial virus-induced inflammation in mice. Parasites Hosts Dis 2026;64(1):7-17.

contributed to the formulation of the "hygiene hypothesis" in the late 1980s, which posited that reduced exposure to parasitic infections during early life results in insufficient immune stimulation, thereby increasing susceptibility to allergic and autoimmune diseases that are highly prevalent in developed countries [5]. Supporting this hypothesis, helminth-induced amelioration of inflammatory and autoimmune diseases has been documented in humans. For instance, patients with multiple sclerosis who harbored intestinal parasitic infections exhibited fewer disease exacerbations and reduced pathological changes compared with uninfected controls [6]. Similarly, colonization of the intestine by *Trichuris trichiura* promoted a Th2-skewed immune response that alleviated ulcerative colitis through mechanisms involving increased mucus secretion and goblet cell hyperplasia [7]. These findings suggest that helminths, or antigens derived from them, may serve as promising candidates for the development of novel therapeutic strategies against autoimmune and inflammatory diseases, thereby warranting further investigations of individual species with distinct immunomodulatory properties.

Trichinella spiralis is a helminth well recognized for its immunomodulatory and anti-inflammatory properties across a wide range of diseases. For example, serine protease inhibitors secreted by *T. spiralis* muscle larvae have been shown to inactivate the NF-κB signaling cascade, thereby ameliorating tissue damage associated with non-alcoholic fatty liver disease [8]. Similarly, *T. spiralis* infection alleviated vincristine-induced peripheral neuropathy in mice by suppressing neuroinflammation [9]. Importantly, the immunomodulatory effects of *T. spiralis* are not restricted to autoimmune conditions but extend to infections with co-inhabiting pathogens, as demonstrated in experimental models of respiratory disease. Worm extracts derived from *T. spiralis* have been reported to attenuate sepsis-induced acute lung injury in mice [10]. Moreover, pre-existing *T. spiralis* infection in C57BL/6 mice promoted a Th2-biased immune response, which reduced neutrophil recruitment and the influx of proinflammatory cytokines following *Pseudomonas aeruginosa* infection [11]. In another study, excretory–secretory antigens of *T. spiralis* exerted protective effects against coronavirus infection in mice [12]. Chronic *T. spiralis* infection was also shown to dampen allergic airway remodeling induced by exposure to house dust mite allergens [13], highlighting its therapeutic potential in modulating host immune responses to inflammatory disorders.

Consistent with previous findings demonstrating the ability of *T. spiralis* to mitigate inflammatory responses, our earlier work showed that *T. spiralis* infection attenuates pulmonary inflammation induced by respiratory syncytial virus (RSV) exposure in mice [14]. Despite our previous histopathological and cytokine-level analyses demonstrating that *T. spiralis* infection suppresses RSV-induced inflammation, the molecular pathways and cellular networks underlying this protective effect remain undefined. To address this gap, we performed RNA sequencing (RNA-seq) to identify the host genetic factors underlying these protective effects and to obtain a comprehensive overview of gene-expression changes associated with *T. spiralis*-mediated modulation of RSV pathogenesis. This systems-level approach enables the unbiased identification of immunoregulatory pathways including cytokine signaling cascades and interferon-stimulated genes that are not readily discernible through conventional assays. By integrating differential gene-expression profiles with pathway and network analyses, we sought to delineate how *T. spiralis*-induced regulatory programs reshape antiviral and inflammatory responses in the lung. These transcriptomic insights extend beyond prior phenotypic observations and provide a mechanistic framework for the development of novel immunomodulatory strategies for virus-induced pulmonary diseases.

Methods

Ethics statement

All experiments involving animals were approved by Kyung Hee University's Institutional Animal Care and Use Committee (accession No. KHUASP-SE-22). Mice were housed in an institution-approved facility under specific-pathogen-free conditions. Mice were randomly assigned to experimental groups and maintained under controlled environmental conditions with standard enrichment, a 12 h light/dark cycle, and ad libitum access to food and water. All experimental procedures were conducted in accordance with institutional guidelines for animal care and welfare. Efforts were made to minimize animal suffering, and mice exhibiting signs of severe distress were humanely euthanized by CO_2 inhalation followed by cervical dislocation.

Cell, parasites, and virus culture

T. spiralis muscle larvae were serially passaged in Sprague–Dawley rats and recovered using an artificial digestion method, as previously described [15]. Briefly, skeletal muscles from infected rats were digested in a pepsin–HCl solution, and released larvae were filtered through a wire mesh to remove residual tissue debris. The sedimented larvae were washed repeatedly with 0.85% saline until the supernatant became clear,

https://doi.org/10.3347/PHD.25067

after which they were enumerated microscopically prior to infection. RSV was propagated in HEp-2 cells and titrated by plaque assay, as previously described [16]. Confluent HEp-2 cell monolayers were infected with the RSV A2 strain at a multiplicity of infection of 0.1 in serum-free DMEM (Welgene) and incubated for 48 h at 37°C in 5% CO_2. Upon observation of cytopathic effects, cells were harvested using a cell scraper and centrifuged at 2,000 rpm for 5 min at 4°C. The supernatant was discarded, and the cell pellet was sonicated to release progeny virus. Following titration, virus stocks were aliquoted and stored at -80°C until use.

Experimental infection of mice, lung tissue sampling, and RNA preparation

BALB/c mice were obtained from NARA Biotech and assigned to 1 of 4 groups ($n=6$ per group): infection with 400 *T. spiralis* muscle larvae (Ts), infection with 3×10^6 plaque-forming units of RSV, co-infection with both pathogens (Ts-RSV), or uninfected naïve controls. *T. spiralis* larvae were administered via orogastric tube on day 0, whereas RSV was delivered intranasally on day 12. All mice were sacrificed on day 16, and whole lung tissues were collected. Lungs were homogenized, and total RNA was extracted using the RNeasy Kit (Qiagen) according to the manufacturer's protocol. RNA concentration and purity were assessed with a NanoDrop One spectrophotometer (Thermo Fisher Scientific), and samples were stored at -80°C until further use. Whole lung tissue from 1 representative mouse in each experimental group was used for RNA-seq, while lung tissues from the remaining 5 mice were used for other downstream assays.

Quantifying lung RSV titer, hematoxylin and eosin staining of lung tissues

Mice were sacrificed for lung virus titer quantification and histopathological analysis. Half of the left lobes were homogenized and processed for plaque assay, while the remaining half were prepared for hematoxylin and eosin (H&E) staining. For plaque assays, lung tissues were homogenized in cold phosphate-buffered saline (PBS) and filtered through a cell strainer. Homogenates were centrifuged at 3,000 rpm for 5 min at 4°C, and the supernatants were collected. HEp-2 cells were seeded in 12-well culture plates and grown to confluence in complete DMEM (Welgene) supplemented with 10% fetal bovine serum and 1% penicillin–streptomycin at 37°C in 5% CO_2. After aspirating the culture medium, cells were washed with PBS and incubated with serially diluted lung supernatants in serum-free DMEM for 1 h at 37°C. Following viral adsorption, the inoculum was removed and cells were overlaid with 1% noble agar. Plates were incubated for 3 days at 37°C in 5% CO_2 until plaques developed. After incubation, agar overlays were carefully removed, and cells were fixed in a methanol–acetone solution (1:1) for 20 min at room temperature. Wells were blocked with 5% skim milk in PBS containing 0.1% Tween-20 for 1 h at room temperature. Monoclonal antibodies specific for the RSV fusion protein (Merck Millipore) diluted in PBS were added and incubated for 1 h at 37°C, followed by horseradish peroxidase-conjugated anti-mouse IgG secondary antibodies. Plaques were visualized by adding 3,3′-diaminobenzidine (Invitrogen), and viral titers were determined by plaque counting. For histopathological evaluation, the lung tissues were immersed in 10% neutral-buffered formalin, paraffin-embedded, and sectioned using a microtome. Tissue sections were stained with H&E, and immune cell infiltration and inflammatory severity were assessed microscopically at 100× magnification.

RNA-seq via Massive Analysis of cDNA Ends, data analysis, and pathway mapping

Total RNA was extracted from the whole lungs of 1 representative mouse per group and subjected to RNA sequencing. The resulting transcriptomic profiles were used for exploratory comparison of gene-expression patterns among groups. RNA-seq and data analysis was performed by Ebiogen. For control and test RNAs, the construction of library was performed using QuantSeq 3′mRNA-Seq Library Prep Kit (Lexogen) following the manufacturer's instructions. In brief, each 500 ng total RNA were prepared and an oligo-dT primer containing an Illumina-compatible sequence at its 5′end was hybridized to the RNA and reverse transcription was performed. After degradation of the RNA template, second strand synthesis was initiated by a random primer containing an Illumina-compatible linker sequence at its 5′end. The double-stranded library was purified using magnetic beads to remove all reaction components. The library was amplified to add the complete adapter sequences required for cluster generation. The finished library is purified from PCR components. High-throughput sequencing was performed as single-end 75 sequencing using NextSeq 500 (Illumina). For data analysis, QuantSeq 3′mRNA-Seq reads were aligned using Bowtie2. Bowtie2 indices were either generated from genome assembly sequence or the representative transcript sequences for aligning to the genome and transcriptome. The alignment file was used for assembling transcripts, estimating their abundances and detecting differential expression of genes. Differentially expressed genes (DEGs) were determined based on counts from unique and multiple alignments

using coverage in BEDTools. The read count data were processed based on quantile normalization method using EdgeR within R using Bioconductor [17]. Gene classification was based on searches done by the Database for Annotation, Visualization and Integrated Discovery (https://davidbioinformatics.nih.gov/) and Medline databases (http://www.ncbi.nlm.nih.gov/). Data mining and graphic visualization were performed using the Excel-based Differentially Expressed Gene Analysis (ExDEGA; Ebiogen). Raw reads were processed using the ExDEGA pipeline (Ebiogen) and aligned to the *Mus musculus* reference genome (mm10, GRCm38 assembly) obtained from the UCSC Genome Browser database. Genes showing an absolute twofold or greater change in expression with a false discovery rate of less than 0.05 were considered differentially expressed. The Kyoto Encyclopedia of Genes and Genomes (KEGG) pathway for "*mmu04060: Cytokine-cytokine receptor interaction*" was obtained from the KEGG database [18]. DEGs identified by RNA-seq were mapped onto this pathway using KEGG Mapper, and nodes were color-coded according to up regulation or downregulation based on the *T. spiralis* plus RSV (Ts-RSV) versus RSV comparison.

Quantitative real-time PCR

Mice from each experimental group were sacrificed for lung tissue collection, and total RNA was extracted from the right lungs for quantitative real-time PCR (qPCR). cDNA was synthesized using the PrimeScript First Strand cDNA Synthesis Kit (Takara) according to the manufacturer's instructions. qPCR was performed on a Mic qPCR cycler (PhileKorea). Each 20 μl reaction mixture contained 10 μl of Luna Universal qPCR Master Mix (New England Biolabs), 1 μl each of forward and reverse primers, and 20 ng of cDNA template. The thermal cycling protocol consisted of an initial denaturation at 95°C for 2 min, followed by 40 cycles of 95°C for 15 sec and 60°C for 60 sec. Relative mRNA expression levels of C-X-C motif chemokine ligands 9–10 (*Cxcl9*, *Cxcl10*, and *Cxcl11*), serum amyloid A3 (*Saa3*), and tissue inhibitor of metalloproteinase 1 (*Timp1*) were calculated using the comparative cycle threshold method. Gene expressions were normalized to beta-actin (*Actb*). The primer sequences for all genes used in this study are listed in Table 1.

Statistical analysis

Statistical significance was calculated using the GraphPad Prism 8 software. Data were presented as mean ± SD and significance between the groups were determined using either a one-way analysis of variance with Tukey's *post hoc* tests or two-tailed Student's *t*-test. Significant differences between the means were denoted with an asterisk and $P < 0.05$ were considered statistically significant.

Results

Pre-existing *T. spiralis* enhances antiviral immunity and attenuates RSV-induced pulmonary inflammation in mice

To validate the protective effects of *T. spiralis* against RSV infection, lung viral titers and histopathological analyses were performed. As expected, extensive immune cell infiltration was not observed in the lungs of naïve mice (Fig. 1A). Mice with pre-existing *T. spiralis* infection exhibited only mild inflammatory responses, characterized by limited immune cell recruitment. In contrast, RSV-infected mice displayed marked pulmonary inflammation with pronounced cellular influx,

Table 1. Quantitative real-time PCR primers used in this study

Gene	Primer sequence (5' – 3')	GenBank ID
Cxcl9	F: CCGAGGCACGATCCACTACA R: CGAGTCCGGATCTAGGCAGGT	NM_008599.4
Cxcl10	F: ATCATCCCTGCGAGCCTATCCT R: GACCTTTTTTGGCTAAACGCTTTC	NM_021274.2
Cxcl11	F: CCGAGTAACGGCTGCGACAAAG R: CCTGCATTATGAGGCGAGCTTG	NM_019494.1
Saa3	F: CGCAGCACGAGCAGGAT R: CCAGGATCAAGATGCAAAGAATG	NM_011315.3
Timp1	F: GTGGGAAATGCCGCAGAT R: GGGCATATCCACAGAGGCTTT	NM_001044384.1
Actb	F: CCACCATGTACCCAGGCATT R: CGGACTCATCGTACTCCTGC	NM_007393.5

https://doi.org/10.3347/PHD.25067

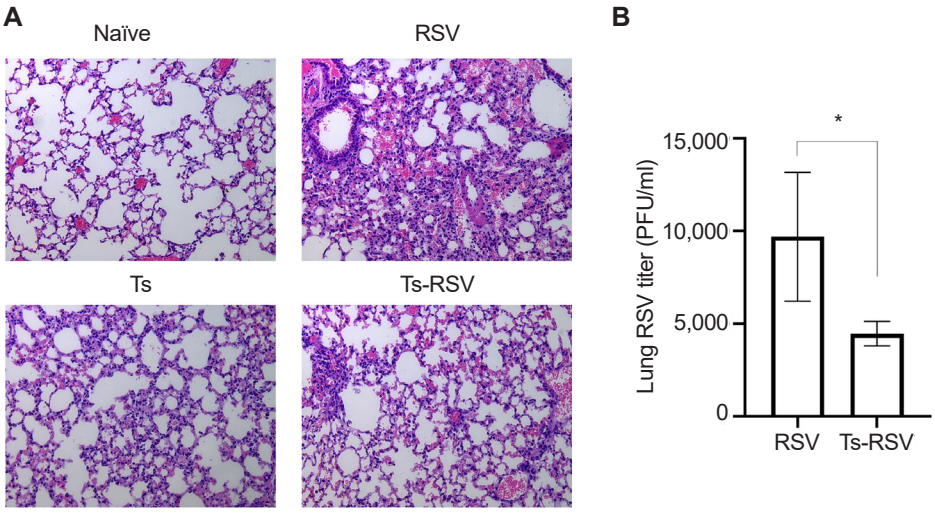

Fig. 1. Anti-inflammatory effects of *Trichinella spiralis* (Ts) infection in mice. The effect of pre-existing Ts infection on respiratory syncytial virus (RSV)-induced inflammation in mice (n=5 per group) were evaluated via lung tissue staining and plaque assay. Hematoxylin and eosin-stained lung tissue sections were visualized under a microscope and images were acquired under 100× magnification (A). RSV titers in the lung homogenates of mice were quantified by performing plaque assays using confluent monolayers of HEp-2 cells (B). Data are presented as mean±SD ($^{*}P$<0.05).

which was substantially reduced in mice co-infected with *T. spiralis* and RSV. To further assess whether *T. spiralis* infection limits viral replication in the lungs, plaque assays were conducted (Fig. 1B). Compared with RSV-infected controls, mice with prior *T. spiralis* exposure demonstrated a significant reduction in lung viral titers. Collectively, these findings confirm that pre-existing *T. spiralis* infection alleviates RSV-induced pulmonary inflammation and suppresses viral propagation in the lungs.

Massive Analysis of cDNA Ends analysis of *T. spiralis*-mediated transcriptomic changes in the lungs

RNA sequencing was performed to identify *T. spiralis*-induced alterations in pulmonary gene expression that may contribute to protection against subsequent RSV infection. Gene expression profiles from infected mice were normalized to those of naïve controls and designated as R/N (RSV vs. naïve), T/N (*T. spiralis* vs. naïve), and TR/N (co-infection vs. naïve). A total of 23,282 genes were detected, of which 407 were DEGs exhibiting ≥2-fold changes. A Venn diagram depicting upregulated, downregulated, and contra-regulated DEGs is shown in Fig. 2A. Notably, no contra-regulated genes were identified between T/N and TR/N or between R/N and TR/N, whereas 11 contra-regulated genes were detected between T/N and R/N. Next, fold enrichment analysis was performed for the TR/N group (Fig. 2B). DEGs were categorized into the 3 principal Gene Ontology (GO) domains: Biological Process, Cellular Component, and Molecular Function. The top 10 upregulated and downregulated pathways were identified for each domain. Among these, the most strongly regulated category was "cytoplasm" within the Cellular Component domain, which contained both the highest upregulated and downregulated genes.

To further characterize these transcriptional changes, we analyzed the distribution of DEGs across GO categories in R/N and TR/N (Fig. 3A, B). Because our focus was on *T. spiralis*-induced pathways associated with reduced pulmonary inflammation and viral load, 2 GO terms of particular relevance were included: "inflammatory response" (GO:0006954) and "defense response to virus" (GO:0051607). In RSV-infected mice, these categories accounted for 10.31% and 5.52% of all significant DEGs, respectively. By contrast, in the TR/N group, these proportions were reduced approximately by half, to 5.34% and 3.56%. Additional decreases in DEG proportions were observed in categories such as aging, cell differentiation, and cell cycle. Conversely, increases were detected in GO terms associated with secretion and RNA splicing, while angiogenesis-related DEGs remained unchanged between R/N and TR/N.

Validation of RNA-seq results via qPCR

Of the 407 DEGs identified with ≥2-fold changes, 71 genes were classified under either the "inflammatory response" (GO:0006954) or "defense response to virus" (GO:0051607) categories. These 71 DEGs were visualized in a heatmap, illustrating their relative fold-changes compared with naïve con-

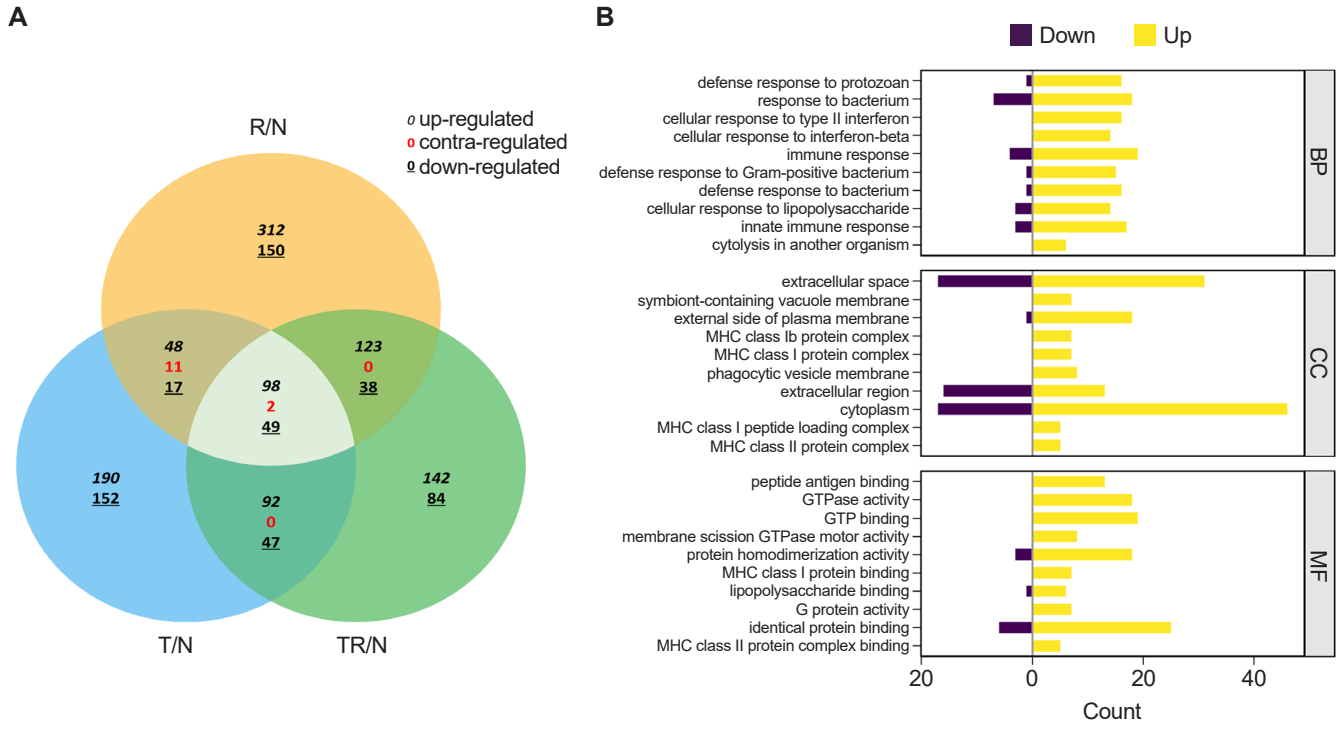

Fig. 2. Transcriptome profiling of lung tissues from infected mice. A Venn diagram depicting the concordance of differentially expressed genes between R/N (respiratory syncytial virus vs. naïve), T/N (*T. spiralis* vs. naïve), and TR/N (co-infection vs. naïve) groups (A). Enriched genes classified under the 3 principal Gene Ontology domains are shown, with downregulated genes indicated in purple and upregulated genes in yellow (B). BP, Biological Process; CC, Cellular Component; MF, Molecular Function.

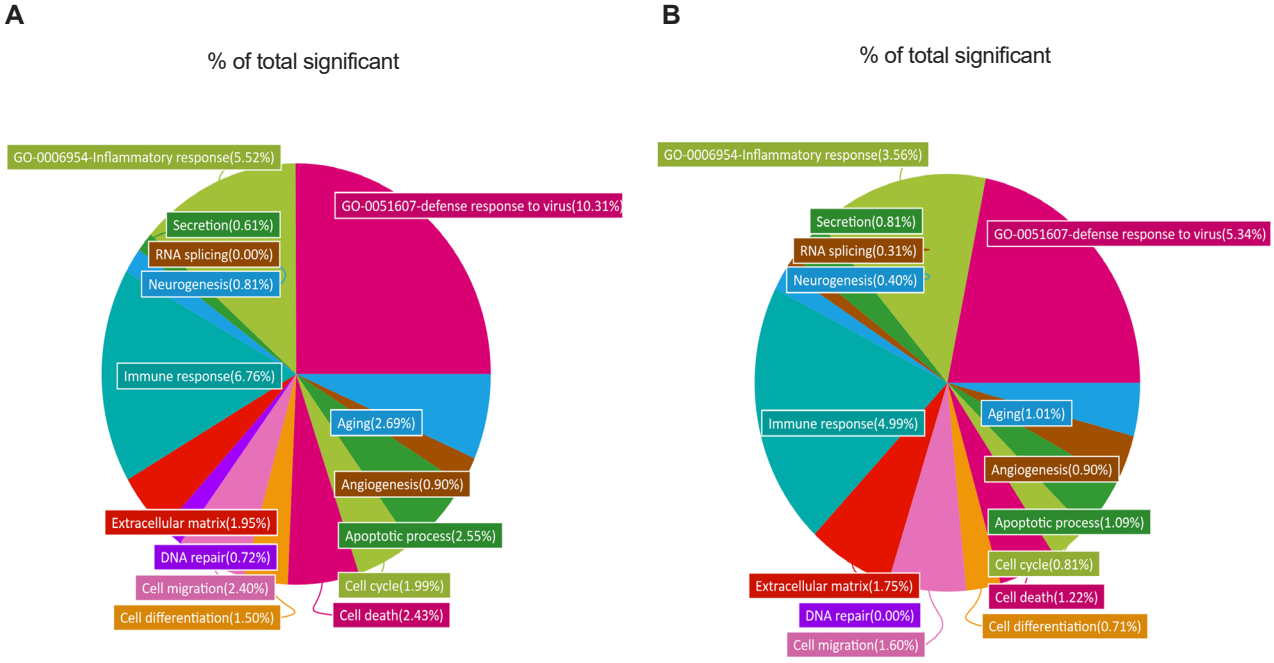

Fig. 3. Gene Ontology (GO) analysis of lung transcriptomes from respiratory syncytial virus–infected and co-infected mice. Enriched GO terms were identified from RNA sequencing data, and the relative proportion of genes associated with each GO term is shown as a percentage of the total significant categories. Differentially expressed gene categories and their relative proportions were analyzed for respiratory syncytial virus vs. naïve (A) and co-infection vs. naïve (B).

https://doi.org/10.3347/PHD.25067

trols (Fig. 4A). To validate the RNA-seq results, qPCR was performed on selected genes previously implicated in RSV-induced inflammation. Specifically, RSV-induced changes to *Cxcl9*, *Cxcl10*, *Cxcl11*, *Saa3*, and *Timp1* expressions were evaluated (Fig. 4B). Consistent with RNA-seq data, *Cxcl9* expression was strongly upregulated in RSV-infected mice but was significantly suppressed in the presence of *T. spiralis*. A similar pattern was observed for *Cxcl11*, *Cxcl10*, and *Saa3*, all of which were markedly induced by RSV but attenuated in co-infected mice. In contrast, expression of *Timp1*, despite its known roles in inflammation and tissue repair, remained at basal levels across all groups. This observation differed from the RNA-seq heatmap, which suggested a gradual reduction in *Timp1* expression in *T. spiralis*-exposed mice. An overview of how *T. spiralis* infection modulated RSV-induced inflammatory response was obtained through KEGG pathway analysis (Fig. 5) [18]. Genes upregulated and downregulated in the Ts-RSV group relative to RSV alone were color-coded in red and blue, respectively. Consistent with the RNA-seq data, several chemokines such as CXCL9-11, CCL2, and CCL7 were markedly downregulated, indicating attenuated recruitment of monocytes and Th1-associated effector cells. In contrast, receptors including CCR3 and CXCR2 were upregulated, suggesting a shift toward eosinophilic or tissue repair-associated chemotaxis. Cytokines within the TNF family and interferon families, including IFN-γ also exhibited reduced expression, indicating a general attenuation of cytokine-cytokine receptor signaling in the lungs of Ts-RSV mice.

Discussion

Helminth-mediated attenuation of inflammatory responses is a well-documented phenomenon observed across numerous parasitic species, and *T. spiralis* is no exception. Multiple studies have highlighted the immunomodulatory properties of *T. spiralis* in the context of refractory and chronic immune-mediated disorders [19]. In the present study, we characterized transcriptomic alterations in mice with pre-existing *T. spiralis* infection that were subsequently challenged with RSV. Our findings demonstrate that helminth exposure induces extensive changes in pulmonary gene expression, ultimately contributing to the suppression of virus-induced inflammatory

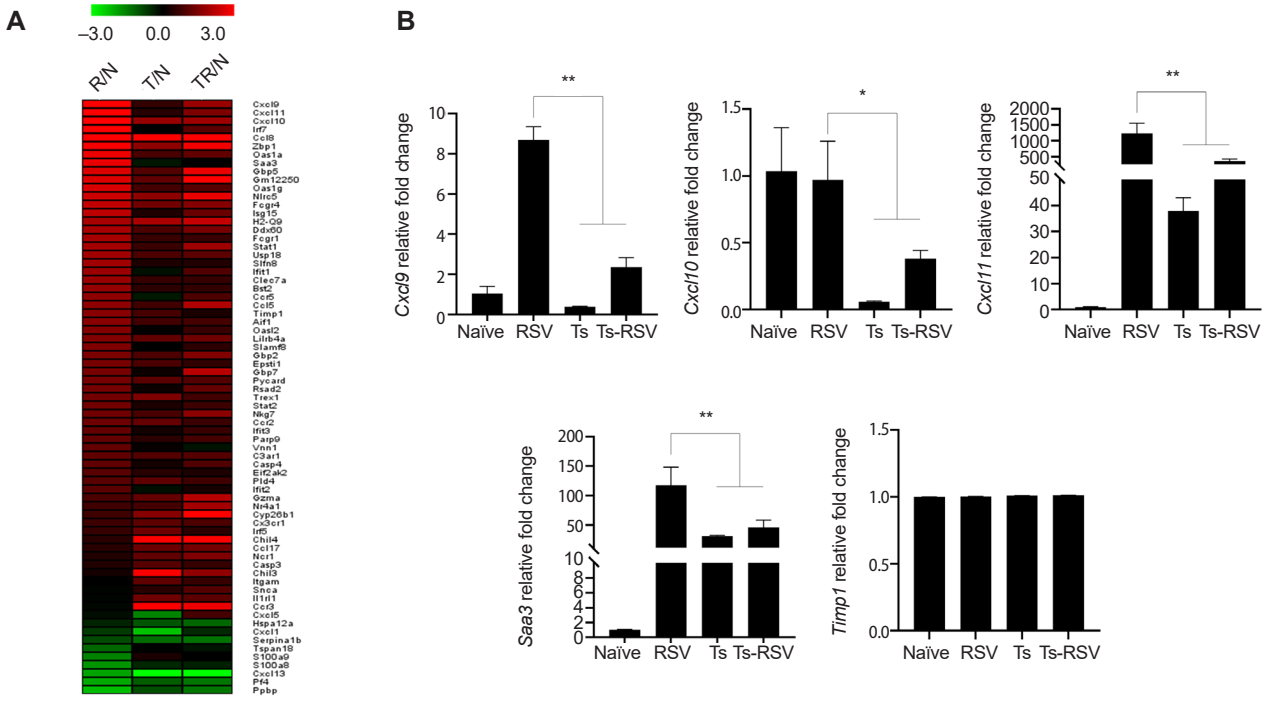

Fig. 4. Heatmap of genes upregulated and downregulated by *Trichinella spiralis* (Ts) infection in the lungs. Differentially expressed genes categorized under GO:0006954 and GO:0051607 were compiled and a heatmap was drawn using the MeV software (A). Expression of genes whose association with respiratory syncytial virus (RSV)-induced inflammation was validated through quantitative real-time PCR from the right lung lobes of mice (n=5 per group) (B). All gene expression values were normalized to beta-actin (*Actb*). Data are presented as mean±SD ($^{*}P$<0.05, $^{**}P$<0.01). R/N, RSV vs. naïve; T/N, *T. spiralis* vs. naïve; TR/N, co-infection vs. naïve.

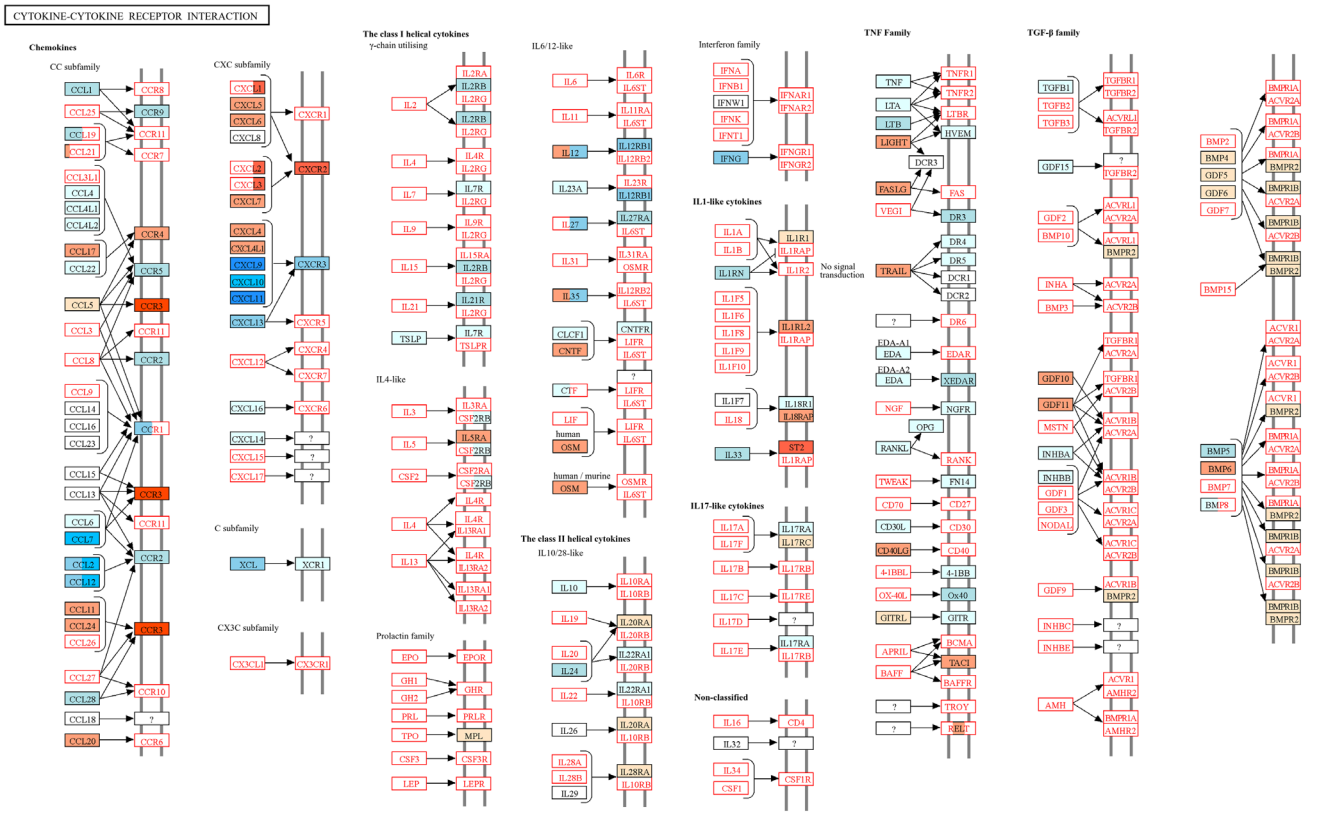

Fig. 5. Kyoto Encyclopedia of Genes and Genomes (KEGG) pathway analysis of cytokine-cytokine receptor interactions in the lungs of *Trichinella spiralis* (Ts) plus respiratory syncytial virus (RSV) mice. Differentially expressed genes identified from RNA sequencing data were mapped onto the KEGG pathway *mmu04060* using KEGG Mapper. Genes upregulated or downregulated in the Ts-RSV group relative to RSV control group are indicated in red and blue, respectively. Pathway map modified from KEGG with permission from Kanehisa Laboratories [18].

responses.

RSV infection is known to activate multiple signaling pathways, including those involved in immune cell adhesion (e.g., *Cxcl* family chemokines), acute-phase responses mediated by *Saa3*, and Toll-like receptor signaling cascades, among others [20]. Consistent with these reports, transcriptomic profiling of murine lungs in our study revealed significant upregulation of genes associated with chemoattraction and inflammation [21,22]. For example, it is well established that the inflammatory cytokine IFN-γ induces the expression of *Cxcl9*, *Cxcl10*, and *Cxcl11* [23]. In our previous work, we demonstrated that pre-existing *T. spiralis* infection significantly reduced IFN-γ production in the lungs of RSV-infected mice, consistent with the RNA-seq results presented in this study [14]. Moreover, other studies have reported that IFN-γ–inducible genes can be drastically overexpressed, with fold changes exceeding 10,000 following infection with the RSV A2 strain [24]. It is well established that helminth infections induce a shift toward Th2-biased immunity, characterized by the activation of Th2 cytokines and eosinophils, which are essential for parasite clearance. In parallel, helminths promote immunoregulatory responses through induction of IL-10, TGF-β, and regulatory T cells, thereby establishing an anti-inflammatory environment [25]. In agreement with this paradigm, we observed upregulation of genes associated with Th2 immunity in mice with pre-existing *T. spiralis* infection. Notably, the expression of *Chil3* and *Chil4* (encoding chitinase-like proteins 3 and 4) was increased, as shown in the heatmap, both of which are implicated in Th2 polarization and the activation of alternatively activated macrophages [26,27]. Similar findings have been reported in the lungs of *Nippostrongylus brasiliensis*-infected mice, where acute upregulation of *Chil3*/*Chil4* expression led to alternatively activated macrophage activation and subsequent attenuation of pulmonary inflammation [28]. However, certain discrepancies were observed between our findings and those of previous studies regarding the expression of inflammation-associated genes. In our study, inflammation-associated genes were upregulated to a greater extent

https://doi.org/10.3347/PHD.25067

than previously reported, which is likely attributable to the higher RSV inoculum used—approximately threefold greater than in earlier experiments. Other inconsistencies were also noted. For example, while pre-existing *T. spiralis* infection was expected to suppress *Timp1* expression, transcriptome analysis indicated upregulation in RSV-infected mice. In contrast, qPCR validation revealed that *Timp1* expression remained near basal levels across all groups. Such discrepancies are not unexpected, as RNA-seq, despite its robustness, does not always yield results concordant with qPCR or microarray analyses. Indeed, transcriptomic studies have shown that 15%–20% of expressed genes may display non-concordance, either through differential directionality of expression or by the identification of DEGs in 1 platform but not in another [29].

There are several limitations that must be acknowledged. First, RNA-seq analysis was performed using a single biological sample per experimental group. Consequently, the differential-expression data should be regarded as exploratory rather than inferential, since statistical confidence metrics such as *P*-values and false discovery rates cannot be fully validated without biological replication. Nevertheless, the observed transcriptomic trends and the enrichment of regulatory pathways were consistent with our histopathological and cytokine findings, lending biological plausibility to the proposed immunomodulatory effects of *T. spiralis* pre-infection. Future studies including replicate samples and cell-type specific transcriptomic profiling will be important to confirm and refine these mechanistic insights. Another limitation of this study is that cytokine concentrations and immune-cell subsets were not directly measured. Although the transcriptomic data indicated activation of Th2-associated and regulatory pathways, these findings were inferred from gene-expression profiles rather than confirmed by functional assays. Future studies incorporating cytokine quantification and immunophenotyping of regulatory T cells and alternatively activated macrophages will be important to validate the transcriptional predictions and clarify the cellular mechanisms underlying *T. spiralis*–mediated immunomodulation.

While our findings demonstrate that helminth-mediated immunomodulation can be elicited by *T. spiralis* and that such responses confer protection against RSV infection, several key questions remain unresolved. First, our study did not determine whether the protective effects and associated gene expression changes were driven primarily by live infection or by specific parasite-derived molecules. Notably, randomized clinical trials in humans have shown that administration of *Trichuris suis* ova did not significantly alleviate allergic rhinitis [25], suggesting that either persistent infection or parasite-derived secretory products may be necessary to induce protection. Second, the infection dose required to achieve immunomodulation while minimizing host pathology remains unclear. For example, protection against airway hyperresponsiveness in Wistar rats was reported following infection with 5,000 *Strongyloides venezuelensis* L3 larvae [30]. By contrast, inoculation with 5,000 *T. spiralis* muscle larvae is not feasible, particularly in humans, who are highly susceptible to *T. spiralis* infection; ingestion of even a small number of larvae in contaminated meat poses a risk for trichinosis [31]. *T. spiralis*-derived excretory-secretory (ES) antigens have emerged as more realistic therapeutic candidates because direct application of live *T. spiralis* is not feasible due to safety concerns. Several *T. spiralis* components have demonstrated anti-inflammatory properties in animal models. For example, *T. spiralis* cystatin regulates macrophage polarization toward an anti-inflammatory phenotype, thereby ameliorating sepsis-induced inflammation and improving survival in mice [32]. Likewise, *T. spiralis* chitinase markedly reduces allergic airway inflammation by suppressing Th2-associated immune responses [33]. Because individual *T. spiralis* antigen likely act through distinct mechanisms and some may even exacerbate inflammation [34], careful selection and rigorous preclinical evaluation of candidate molecules will be essential for their safe therapeutic application. Finally, the duration of infection may critically influence the extent of helminth-mediated protection. In our study, RSV infection was introduced 12 days post-*T. spiralis* infection, based on prior reports indicating that this is the last time point at which migratory larvae can still be detected in the lungs [35]. However, we did not investigate whether encysted muscle-stage larvae are capable of modulating immune responses in distal organs such as the lungs. Collectively, these lingering questions highlight the need for future studies to determine whether protection is mediated by live infection or parasite-derived products, to establish safe and effective dosing strategies, and to define the temporal window during which *T. spiralis* exerts its immunomodulatory effects.

In conclusion, this study demonstrates that pre-existing *T. spiralis* infection induces transcriptomic changes in the lungs that attenuate RSV-induced pulmonary inflammation and tissue damage. Although the precise mechanisms underlying this protective effect remain to be elucidated, our findings suggest that *T. spiralis* possesses therapeutic potential in modulating pathogen-induced inflammatory diseases. Future studies aimed at identifying the specific components of *T. spi-*

ralis responsible for these anti-inflammatory effects will not only advance our understanding of helminth-derived immunomodulation but may also facilitate the development of novel prophylactic or therapeutic strategies for managing inflammatory disorders.

Author contributions

Conceptualization: Chu KB, Quan FS. Funding acquisition: Chu KB. Investigation: Chu KB. Project administration: Quan FS. Supervision: Quan FS. Visualization: Chu KB. Writing – original draft: Chu KB. Writing – review & editing: Chu KB, Quan FS.

Conflict of interest

Fu-Shi Quan serves as an editor of Parasites, Hosts and Diseases but had no involvement in the decision to publish this article. No other potential conflicts of interest relevant to this study were reported.

Funding

This work was supported by the 2024 Inje University research grant.

ORCID

Ki Back Chu, https://orcid.org/0000-0002-2126-3366
Fu-Shi Quan, https://orcid.org/0000-0003-0419-9339

References

1. Ryan SM, Eichenberger RM, Ruscher R, Giacomin PR, Loukas A. Harnessing helminth-driven immunoregulation in the search for novel therapeutic modalities. PLoS Pathog 2020;16:e1008508. https://doi.org/10.1371/journal.ppat.1008508
2. Chen J, Gong Y, Chen Q, Li S, Zhou Y. Global burden of soil-transmitted helminth infections, 1990-2021. Infect Dis Poverty 2024;13:77. https://doi.org/10.1186/s40249-024-01238-9
3. Parker W, Ollerton J. Evolutionary biology and anthropology suggest biome reconstitution as a necessary approach toward dealing with immune disorders. Evol Med Public Health 2013;2013:89-103. https://doi.org/10.1093/emph/eot008
4. Gerrard JW, Geddes CA, Reggin PL, Gerrard CD, Horne S. Serum IgE levels in white and metis communities in Saskatchewan. Ann Allergy 1976;37:91-100.
5. Evans H, Mitre E. Worms as therapeutic agents for allergy and asthma: understanding why benefits in animal studies have not translated into clinical success. J Allergy Clin Immunol 2015;135:343-53. https://doi.org/10.1016/j.jaci.2014.07.007
6. Correale J, Farez M. Association between parasite infection and immune responses in multiple sclerosis. Ann Neurol 2007;61:97-108. https://doi.org/10.1002/ana.21067
7. Broadhurst MJ, Leung JM, Kashyap V, et al. IL-22+ CD4+ T cells are associated with therapeutic trichuris trichiura infection in an ulcerative colitis patient. Sci Transl Med 2010;2:60ra88. https://doi.org/10.1126/scitranslmed.3001500
8. Tong M, Yang X, Qiao Y, et al. Serine protease inhibitor from the muscle larval *Trichinella spiralis* ameliorates non-alcoholic fatty liver disease in mice via anti-inflammatory properties and gut-liver crosstalk. Biomed Pharmacother 2024;172:116223. https://doi.org/10.1016/j.biopha.2024.116223
9. Jo YR, Park HT, Yu HS, Kong HH. *Trichinella* infection ameliorated vincristine-induced neuroinflammation in mice. Korean J Parasitol 2022;60:247-54. https://doi.org/10.3347/kjp.2022.60.4.247
10. Li H, Qiu D, Yang H, et al. Therapeutic efficacy of excretory-secretory products of *Trichinella spiralis* adult worms on sepsis-induced acute lung injury in a mouse model. Front Cell Infect Microbiol 2021;11:653843. https://doi.org/10.3389/fcimb.2021.653843
11. Long SR, Shang WX, Jiang M, et al. Preexisting *Trichinella spiralis* infection attenuates the severity of *Pseudomonas aeruginosa*-induced pneumonia. PLoS Negl Trop Dis 2022;16:e0010395. https://doi.org/10.1371/journal.pntd.0010395
12. Cao Z, Wang J, Liu X, et al. Helminth alleviates COVID-19-related cytokine storm in an IL-9-dependent way. mBio 2024;15:e0090524. https://doi.org/10.1128/mbio.00905-24
13. Elmehy DA, Abdelhai DI, Elkholy RA, et al. Immunoprotective inference of experimental chronic *Trichinella spiralis* infection on house dust mites induced allergic airway remodeling. Acta Trop 2021;220:105934. https://doi.org/10.1016/j.actatropica.2021.105934
14. Chu KB, Lee HA, Kang HJ, Moon EK, Quan FS. Preliminary *Trichinella spiralis* infection ameliorates subsequent RSV infection-induced inflammatory response. Cells 2020;9:1314. https://doi.org/10.3390/cells9051314
15. Chu KB, Kim SS, Lee SH, et al. Immune correlates of resistance to *Trichinella spiralis* reinfection in mice. Korean J Parasitol 2016;54:637-43. https://doi.org/10.3347/kjp.2016.54.5.637
16. Chu KB, Lee DH, Kang HJ, Quan FS. The resistance against *Trichinella spiralis* infection induced by primary infection with respiratory syncytial virus. Parasitology 2019;146:634-42. https://doi.org/10.1017/S0031182018001889
17. Robinson MD, McCarthy DJ, Smyth GK. edgeR: a Bioconductor package for differential expression analysis of digital gene expression data. Bioinformatics 2010;26:139-40. https://doi.org/10.1093/bioinformatics/btp616
18. Ogata H, Goto S, Sato K, et al. KEGG: Kyoto Encyclopedia of Genes and Genomes. Nucleic Acids Res 1999;27:29-34. https://doi.

org/10.1093/nar/27.1.29

19. Cho M, Yu HS. Therapeutic potentials of *Trichinella spiralis* in immune disorders: from allergy to autoimmunity. Parasites Hosts Dis 2025;63:123-34. https://doi.org/10.3347/PHD.24086
20. Marzec J, Cho HY, High M, et al. Toll-like receptor 4-mediated respiratory syncytial virus disease and lung transcriptomics in differentially susceptible inbred mouse strains. Physiol Genomics 2019;51:630-43. https://doi.org/10.1152/physiolgenomics.00101.2019
21. Janssen R, Pennings J, Hodemaekers H, et al. Host transcription profiles upon primary respiratory syncytial virus infection. J Virol 2007;81:5958-67. https://doi.org/10.1128/JVI.02220-06
22. Schuurhof A, Bont L, Pennings JL, et al. Gene expression differences in lungs of mice during secondary immune responses to respiratory syncytial virus infection. J Virol 2010;84:9584-94. https://doi.org/10.1128/JVI.00302-10
23. Han JH, Suh CH, Jung JY, et al. Elevated circulating levels of the interferon-γ-induced chemokines are associated with disease activity and cutaneous manifestations in adult-onset Still's disease. Sci Rep 2017;7:46652. https://doi.org/10.1038/srep46652
24. Feng Q, Feng Z, Yang B, et al. Metatranscriptome reveals specific immune and microbial signatures of respiratory syncytial virus infection in children. Microbiol Spectr 2023;11:e0410722. https://doi.org/10.1128/spectrum.04107-22
25. Helmby H. Human helminth therapy to treat inflammatory disorders: where do we stand? BMC Immunol 2015;16:12. https://doi.org/10.1186/s12865-015-0074-3
26. Kang Q, Li L, Pang Y, Zhu W, Meng L. An update on Ym1 and its immunoregulatory role in diseases. Front Immunol 2022;13:891220. https://doi.org/10.3389/fimmu.2022.891220
27. Nutman TB. Looking beyond the induction of Th2 responses to explain immunomodulation by helminths. Parasite Immunol 2015;37:304-13. https://doi.org/10.1111/pim.12194
28. Reece JJ, Siracusa MC, Scott AL. Innate immune responses to lung-stage helminth infection induce alternatively activated alveolar macrophages. Infect Immun 2006;74:4970-81. https://doi.org/10.1128/IAI.00687-06
29. Coenye T. Do results obtained with RNA-sequencing require independent verification? Biofilm 2021;3:100043. https://doi.org/10.1016/j.bioflm.2021.100043
30. Negrão-Corrêa D, Silveira MR, Borges CM, Souza DG, Teixeira MM. Changes in pulmonary function and parasite burden in rats infected with *Strongyloides venezuelensis* concomitant with induction of allergic airway inflammation. Infect Immun 2003;71:2607-14. https://doi.org/10.1128/IAI.71.5.2607-2614.2003
31. Teunis PF, Koningstein M, Takumi K, van der Giessen JW. Human beings are highly susceptible to low doses of *Trichinella* spp. Epidemiol Infect 2012;140:210-8. https://doi.org/10.1017/S0950268811000380
32. Li H, Qiu D, Yuan Y, et al. *Trichinella spiralis* cystatin alleviates polymicrobial sepsis through activating regulatory macrophages. Int Immunopharmacol 2022;109:108907. https://doi.org/10.1016/j.intimp.2022.108907
33. Xu J, Yao Y, Zhuang Q, et al. Characterization of a chitinase from *Trichinella spiralis* and its immunomodulatory effects on allergic airway inflammation in mice. Parasit Vectors 2025;18:6. https://doi.org/10.1186/s13071-024-06656-0
34. Wang R, Zhang Y, Li Z, et al. Effects of *Trichinella spiralis* and its serine protease inhibitors on intestinal mucosal barrier function. Vet Res 2025;56:7. https://doi.org/10.1186/s13567-024-01446-z
35. Harley JP, Gallicchio V. *Trichinella spiralis*: migration of larvae in the rat. Exp Parasitol 1971;30:11-21. https://doi.org/10.1016/0014-4894(71)90064-6

Original Article

Parasites Hosts Dis 2026;64(1):18-26
https://doi.org/10.3347/PHD.25039

Parasites, Hosts and Diseases

pISSN 2982-5164 • eISSN 2982-6799

A human case of cercarial dermatitis and molecular characterization of *Trichobilharzia* cercariae from *Radix plicatula* of paddy field in Tokyo, Japan

Azusa Banzai[1,*], Hiromu Sugiyama[1,2], Kentaro Wada[1], Hirotaka Katahira[1], Rei Hirasawa[1], Ryota Tanabe[3], Sou Saito[3], Kunitaka Kobayashi[4]

[1]School of Life and Environmental Science, Azabu University, Kanagawa, Japan; [2]Department of Parasitology, National Institute of Infectious Diseases, Japan Institute for Health Security, Tokyo, Japan; [3]Ecosystem Conservation Society-Japan, Tokyo, Japan; [4]Japan Greenery Research and Development Center, Tokyo, Japan

Avian schistosomes, mainly belonging to the genus *Trichobilharzia*, are the etiological agents of cercarial dermatitis in humans. The aims of this study were to report a human case of cercarial dermatitis contracted in a paddy field in a natural regeneration area in Tokyo, Japan, and identify the etiological agents of this case using molecular phylogenetic analyses. A snail survey was conducted between 2021 and 2023 in a rice paddy field where a case of cercarial dermatitis occurred, and molecular phylogenetic analyses of the furcocercariae and parasitized lymnaeid snails were performed based on the partial sequence of the mtDNA *cox1* gene. Furcocercariae were detected in 11 (2.7%) of the 413 lymnaeid snails examined, and all 120 pleurocerid snails tested negative for cercariae. The cercarial larvae possessed a pair of eye spots and a characteristic bifurcated tail. Phylogenetic analyses of the *cox1* genes identified the furcocercariae as *Trichobilharzia* sp., and the lymnaeid snails were *Radix plicatula*. This study demonstrated that the life cycle of a *Trichobilharzia* sp., using *R. plicatula* as an intermediate host, is established in an urban natural restoration area in Tokyo, serving as a source of human cercarial dermatitis. This study emphasizes the need for an increased awareness of cercarial dermatitis as a potential public health concern.

Keywords: Cercarial dermatitis, paddy field dermatitis, *Trichobilharzia*, *Radix plicatula*, Japan

Introduction

Schistosomatidae (Platyhelminthes, Neodermata, Trematoda) are widely known blood flukes that parasitize birds and mammals, including humans. The genus *Trichobilharzia* Skrjabin and Zakharov, 1920, is the most speciose within this family, encompassing approximately 40 nominal species [1,2]. *Trichobilharzia* spp. utilize wild waterfowl as definitive hosts and freshwater snails as intermediate hosts, but incidental cercarial infections of humans can occur [3]. Humans are "dead-end" hosts, meaning that invading cercariae ultimately die within the host. However, invading cercariae have the potential to induce a strong allergic reaction in human hosts. Initial symptoms include erythema and itching, followed by development of a maculopapular rash on areas of skin that have been submerged in water within 12–48 h of exposure [4,5].

Cercarial dermatitis was observed by Dr. William W. Cort at Douglas Lake, Michigan, USA, when collecting snails for biological specimens in 1928. He found that the cercariae of avian schistosomes, *Cercaria elvae* from snails, induced a rash after

Received: May 20, 2025 Accepted: October 1, 2025
*Correspondence: umehara@azabu-u.ac.jp

Citation
Banzai A, Sugiyama H, Wada K, Katahira H, Hirasawa R, Tanabe R, Saito S, Kobayashi K. A human case of cercarial dermatitis and molecular characterization of *Trichobilharzia* cercariae from *Radix plicatula* of paddy field in Tokyo, Japan. Parasites Hosts Dis 2026;64(1):18-26.

penetrating the skin, and he described this allergic reaction as cercarial dermatitis [6]. Since that time, cases of cercarial dermatitis have been reported worldwide. This is because the pathogens parasitize migratory birds, which facilitates widespread dispersal of parasite eggs.

Tanabe [7] was the first to report the cause of a well-known dermatitis among paddy field workers in the valley area adjacent to Lake Shinji in Shimane Prefecture, Japan. Known locally in Japan as "Koganbyo" (lakeside disease), his report indicates that the condition was caused by penetration of the skin by cercariae of *Gigantobilharzia sturniae*. Cort reported that this dermatitis was similar to the condition commonly referred to as "swimmer's itch" in many parts of the world [8]. Thereafter, cases of dermatitis resulting from skin penetration by cercariae of *T. physellae* and *T. szidati* (formerly referred to as *T. ocellata*, see [9]) at Oki Island, Shimane Prefecture [10], Japan, and *T. brevis* in Saitama Prefecture, Japan [11], were also reported, indicating that paddy fields could serve as sources of cercarial dermatitis in various parts of Japan. However, since the 1990s, few reports of cercarial dermatitis have been reported in Japan, and as a result, it has become one of the lesser-known parasitic diseases.

In 2021, a worker developed an itchy skin rash on his legs after working in a paddy field in Tokyo, Japan. This paddy field is located within a natural restoration area, and the flight of ducks to the paddy field and the presence of snails have been confirmed. Therefore, we suspected it to be a case of cercarial dermatitis. The aims of this study were to report a human case of cercarial dermatitis contracted in a paddy field in a natural regeneration area in Tokyo, Japan, and identify the etiological agents of this case and its intermediate snail hosts using molecular phylogenetic analyses. Although identification of cercariae at the family level is generally possible based on morphology, more specific identification requires the use of molecular tools. Several studies have demonstrated that morphological characterization of cercariae is unreliable for identifying species of the genus *Trichobilharzia* [1,12-14]. Accurate identification of the snail species is often critical for precise identification of schistosome species, as schistosomes exhibit a strong preference for particular snail species as hosts [1,15]. Based on these considerations, molecular analyses were conducted in this study to identify both the schistosome species and their snail hosts. As a result, we demonstrated the life cycle of *Trichobilharzia* in an urban natural restoration area, indicating an emerging interface between wildlife parasites and human activities. This study highlights the importance of recognizing the potential risk of cercarial dermatitis and the need for integrated approaches to both biodiversity and public health management for this zoonotic disease.

Methods

Ethics statement

This study was conducted in accordance with institutional guidelines. Ethical approval was not required because this was a single anonymized case report. Written informed consent was obtained from the patient for the publication of this case report and the accompanying images.

Description of a cercarial dermatitis case

In June 2021, a male worker in a natural restoration paddy field in Tokyo, Japan, presented with an itchy rash on his legs, which had been submerged in paddy field water (Fig. 1). Lesions developed within hours of contact with the paddy field water. The worker reported that dermatologic symptoms, including itching, had been observed in other individuals who had been in contact with the paddy field water within approximately the last year.

Fig. 1. The leg of the paddy field worker in the present case. Multiple erythematous papules appeared on the areas that had been submerged in paddy field water. Scale bar=5 cm.

Collection of freshwater snails and examination of schistosome cercariae

Snail samples were collected by hand from the abovementioned small paddy field 4 to 7 times per year between 2021 and 2023. Snail sampling was basically performed until consecutive negative results for cercariae of avian schistosomes were confirmed. The collected snails were transported to the laboratory after being placed in plastic containers filled with paddy field water. At the laboratory, the snails were cracked open with pliers in a petri dish filled with distilled water and examined under a stereomicroscope for the presence of cercariae. Cercariae with a bifurcated tail were identified as furcocercariae. Detected furcocercariae were transferred to water for injection, and each was placed in a PCR tube with 10 μl of water using a micropipette and stored at -20°C until DNA extraction. The remaining furcocercariae were preserved in 70% alcohol as preliminary samples for molecular identification. For each snail, a small piece of the posterior foot was trimmed and stored at -20°C for DNA extraction.

DNA extraction, PCR amplification, and sequencing of cercarial DNA

In this study, we used molecular analysis to identify the species of 5 furcocercariae randomly selected from each snail. DNA was extracted using an alkaline lysis method. Whole furcocercariae were lysed in 25 μl of 0.02 N NaOH at 99°C for 30 min.

First, PCR amplification of nuclear 28S ribosomal DNA (rDNA) was carried out according to a previous report [16]. The primer pair LSU-5 (5′-TAGGTCGACCCGCTGAAYTTAAGCA-3′) and 1500R (5′-GCTATCCTGAGGGAAACTTCG-3′) was utilized for PCR. These primers were also used for sequencing. Three additional primers were synthesized and used to focus on regions not accessible using the PCR primers: 300F (5′-CAAGTACCGTGAGGGAAAGTT-3′), 300FR (5′-AACTTTCCCTCACGGTACTTG-3′), ECD2 (5′-CTTGGTCCGTGTTTCAAGACGGG-3′), and ECD2R-for (5′- CCCGTCTTGAAACACGGACCAAG-3′). For identification of *Trichobilharzia* spp., PCR amplification of mitochondrial cytochrome *c* oxidase subunit 1 (*cox1*) was performed using the following degenerate primer pair, CO1F15 (forward: 5'-TTTNTYTCTTTRGATCATAAGC-3′) with CO1R15 (reverse: 5'-TGAGCWAYHACAAAYCAHGTATC-3′) [2]. PCR conditions were as follows: initial DNA denaturation at 94°C for 3 min, followed by 35 cycles of 94°C for 30 sec, 45°C for 1 min, and 72°C for 1 min 30 sec, followed by a final extension step of 10 min at 72°C. PCR amplification of the *cox1* gene was carried out in a 25-μl reaction containing 1 μl of template DNA, 0.6 U of TaKaRa EX Taq (TaKaRa Bio), 0.6 μM each primer, and the manufacturer's 1× Ex Taq buffer, using a Gene Atlas G02 gradient thermal cycler (Astec). Water for injection was used instead of the DNA template as a negative control. The PCR products were directly sequenced in both directions by Eurofins Genomics using the primers described above.

DNA extraction, PCR amplification, and sequencing of lymnaeid snails

Total DNA was extracted from a small piece of tissue from each of 8 snails (4 infected and 4 uninfected) using a QIAamp DNA Mini kit (Qiagen), following the manufacturer's instructions. PCR amplification of the *cox1* gene was performed utilizing the primer pair LCO1490 (5'-GGTCAACAAATCATAAAGATATTGG-3') and HCO2198 (5'-TAAACTTCAGGGTGACCAAAAAATCA-3') [17]. Template DNA or water for injection (as a negative control) was added to 25 μl PCR preparations. The PCR conditions were as follows: initial DNA denaturation at 94°C for 3 min, followed by 35 cycles of 94°C for 30 sec, 45°C for 30 sec, and 72°C for 30 sec, followed by a final extension step of 72°C for 10 min. Direct sequencing analysis was performed in both directions using PCR primers.

Sequence analysis

The resulting sequences obtained by PCR were analyzed using GeneStudio Pro version 2.2 (GeneStudio) and compared with sequences in the GenBank database using the NCBI BLAST program (https://blast.ncbi.nlm.nih.gov/Blast.cgi). The sequences obtained in this study were aligned with those of respective *Trichobilharzia* species or respective lymnaeid snail species previously deposited in GenBank using the MUSCLE program. In addition, pairwise distance (p-distance) values were calculated among sequences within the genus *Trichobilharzia* using MEGA X software [18]. Phylogenetic analyses were subsequently performed using the maximum-likelihood method with MEGA X software. *Schistosoma bovis* (AY157212) was used as the outgroup for analyses of *Trichobilharzia* species, and *Physella acuta* (JQ390525) was used as the outgroup for analyses of lymnaeid snails. The best-fit nucleotide substitution models for phylogenetic analyses were selected based on the Akaike Information Criterion. The TN93+G+I model was employed for *Trichobilharzia*, whereas the GTR+G+I model was employed for snails. Individual nodes were evaluated by bootstrap resampling with 1,000 replications.

https://doi.org/10.3347/PHD.25039

Results

Prevalence of schistosome cercariae

Lymnaeid snails were collected in July and September 2021 and then again in April to September 2022 and April to October 2023. Conversely, the survey of pleurocerid snails was concluded in July 2021 because the absence of cercariae was confirmed in 2 consecutive surveys. A total of 413 lymnaeid snails and 120 pleurocerid snails were analyzed, and furcocercariae were found in 11 lymnaeid snails (2.7%). The prevalence of furcocercariae by collection date over 3 years is shown in Table 1. The detected cercarial larvae possessed a pair of eye spots, a ventral sucker, and a characteristic bifurcated tail (Fig. 2).

28S rDNA sequencing for genus-level identification

Sequencing of 28S rDNA from a furcocercaria indicated a length of 1,304 bp. A database search of that sequence using NCBI BLAST showed the highest similarity (99.8%) with the sequence of *Trichobilharzia* sp. (OK104140) and hits with members of the genus *Trichobilharzia* with ≥97% identity. Accordingly, this cercaria was identified as belonging to the genus *Trichobilharzia*. The sequence was submitted to GenBank under accession number LC860981.

Phylogenetic analysis of furcocercariae based on sequencing of the *cox1* gene

The partial sequence of the mitochondrial *cox1* gene proved to be a valuable tool for distinguishing between species of the genus *Trichobilharzia* due to its requisite variation for species discrimination. The *cox1* products of approximately 1,000 bp were generated through PCR. Subsequently, the obtained DNA sequences were trimmed of low-quality regions at both ends, resulting in a determined sequence of 800 bp in both directions. No differences were detected in the sequences between the worms. The sequence was submitted to GenBank under the number LC860982.

BLASTn analysis revealed that the sequence showed the highest similarity (94.0%) with that of *Trichobilharzia* sp. B (FJ174528), which was reported in the United States. A phylogenetic tree was constructed based on the partial *cox1* sequences of the obtained cercariae and those of additional related species of the genus *Trichobilharzia* available from GenBank. Phylogenetic analyses indicated that the isolates in the present study did not group with known species in the tree and thus did not allow for species identification (Fig. 3).

Uncorrected p-distances between and within *Trichobilharzia* species, as estimated from *cox1* gene sequences, are presented in Table 2. The estimated uncorrected p-distance between and within these species ranged from 7.2% to 12.1% and 0.1% to 2.2%, respectively. Furthermore, the uncorrected p-distance between *Trichobilharzia* sp. B and the cercariae of *Trichobilharzia* sp. in the present study was 6.0%.

Table 1. Prevalence of *Trichobilharzia* sp. cercariae in lymnaeid snails, *Radix plicatula*, by survey date

Date		No. of snails		
		Examined	Infected	% infected
2021	Jul 22	53	1	1.9
	Jul 30	62	5	8.1
	Sep 15	68	0	0
	Sep 28	8	0	0
2022	Apr 22	11	0	0
	May 30	23	1	4.3
	Jun 27	24	1	4.2
	Jul 26	10	0	0
	Aug 30	20	0	0
2023	Apr 17	44	0	0
	May 19	18	1	5.6
	Jun 12	15	0	0
	Jul 7	10	0	0
	Aug 9	25	2	8.0
	Sep 8	14	0	0
	Oct 6	8	0	0
Total		413	11	2.7

Fig. 2. A furcocercaria isolated from an infected lymnaeid snail (live specimen). Scale bar=100 μm.

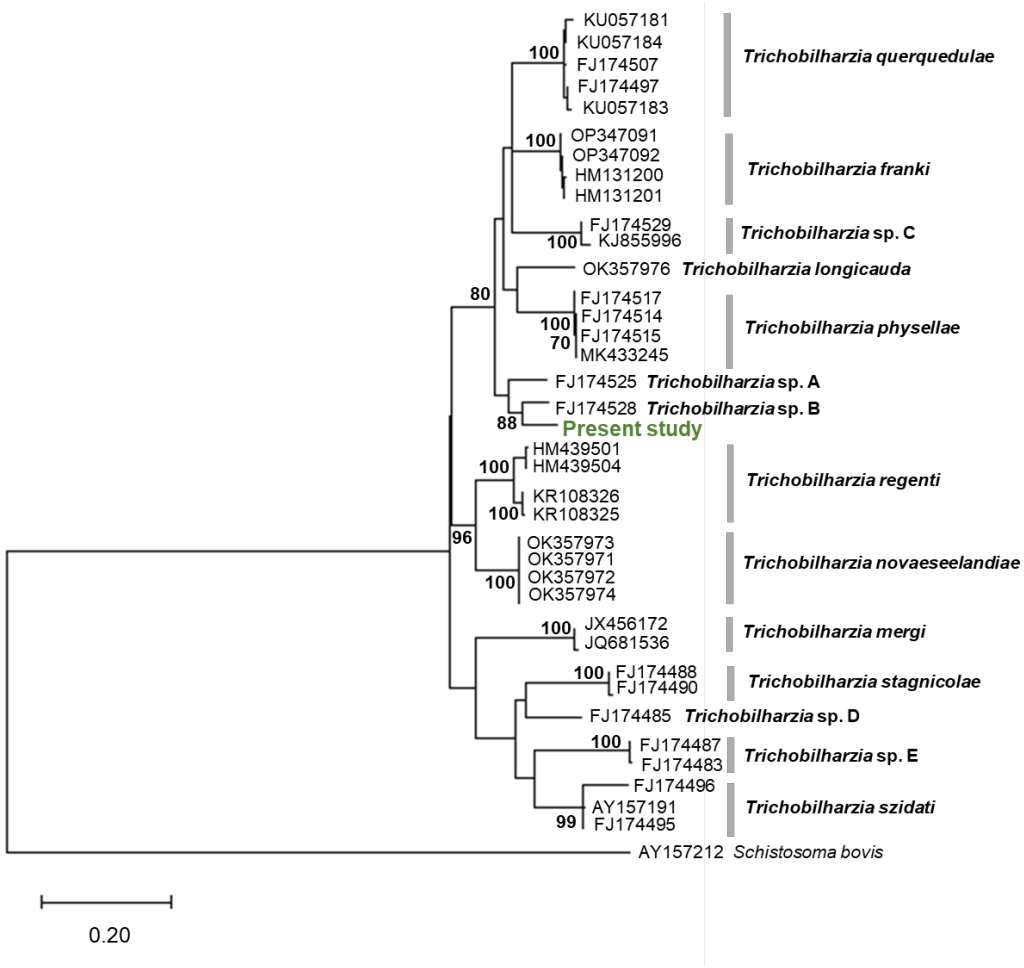

Fig. 3. Maximum-likelihood tree of *Trichobilharzia* species based on the sequence of the mtDNA *cox1* gene. Bootstrap values >70 (percentage of 1,000 replicates) are shown at the branches. *Schistosoma bovis* (AY157212) was used as an outgroup.

Table 2. Mean uncorrected pairwise distance (p-distance, %) between *Trichobilharzia* species based on the sequence of the mitochondrial cytochrome *c* oxidase subunit 1 gene

No.	Species	1	2	3	4	5	6	7	8	9	10
1	*Trichobilharzia querquedulae*	1.3[a]									
2	*Trichobilharzia physellae*	9.1	0.1[a]								
3	*Trichobilharzia* sp. A	9.4	10.0	-							
4	*Trichobilharzia* sp. B	8.4	9.3	7.2	-						
5	*Trichobilharzia* sp. C	9.0	9.9	9.3	9.8	1.4[a]					
6	*Trichobilharzia franki*	8.4	9.7	8.9	8.5	9.3	0.4[a]				
7	*Trichobilharzia regenti*	12.0	11.4	10.6	9.5	11.5	11.0	2.2[a]			
8	*Trichobilharzia novaeseelandiae*	11.6	10.5	9.8	10.5	12.1	11.3	8.0	0.2[a]		
9	*Trichobilharzia longicauda*	8.2	9.2	8.3	9.5	10.0	9.3	10.3	10.4	-	
10	Present study	7.3	9.3	7.5	6.0	9.8	9.3	11.4	10.1	10.2	-

[a]Mean intraspecific genetic variability.

Phylogenetic analysis of lymnaeid snails based on sequencing of the *cox1* gene

The lymnaeid snail *cox1* sequence was analyzed, and the length was determined as 660 bp. No sequence differences were detected among the snails examined. The lymnaeid snail sequence was submitted to GenBank under the accession num-

https://doi.org/10.3347/PHD.25039

ber LC860983. The sequence was queried using the BLAST algorithm in the NCBI database and exhibited high similarity (99.9%) to the sequence from *Radix plicatula* (LC658512) isolated in Ehime Prefecture, Japan. A phylogenetic tree based on the *cox1* gene was constructed using the nucleotide sequences of lymnaeid snails in the present study and those of 3 *Radix* species, together with sequences of *Galba truncatula* and *Austropeplea ollula* available from GenBank. The resulting constructed phylogenetic tree indicated that the snail specimens in this study grouped with *R. plicatula* (Fig. 4).

Discussion

The emergence of dermatitis contracted from the paddy field in Tokyo, Japan, in 2021 was attributed to skin invasion by the cercariae of *Trichobilharzia* sp., with *R. plicatula* as the intermediate host. This was based on the observed clinical symptoms and determination of the cercariae species found in resident snails. According to the Bureau of Environment of the Tokyo Metropolitan Government [19], in urban areas, ecological network plans are often promoted to maintain and enhance the biodiversity of limited natural environments by preserving the remaining habitats and organically connecting them through "green" corridors and relay points. The paddy field at the present study site was located within a natural restoration area designed to integrate local greenery and riverine nature as part of the overall ecological network. The establishment of the life cycle of *Trichobilharzia* in a restored natural environment provides evidence that an ecological relationship has been established between waterfowl and freshwater snails (*R. plicatula*). Bird monitoring surveys have indicated that 2 waterfowl species, the spot-billed duck (*Anas* sp.) and grey heron (*Ardea cinerea*), have visited the paddy field annually since 2015. Given that members of the genus *Trichobilharzia* are primarily transmitted to ducks, geese, or swans [1], the spot-billed duck is the most likely definitive host. Furthermore, although drainage of paddy fields is important for maintaining an optimal environment for crop growth, this practice has not been implemented in the study site because it reportedly reduces the number of aquatic organisms inhabiting paddy fields [20]. Therefore, it is

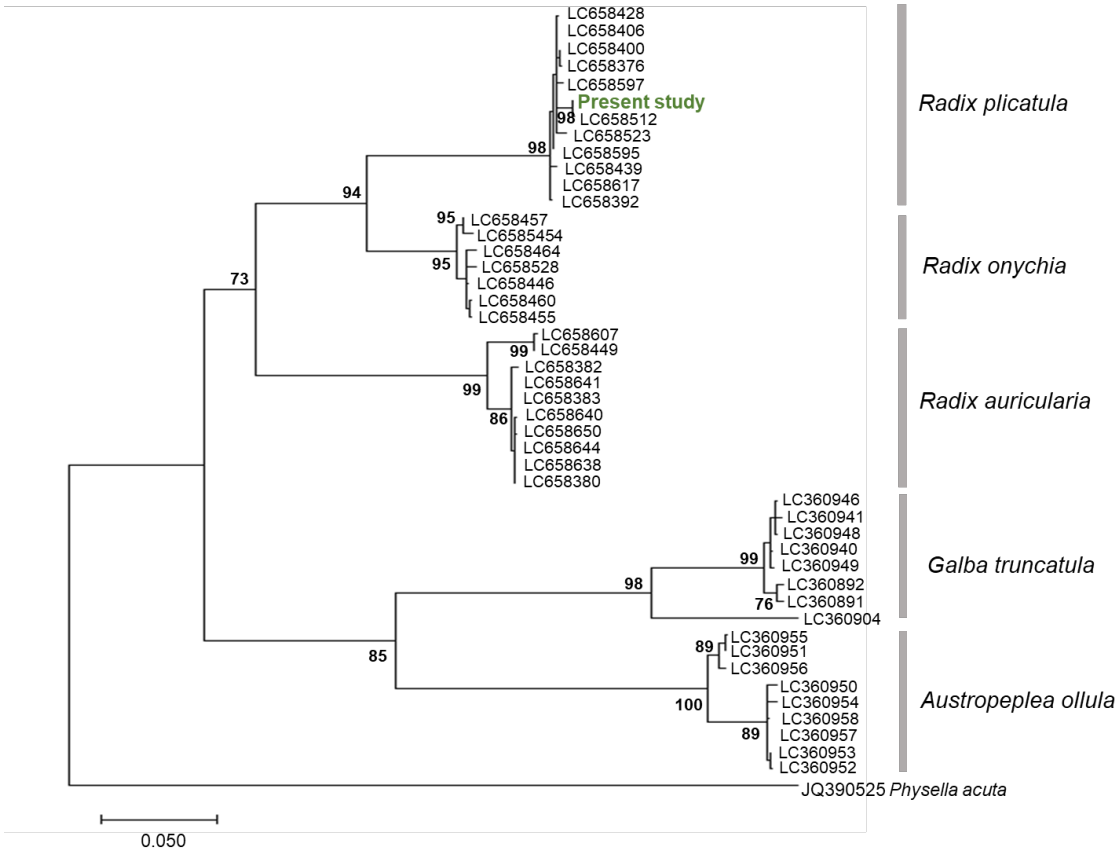

Fig. 4. Maximum-likelihood tree of *Radix* spp., *Galba truncatula* and *Austropeplea ollula*, based on the sequence of the mtDNA *cox1* gene. Bootstrap values >70 (percentage of 1,000 replicates) are shown at the branches. *Physella acuta* (JQ390525) was used as an outgroup.

considered that the reduction in the abundance of snails due to drainage did not occur. Based on the monthly temperature data from 2021 to 2023 in Tokyo (Japan Meteorological Agency, https://www.data.jma.go.jp/stats/etrn/index.php), the average temperature for each month consistently exceeded 20°C from June to September every year. This temperature range is crucial, as Ozu et al. [11] reported an increase in cercarial dermatitis when the mean temperature exceeds 20°C and stabilizes between 20°C and 25°C. Additionally, rising temperatures promote the development of the cercarial stage and cercarial emission rates, suggesting that even a slight temperature increase can increase transmission success [5]. Given these findings and the results of this study, individuals working in the paddy field where the present case originated, should wear rubber boots and gloves from May to August to avoid skin exposure to water, particularly during the planting season (May to June).

Molecular analyses of the schistosome species revealed that the furcocercariae isolated in this study were most closely related to *Trichobilharzia* sp. B isolated from American widgeons (*Anas americana*) in the United States. In contrast, no species were grouped in the same phylogenetic position as the isolates identified in this study. The calculated p-distances between the *cox1* gene sequences of the furcocercariae in this study and *Trichobilharzia* sp. B was 6.0%, which was lower than the interspecies values determined for other known species (7.2%–12.1%), but significantly greater than the intraspecies values (0.1%–2.2%). Previous studies have selected a p-distance >5% difference in COI or ND1 mtDNA markers as an indicator of separate species [2,21-25]. Although the phylogenetic analysis results and p-distance values for *cox1* in the present study identified the isolated furcocercariae as *Trichobilharzia* species, they were distinct from the species registered in the database. In Japan, the genus *Trichobilharzia* was previously reported by at least 3 species: *T. physellae*, *T. szidati*, and *T. brevis* [26]. Of these, the nucleotide sequence of *T. brevis* has not yet been registered in the database. Consequently, the molecular phylogenetic relationship between *T. brevis* and the furcocercariae isolated in this study could not be verified. There is a scarcity of *Trichobilharzia* sp. sequences in the GenBank DNA database; therefore, this poses a challenge for definitive molecular identification. *R. plicatula*, which was infected with furcocercariae in this study, has been reported to be an intermediate host of *T. paoi*, which is common across China [27]. Based on the strong host specificity for certain intermediate host species of the genus *Trichobilharzia*, it is possible that the infection in this study was caused by a species of *Trichobilharzia* that has not yet been described in Japan.

Of the 3 species of *Trichobilharzia* reported in Japan, neither *T. physellae* nor *T. szidati* has been reported as a cause of dermatitis since 1965. According to Suzuki et al. [26], the absence of reports on dermatitis caused by these species has been attributed to a decline in the number of intermediate hosts, *R. auricularia*, resulting from pesticide use or environmental changes in paddy fields. Conversely, *T. brevis* utilizing *A. ollula* as an intermediate host was reported as a new cause of dermatitis in Japan in the late 1960s [11,26,28,29]. Although subsequent outbreaks of cercarial dermatitis caused by *T. brevis* have occurred in many parts of the country, reports of dermatitis caused by this species also declined dramatically in the 1990s. In Japan, cercarial dermatitis remains poorly recognized because a continuous epidemiological study on cercarial dermatitis has not been conducted for approximately 35 years. However, this does not necessarily mean that the disease is rare. This is because the symptoms are pathologically benign and are confused with other allergic reactions or insect bites [30]. Meanwhile, recent studies have pointed out that changes in the populations of waterfowl and freshwater snails due to climate change may lead to the re-emergence of cercarial dermatitis [31]. Indeed, an increase in the incidence of the disease has been noted, and cercarial dermatitis is now considered an emerging or re-emerging disease not only in Europe but also in the United States [5,30,32].

Given these circumstances, our report on this zoonotic disease in Japan is highly significant, reaffirming its existence. Therefore, it is important to increase awareness of cercarial dermatitis through additional case reports, targeting not only agricultural workers but also environmental educators. Although paddy fields are semi-natural environments created for rice production, they perform some of the functions of natural wetlands and provide habitats and feeding sites for various organisms. Consequently, the government has encouraged environmental education to increase the understanding and awareness of biodiversity through rice cultivation [33]; thus, paddy fields are also used as sites for environmental education for residents and children. As urban ecological restoration projects continue to expand, monitoring parasitic diseases at the wildlife-human interface is becoming increasingly important for public health management.

Author contributions

Conceptualization: Banzai A, Sugiyama H. Data curation: Banzai A, Sugiyama H. Formal analysis: Banzai A. Investigation: Banzai A, Wada K, Katahira H, Hirasawa R. Project administra-

https://doi.org/10.3347/PHD.25039

tion: Banzai A, Sugiyama H. Resources: Tanabe R, Saito S, Kobayashi K. Supervision: Sugiyama H. Validation: Banzai A, Katahira H. Writing – original draft: Banzai A.

Conflict of interest

The authors have no conflicts of interest to declare.

Acknowledgments

We would like to thank Kouzo Iwaki, Ecosystem Conservation Society-Japan, and Sae Hayashida, Azabu University, for their strong support and help in this investigation.

ORCID

Azusa Banzai, https://orcid.org/0009-0004-0052-8910
Hiromu Sugiyama, https://orcid.org/0000-0002-5001-5169
Kentaro Wada, https://orcid.org/0009-0008-3103-2212
Hirotaka Katahira, https://orcid.org/0000-0002-8376-8968
Rei Hirasawa, https://orcid.org/0009-0007-3733-4513
Ryota Tanabe, https://orcid.org/0009-0006-4355-8874
Sou Saito, https://orcid.org/0009-0009-9407-0192
Kunitaka Kobayashi, https://orcid.org/0009-0002-9020-9571

References

1. Horák P, Kolárová L, Adema CM. Biology of the schistosome genus *Trichobilharzia*. Adv Parasitol 2002;52:155-233. https://doi.org/10.1016/s0065-308x(02)52012-1
2. Brant SV, Loker ES. Molecular systematics of the avian schistosome genus *Trichobilharzia* (Trematoda: Schistosomatidae) in North America. J Parasitol 2009;95:941-63. https://doi.org/10.1645/GE-1870.1
3. Horak P, Schets L, Kolarova L, Brant SV. *Trichobilharzia*. In: Liu D, editors. Molecular detection of human parasitic pathogen. CRC Press; 2012. p. 455-66.
4. Kolářová L, Horák P, Skírnisson K, Marečková H, Doenhoff M. Cercarial dermatitis, a neglected allergic disease. Clin Rev Allergy Immunol 2013;45:63-74. https://doi.org/10.1007/s12016-012-8334-y
5. Horák P, Mikeš L, Lichtenbergová L, et al. Avian schistosomes and outbreaks of cercarial dermatitis. Clin Microbiol Rev 2015;28:165-90. https://doi.org/10.1128/cmr.00043-14
6. Cort WW. Schistosome dermatitis in the United States (Michigan). J Am Med Assoc 1928;90:1027-9. https://doi.org/10.1001/jama.1928.02690400023010
7. Tanabe H. On the cause of Koganbyo. J Yonago Med Assoc 1948;1:2-3.
8. Cort WW. Studies on schistosome dermatitis. XI. Status of knowledge after more than 20 years. Am J Hyg 1950;52:251-307.
9. Rudolfová J, Hampl V, Bayssade-Dufour C, et al. Validity reassessment of *Trichobilharzia* species using *Lymnaea stagnalis* as the intermediate host. Parasitol Res 2005;95:79-89. https://doi.org/10.1007/s00436-004-1262-x
10. Oda T. Schistosome dermatitis in Japan. Prog Med Parasitol Jpn 1973;5:1-63.
11. Ozu S, Aida C, Takei S, Suzuki N, Ishizaki T. The paddy field dermatitis in Saitama Prefecture (I): epidemiological studies. J Jpn Assoc Rural Med 1972;21:361-7.
12. Blair D, Islam KS. The life cycle and morphology of *Trichobilharzia australis* n. sp. (Digenea: Schistosomatidae) from the nasal blood vessels of the black duck (*Anas superciliosa*) in Australia, with a review of the genus *Trichobilharzia*. Syst Parasitol 1983;5:89-117. https://doi.org/10.1007/BF00049237
13. Podhorsky M, Huuzova Z, Mikes L, Horak P. Cercarial dimensions and surface structures as a tool for species determination of *Trichobilharzia* spp. Acta Parasitol 2009;54:28-36. https://doi.org/10.2478/s11686-009-0011-9
14. McPhail BA, Froelich K, Reimink RL, Hanington PC. Simplifying schistosome surveillance: using molecular cercariometry to detect and quantify cercariae in water. Pathogens 2022;11:565. https://doi.org/10.3390/pathogens11050565
15. Sapp KK, Loker ES. Mechanisms underlying digenean-snail specificity: role of miracidial attachment and host plasma factors. J Parasitol 2000;86:1012-9. https://doi.org/10.1645/0022-3395(2000)086[1012:MUDSSR]2.0.CO;2
16. Olson PD, Cribb TH, Tkach VV, Bray RA, Littlewood DT. Phylogeny and classification of the Digenea (Platyhelminthes: Trematoda). Int J Parasitol 2003;33:733-55. https://doi.org/10.1016/S0020-7519(03)00049-3
17. Folmer O, Black M, Hoeh W, Lutz R, Vrigenhoek R. DNA primers for amplification of mitochondrial cytochrome *c* oxidase subunit I from diverse metazoan invertebrates. Mol Mar Biol Biotechnol 1994;3:294-9.
18. Kumar S, Stecher G, Li M, Knyaz C, Tamura K. MEGA X: Molecular Evolutionary Genetics Analysis across computing platforms. Mol Biol Evol 2018;35:1547-9. https://doi.org/10.1093/molbev/msy096
19. Bureau of Environment of the Tokyo Metropolitan Government. Tokyo biodiversity strategy for 2030 [Internet]. 2023 [cited 2025 Aug 14]. Available from: https://www.kankyo.metro.tokyo.lg.jp/documents/d/english/Tokyo-Biodiversity-Strategy_en
20. Ichikawa N. The present condition and the preservation of pond insects lived in village. Jpn J Environ Entomol Zool 2008;19:47-50.
21. Vilas R, Criscione CD, Blouin MS. A comparison between mitochondrial DNA and the ribosomal internal transcribed regions in prospecting for cryptic species of platyhelminth parasites. Parasitology 2005;131:839-46. https://doi.org/10.1017/S0031182005008437

22. Ebbs ET, Loker ES, Davis NE, et al. Schistosomes with wings: how host phylogeny and ecology shape the global distribution of *Trichobilharzia querquedulae* (Schistosomatidae). Int J Parasitol 2016;46:669-77. https://doi.org/10.1016/j.ijpara.2016.04.009
23. Fakhar M, Ghobaditara M, Brant SV, et al. Phylogenetic analysis of nasal avian schistosomes (*Trichobilharzia*) from aquatic birds in Mazandaran Province, northern Iran. Parasitol Int 2016;65:151-8. https://doi.org/10.1016/j.parint.2015.11.009
24. Laidemitt MR, Zawadzki ET, Brant SV, et al. Loads of trematodes: discovering hidden diversity of paramphistomoids in Kenyan ruminants. Parasitology 2017;144:131-47. https://doi.org/10.1017/S0031182016001827
25. Davis NE, Blair D, Brant SV. Diversity of *Trichobilharzia* in New Zealand with a new species and a redescription, and their likely contribution to cercarial dermatitis. Parasitology 2022;149:380-95. https://doi.org/10.1017/S0031182021001943
26. Suzuki N, Kawanaka M, Murata I, Ozu S. Recent paddy field dermatitis due to avian schistosome. Jpn Med J 1979;2890:43-6.
27. Attwood SW, Cottet M. Malacological and parasitological surveys along the Xe Bangfai and its tributaries in Khammouane Province, Lao PDR. Hydroecol Appl 2016;19:245-70. https://doi.org/10.1051/hydro/2015003
28. Suzuki N, Ozu S, Aida C, Takei S, Sawaura S. The paddy field dermatitis in Saitama Prefecture II: survey on the snails. J Jpn Assoc Rural Med 1973;484-90.
29. Suzuki N, Kawanaka M. *Trichobilharzia brevis* Basch, 1966, as a cause of an outbreak of cercarial dermatitis in Japan. Jpn J Parasitol 1980;29:1-11.
30. Kerr O, Juhász A, Jones S, Stothard JR. Human cercarial dermatitis (HCD) in the UK: an overlooked and under-reported nuisance? Parasit Vectors 2024;17:83. https://doi.org/10.1186/s13071-024-06176-x
31. Bispo MT, Calado M, Maurício IL, Ferreira PM, Belo S. Zoonotic threats: the (re)emergence of cercarial dermatitis, its dynamics, and impact in Europe. Pathogens 2024;13:282. https://doi.org/10.3390/pathogens13040282
32. De Liberato C, Berrilli F, Bossù T, et al. Outbreak of swimmer's itch in Central Italy: description, causative agent and preventive measures. Zoonoses Public Health 2019;66:377-81. https://doi.org/10.1111/zph.12570
33. Ministry of Agriculture, Forestry and Fisheries. The biodiversity strategy of the Ministry of Agriculture, Forestry and Fisheries [Internet]. 2023 [cited 2025 Mar 12]. Available from: https://www.maff.go.jp/e/policies/env/env_policy/attach/pdf/biodivstrategy-6.pdf

https://doi.org/10.3347/PHD.25039

Original Article

Parasites Hosts Dis 2026;64(1):27-36
https://doi.org/10.3347/PHD.25058

Parasites, Hosts and Diseases

pISSN 2982-5164 • eISSN 2982-6799

Exploration of *Naegleria*-preferentially secreted proteins for identifying diagnostic candidates to detect *Naegleria fowleri*

Hye-Jeong Jo[1,†], Hae-Ahm Lee[2,†], Fu-Shi Quan[2,3], Hyun-Hee Kong[4], Eun-Kyung Moon[2,*]

[1]Department of Biomedical Science, Graduate School, Kyung Hee University, Seoul, Korea; [2]Department of Medical Zoology, Kyung Hee University School of Medicine, Seoul, Korea; [3]Medical Research Center for Bioreaction to Reactive Oxygen Species and Biomedical Science Institute School of Medicine, Graduate School, Kyung Hee University, Seoul, Korea; [4]Department of Parasitology, Dong-A University College of Medicine, Busan, Korea

Naegleria fowleri is a free-living amoeba that can cause primary amebic meningoencephalitis (PAM), a very serious infection of the central nervous system. Early diagnosis of PAM is challenging, and the condition is almost always fatal. In this study, we conducted 2-dimensional gel electrophoresis (2-DE) analysis using *N. fowleri* trophozoite lysates and conditioned media to identify preferentially secreted proteins. As a result of the 2-dimensional gel electrophoresis analysis, 1 protein was found to increase, 5 proteins were found to decrease, 3 proteins showed a qualitative increase, and 15 proteins showed a qualitative decrease in the conditioned media compared to the proteins in the trophozoite lysates. Using cDNA from *N. fowleri*, *Acanthamoeba castellanii*, and *Balamuthia mandrillaris*, all of which can cause encephalitis, real-time PCR was performed on 5 genes corresponding to the p23-like domain-containing protein, cystatin-like domain-containing protein, fowlerpain-2, hemerythrin family non-heme iron protein, and an uncharacterized protein. The results showed that all 5 genes were highly expressed in *N. fowleri*. In animal models infected with *N. fowleri* resulting in PAM, real-time PCR analysis of brain tissue revealed significant overexpression of the p23-like domain-containing protein and fowlerpain-2. These results suggest that the 2 secreted proteins could provide valuable insights for developing antibody-based or molecular diagnostic methods to detect *N. fowleri* in patients with PAM.

Keywords: *Naegleria fowleri*, primary amebic meningoencephalitis, secreted protein

Introduction

Primary amebic meningoencephalitis (PAM) is a rare but deadly disease caused by an infection with *Naegleria fowleri* in the human body [1,2]. *N. fowleri* are free-living amoebae that inhabit warm freshwater environments such as hot springs, ponds, rivers, and lakes [3]. *Naegleria* infection can occur through activities such as swimming in freshwater, washing the nasal cavity with unsterilized water, or, in rare cases, using recreational waters such as poorly managed swimming pools and surf parks [4,5]. Generally, *N. fowleri* is introduced through the nasal cavity, travels through the olfactory nerve to the brain, and destroys central nervous system tissues. Symptoms often develop within 24 h to 1 week of infection, frequently leading to death [6,7]. Due to global warming, the risk of infection is increasing worldwide as the environments where *N. fowleri* can thrive are expanding [8]. Currently, there is no definitive treatment, and the clinical symptoms of PAM and bacterial meningitis are very similar, complicating rapid and accurate treatment [9]. PAM was first reported in the 1960s, and its incidence

Received: July 31, 2025 Accepted: November 12, 2025
*Correspondence: ekmoon@khu.ac.kr

†These authors contributed equally to this work.

Citation
Jo HJ, Lee HA, Quan FS, Kong HH, Moon EK. Exploration of *Naegleria*-preferentially secreted proteins for identifying diagnostic candidates to detect *Naegleria fowleri*. Parasites Hosts Dis 2026;64(1):27-36.

rate has been gradually increasing [10]. Therefore, it is crucial to quickly and accurately diagnose this deadly disease at an early stage.

Currently, PAM diagnosis is performed using CT or MRI to identify brain lesions such as diffuse cerebral edema, followed by cerebrospinal fluid (CSF) collection for microscopic examination. This examination uses Wright-Giemsa stain, hematoxylin and eosin stain, and periodic acid-Schiff stain, or involves culturing CSF and brain tissue [11]. Additionally, real-time PCR or PCR is used to diagnose *N. fowleri* infection in CSF samples [12,13]. However, these methods require specialized expertise and equipment and are time-consuming, making early diagnosis challenging [14,15]. Therefore, there is a need for a diagnostic method that is quick, accurate, and easy to perform.

Several studies have focused on secreted proteins as targets for vaccine development, treatment, and diagnosis of amoeba infections. One study compared protein expression profiles between axenically cultured low-virulence amoebae and mouse-passaged high-virulence amoebae using 2-dimensional gel electrophoresis (2-DE) and liquid chromatography–tandem mass spectrometry (LC-MS/MS) to identify potential therapeutic targets for limiting PAM. Proteins such as RhoA signaling-related proteins, heat shock protein 70, and Mp2CL5 were found to be associated with high virulence, suggesting that the pathogenicity of *N. fowleri* involves multiple proteins that facilitate host cell invasion [16]. In another study, proteins related to pathogenicity among *N. fowleri* excretory–secretory proteins were identified. Proteins were separated by 2-DE and reacted with *N. fowleri* infection or immune sera to identify immunodominant excretory–secretory proteins, leading to the identification of 6 proteins expected to play important roles in the pathogenicity of *N. fowleri* [17]. Another study analyzed the electrophoretic patterns of membrane proteins from *N. fowleri* and compared them with those from *N. lovaniensis* and *N. gruberi*, which are known to be nonpathogenic *Naegleria* species. This study aimed to identify a membrane protein, Nf23, that may be involved in the virulence of *N. fowleri* [18]. In another study, extracellular vesicles secreted by *N. fowleri* were reported to act as pathogenic factors that trigger host inflammatory responses [19]. However, research on the development of antibodies preferentially expressed in *N. fowleri* for its detection remains limited.

In this study, we investigated secreted proteins of *N. fowleri* that could be useful for producing antibodies capable of preferentially detecting *N. fowleri*. To achieve this, we compared the proteins present in the lysate of *N. fowleri* trophozoites with those in the cell-conditioned media using 2-DE analysis to identify proteins secreted by *N. fowleri*. We then confirmed the gene expression of those proteins using real-time PCR.

Methods

Ethics statement

All experiments involving animals were conducted in adherence to the ARRIVE (Animal Research: Reporting of In Vivo Experiments) guidelines. The study was approved by the Kyung Hee University Institutional Animal Care and Use Committee (approval No. KHSASP-24-681).

Cell cultures

N. fowleri (ATCC 30894), *Acanthamoeba castellanii* (ATCC 30868), and *Balamuthia mandrillaris* (ATCC 50209) were obtained from the American Type Culture Collection. Vero cells were sourced from the Korean Cell Line Bank. *N. fowleri* were axenically cultured in Nelson's medium (4 mg/L $MgSO_4 \cdot 7H_2O$, 4 mg/L $CaCl_2 \cdot 2H_2O$, 142 mg/L Na_2HPO_4, 136 mg/L KH_2PO_4, 120 mg/L NaCl, 1.7 g/L liver infusion, and 1.7 g/L glucose) at 37°C. *A. castellanii* were cultured in peptone-yeast-glucose medium (20 g/L proteose peptone, 1 g/L yeast extract, 0.1 M glucose, 4 mM $MgSO_4$, 0.4 mM $CaCl_2$, 3.4 mM sodium citrate, 0.05 mM $Fe(NH_4)_2(SO_4)_2$, 2.5 mM Na_2HPO_4, and 2.5 mM KH_2PO_4) at 25°C. Vero cell were cultured in RPMI 1640 medium (WelGENE) with 10% fetal bovine serum (GenDEPOT) in a 37°C incubator with 5% CO_2. When the Vero cell monolayer reached approximately 80% confluency, the culture supernatant was carefully aspirated, and *B. mandrillaris* was inoculated onto the monolayer along with fresh culture medium.

Sample preparation and 2-DE analysis

N. fowleri trophozoites were detached from the culture flask and centrifuged at 2,000 rpm for 5 min. Protein extracts were prepared by lysing samples in a denaturing buffer (7 M urea, 2 M thiourea, 4% CHAPS, 2.5% DTT, and protease inhibitors), followed by homogenization and clarification through centrifugation at 15,000 g for 20 min. Conditioned media from *N. fowleri* were collected after 7 days of cultivation and concentrated using an Amicon Ultra-4 Centrifugal Filter Unit (Merck KGaA) at 3,000 rpm for 10 min. Protein concentration was measured using Bradford assay. For 2-DE, 600 μg of each sample was applied to pH 4-7 immobilized pH gradient strips (GE Healthcare Life Sciences), focused using an IPGphor III system, and then separated on 10% SDS-PAGE gels. Gels were fixed in 40% methanol containing 5% phosphoric acid, stained with Colloidal Coomassie Blue G-250, destained in water, and scanned for im-

https://doi.org/10.3347/PHD.25058

aging. Spot detection and matching (with at least 25 landmarks per gel) were performed with ImageMaster 2D Platinum software (Amersham Biosciences).

LC-MS/MS for protein analysis

Protein spots from SDS-PAGE gels were excised and cut into pieces. These gel pieces were washed for 1 h in a solution of 25 mM ammonium bicarbonate buffer (pH 7.8) containing 50% acetonitrile. After dehydration in a centrifugal vacuum concentrator for 10 min, gel pieces were rehydrated in 50 ng of sequencing-grade trypsin solution (Promega). Following an overnight incubation at 37°C in 25 mM ammonium bicarbonate buffer, the tryptic peptides were extracted with 5 μl of 0.5% formic acid with 50% acetonitrile for 40 min under mild sonication. The extracted solution was concentrated using a centrifugal vacuum concentrator.

LC-MS/MS analysis was conducted using an agilent 1100 series nano-LC coupled with an LTQ mass spectrometer (Thermo Electron). Peptides were separated on a 150 mm × 75 μm Magic C18 capillary column (Proxeon). The mobile phase for liquid chromatography consisted of 2 solutions: mobile phase A was 0.1% formic acid in water, and mobile phase B was 0.1% formic acid in acetonitrile. A linear gradient was applied, starting from 6% to 50% of mobile phase B over 22 min, then ramping to 95% B over 5 min, before returning to 6% B over the next 13 min.

For tandem mass spectrometry, mass spectra were acquired using data-dependent acquisition with a full mass scan range of 350–1,800 m/z followed by MS/MS of the top precursors (1 microscan, normalized collision energy 35%). The ion transfer tube was set at 200°C, and the spray voltage was between 1.5 and 2.0 kV. Raw spectra were processed using SEQUEST (Thermo Quest) and searched against an in-house database using MASCOT (Matrix Science Ltd.). The MS analyses included modifications of methionine oxidation, cysteine alkylation, arginine methylation, and serine/threonine/tyrosine phosphorylation. The peptide mass tolerance was set at 10 ppm with an MS/MS ion mass tolerance of 0.8 Da. An allowance for 1 missed cleavage was given, and charge states +2 and +3 were considered during data analysis. MS/MS spectra underwent further de novo sequencing using the PepNovo software (open source, available at http://proteomics.ucsd.edu/Software/PepNovo.html), followed by MS-BLAST validation. All procedures were conducted with the assistance of Protia and were performed exactly as detailed in our previous publication [20].

Gene expression analysis by real-time PCR

The expression of the 5 selected target genes was analyzed by real-time PCR, using 18S rDNA as the internal control. Total RNA from *N. fowleri*, *A. castellanii*, and *B. mandrillaris* was extracted with the RNeasy Mini Kit (Qiagen). cDNA was synthesized using the RevertAid First Strand cDNA Synthesis Kit (Fermentas), following the manufacturer's instructions. Real-time PCR was performed on a Magnetic Induction Cycler PCR system (PhileKorea) according to a previously established protocol [21]: pre-incubation at 95°C for 1 min, followed by 40 cycles of 95°C for 15 sec and 60°C for 30 sec. All reaction mixtures were prepared using Luna Universal qPCR Master Mix (New England Biolabs), with specific primers listed in Table 1. The relative expression levels were calculated by normalizing the critical threshold (Ct) values to that of the internal control (18S rDNA), and graphs were presented using the 2^-ΔCt method.

Establishment of PAM mouse model and brain tissue collection

A total of 8 3-week-old female Balb/c mice were purchased from NARA Biotech. After a 1-week acclimation period, they were divided into a control group ($n=4$) and an infected group ($n=4$). Dexamethasone (Sigma-Aldrich) was administered intraperitoneally to the infected group at a dose of 5 mg/kg once daily for 4 consecutive days. Mice were then intranasally infected with 1×10^5 *N. fowleri* trophozoites in 50 μl PBS. They were monitored daily for clinical signs and mortality following *N. fowleri* infection.

Brains were collected from mice that either died or showed severe clinical deterioration, such as ruffled fur and marked reduction in mobility, following infection. Brains were also collected from control group mice. The brains were fixed in 4% paraformaldehyde (Yakuri Pure Chemicals) for 24 h, cryoprotected in 30% sucrose (Duksan Pure Chemicals), and subsequently embedded in OCT compound (Sigma-Aldrich), then stored at -80°C until use.

Gene expression analysis of brain tissues by real-time PCR

Brains were sliced to a depth of 20 μm using a cryostat (Leica Microsystems). RNA was extracted from the brain tissues using the RNeasy FFPE Kit (Qiagen). cDNA was synthesized using the RevertAid First Strand cDNA Synthesis Kit (Fermentas), following the manufacturer's instructions. Real-time PCR was performed as described above, using specific primers (Table 1). The relative expression levels were calculated by normalizing the Ct values to that of the control, and graphs were presented using the 2^-ΔCt method.

Table 1. Primer sequences for real-time PCR

No.	Group ID	Product	Primer sequences (5'→3')
1	QD06	Hypothetical protein (p23_like domain)	F: GTGGACTGGTCGAAATGGGT R: CCTCCTCTTCTTCATCACCCG
2	QD09	Hypothetical protein (cystatin-like domain)	F: GAACAAAAGCTCGGCAAGACA R: CTCACCTGTCTTGACGCCAT
3	DE05, QI14, QD15	Fowlerpain-2 (cysteine protease)	F: AGTGGATCATTGGCTGGTGG R: TCCAAACCCCAGTCAACTCC
4	QD10	Hypothetical protein (hemerythrin family non-heme iron protein)	F: CTGGGACTCTTCTTTCTGCGT R: TGCGAACAAGTCCTCCTCAG
5	QD08	Uncharacterized protein	F: GTTCCTTCACTGGAGGCTCA R: ACTGGTGAGAAGAAGAAGAATTTGC
6	Control_Nf	*Naegleria fowleri* 18S rDNA	F: GGAGAGGGAGCCTGAGAGAT R: CTGGCACCAGACTTTTCCTC
7	Control_Ac	*Acanthamoeba castellanii* 18S rDNA	F: CGTGCTGGGGATAGATCATT R: AAAGGGGAGACCTCACAACC
8	Control_Bm	*Balamuthia mandrillaris* 18S rDNA	F: TGACTCAACACGGGGAAACT R: TCACCCCCTGGTTTTGAATA

Statistical analysis

All statistical analyses were performed using GraphPad Prism 8 software (GraphPad Software Inc.). Data are presented as mean ± SD from 3 independent experiments. Statistical significance was assessed using Student *t*-test. *P*-values less than 0.05 were considered statistically significant and are denoted by asterisks ($^{*}P<0.05$, $^{**}P<0.01$).

Results

Comparison of proteins between trophozoite lysates and conditioned media of *N. fowleri*

To identify *Naegleria*-preferentially secreted proteins, a comparison was made between trophozoite cell lysates (Fig. 1A) and conditioned media (Fig. 1B) of *N. fowleri* using 2-DE analysis. Protein spots were found to be weakly acidic, concentrating along the center of the pH 3–10 gradient strip (data not shown). Optimal protein spot distribution and resolution were achieved using a pH 4–7 strip and 10% SDS-PAGE (Fig. 1). The 2-DE analysis identified 24 proteins with differential expression in the conditioned media relative to the trophozoite lysates. The analysis revealed 1 increased protein (IN01), 5 decreased proteins (DE02 to DE06), 3 qualitative increased proteins (QI12 to QI14), and 15 qualitative decreased proteins (QD01 to QD15). Each protein spot was labeled with a number (Fig. 1C, D), and the number of spots classified by expression patterns was organized into a table (Fig. 1E).

Identification of *N. fowleri*–preferential proteins

LC-MS/MS analysis of proteins isolated from 2-DE gels identified various proteins derived from *Naegleria* spp. To search for sequence similarity matches specific to a taxonomy group or species, the UniProt (https://www.uniprot.org) and NCBI BLAST (https://blast.ncbi.nlm.nih.gov) databases were utilized. Of the 24 proteins that exhibited differential expression in the 2-DE analysis, 18 were confirmed to be proteins of *N. fowleri* (Table 2). According to NCBI BLAST results, among these 18 *N. fowleri* proteins, 15 were identified as hypothetical proteins, and 3 showed high similarity to fowlerpain-2. The protein analysis results for all spots are shown in Table 2.

Gene expression of 5 genes in *N. fowleri* by real-time PCR

From the *Naegleria*-preferential proteins identified in the 2-DE analysis, 5 proteins were selected based on their putative functions according to UniProt search results. These proteins were chosen to verify their preferential expression in *N. fowleri* among free-living amoebae. Primers targeting each gene were designed for the following proteins: p23-like domain–containing protein (p23), cystatin-like domain–containing protein (CYST), fowlerpain-2 (FLP), hemerythrin family non-heme iron protein (HLDP), and uncharacterized protein (UNCH). These along with the 18S reference gene, are listed in Table 1. The cDNA synthesized from total the RNA of *N. fowleri*, *A. castellanii*, and *B. mandrillaris* was subjected to real-time PCR. All 5 genes were found to be signifi-

https://doi.org/10.3347/PHD.25058

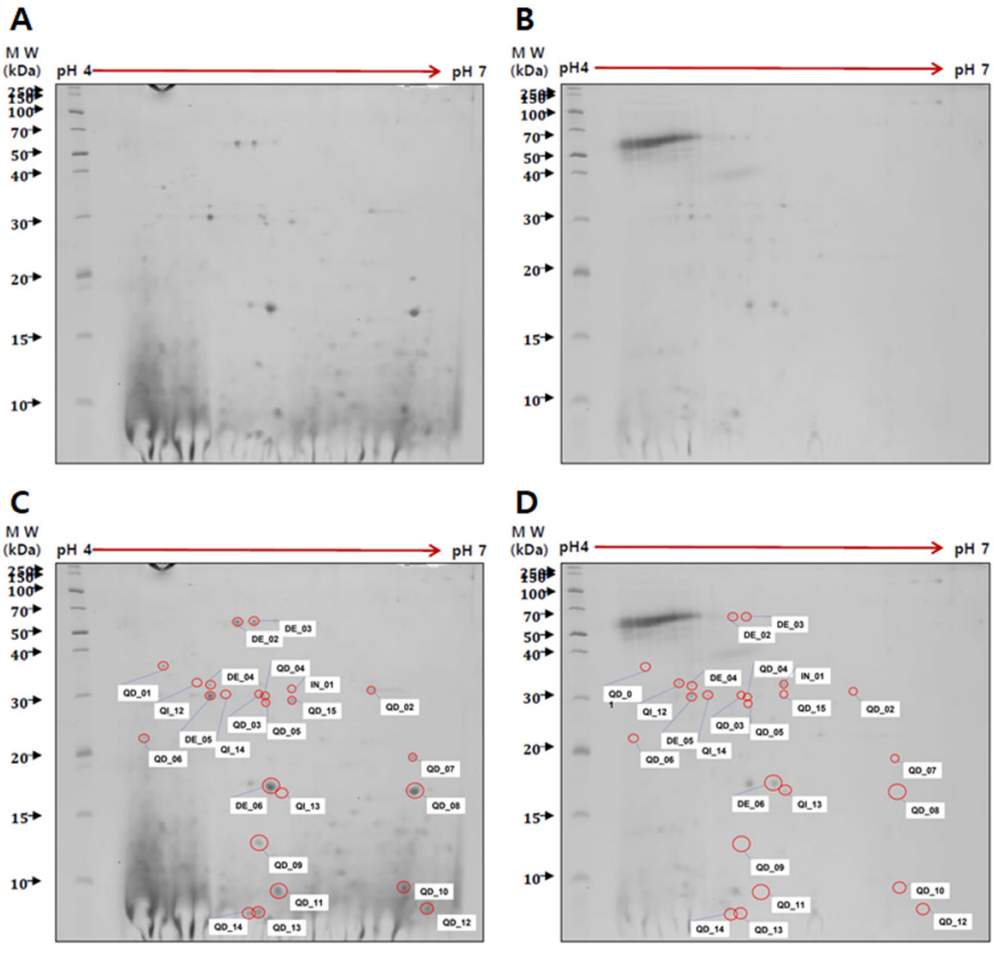

E

	IN	DE	QI	QD	Total
No. of spots	1	5	3	15	24

Fig. 1. Two-dimensional gel electrophoresis of proteins in *Naegleria fowleri* lysates and conditioned media. A comparison of proteins between trophozoite lysates (A) and conditioned media (B) revealed 24 proteins with differential expression. Each protein spot was labeled with a number indicating whether the protein was increased (IN), decreased (DE), qualitative increased (QI), or qualitative decreased (QD) in the conditioned media compared to the trophozoite lysates (C, D). The number of spots classified by expression patterns was organized into a table (E). MW, molecular weight.

cantly expressed in *N. fowleri* and not in *A. castellanii* and *B. mandrillaris* (Fig. 2A-E). However, the CYST gene was observed to be slightly expressed in *Acanthamoeba* and *Balamuthia* (Fig. 2B).

Gene expression in PAM animal models by real-time PCR

To evaluate the potential of *N. fowleri*-preferentially secreted proteins as diagnostic candidates, PAM animal models were developed by infecting them with *N. fowleri*, and real-time PCR was performed using brain tissue (Fig. 3). All 4 mice with induced PAM succumbed to the infection between days 8 and 12, showing similar patterns of inflammation in the frontal brain regions (Fig. 3A, indicated by an arrow). RNA was extracted from the brain tissue of the PAM models, followed by cDNA synthesis. Real-time PCR was performed for the 5 mentioned protein genes, revealing significant overexpression of the p23-like domain-containing protein (p23) and fowlerpain-2 (FLP) in the PAM models. The p23-like domain-containing protein gene was overexpressed in PAM mice by 101.9, 81.2, 45.2, and 35.7 times compared to the control group (Fig. 3B). Similarly, the fowlerpain-2 protein gene was overex-

Table 2. Secreted proteins from *Naegleria fowleri* trophozoites

No.	Group ID	Uniprot		NCBI		Score	Mass (Da)
		Name	Accession No.	Name	Accession No.		
1	IN01	Profilin	tr|A0A6A5BHQ3|A0A6A5BHQ3_NAEFO	Hypothetical protein FDP41_006373 [*Naegleria fowleri*]	KAF0974341.1	126	14,000
2	DE02	Triosephosphate isomerase	tr|A0A6A5BWU3|A0A6A5BWU3_NAEFO	Hypothetical protein FDP41_012394 [*N. fowleri*]	KAF0981737.1	324	27,879
3	DE03	Triosephosphate isomerase	tr|A0A6A5BWU3|A0A6A5BWU3_NAEFO	Hypothetical protein FDP41_012394 [*N. fowleri*]	KAF0981737.1	137	27,879
4	DE04	Uncharacterized protein	tr|A0AA88KE97|A0AA88KE97_NAELO	Hypothetical protein C9374_009233 [*N. lovaniensis*]	KAG2377322.1	27	108,339
5	DE05	Fowlerpain-2	tr|A0A1L1XWF9|A0A1L1XWF9_NAEFO	Fowlerpain-2 [*N. fowleri*]	AKC55968.1	751	34,550
6	DE06	Uncharacterized protein	tr|A0AAW2Z485|A0AAW2Z485_9EUKA	Hypothetical protein AKO1_013992 [*N. fowleri*]	KAL0483734.1	23	42,132
7	QI12	Histidine kinase	tr|D2VZJ1|D2VZJ1_NAEGR	Predicted protein [*N. gruberi*]	EFC37856.1	18	61,785
8	QI13	NUC153 domain-containing protein	tr|A0A6A5CCI8|A0A6A5CCI8_NAEFO	Hypothetical protein FDP41_007451 [*N. fowleri*]	KAF0984274.1	21	93,035
9	QI14	Fowlerpain-2	tr|A0A1L1XWF9|A0A1L1XWF9_NAEFO	Fowlerpain-2 [*Naegleria fowleri*]	AKC55968.1	794	34,550
10	QD01	ABC transporter protein ARB1	tr|A0AAW2YMA9|A0AAW2YMA9_9EUKA	ABC transporter protein ARB1 [*Acrasis kona*]	KAL0478427.1	21	66,226
11	QD02	Carboxypeptidase	tr|A0A6A5CIS9|A0A6A5CIS9_NAEFO	Hypothetical protein FDP41_000254 [*N. fowleri*]	KAF0985215.1	67	56,379
12	QD03	Dopey N-terminal domain-containing protein	tr|A0A6A5C095|A0A6A5C095_NAEFO	Hypothetical protein FDP41_001661 [*N. fowleri*]	KAF0979318.1	96	214,996
13	QD04	Dopey N-terminal domain-containing protein	tr|A0A6A5C095|A0A6A5C095_NAEFO	Hypothetical protein FDP41_001661 [*N. fowleri*]	KAF0979318.1	116	214,996
14	QD05	Dopey N-terminal domain-containing protein	tr|A0A6A5C095|A0A6A5C095_NAEFO	Hypothetical protein FDP41_001661 [*N. fowleri*]	KAF0979318.1	35	214,996
15	QD06	CS domain-containing protein	tr|A0A6A5BBV5|A0A6A5BBV5_NAEFO	Hypothetical protein FDP41_006609 [*N. fowleri*]	KAF0974577.1	189	20,010
16	QD07	Uncharacterized protein	tr|A0A6A5BFT0|A0A6A5BFT0_NAEFO	Hypothetical protein FDP41_003988 [*N. fowleri*]	KAF0976693.1	60	18,525
17	QD08	Uncharacterized protein	tr|A0A6A5BFT0|A0A6A5BFT0_NAEFO	Hypothetical protein FDP41_003988 [*N. fowleri*]	KAF0976693.1	130	18,525
18	QD09	Cystatin domain-containing protein	tr|A0A6A5BX69|A0A6A5BX69_NAEFO	Hypothetical protein FDP41_002161 [*N. fowleri*]	KAF0979091.1	157	10,408
19	QD10	Hemerythrin-like domain-containing protein	tr|A0A6A5BCB0|A0A6A5BCB0_NAEFO	Hypothetical protein FDP41_010118 [*N. fowleri*]	KAF0971589.1	1,750	13,452
20	QD11	Uncharacterized protein	tr|A0AAW2Z485|A0AAW2Z485_9EUKA	Hypothetical protein AKO1_013992 [*A. kona*]	KAL0483734.1	36	42,132
21	QD12	Glutamyl-tRNA reductase	tr|A0AAW2YMP3|A0AAW2YMP3_9EUKA	Glutamyl-tRNA reductase [*A. kona*]	KAL0478153.1	16	31,447
22	QD13	Predicted protein	tr|D2VNK6|D2VNK6_NAEGR	Predicted protein [*N. gruberi*]	EFC41752.1	29	59,920
23	QD14	Dopey N-terminal domain-containing protein	tr|A0A6A5C095|A0A6A5C095_NAEFO	Hypothetical protein FDP41_001661 [*N. fowleri*]	KAF0979318.1	25	214,996
24	QD15	Fowlerpain-2	tr|A0A1L1XWF9|A0A1L1XWF9_NAEFO	Fowlerpain-2 [*N. fowleri*]	AKC55968.1	250	34,550

IN, increased; DE, decreased; QI, qualitative increased; QD, qualitative decreased.

https://doi.org/10.3347/PHD.25058

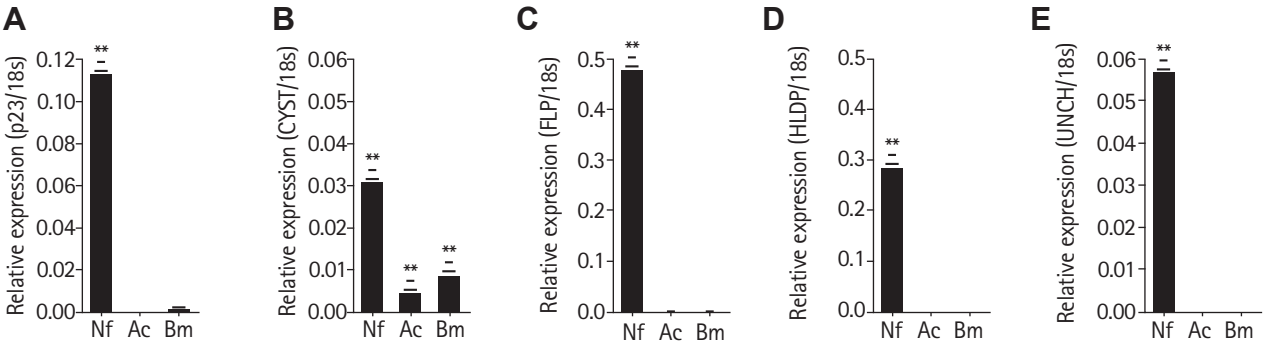

Fig. 2. Real-time PCR for mRNA quantitation. Real-time PCR was performed on cDNA synthesized from the total RNA of *Naegleria fowleri* (Nf), *Acanthamoeba castellanii* (Ac), and *Balamuthia mandrillaris* (Bm). The relative expression levels were normalized to the 18S rDNA of each sample and calculated using the formula 2^−ΔCt (where ΔCt = Ct_target − Ct_18S). Bars represent the mean±SD (n=3). The p23-like domain–containing protein (p23), cystatin-like domain–containing protein (CYST), fowlerpain-2 (FLP), hemerythrin family non-heme iron protein (HLDP), and uncharacterized protein (UNCH) each exhibited their highest expression in *N. fowleri* (A-E). Data are expressed as mean±SD, and asterisks denote statistically significant differences between the target gene and 18S rDNA ($^{**}P$<0.01).

pressed by 27.7, 24.2, 47.8, and 23.0 times (Fig. 3C). The cystatin-like domain–containing protein, hemerythrin family non-heme iron protein, and uncharacterized protein genes were either not significantly expressed or showed large error margins in the brain tissue of the PAM model (data not shown).

Discussion

Based on the comparative analysis of proteins though 2-DE analysis between trophozoite lysates and conditioned media of *N. fowleri*, 24 proteins with altered expression in conditioned media were identified. Further utilization of LC-MS/MS enabled the identification of 18 *N. fowleri*-preferential proteins. Gene expression analysis through real-time PCR provided additional evidence of the specificity of 5 proteins to *N. fowleri*.

Due to the lack of extensive database information on *N. fowleri*, the results of the LC-MS/MS analysis were searched for similarity using the UniProt and NCBI BLAST websites (Table 2). UniProt and NCBI BLAST are valuable bioinformatics resources with different, albeit related, purposes. NCBI BLAST is primarily used for sequence similarity searching, comparing a query sequence against a database to find homologous sequences and infer functional relationships. In contrast, UniProt is a comprehensive protein knowledgebase that integrates sequence, structure, function, and other relevant data. While UniProt also offers a BLAST tool for sequence similarity searches, its core function is to provide a curated and annotated resource for protein information. According to the NCBI BLAST results, most of the proteins identified by 2-DE analysis were classified as hypothetical proteins. However, in this study, 5 proteins were selected for further analysis based on their putative functions from the UniProt search results.

Spot QD06 was identified as a p23-like domain-containing protein, known to act as a co-chaperone of Hsp90 and facilitate the folding of various regulatory proteins [22]. However, since multiple Hsp90-encoding genes have been reported in the *N. fowleri* genome and none appear to be species-preferential, this protein was excluded from antibody development [23]. Spot QD09 corresponded to a protein containing a cystatin-like domain, classified within the cystatin family of cysteine protease inhibitors. These proteins typically consist of a single domain and are upregulated in brain tissue environments, where they suppress the activity of host cathepsins K and L, thereby enhancing parasite survival and pathogenicity [24]. Spots DE05, QI14, and QD15 were identified as fowlerpain-2, a cysteine protease secreted by *N. fowleri* that contributes to host tissue destruction, traversal of the blood–brain barrier, and invasion of the central nervous system [25]. Spot QD10 was a member of the hemerythrin family, which binds and consumes nitric oxide produced by macrophages, thus neutralizing nitric oxide–mediated amoebicidal mechanisms and promoting immune evasion [24]. Spot QD08 was an uncharacterized protein, and due to the lack of functional information, it was excluded from further investigation. To evaluate whether these genes were preferentially expressed in *N. fowleri*, real-time PCR analysis was conducted using *A. castellanii* and *B. mandrillaris*, 2 other free-living amoebae associated with encephalitis. All 5 genes were expressed at the highest levels in *N. fowleri*, while their expression in *A. castellanii* and *B. mandrillaris* was significantly lower or not expressed

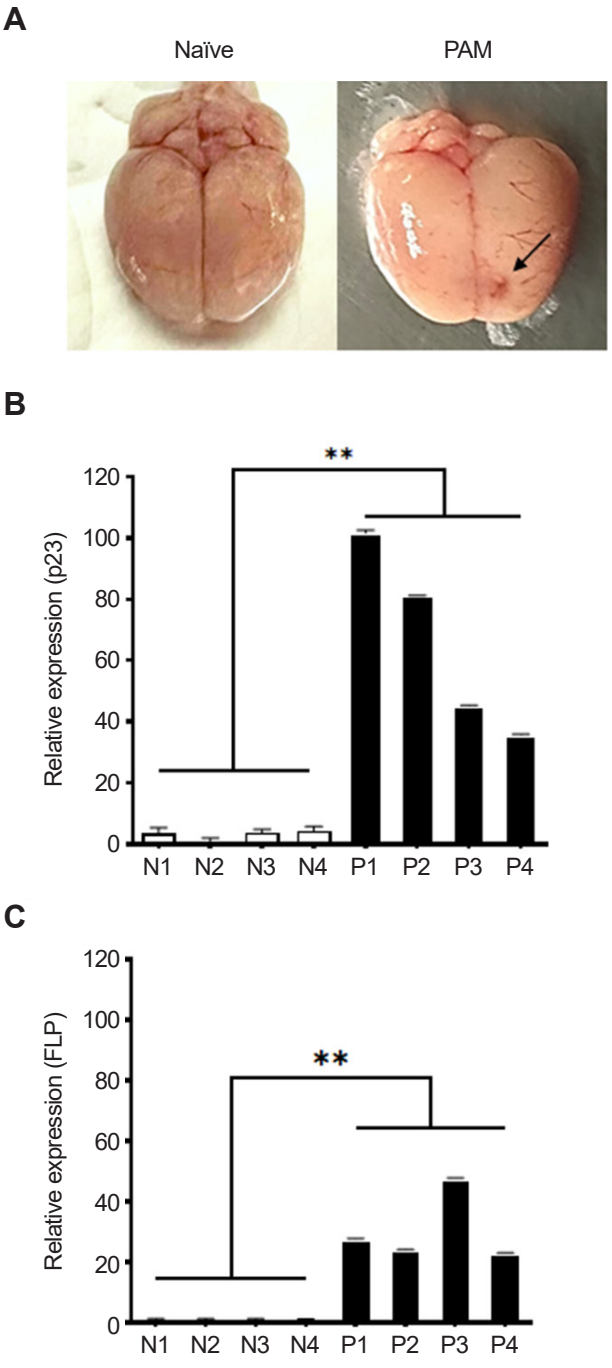

Fig. 3. Detection of *Naegleria fowleri*–preferential proteins in primary amebic meningoencephalitis (PAM) animal models. PAM animal models were developed by infecting them with *N. fowleri* (A, indicated by an arrow), and real-time PCR was performed using cDNA synthesized from the total RNA of brain tissue (B, C). The p23-like domain-containing protein and the fowlerpain-2 gene were significantly overexpressed in PAM brain tissue compared to the control group. Naïve refers to the brain of the negative control group (N), and PAM refers to the brain of the *N. fowleri*–infected group (P). Data are expressed as mean±SD, and asterisks denote statistical significance between the means of the 2 groups ($^{**}P<0.01$).

(Fig. 2). Among these, the genes for the p23-like domain-containing protein (QD06) and fowlerpain-2 (DE05, QI14, and QD15) were significantly overexpressed in the brain tissue of the PAM mouse model (Fig. 3). Based on these results, the proteins corresponding to spots DE05, QI14, and QD15 were selected as *N. fowleri*-preferentially secreted proteins, and further research is underway.

In previous studies exploring the secreted pathogenic proteins of *A. castellanii*, a wide variety of secreted proteins were identified through 2-DE analysis [20]. However, in this study, the number of secreted proteins identified in *N. fowleri* was much smaller than expected. This was likely due to our use of serum-free conditioned media, which was employed to minimize strong background signals caused by residual fetal bovine serum proteins. However, the serum-free conditions may have compromised the physiological activity of *N. fowleri*, leading to reduced protein secretion and a consequent decrease in the number of detectable spots. As a result, the range of candidate proteins available for screening of *N. fowleri*–preferentially secreted proteins was limited. Further studies should focus on optimizing culture conditions to enhance secreted protein yield and validate the diagnostic utility of the selected proteins in clinical and experimental models. Meanwhile, some protein genes showed non-significant or highly variable real-time PCR results in the brain tissue of the PAM animal model (data not shown). This variability may be influenced by differences in the severity of PAM symptoms and the specific brain regions sampled. To address this, further validation of PCR results in a larger number of PAM animal models is warranted.

In summary, the comprehensive proteomic and gene expression analyses of *N. fowleri* provide a foundational understanding of its secretome and highlight potential targets for the development of antibody-based and molecular biological diagnostic methods. Further studies should focus on the functional characterization of identified proteins to enhance our understanding of *N. fowleri* biology and to develop strategies to combat infections caused by free-living amoebae including *N. fowleri*.

Author contributions

Conceptualization: Moon EK. Data curation: Lee HA, Quan FS, Kong HH, Moon EK. Funding acquisition: Moon EK. Investigation: Jo HJ, Lee HA, Moon EK. Methodology: Jo HJ, Lee HA, Quan FS, Kong HH, Moon EK. Validation: Moon EK. Writing – original draft: Jo HJ. Writing – review & editing: Lee HA, Quan FS, Kong HH, Moon EK.

https://doi.org/10.3347/PHD.25058

Conflict of interest

Fu-Shi Quan serves as an editor of Parasites, Hosts and Diseases but had no involvement in the decision to publish this article. No other potential conflicts of interest relevant to this study were reported.

Funding

This work was supported by the National Research Foundation of Korea (NRF) grant funded by the Korea government (MSIT) (RS-2024-00346635).

ORCID

Hye-Jeong Jo, https://orcid.org/0009-0003-7079-087X
Hae-Ahm Lee, https://orcid.org/0000-0002-4279-4705
Fu-Shi Quan, https://orcid.org/0000-0003-0419-9339
Hyun-Hee Kong, https://orcid.org/0000-0003-1075-0051
Eun-Kyung Moon, https://orcid.org/0000-0003-1121-2052

References

1. Alanazi A, Younas S, Ejaz H, et al. Advancing the understanding of *Naegleria fowleri*: global epidemiology, phylogenetic analysis, and strategies to combat a deadly pathogen. J Infect Public Health 2025;18:102690. https://doi.org/10.1016/j.jiph.2025.102690
2. Ben Youssef M, Omrani A, Sifaoui I, et al. Amoebicidal thymol analogues against brain-eating amoeba, *Naegleria fowleri*. Bioorg Chem 2025;159:108346. https://doi.org/10.1016/j.bioorg.2025.108346
3. Stahl LM, Olson JB. Environmental abiotic and biotic factors affecting the distribution and abundance of *Naegleria fowleri*. FEMS Microbiol Ecol 2020;97:fiaa238. https://doi.org/10.1093/femsec/fiaa238
4. Mungroo MR, Khan NA, Siddiqui R. *Naegleria fowleri*: diagnosis, treatment options and pathogenesis. Expert Opin Orphan Drugs 2019;7:67-80. https://doi.org/10.1080/21678707.2019.1571904
5. Miko S, Cope JR, Hlavsa MC, et al. A case of primary amebic meningoencephalitis associated with surfing at an artificial surf venue: environmental investigation. ACS ES T Water 2023;3:1126-33. https://doi.org/10.1021/acsestwater.2c00592
6. Jarolim KL, McCosh JK, Howard MJ, John DT. A light microscopy study of the migration of *Naegleria fowleri* from the nasal submucosa to the central nervous system during the early stage of primary amebic meningoencephalitis in mice. J Parasitol 2000;86:50-5. https://doi.org/10.1645/0022-3395(2000)086[0050:ALMSOT]2.0.CO;2
7. Visvesvara GS, Moura H, Schuster FL. Pathogenic and opportunistic free-living amoebae: *Acanthamoeba* spp., *Balamuthia mandrillaris*, *Naegleria fowleri*, and *Sappinia diploidea*. FEMS Immunol Med Microbiol 2007;50:1-26. https://doi.org/10.1111/j.1574-695X.2007.00232.x
8. Heilmann A, Rueda Z, Alexander D, Laupland KB, Keynan Y. Impact of climate change on amoeba and the bacteria they host. J Assoc Med Microbiol Infect Dis Can 2024;9:1-5. https://doi.org/10.3138/jammi-2023-09-08
9. Zahid MF, Saad Shaukat MH, Ahmed B, et al. Comparison of the clinical presentations of *Naegleria fowleri* primary amoebic meningoencephalitis with pneumococcal meningitis: a case-control study. Infection 2016;44:505-11. https://doi.org/10.1007/s15010-016-0878-y
10. Maciver SK, Piñero JE, Lorenzo-Morales J. Is *Naegleria fowleri* an emerging parasite? Trends Parasitol 2020;36:19-28. https://doi.org/10.1016/j.pt.2019.10.008
11. Chen S, Che C, Lin W, et al. Recognition of devastating primary amoebic meningoencephalitis (PAM) caused by *Naegleria fowleri*: another case in south China detected via metagenomics next-generation sequencing combined with microscopy and a review. Front Trop Dis 2022;3:899700. https://doi.org/10.3389/fitd.2022.899700
12. Maďarová L, Trnková K, Feiková S, Klement C, Obernauerová M. A real-time PCR diagnostic method for detection of *Naegleria fowleri*. Exp Parasitol 2010;126:37-41. https://doi.org/10.1016/j.exppara.2009.11.001
13. Aykur M, Dirim Erdogan D, Selvi Gunel N, et al. Genotyping and molecular identification of *Acanthamoeba* genotype T4 and *Naegleria fowleri* from cerebrospinal fluid samples of patients in Turkey: is it the pathogens of unknown causes of death? Acta Parasitol 2022;67:1372-83. https://doi.org/10.1007/s11686-022-00597-3
14. McKenna JP, Fairley DJ, Shields MD, et al. Development and clinical validation of a loop-mediated isothermal amplification method for the rapid detection of *Neisseria meningitidis*. Diagn Microbiol Infect Dis 2011;69:137-44. https://doi.org/10.1016/j.diagmicrobio.2010.10.008
15. Mahittikorn A, Mori H, Popruk S, et al. Development of a rapid, simple method for detecting *Naegleria fowleri* visually in water samples by loop-mediated isothermal amplification (LAMP). PLoS One 2015;10:e0120997. https://doi.org/10.1371/journal.pone.0120997
16. Jamerson M, Schmoyer JA, Park J, Marciano-Cabral F, Cabral GA. Identification of *Naegleria fowleri* proteins linked to primary amoebic meningoencephalitis. Microbiology (Reading) 2017;163:322-32. https://doi.org/10.1099/mic.0.000428
17. Kim JH, Yang AH, Sohn HJ, et al. Immunodominant antigens in *Naegleria fowleri* excretory: secretory proteins were potential pathogenic factors. Parasitol Res 2009;105:1675-81. https://doi.org/10.1007/s00436-009-1610-y

18. Flores-Huerta N, Sánchez-Monroy V, Rodríguez MA, Serrano-Luna J, Shibayama M. A comparative study of the membrane proteins from *Naegleria* species: a 23-kDa protein participates in the virulence of *Naegleria fowleri*. Eur J Protistol 2020;72:125640. https://doi.org/10.1016/j.ejop.2019.125640
19. Lê HG, Kang JM, Võ TC, Yoo WG, Na BK. *Naegleria fowleri* extracellular vesicles induce proinflammatory immune responses in BV-2 microglial cells. Int J Mol Sci 2023;24:13623. https://doi.org/10.3390/ijms241713623
20. Moon EK, Choi HS, Park SM, Kong HH, Quan FS. Comparison of proteins secreted into extracellular space of pathogenic and non-pathogenic *Acanthamoeba castellanii*. Korean J Parasitol 2018;56:553-8. https://doi.org/10.3347/kjp.2018.56.6.553
21. Kim MJ, Moon EK, Jo HJ, Quan FS, Kong HH. Identifying the function of genes involved in excreted vesicle formation in *Acanthamoeba castellanii* containing *Legionella pneumophila*. Parasit Vectors 2023;16:215. https://doi.org/10.1186/s13071-023-05824-y
22. Weaver AJ, Sullivan WP, Felts SJ, Owen BAL, Toft DO. Crystal structure and activity of human p23, a heat shock protein 90 co-chaperone. J Biol Chem 2000;275:23045-52. https://doi.org/10.1074/jbc.M003410200
23. Joseph SJ, Park S, Kelley A, et al. Comparative genomic and transcriptomic analysis of *Naegleria fowleri* clinical and environmental isolates. mSphere 2021;6:e0063721. https://doi.org/10.1128/msphere.00637-21
24. Malych R, Folgosa F, Pilátová J, et al. Eating the brain: a multidisciplinary study provides new insights into the mechanisms underlying the cytopathogenicity of *Naegleria fowleri*. PLoS Pathog 2025;21:e1012995. https://doi.org/10.1371/journal.ppat.1012995
25. Aldape K, Huizinga H, Bouvier J, McKerrow J. *Naegleria fowleri*: characterization of a secreted histolytic cysteine protease. Exp Parasitol 1994;78:230-41. https://doi.org/10.1006/expr.1994.1023

https://doi.org/10.3347/PHD.25058

Original Article

Parasites Hosts Dis 2026;64(1):37-44
https://doi.org/10.3347/PHD.25080

Parasites, Hosts and Diseases

pISSN 2982-5164 • eISSN 2982-6799

The effect of *Legionella pneumophila* infection on the encystation of *Acanthamoeba castellanii*

Hye-Jeong Jo[1], Hae-Ahm Lee[2], Fu-Shi Quan[2,3], Hyun-Hee Kong[4,*], Eun-Kyung Moon[2,*]

[1]Department of Biomedical Science, Graduate School, Kyung Hee University, Seoul, Korea; [2]Department of Medical Zoology, Kyung Hee University, School of Medicine, Seoul, Korea; [3]Medical Research Center for Bioreaction to Reactive Oxygen Species and Biomedical Science Institute School of Medicine, Graduate School, Kyung Hee University, Seoul, Korea; [4]Department of Parasitology, Dong-A University College of Medicine, Busan, Korea

Acanthamoeba is a genus of free-living amoebae commonly found in soil, water, and other habitats. This organism undergoes 2 distinct stages in its life cycle, the trophozoite and the cyst. Under adverse conditions, trophozoites transform into cysts, which are notably resistant to harsh physical and chemical conditions. Infection by *Legionella pneumophila* has been shown to decrease the number of cysts in its host *Acanthamoeba* species, although the mechanisms responsible for this effect remain poorly understood. In this study, *A. castellanii* was co-cultured with either *L. pneumophila* or *Escherichia coli* to assess the impact on encystation and to explore the genes involved in this process. Following a 72-h encystation induction period, it was observed that *Acanthamoeba* infected with *Legionella* exhibited a 45.8% reduction in cyst formation compared to the control group. In contrast, *Acanthamoeba* that phagocytosed *E. coli* showed a 21.7% decrease. To identify the genes involved in this phenomenon, real-time PCR analysis was conducted on 20 genes known to be upregulated during encystation. This analysis was performed to verify their expression patterns at 24, 48, and 72 h. Notably, ten genes, including cyst-specific protein 21, glycosyltransferase, RSNARE, and cellulose synthase, did not exhibit increased expression in *Legionella*-infected *Acanthamoeba*. However, these genes showed elevated expression levels in both the control group and the bacteria-phagocytosed *Acanthamoeba*. This suggests that several cellular processes, including cell wall formation, are inhibited in *Acanthamoeba* infected with *Legionella*, resulting in reduced encystation.

Keywords: *Acanthamoeba castellanii*, *Legionella pneumophila*, encystation

Introduction

Acanthamoeba spp. are ubiquitous free-living amoebae prevalent in diverse aquatic environments, capable of causing significant human diseases such as amoebic keratitis and granulomatous amoebic encephalitis [1]. These amoebae exist in 2 distinct forms: the motile, feeding trophozoite stage and the dormant, resistant cyst stage [2]. While the trophozoite represents the active form, the cyst serves as a vital survival mechanism, especially under harsh environmental conditions. This encystation process is crucial for their persistence in extreme habitats. Beyond their role as passive environmental inhabitants, *Acanthamoeba* spp. serve as hosts for various pathogenic bacteria. *Acanthamoeba* are often referred to as the 'Trojan horse' of microorganisms including *Escherichia coli* O157, *Legionella pneumophila*, *Coxiella burnetii*, *Helicobacter pylori*, *Chlamydophila pneumoniae*, *Vibrio cholerae*, *Listeria monocytogenes*, *Campylobacter jejuni*, *Mycobacterium leprae* and *Pseudomonas*

Received: September 5, 2025 Accepted: December 11, 2025
*Correspondence: hhk, hhkong@dau.ac.kr; ekm, ekmoon@khu.ac.kr

Citation
Jo HJ, Lee HA, Quan FS, Kong HH, Moon EK. The effect of *Legionella pneumophila* infection on the encystation of *Acanthamoeba castellanii*. Parasites Hosts Dis 2026;64(1):37-44.

aeruginosa [3-5].

Among these, *L. pneumophila*, the causative agent of Legionnaires' disease, is an intracellular pathogen that exploits protozoa including *Acanthamoeba*, as reservoirs and vectors for transmission to humans [6]. *A. castellanii* can harbor *L. pneumophila* within their cells, provides a protective niche, shielding them from disinfection processes. Despite this symbiotic protection, the presence of *L. pneumophila* exerts a profound impact on the biology of *Acanthamoeba*, notably inhibiting DNA replication and cell division, which ultimately leads to the arrest in the proliferation of the host [7,8]. *Legionella* infection disrupts the normal life cycle of *Acanthamoeba*, particularly affecting the encystation process by altering cellular proliferation, morphology, and gene expression linked to encystment. Notably, *Legionella* amylase A (LamA)-mediated glycogenolysis depletes cytosolic glycogen reserves and hinders the synthesis of the cellulose-rich cyst wall, effectively subverting the encystation process [9]. Despite emerging evidence of *Legionella*'s impact on *Acanthamoeba* encystation, the precise molecular mechanisms remain inadequately understood. Specifically, understanding how *L. pneumophila* infection modulates the gene expression associated with encystation could provide valuable insights into the survival strategies of both the *Acanthamoeba* and the *Legionella*.

This study aims to elucidate the effects of *L. pneumophila* infection on the encystation of *A. castellanii*. Previous research has identified essential genes involved in the encystation of *A. castellanii* through mRNA sequencing and real-time PCR analysis [10-15]. Building on this knowledge, we compare the encystation rates and gene expression profiles of *A. castellanii* infected with *L. pneumophila* to those of amoebae that have phagocytosed non-pathogenic *E. coli*. Through this comparison, we seek to unravel the molecular mechanisms underlying these interactions. Our findings will enhance the understanding of amoebal-bacterial interactions and may inform future strategies for controlling *Legionella* outbreaks and *Acanthamoeba* encystation in the environmental contexts.

Methods

Ethics statement

Not applicable.

Cell cultures

A. castellanii (ATCC 30868) was cultured axenically in peptone-yeast-glucose (PYG) media (20 g proteose peptone, 1 g yeast extract, 0.1 M glucose, 4 mM $MgSO_4$, 0.4 mM $CaCl_2$, 3.4 mM sodium citrate, 0.05 mM $Fe(NH_4)_2(SO_4)_2$, 2.5 mM Na_2HPO_4, and 2.5 mM K_2HPO_4 in 1 L distilled water with the final pH adjusted to 6.5) at 25°C, and *L. pneumophila* (ATCC 33152) was cultured on a buffered charcoal yeast extract agar plate (Thermo Fisher Scientific) at 37°C with 5% CO_2. *E. coli* (Enzynomics) was cultured in tryptone-yeast-NaCl (Luria–Bertani) media at 37°C using a shaking incubator.

Infection of bacteria

L. pneumophila was diluted in PBS until the OD_{600} absorbance reading reached 1, which corresponds to 10^9 CFU/ml. A total of 1×10^7 *A. castellanii* trophozoites were incubated with 1 ml of the *Legionella* suspension at 37°C with 5% CO_2 for 1 h in PYG medium. After incubation, *Acanthamoeba* was washed with Page's amoeba saline and then incubated with fresh PYG media containing 100 μg/ml of gentamicin for 2 h to kill any extracellular *Legionella*. The *Acanthamoeba* infected with *Legionella* (A+L) were washed with Page's amoeba saline twice and incubated with fresh PYG media for 12 h in a 25°C incubator. *Acanthamoeba* (control) or those that had phagocytosed *E. coli* (A+E) were treated in the same way [16].

Encystation of *Acanthamoeba*

Encystation of *A. castellanii* (control, A+E, and A+L) was induced using an encystment media composed of 95 mM NaCl, 5 mM KCl, 8 mM $MgSO_4$, 0.4 mM $CaCl_2$, 1 mM $NaHCO_3$, 20 mM Tris-HCl at pH 9.0. The encystation process for each group was monitored at 24, 48, and 72 h, with morphological changes observed using light microscopy. Mature cysts were counted under a microscope after treatment with 0.5% SDS to calculate encystation ratios [10,17].

Gene expression analysis by real-time PCR

The expression of target genes was determined by real-time PCR analysis. The total RNA was purified using an RNeasy Mini kit (Qiagen), and the cDNA was synthesized using a RevertAid first-strand cDNA synthesis kit (Thermo Fisher Scientific) following the manufacturer's instructions. Real-time PCR was conducted using a Magnetic Induction Cycler PCR machine (PhileKorea) as manufacturer's instructions: preincubation at 95°C for 1 min, followed by 40 cycles of 95°C for 15 sec and 60°C for 30 sec. All reaction mixtures were made using a Luna Universal qPCR Master Mix (New England Biolabs) with different sense and antisense primers (Table 1). The relative expression levels were calculated by normalizing the critical threshold (Ct) values to that of the internal control (18S rDNA), and graphs were presented using the 2^-ΔΔCt method [18].

https://doi.org/10.3347/PHD.25080

Table 1. Primer sequences for real-time PCR

Product	Primer sequences (5'→3')
Cyst specific protein 21	F: gcttcctgcgcatgtgtaag
	R: cctccctcttgccgatgatc
WH2 motif domain containing protein	F: gaagaagagggcgagctcag
	R: ttgaggttgaactgctgcca
Twin arginine translocation pathway protein	F: gagaccatcacccttcgcaa
	R: ggatgcagtagggcctcttc
Aminotransferase, class III superfamily protein	F: ttcatgaagggtgttcgcga
	R: ggatgtcgggcttgatgtca
Glycosyltransferase, group 2 domain containing protein	F: acctcgagttcaagtggagc
	R: ttttccacgccccagatctc
Betaine homocysteine methyltransferase	F: aatctgtgggaggggaagga
	R: ttcggcgatgacaaagtcca
Kazal type serine protease inhibitor domain containing protein	F: cttctccgagcagctctacg
	R: gacgagaaggggctgtagtc
Golgi family protein, putative	F: agtcgatcgtgaagctccac
	R: ggcgagtcggtgaagaagaa
Cysteine proteinase	F: caccaccatcaccaccatca
	R: gcgtgcttcttgttccagtg
von Willebrand factor type A domain containing protein	F: caccaaccgcatcttcctct
	R: tgaagaagtaggcaccgctg
Multicopper oxidase, type 2	F: tccagttcagagtgtcacgc
	R: gttgatctccaccagcgtca
RSNARE, VAMP72-family	F: agtggcctttgacttcctcg
	R: ccttcttcacgtcctccacc
Armadillo/beta catenin-like repeat domain containing protein	F: cgtccaccaccagaagaaca
	R: tgcaaggccaggttccatag
Autophagy protein 8	F: aagaagttcctggtgcctgc
	R: ctcgtccttgtacttggcgt
Autophagy protein 16	F: tctatgtgctgagctacgcg
	R: cttggaggcgcacatgattg
Encystation-mediating cysteine proteinase	F: ttcgtggaggagttcaaccg
	R: atctgctcctcctcgtcctt
Encystation-mediating serine proteinase	F: caactacacccaggacaccc
	R: gtgccggagatggtgttgta
Glycogen phosphorylase	F: gtccttctcgacgagcagaa
	R: cagaagctcctcctgttggg
UDP-glucose pyrophosphorylase	F: ccccgactctgtcttttccc
	R: tcttgtgagccgctaactgg
Cellulose synthase	F: tctacatgttctgcgccctg
	R: cagttgttgagcatgcggag
18S rDNA	F: cgtgctggggatagatcatt
	R: aaaggggagacctcacaacc

Statistical analysis

All statistical analyses were conducted using GraphPad Prism version 8.0. Data are presented as the mean ± SD. Statistical significance between groups is denoted by asterisks, with *P*-values less than 0.05 considered statistically significant ($^{*}P<0.05$, $^{**}P<0.01$).

Results

Inhibition of encystation of *A. castellanii* by *L. pneumophila* infection

To investigate the effect of *Legionella* infection on the encystation of *Acanthamoeba*, cyst formation experiments were conducted using several groups: control, A+E, and A+L. Encystation was induced over a period of 72 h. Encystation of each group was monitored at 24, 48, and 72 h using microscopy (Fig. 1A), and the number of mature cysts (%) was graphically represented in Fig. 1B.

During the encystation induction periods of 24, 48, and 72 h, the control group showed encystment rates of 12.2%, 25.1%, and 51.9%, respectively. In contrast, the A+L group demonstrated encystation rates of 8.2%, 8.9%, and 6.1% over the same time intervals, and the A+E group showed rates of 13.0%, 16.9%, and 30.2%. The A+L group exhibited a significant reduction in encystment, with a 45.8% decrease compared to the control group (from 51.9% to 6.1%, corresponding to an 88% relative decrease), and the A+E group showed a 21.7% reduction in encystment relative to the control (from 51.9% to 30.2%, corresponding to a 42% relative decreases). These findings suggest that the presence of *L. pneumophila* or *E. coli* negatively impacts the encystation process of *A. castellanii*, with *L. pneumophila* infection significantly reducing encystment more than *E. coli*.

Gene expression analysis during encystation

To further investigate the molecular mechanisms underlying the encystation of *Acanthamoeba* infected by *Legionella*, real-time PCR analysis was conducted on 20 genes previously identified as upregulated during *Acanthamoeba* encystation [10-15]. In previous mRNA sequencing analysis of *A. castellanii* results, 13 genes that showed a significant increase in expression 24 h after encystation induction are summarized in Table 2 [10]. Additionally, 7 genes that showed increased expression related to autophagy or cyst wall formation during the encystation process of *A. castellanii* are also summarized in Table 2 [11-15]. This study observed changes in the expression of these 20 genes when *A. castellanii* formed cysts after being infected with *L. pneumophila* or after phagocytosing *E. coli* (Supplementary Fig. S1).

In *A. castellanii* infected with *L. pneumophila*, 10 out of the 20 genes were downregulated in 24 h encysting cells compared

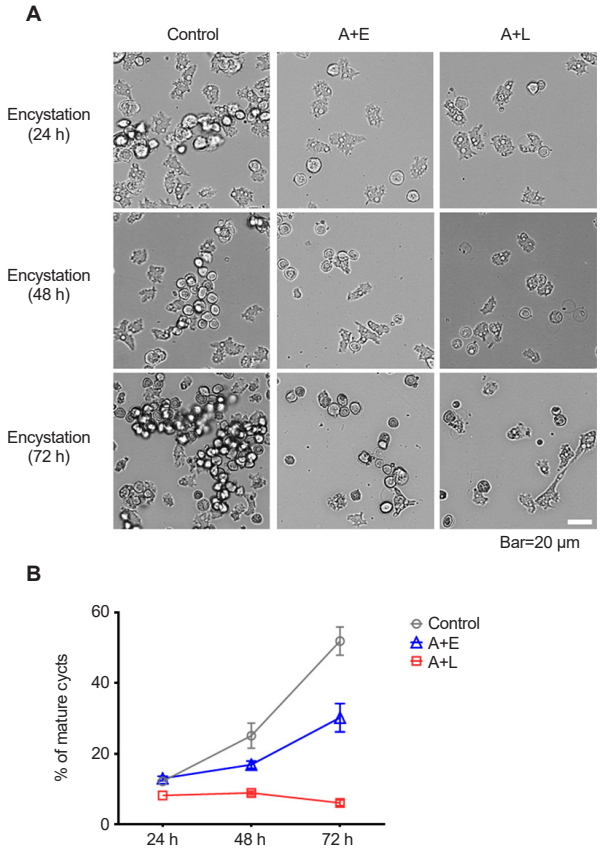

Fig. 1. Encystation rate of *Acanthamoeba castellanii* over 72 h. The encystation rates of *A. castellanii* (control) and those co-cultured with either *Legionella pneumophila* or *Escherichia coli* (A+L or A+E) were assessed by inducing encystation in encystation media over a period of 72 h. The extent of encystation was observed under a microscope at intervals of 24, 48, and 72 h (A), and the data were represented in a graph (B). The A+L group exhibited a 45.8% reduction in encystment, while the A+E group showed a 21.7% decrease compared to the control group.

Table 2. Genes upregulated in *Acanthamoeba castellanii* during encystation

Product	GeneBank No.	Reference
Cyst specific protein 21	XM_004353421.1	[10]
WH2 motif domain containing protein	XM_004333237.1	[10]
Twin arginine translocation pathway protein	XM_004352737.1	[10]
Aminotransferase, class III superfamily protein	XM_004336305.1	[10]
Glycosyltransferase, group 2 domain containing protein	XM_004368209.1	[10]
Betaine homocysteine methyltransferase	XM_004340572.1	[10]
Kazal type serine protease inhibitor domain containing protein	XM_004368049.1	[10]
Golgi family protein, putative	XM_004341407.1	[10]
Cysteine proteinase	XM_004342180.1	[10]
von Willebrand factor type A domain containing protein	XM_004338072.1	[10]
Multicopper oxidase, type 2	XM_004335693.1	[10]
RSNARE, VAMP72-family	XM_004334605.1	[10]
Armadillo/beta catenin-like repeat domain containing protein	XM_004346431.1	[10]
Autophagy protein 8	EU935007.1	[11]
Autophagy protein 16	FJ906697.1	[12]
Encystation-mediating cysteine proteinase	JQ253375.1	[13]
Encystation-mediating serine proteinase	EU365402.1	[14]
Glycogen phosphorylase	JX312797.1	[15]
UDP-glucose pyrophosphorylase	JX312798.1	[15]
Cellulose synthase	JX312799.1	[15]

to the control group, and remained decreased until 72 h (Fig. 2). These genes include key proteins such as the cyst-specific protein 21 (Fig. 2A), WH2 motif domain-containing protein (Fig. 2B), glycosyltransferase (Fig. 2C), betaine homocysteine methyltransferase (Fig. 2D), kazal type serine protease inhibitor domain containing protein (Fig. 2E), golgi family protein (Fig. 2F), multicopper oxidase (Fig. 2G), RSNARE (Fig. 2H), UDP-glucose pyrophosphorylase (Fig. 2I), and cellulose synthase (Fig. 2J) involved in cellular and metabolic processes. The functions of these ten genes seem to be primarily involved in cyst wall formation (Table 3). The lack of upregulation of these genes suggests that *L. pneumophila* may inhibit or alter the normal encystation-related structure components, potentially contributing to the observed reduction in encystment.

Whereas cysteine proteinases and encystation-mediating serine proteinase were increased at 48 and 72 h, and other encystation-related genes (such as twin arginine translocation pathway protein, aminotransferase, von Willebrand factor type A domain containing protein, armadillo/beta catenin-like repeat domain containing protein, autophagy proteins, encystation-mediating cysteine proteinase, and glycogen phosphorylase) were upregulated in *Legionella*-infected *Acanthamoeba* compared to the control group (Supplementary Fig. S1).

Discussion

This study provides significant insights into the interaction between *A. castellanii* and *L. pneumophila*, specifically focusing on how *Legionella* infection affects the encystation pro-

https://doi.org/10.3347/PHD.25080

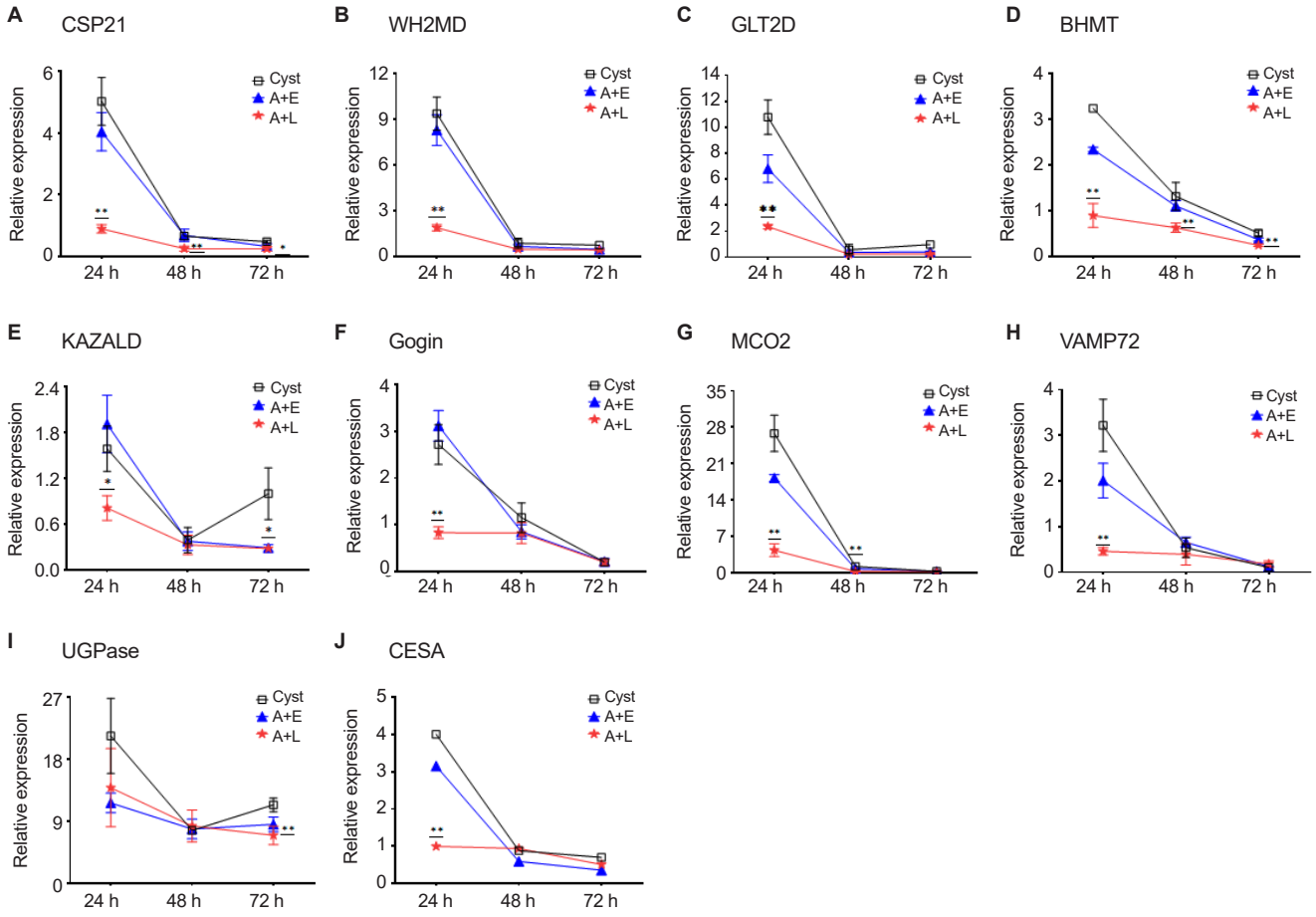

Fig. 2. Real-time PCR analysis of genes related to encystation. The expression changes of 10 out of 20 genes, previously identified to be upregulated during encystation of *Acanthamoeba*, were observed to be downregulated when *A. castellanii* formed cysts after being infected with *Legionella pneumophila* or after phagocytosing *Escherichia coli*. (A) Cyst specific protein 21 (CSP21), (B) WH2 motif domain containing protein (WH2MD), (C) glycosyltransferase, group 2 domain containing protein (GLT2D), (D) betaine homocysteine methyltransferase (BHMT), (E) Kazal type serine protease inhibitor domain containing protein (KAZALD), (F) Golgi family protein, putative (Golgin), (G) multicopper oxidase, type 2 (MCO2), (H) RSNARE, VAMP72-family (VAMP72), (I) UDP-glucose pyrophosphorylase (UGPase), and (J) cellulose synthase (CESA). A+E, *A. castellanii* that phagocytosed *E. coli*; A+L, *A. castellanii* infected with *L. pneumophila*.

cess of *Acanthamoeba*. Our findings reveal that *L. pneumophila* not only significantly reduces encystation rates of *Acanthamoeba* but also disrupts the gene expression program necessary for encystation.

The encystation process is a critical adaptive mechanism for *Acanthamoeba*, allowing it to persist in harsh environmental conditions. Our results showed a marked reduction in encystation rates in *A. castellanii* infected with *L. pneumophila* compared to the control group (Fig. 1). This suggests that *L. pneumophila* infection compromises the ability of *Acanthamoeba* to form protective cysts, potentially increasing the amoeba's susceptibility to environmental stressors. If the encystment of *Acanthamoeba* is inhibited, it also means that its ability to protect the internal *Legionella* from environmental threats is reduced. It is worth considering why *Legionella* would inhibit the encystment of its protective host, *Acanthamoeba*. The reduction in encystation was more pronounced with *L. pneumophila* (A+L) than with non-pathogenic *E. coli* (A+E), indicating a pathogen-specific interaction. The encystation media induce cyst formation in *Acanthamoeba* due to nutrient deprivation. In the A+E group, however, the phagocytosis and digestion of *E. coli* provide nutrients, which is believed to result in a reduced encystation rate.

Gene expression analysis further supported these findings, demonstrating that *L. pneumophila* alters the expression of key genes involved in the encystation pathway. Notably, 10 out of 20 genes typically upregulated during encystation did not show increased expression in the presence of *L. pneumophila* (Fig. 2). This includes genes encoding cyst-specific proteins (Fig. 2A) and enzymes essential for cyst wall biosyn-

Table 3. Functions of encystation-related genes suppressed by *Legionella pneumophila* in *Acanthamoeba castellanii* during encystation

Product	Function
Cyst specific protein 21	Involved in the form of the cyst wall
WH2 motif domain containing protein	A group of proteins that bind to actin monomers, playing a crucial role in regulating the dynamic assembly and disassembly of actin filaments
Glycosyltransferase	Synthesize the glycoproteins and glycolipids required for the cyst wall
Betaine homocysteine methyltransferase	A zinc-dependent enzyme that converts betaine and homocysteine into dimethylglycine and methionine, regulating homocysteine levels
Kazal type serine protease inhibitor domain containing protein	A protein with a specific functional domain that inhibits serine proteases, wide range of biological processes
Golgi family protein	Essential for the transport and processing of cyst wall proteins
Multicopper oxidase	A specific copper-binding site within a class of enzymes that oxidize substrates using oxygen as the final electron acceptor
RSNARE, VAMP72-family	Involved in vesicle trafficking necessary for autophagy and encystation
UDP-glucose pyrophosphorylase	Produce UDP-glucose, a precursor for synthesizing cyst wall components such as cellulose or chitin
Cellulose synthase	Build the cyst wall by catalyzing the formation of cellulose microfibrils from glucose precursors

thesis, such as UDP-glucose pyrophosphorylase and cellulose synthase (Fig. 2I, J). Previous studies have shown that *L. pneumophila* can manipulate host cells by degrading cellular glycogen reserves [9]. This process involves *Legionella* amylase A in glycogenolysis, thereby hindering cyst wall formation. In *Giardia lamblia*, RSNAREs are involved in the encystation pathway, where they contribute to the formation of the cyst wall, a protective structure composed of cyst wall material [19]. Similarly, in *Entamoeba*, RSNAREs play a role in the trafficking of cyst wall components [20]. However, in *L. pneumophila*-infected *A. castellanii*, the expression of Golgi family proteins and RSNARE is notably diminished (Fig. 2F, H). The absence of upregulation in these genes suggests that *L. pneumophila* may interfere with the regulatory pathways that initiate and sustain the cyst wall formation during the encystation process. The mechanism by which *L. pneumophila* exerts these effects may involve the depletion of resources or direct modulation of host cellular pathways.

The transition of *Acanthamoeba* into the cyst form typically involves the upregulation of cysteine and serine proteinase for autophagy and internal digestion [13,14]. These processes were found to be suppressed at 24 h by *L. pneumophila* infection (Supplementary Fig. S1P, Q). However, these 2 genes were observed to increase again at 48 or 72 h. This is presumed to be because *Legionella* delays the delivery to lysosomes in host cells, thereby inhibiting autophagy formation for its survival [21]. Meanwhile, other encystation-related genes (such as twin arginine translocation pathway protein, aminotransferase, von Willebrand factor type A domain containing protein, armadillo/beta catenin-like repeat domain containing protein, autophagy proteins, encystation-mediating cysteine proteinase, and glycogen phosphorylase) were found to increase in *Acanthamoeba* infected with *Legionella* compared to the control group (Supplementary Fig. S1). Further research is needed to understand the reasons and mechanisms behind this.

These findings have broader implications for understanding amoebal-bacterial interactions and the survival strategies employed by intracellular pathogens. The ability of *L. pneumophila* to inhibit encystation could facilitate its persistence and transmission in the environment, as *Acanthamoeba* serves as a reservoir and vector for the bacteria. This interaction highlights the complex ecological relationships between free-living amoebae and pathogenic bacteria, emphasizing the need for further research to uncover the precise molecular mechanisms involved. Future studies should focus on elucidating the signaling pathways disrupted by *L. pneumophila* and identifying potential targets for intervention. Understanding these interactions at a molecular level could inform strategies to prevent *Legionella* outbreaks by targeting its amoebal hosts and disrupting its life cycle within these protozoa. Additionally, since these findings are based on a single amoeba strain (*A. castellanii*) and bacterial isolate (*L. pneumophila*), they cannot be generalized. Therefore, further research involving various amoeba strains and bacterial isolates is considered necessary.

In conclusion, *L. pneumophila* appears to significantly inhibit the cyst formation of *A. castellanii* by suppressing the expression of genes involved in cyst formation, particularly those related to cyst wall formation. This study advances our

https://doi.org/10.3347/PHD.25080

understanding of how *Legionella* influences the encystation of *Acanthamoeba*.

Author contributions

Conceptualization: Moon EK. Data curation: Lee HA, Quan FS, Kong HH, Moon EK. Funding acquisition: Moon EK. Investigation: Jo HJ, Lee HA, Moon EK. Methodology: Jo HJ, Lee HA, Quan FS, Kong HH, Moon EK. Validation: Moon EK. Writing – original draft: Jo HJ. Writing – review & editing: Lee HA, Quan FS, Kong HH, Moon EK.

Conflict of interest

Fu-Shi Quan serves as an editor of Parasites, Hosts and Diseases but had no involvement in the decision to publish this article. No other potential conflicts of interest relevant to this study were reported.

Funding

This work was supported by the National Research Foundation of Korea (NRF) grant funded by the Korea government (MSIT) (RS-2024-00346635).

Supplementary information

Supplementary material is available with this article at https://doi.org/10.3347/PHD.25080.

ORCID

Hye-Jeong Jo, https://orcid.org/0009-0003-7079-087X
Hae-Ahm Lee, https://orcid.org/0000-0002-4279-4705
Fu-Shi Quan, https://orcid.org/0000-0003-0419-9339
Hyun-Hee Kong, https://orcid.org/0000-0003-1075-0051
Eun-Kyung Moon, https://orcid.org/0000-0003-1121-2052

References

1. Siddiqui R, Khan NA. Biology and pathogenesis of *Acanthamoeba*. Parasit Vectors 2012;5:6. https://doi.org/10.1186/1756-3305-5-6
2. Wang Y, Jiang L, Zhao Y, et al. Biological characteristics and pathogenicity of *Acanthamoeba*. Front Microbiol 2023;14:1147077. https://doi.org/10.3389/fmicb.2023.1147077
3. Winiecka-Krusnell J, Linder E. Bacterial infections of free-living amoebae. Res Microbiol 2001;152:613-9. https://doi.org/10.1016/S0923-2508(01)01240-2
4. Greub G, Raoult D. Microorganisms resistant to free-living amoebae. Clin Microbiol Rev 2004;17:413-33. https://doi.org/10.1128/CMR.17.2.413-433.2004
5. Axelsson-Olsson D, Waldenström J, Broman T, Olsen B, Holmberg M. Protozoan *Acanthamoeba polyphaga* as a potential reservoir for *Campylobacter jejuni*. Appl Environ Microbiol 2005;71:987-92. https://doi.org/10.1128/AEM.71.2.987-992.2005
6. Lopez AE, Grigoryeva LS, Barajas A, Cianciotto NP. *Legionella pneumophila* rhizoferrin promotes bacterial biofilm formation and growth within amoebae and macrophages. Infect Immun 2023;91:e0007223. https://doi.org/10.1128/iai.00072-23
7. Mengue L, Régnacq M, Aucher W, et al. *Legionella pneumophila* prevents proliferation of its natural host *Acanthamoeba castellanii*. Sci Rep 2016;6:36448. https://doi.org/10.1038/srep36448
8. Li P, Vassiliadis D, Ong SY, et al. *Legionella pneumophila* infection rewires the *Acanthamoeba castellanii* transcriptome, highlighting a class of sirtuin genes. Front Cell Infect Microbiol 2020;10:428. https://doi.org/10.3389/fcimb.2020.00428
9. Price C, Jones S, Mihelcic M, Santic M, Abu Kwaik Y. Paradoxical pro-inflammatory responses by human macrophages to an amoebae host-adapted *Legionella* effector. Cell Host Microbe 2020;27:571-84.e7. https://doi.org/10.1016/j.chom.2020.03.003
10. Kim MJ, Jo HJ, Quan FS, et al. Identification of essential genes for *Acanthamoeba castellanii* excystation during encystation and excystation. Parasites Hosts Dis 2024;62:399-407. https://doi.org/10.3347/PHD.24062
11. Moon EK, Chung DI, Hong YC, Kong HH. Autophagy protein 8 mediating autophagosome in encysting *Acanthamoeba*. Mol Biochem Parasitol 2009;168:43-8. https://doi.org/10.1016/j.molbiopara.2009.06.005
12. Song SM, Han BI, Moon EK, et al. Autophagy protein 16-mediated autophagy is required for the encystation of *Acanthamoeba castellanii*. Mol Biochem Parasitol 2012;183:158-65. https://doi.org/10.1016/j.molbiopara.2012.02.013
13. Moon EK, Hong Y, Chung DI, Kong HH. Cysteine protease involving in autophagosomal degradation of mitochondria during encystation of *Acanthamoeba*. Mol Biochem Parasitol 2012;185:121-6. https://doi.org/10.1016/j.molbiopara.2012.07.008
14. Moon EK, Chung DI, Hong YC, Kong HH. Characterization of a serine proteinase mediating encystation of *Acanthamoeba*. Eukaryot Cell 2008;7:1513-7. https://doi.org/10.1128/EC.00068-08
15. Moon EK, Kong HH. Short-cut pathway to synthesize cellulose of encysting *Acanthamoeba*. Korean J Parasitol 2012;50:361-4. https://doi.org/10.3347/kjp.2012.50.4.361
16. Moon EK, Kim MJ, Lee HA, Quan FS, Kong HH. Comparative analysis of differentially expressed genes in *Acanthamoeba* after ingestion of *Legionella pneumophila* and *Escherichia coli*. Exp Parasitol 2022;232:108188. https://doi.org/10.1016/j.exppara.2021.108188
17. Aung JM, Joo SY, Na BK, et al. Establishing a Cre/loxP-based genetic manipulation system for *Acanthamoeba*: targeted genome editing and stable reporter expression. Parasites Hosts Dis 2025;63:25-36.

https://doi.org/10.3347/PHD.24078

18. Livak KJ, Schmittgen TD. Analysis of relative gene expression data using real-time quantitative PCR and the 2(-Delta Delta C(T)) method. Methods 2001;25:402-8. https://doi.org/10.1006/meth.2001.1262
19. Marti M, Hehl AB. Encystation-specific vesicles in *Giardia*: a primordial Golgi or just another secretory compartment? Trends Parasitol 2003;19:440-6. https://doi.org/10.1016/s1471-4922(03)00201-0
20. Herman E, Siegesmund MA, Bottery MJ, et al. Membrane trafficking modulation during *Entamoeba* encystation. Sci Rep 2017;7:12854. https://doi.org/10.1038/s41598-017-12875-6
21. Rolando M, Escoll P, Buchrieser C. *Legionella pneumophila* restrains autophagy by modulating the host's sphingolipid metabolism. Autophagy 2016;12:1053-4. https://doi.org/10.1080/15548627.2016.1166325

Original Article

Parasites Hosts Dis 2026;64(1):45-51
https://doi.org/10.3347/PHD.25079

Parasites, Hosts and Diseases

pISSN 2982-5164 • eISSN 2982-6799

IKK2, calcium, MAP kinase, and PI3 kinase are required for exocytosis and interleukin-8 production in human mast cells stimulated by *Trichomonas vaginalis*-derived secretory products

Shin Hye Park[1], Young Ah Lee[2,*], Myeong Heon Shin[1,*]

[1]Department of Tropical Medicine and Institute of Tropical Medicine, Yonsei University College of Medicine, Seoul, Korea; [2]Department of Environmental Medical Biology, Jeju National University College of Medicine, Jeju, Korea

Trichomonas vaginalis infection causes vaginitis and cervicitis in women, and asymptomatic urethritis and prostatitis in men. Mast cells play a key role in the inflammatory response against *T. vaginalis* infection. In this study, we examined the signaling pathways involved in mast cell activation induced by *T. vaginalis*-derived secretory products (TvSP), focusing on IKK2, calcium, MAP kinase (MAPK), and PI3 kinase (PI3K). TvSP stimulation induced phosphorylation and degradation of IκB, indicating NF-κB activation, and triggered phosphorylation of ERK1/2, p38 MAPK, and AKT. TvSP also increased the surface expression of CD63, a marker of exocytosis, which was reduced by IKK inhibition, calcium chelation, or blockade of PI3K and PKC. Furthermore, inhibition of PI3K or MAPKs decreased TvSP-induced interleukin-8 production. These results suggest that IKK2 and calcium are critical for TvSP-induced degranulation, while PI3K and MAPK pathways contribute to interleukin-8 production in mast cells.

Keywords: *Trichomonas vaginalis*, mast cells, CD63, IKK2, exocytosis, interleukin-8

Introduction

Trichomonas vaginalis is a flagellated protozoan parasite and the causative agent of trichomoniasis, one of the most common non-viral sexually transmitted infections worldwide [1-3]. The World Health Organization estimates 156 million new cases annually, highlighting its public health importance [4]. Infections are often asymptomatic in men but cause vaginitis, cervicitis, and urethritis in women, increasing the risk of preterm birth, pelvic inflammatory disease, and HIV acquisition [5]. *T. vaginalis* secretes virulence factors such as cysteine proteases, lipophosphoglycan, and leukotriene B_4 (LTB_4) [6-8], which modulate host innate immunity by promoting local inflammation and inflammatory cell recruitment [9]. *T. vaginalis*-derived secretory products (TvSP) activate neutrophils, macrophages, and mast cells [8-11], inducing pro-inflammatory cytokines including interleukin-8 (IL-8), a major mediator of neutrophil recruitment and mucosal inflammation [9]. However, the upstream signaling pathways controlling TvSP-induced IL-8 production remain unclear, particularly the roles of MAP kinase (MAPK) and PI3 kinase (PI3K).

Mast cells are long-lived immune cells abundant in mucosal tissues, where they mediate allergic and antimicrobial responses [12-15]. Upon activation, they undergo exocytotic degranulation, releasing histamine, tryptase, and TNF-α, followed by cytokine and chemokine synthesis. *T. vaginalis* induces mast-

Received: September 5, 2025 Accepted: November 5, 2025
*Correspondence: yal, afri00@jejunu.ac.kr; mhs, myeong@yuhs.ac

Citation
Park SH, Lee YA, Shin MH. IKK2, calcium, MAP kinase, and PI3 kinase are required for exocytosis and interleukin-8 production in human mast cells stimulated by *Trichomonas vaginalis*-derived secretory products. Parasites Hosts Dis 2026;64(1):45-51.

cell activation, promoting β-hexosaminidase release and IL-8, TNF-α, and histamine secretion [16-18]. TvSP components such as LTB_4 also enhance NF-κB activation and IL-8 secretion via BLT1 signaling [19], yet the intracellular mechanisms regulating this response remain largely unknown.

IKK2 (IKKβ) is a central regulator of the canonical NF-κB pathway, phosphorylating IκBα and leading to NF-κB–dependent transcription of pro-inflammatory genes [20,21]. While this pathway contributes to mast-cell degranulation and cytokine production, its role in TvSP-induced exocytosis has not been defined. In addition, calcium (Ca^{2+}) signaling is crucial for mast-cell activation and function [13,22,23] and interacts with MAPK and PI3K cascades that regulate vesicle fusion, degranulation, and cytokine production [21,24].

Therefore, this study aimed to elucidate the intracellular signaling mechanisms underlying mast-cell activation by TvSP, focusing on the roles of IKK2/NF-κB and Ca^{2+} signaling in exocytosis, and MAPK and PI3K pathways in IL-8 production.

Methods

Ethics statement

Not applicable.

Reagents

IMD-0354 (MedChemExpress), LTB_4 (Enzo Life Sciences), and platelet-activating factor (PAF, Cayman) were used as stimulants or inhibitors. EDTA, EGTA, wortmannin, LY294002, Ro-31-8220, PD98059, SB203580, and SP600125 were obtained from Sigma-Aldrich. Antibodies against NF-κB (p65), phospho-ERK1/2 (p-p44/42 MAPK), ERK1/2, phospho-p38 (Thr180/Tyr182), p38, phospho-AKT (Ser473), AKT, and β-actin were from Cell Signaling Technology. Anti-phospho-IκBα (S32) antibody was from ABclonal Technology, and anti-IκBα from Santa Cruz Biotechnology. PE-conjugated anti-human CD63 antibody was purchased from BioLegend, and the mouse IgG1 isotype control from Novus Biologicals.

Cultivation of *T. vaginalis* and preparation of TvSP

T. vaginalis strain T016 was axenically cultured at 37°C in TYM medium supplemented with 10% heat-inactivated horse serum (Gibco). For TvSP preparation, trichomonads (1×10^7) were washed twice with Hank's balanced salt solution (Gibco/Invitrogen), resuspended in 1 ml Hank's balanced salt solution, and incubated for 1 h at 37°C. The supernatant was collected by centrifugation (12,000 rpm, 10 min) and filtration through a 0.22 μm filter. TvSP concentration was determined using a BCA protein assay kit (Thermo).

Human mast cell (HMC-1) culture

The human mast cell line HMC-1 was cultured in Iscove's Modified Dulbecco's Medium (Gibco) supplemented with 10% heat-inactivated fetal bovine serum (Corning) and 1% penicillin-streptomycin. Cells were maintained at 37°C in a humidified incubator with 5% CO_2 under sterile conditions.

Stimulation of HMC-1 cells and pretreatment with pharmacological inhibitors

HMC-1 cells (1×10^5 /well) were seeded in 6-well plates and pretreated with inhibitors before stimulation with TvSP, LTB_4, or PAF. Cells were treated with the IKK2 inhibitor IMD-0354 (0.1–10 μM) for 24 h, or with Ca^{2+} chelators EDTA (20 mM) and EGTA (10 mM) for 30 min. PI3K inhibitor (wortmannin, 2 μM; LY294002 10 or 20 μM), PKC inhibitor (Ro-31-8220, 10 μM), and MAPK inhibitors (PD98059 for ERK, SB203580 for p38, SP600125 for JNK; all 10 μM) were applied for 30 min prior to stimulation. Cells were then stimulated for 1 or 16 h, depending on the experimental design.

CD63 measurement in MHC-1 cells

Surface expression of CD63, a marker of exocytotic degranulation, was analyzed by flow cytometry. HMC-1 cells (1×10^5/well) were pretreated with inhibitors and stimulated with TvSP, LTB_4, or PAF for up to 60 min. After stimulation, cells were stained at 4°C for 30 min with PE-conjugated anti-human CD63 or an isotype control antibody, washed twice with PBS containing 1% fetal bovine serum, and analyzed using a BD FACSymphony A5 cytometer. CD63 expression was quantified as mean fluorescence intensity from at least 10,000 events per sample.

Immunoblotting

HMC-1 cells (1×10^6) were stimulated with or without TvSP for the indicated times and lysed on ice for 20 min in buffer containing 50 mM Tris-HCl (pH 8.0), 150 mM NaCl, 1% NP-40, 0.5% sodium deoxycholate, 0.1% SDS, 1 mM EDTA, 1 mM PMSF, 1 mM sodium orthovanadate, and protease inhibitors. Lysates were centrifuged (12,000 rpm, 10 min), and supernatants were mixed with SDS-PAGE buffer and heated at 100°C for 3 min. Proteins were separated by 10% SDS-PAGE and transferred onto PVDF membranes (Millipore). Membranes were blocked with 5% skim milk in Tris-Buffered Saline with Tween-20 for 1 h at room temperature, incubated overnight at 4°C with primary antibodies, washed, and then incubated with horseradish peroxidase-conjugated secondary antibodies for 1

https://doi.org/10.3347/PHD.25079

h. Bands were visualized using ECL select (Cytiva).

IL-8 ELISA

HMC-1 cells (1×10^5/well) were seeded in 6-well plates, pretreated with specific signaling inhibitors for 30 min, and stimulated with TvSP for 16 h at 37°C in a 5% CO_2 incubator. Supernatants were collected, and IL-8 levels were measured using a human IL-8 ELISA kit (Thermo Scientific) following the manufacturer's instructions.

Statistical analysis

Data are presented as mean ± SE from at least 3 independent experiments. Statistical comparisons between experimental and control groups were conducted using Student *t*-test. A *P*-value of < 0.05 was considered statistically significant.

Results

IκB phosphorylation and degradation in HMC-1 cells stimulated with TvSP

To determine whether TvSP activates the NF-κB pathway in HMC-1 cells, phosphorylation and degradation of IκB and cytosolic NF-κB levels were examined. TvSP induced a time-dependent increase in IκB phosphorylation, detectable at 5 min and maximal at 60 min (Fig. 1A). Correspondingly, total IκB levels decreased over time, indicating its degradation (Fig. 1B). Cytosolic NF-κB was strongly detected at 5–15 min but declined at 30–60 min after TvSP stimulation. In contrast, IκB and NF-κB levels remained unchanged in medium-treated control cells (Fig. 1B)

TvSP induces phosphorylation of ERK, p38 MAPK, and AKT in HMC-1 cells

To investigate intracellular signaling activated by TvSP, phosphorylation of key MAPK and AKT pathway proteins was examined. TvSP stimulation rapidly increased ERK1/2 phosphorylation within 5 min, which was sustained up to 15 min, without affecting total ERK1/2 (Fig. 2A). Similarly, p38 phosphorylation increased in a time-dependent manner, while total p38 remained unchanged (Fig. 2B). In addition, AKT phosphorylation was enhanced by TvSP in a dose-dependent manner (10–100 μg/ml), with total AKT levels unaffected (Fig. 2C).

Involvement of IKK2, Ca^{2+}, and PI3K/PKC in TvSP-induced exocytic degranulation in HMC-1 cells

To investigate the signaling mechanisms of TvSP-induced degranulation, HMC-1 cells were pretreated with inhibitors targeting IKK2, Ca^{2+}, and PI3K/PKC pathways before stimulation with TvSP or PAF. Pretreatment with the IKK2 inhibitor IMD-0354 suppressed TvSP-induced degranulation in a dose-dependent manner, and a similar inhibition was observed in LTB_4-stimulated cells (Fig. 3A). Ca^{2+} chelation with EDTA or EGTA markedly reduced CD63 expression in both TvSP- and PAF-stimulated cells compared with control (Fig. 3B). TvSP stimulation increased CD63 surface expression, whereas pretreatment with PI3K inhibitors (wortmannin, LY294002) or the PKC inhibitor Ro-31-8220 significantly attenuated this response (Fig. 3C).

PI3K, ERK, and p38 MAPK signaling pathway mediates IL-8 production in HMC-1 cells induced by TvSP

To examine the role of PI3K signaling in TvSP-induced IL-8

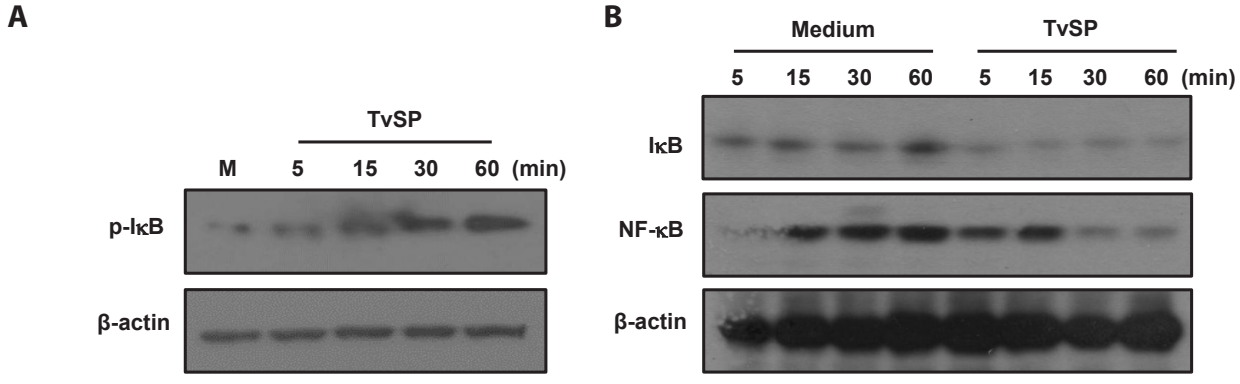

Fig. 1. *Trichomonas vaginalis*-derived secretory products (TvSP) induces IκB phosphorylation (A) and degradation (B) in HMC-1 cells. HMC-1 cells were treated with or without TvSP collected from 1×10^7 trichomonads for the indicated time, respectively. After stimulation, whole cell lysates were subjected to SDS-PAGE and immunoblotted with antibodies specific for phospho-IκB (p-IκB), total IκB, total NF-κB, and β-actin. Representative results from 3 independent experiments are shown. M indicates the medium.

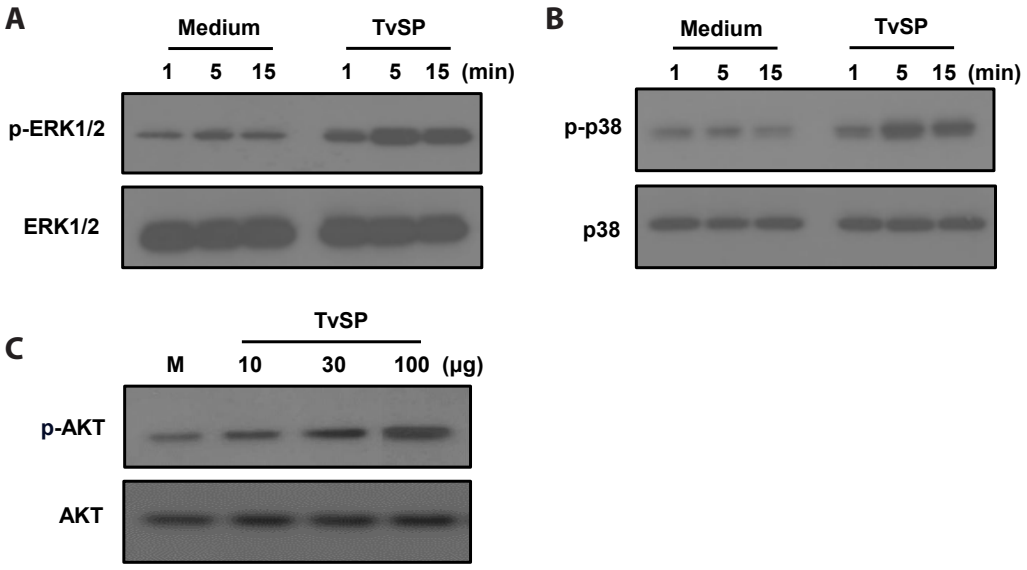

Fig. 2. *Trichomonas vaginalis*-derived secretory products (TvSP) induces phosphorylation of ERK (A), p38 MAPK (B), and AKT (C) in HMC-1 cells. HMC-1 cells were stimulated with or without TvSP for the indicated times. Whole cell lysates were analyzed by SDS-PAGE followed by immunoblotting with antibodies specific for phospho-ERK1/2 (p-ERK1/2), total ERK1/2, phospho-p38 (p-p38), total p38, phospho-AKT (p-AKT), or total AKT. Representative results from 3 independent experiments are shown. M indicates the medium.

production, HMC-1 cells were pretreated with the PI3K inhibitor LY294002. TvSP markedly increased IL-8 secretion compared with the medium control, whereas LY294002 pretreatment significantly reduced IL-8 levels in a dose-dependent manner (Fig. 4A). Inhibition of MAPK pathways with PD98059 (ERK), SB203580 (p38), or SP600125 (JNK) also significantly suppressed TvSP-induced IL-8 secretion, indicating that ERK, p38, and JNK activation contributes to IL-8 production in response to TvSP (Fig. 4B).

Discussion

This study demonstrates that TvSP activate mast cells through multiple intracellular signaling pathways regulating exocytotic degranulation and IL-8 production. TvSP stimulation induced phosphorylation and degradation of IκB, indicating activation of the canonical NF-κB pathway via IKK2. TvSP also triggered phosphorylation of ERK, p38 MAPK, and AKT, which contributed to IL-8 production. Inhibition studies revealed that PI3K and PKC regulate degranulation, whereas IL-8 production is mediated by PI3K and MAPK pathways. In addition, IKK2 and Ca^{2+} are essential for TvSP- and LTB_4-induced exocytosis. Collectively, these results highlight IKK2 and Ca^{2+} as central mediators of mast cell activation, with additional input from PI3K, PKC, and MAPK pathways.

IKK2 functions as a critical regulator of mast cell degranulation by phosphorylating IκBα and promoting NF-κB activation [20]. Loss of IKK2 results in impaired IκBα phosphorylation and defective NF-κB signaling [20,25]. Consistent with this, TvSP-induced degranulation was markedly suppressed by IMD-0354, confirming the essential role of IKK2 in mast cell exocytosis. Beyond transcriptional regulation, IKK2 may also mediate non-transcriptional effects, as previous studies reported IKK2-dependent phosphorylation of SNAP23 facilitating vesicle–plasma membrane fusion [26]. Our earlier work also demonstrated that SNAP23 is crucial for NOX2-mediated degranulation induced by *T. vaginalis*-secreted LTB_4 [26,27]. Although the direct link between IKK2 and SNAP23 was not examined here, it is plausible that IKK2 contributes to TvSP-induced degranulation through both NF-κB–dependent and SNAP23-related mechanisms during *T. vaginalis*–host interactions.

Ca^{2+} plays a pivotal role in mast cell exocytosis. Intracellular Ca^{2+} influx initiates granule–plasma membrane fusion and mediator release [22,23,28,29]. Consistent with this, Ca^{2+} chelation significantly inhibited TvSP-induced degranulation in HMC-1 cells. Our previous study showed that LTB_4 in TvSP binds to BLT1 receptors on HMC-1 cells [27], supporting that Ca^{2+} influx through GPCR-mediated signaling is required for degranulation, as seen with other stimuli such as silver nanoparticles or FcεRI activation [23,30].

Pharmacological inhibition of PI3K and PKC significantly re-

https://doi.org/10.3347/PHD.25079

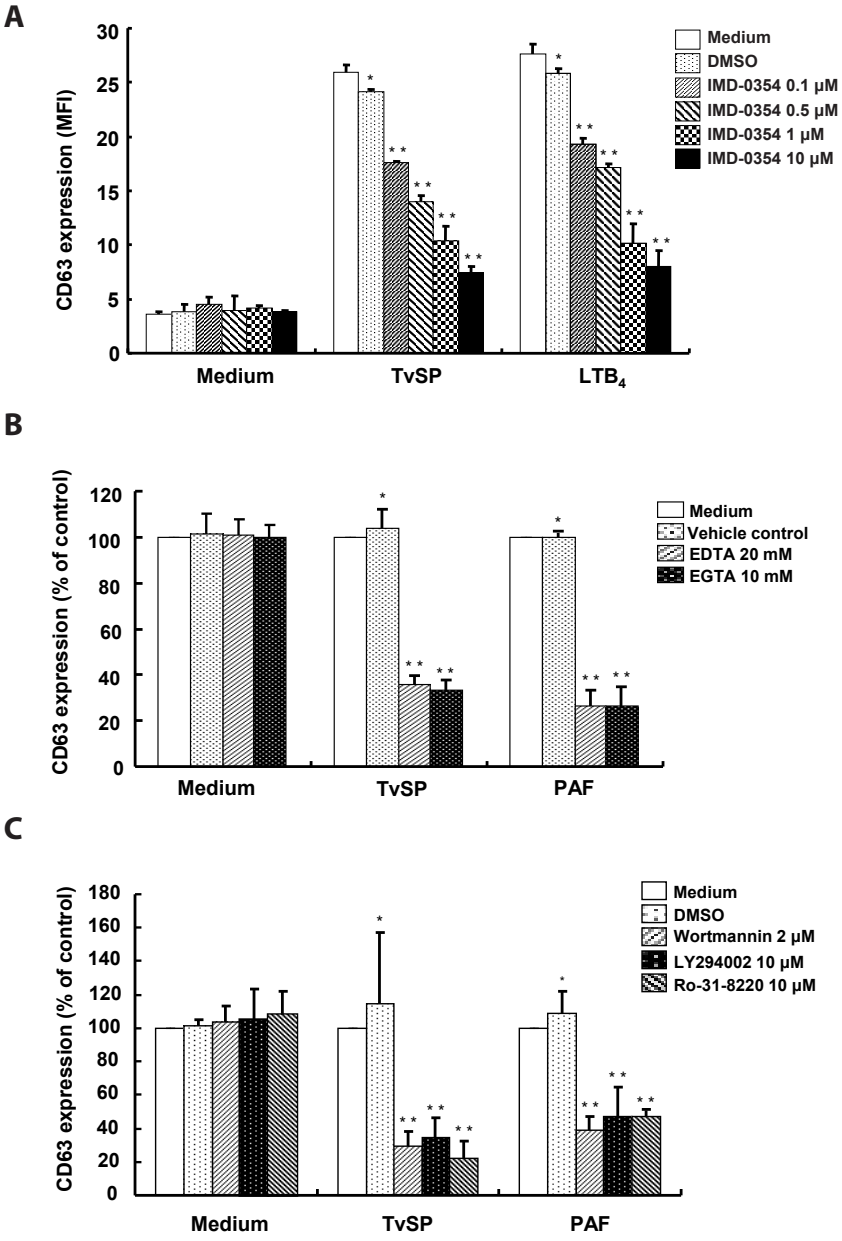

Fig. 3. IKK2, calcium and PI3K/PKC signaling pathway are involved in *Trichomonas vaginalis*-derived secretory products (TvSP)–induced degranulation in HMC-1 cells. (A) HMC-1 cells were pretreated with IMD-0354 for 24 h, then stimulated with TvSP or leukotriene B_4 (LTB_4, 100 nM) for 1 h. (B) Cells were pretreated with calcium chelators EDTA (20 mM) or EGTA (10 mM) for 30 min, followed by TvSP or platelet-activating factor (PAF) stimulation for 1 h. Values are expressed as percentages against HMC-1 (white bar, % of control) of each group. Basal activity (100% values, mean fluorescence intensity [MFI]) of CD63 expression for each group was 2.09 (medium), 21.89 (TvSP), 31.62 (PAF). (C) Cells were pretreated with PI3K inhibitors (wortmannin, 2 μM; LY294002, 10 μM) or the PKC inhibitor Ro-31-8220 (10 μM) for 30 min, then stimulated with TvSP or PAF for 1 h. Surface CD63 expression was analyzed by flow cytometry and presented as MFI. Values are expressed as percentages against HMC-1 (white bar, % of control) of each group. Basal activity (100% values, MFI) of CD63 expression for each group was 3.47 (medium), 31.71 (TvSP), and 47.01 (PAF). Data represent means±SD from 3 independent experiments $^*P<0.05$, $^{**}P<0.01$ (compared with the medium control).

duced TvSP-induced degranulation, indicating their importance in exocytosis. PI3K signaling promotes cytoskeletal rearrangement and granule transport via PIP_3 and downstream effectors such as AKT and Rac [21,30]. AKT regulates mast cell degranulation and cytokine production [21]. In this study, TvSP increased AKT phosphorylation without altering total AKT levels. PKC isoforms (PKCα and PKCβ) facilitate granule priming and fusion through phosphorylation of SNARE and Munc proteins [24,28]. These findings support a model in which TvSP-induced degranulation is mediated by coordinated activation of

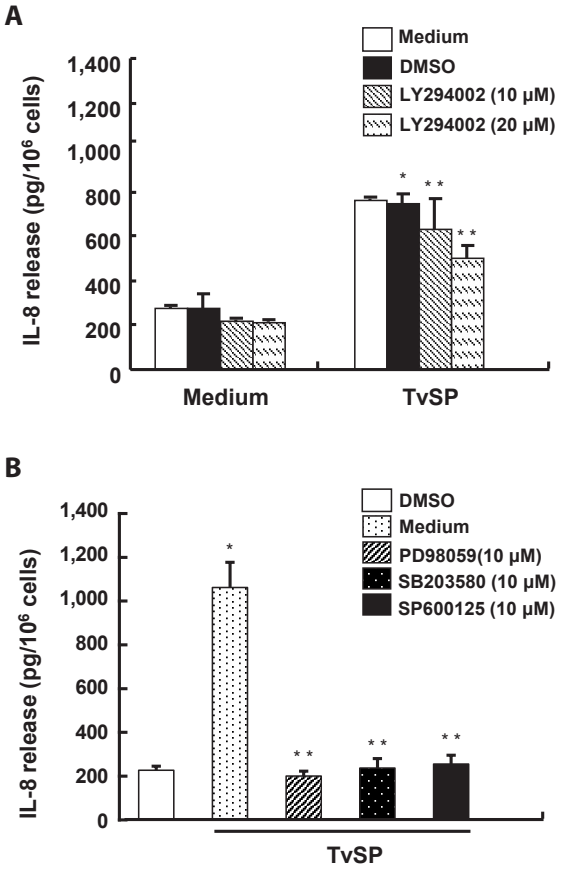

Fig. 4. PI3K, ERK and p38 MAPK contribute to interleukin-8 (IL-8) production in *Trichomonas vaginalis*-derived secretory products (TvSP)–stimulated HMC-1 cells. (A) For PI3K inhibition, cells were pretreated with LY294002 (10, 20 μM) for 30 min and stimulated with TvSP for 16 h; IL-8 levels were measured by ELISA. (B) To assess MAPK involvement, cells were pretreated for 30 min with PD98059 (10 μM), SB203580 (10 μM), or SP600125 (10 μM) and then stimulated with TvSP for 16 h. Data are mean±SD of 3 independent experiments performed in duplicate **P*<0.05, ***P*<0.01 (compared with the medium control).

IKK2, Ca^{2+}, PI3K, and PKC signaling pathways.

IL-8 production in mast cells is regulated by PI3K, PKC, MAPK, and NF-κB pathways [8,21,30]. Activation of PI3K and PKC leads to AKT phosphorylation and NF-κB activation, while ERK and p38 MAPK promote IL-8 gene transcription through AP-1 and CREB [8,10,21]. Consistent with previous reports, TvSP stimulation induced ERK1/2, p38, and AKT phosphorylation, and inhibition of PI3K and MAPK pathways suppressed IL-8 secretion. TvSP also induced IκB phosphorylation and degradation, suggesting NF-κB activation. Although IKK2 inhibition was not directly tested for IL-8 regulation, its suppression of TvSP-induced degranulation implies upstream involvement in cytokine signaling.

In summary, TvSP activates mast cells through an integrated network of IKK2, Ca^{2+}, PI3K, PKC, and MAPK pathways. IKK2, Ca^{2+}, and PI3K are key regulators of exocytotic degranulation, while PI3K and MAPK pathways are involved in IL-8 production. Although the role of PKC in IL-8 production was not directly examined in this study, our findings that PKC regulates degranulation, together with previous reports, suggest that PKC may also contribute to IL-8 production. IKK2 may mediate mast cell exocytosis through both NF-κB–dependent transcription and a SNAP23-associated non-transcriptional mechanism. These findings enhance understanding of *T. vaginalis*-induced inflammation and underscore the importance of host–parasite signaling crosstalk in trichomoniasis pathogenesis.

Author contributions

Conceptualization: Lee YA, Shin MH. Funding acquisition: Lee YA, Shin MH. Investigation: Park SH, Lee YA. Methodology: Lee YA. Project administration: Shin MH. Supervision: Shin MH. Writing – original draft: Park SH, Lee YA. Writing – review & editing: Lee YA, Shin MH.

Conflict of interest

Myeong Heon Shin serves as an editor of Parasites, Hosts and Diseases but had no involvement in the decision to publish this article. No other potential conflicts of interest relevant to this study were reported.

Funding

This study was supported by a faculty research grant from the Yonsei University College of Medicine (6-2021-0238) to MH Shin and by a National Research Foundation of Korea (NRF) grant funded by the Korean Government (MEST) (NRF-2020R1I1A1A01064838) to YA Lee.

ORCID

Shin Hye Park, https://orcid.org/0000-0003-4661-4190
Young Ah Lee, https://orcid.org/0000-0002-0414-842X
Myeong Heon Shin, https://orcid.org/0000-0001-8207-6110

References

1. Van der Pol B. *Trichomonas vaginalis* infection: the most prevalent nonviral sexually transmitted infection receives the least public health attention. Clin Infect Dis 2007;44:23-5. https://doi.org/10.1086/509934
2. Rowley J, Vander Hoorn S, Korenromp E, et al. Chlamydia, gonorrhoea, trichomoniasis and syphilis: global prevalence and incidence estimates, 2016. Bull World Health Organ 2019;97:548-62P. https://doi.org/10.2471/BLT.18.228486

https://doi.org/10.3347/PHD.25079

3. Kissinger P. *Trichomonas vaginalis*: a review of epidemiologic, clinical and treatment issues. BMC Infect Dis 2015;15:307. https://doi.org/10.1186/s12879-015-1055-0
4. World Health Organization. Global health sector strategy on sexually transmitted infections 2016-2021 [Internet]. The Organization; 2016 [cited 2025 Sep 1]. Available from: https://www.who.int/publications/i/item/WHO-RHR-16.09
5. Ryu JS, Min DY. *Trichomonas vaginalis* and trichomoniasis in the Republic of Korea. Korean J Parasitol 2006;44:101-16. https://doi.org/10.3347/kjp.2006.44.2.101
6. Petrin D, Delgaty K, Bhatt R, Garber G. Clinical and microbiological aspects of *Trichomonas vaginalis*. Clin Microbiol Rev 1998;11:300-17. https://doi.org/10.1128/CMR.11.2.300
7. Fichorova RN, Trifonova RT, Gilbert RO, et al. *Trichomonas vaginalis* lipophosphoglycan triggers a selective upregulation of cytokines by human female reproductive tract epithelial cells. Infect Immun 2006;74:5773-9. https://doi.org/10.1128/IAI.00631-06
8. Nam YH, Min D, Kim HP, et al. Leukotriene B_4 receptor BLT-mediated phosphorylation of NF-κB and CREB is involved in IL-8 production in human mast cells induced by *Trichomonas vaginalis*-derived secretory products. Microbes Infect 2011;13:1211-20. https://doi.org/10.1016/j.micinf.2011.07.006
9. Fichorova RN. Impact of *T. vaginalis* infection on innate immune responses and reproductive outcome. J Reprod Immunol 2009;83:185-9. https://doi.org/10.1016/j.jri.2009.08.007
10. Nam YH, Min D, Park SJ, et al. NF-κB and CREB are involved in IL-8 production of human neutrophils induced by *Trichomonas vaginalis*-derived secretory products. Korean J Parasitol 2011;49:291-4. https://doi.org/10.3347/kjp.2011.49.3.291
11. Kim KS, Moon HS, Kim SS, Ryu JS. Involvement of macrophages in proliferation of prostate cancer cells infected with *Trichomonas vaginalis*. Korean J Parasitol 2021;59:557-64. https://doi.org/10.3347/kjp.2021.59.6.557
12. Galli SJ, Tsai M. IgE and mast cells in allergic disease. Nat Med 2012;18:693-704. https://doi.org/10.1038/nm.2755
13. Abraham SN, St John AL. Mast cell-orchestrated immunity to pathogens. Nat Rev Immunol 2010;10:440-52. https://doi.org/10.1038/nri2782
14. Marshall JS. Mast-cell responses to pathogens. Nat Rev Immunol 2004;4:787-99. https://doi.org/10.1038/nri1460
15. Kalesnikoff J, Galli SJ. New developments in mast cell biology. Nat Immunol 2008;9:1215-23. https://doi.org/10.1038/ni.f.216
16. Han IH, Park SJ, Ahn MH, Ryu JS. Involvement of mast cells in inflammation induced by *Trichomonas vaginalis* via crosstalk with vaginal epithelial cells. Parasite Immunol 2012;34:8-14. https://doi.org/10.1111/j.1365-3024.2011.01338.x
17. Im SJ, Ahn MH, Han IH, et al. Histamine and TNF-alpha release by rat peritoneal mast cells stimulated with Trichomonas vaginalis. Parasite 2011;18:49-55. https://doi.org/10.1051/parasite/2011181049
18. Lee YA, Nam YH, Min A, Shin MH. *Trichomonas vaginalis*-secreted cysteinyl leukotrienes promote migration, degranulation and MCP-1 production in mast cells. Parasite Immunol 2020;42:e12789. https://doi.org/10.1111/pim.12789
19. Lee YA, Shin MH. Dynamin 2-mediated endocytosis of BLT1 is required for IL-8 production in HMC-1 cells induced by *Trichomonas vaginalis*-derived secretory products. Parasites Hosts Dis 2024;62:281-93. https://doi.org/10.3347/PHD.24049
20. Oeckinghaus A, Ghosh S. The NF-kappaB family of transcription factors and its regulation. Cold Spring Harb Perspect Biol 2009;1:a000034. https://doi.org/10.1101/cshperspect.a000034
21. Gilfillan AM, Tkaczyk C. Integrated signalling pathways for mast-cell activation. Nat Rev Immunol 2006;6:218-30. https://doi.org/10.1038/nri1782
22. Bell E. The ins and outs of Ca^{2+} signalling in mast cells. Nat Rev Immunol 2008;8:7-15. https://doi.org/10.1038/nri2245
23. Chen YC, Chang YC, Chang HA, et al. Differential Ca^{2+} mobilization and mast cell degranulation by FcεRI- and GPCR-mediated signaling. Cell Calcium 2017;67:31-9. https://doi.org/10.1016/j.ceca.2017.08.002
24. Blank U, Madera-Salcedo IK, Danelli L, et al. Vesicular trafficking and signaling for cytokine and chemokine secretion in mast cells. Front Immunol 2014;5:453. https://doi.org/10.3389/fimmu.2014.00453
25. Nakagomi D, Suzuki K, Nakajima H. Critical roles of IκB kinase subunits in mast cell degranulation. Int Arch Allergy Immunol 2012;158 Suppl 1:92-5. https://doi.org/10.1159/000337800
26. Suzuki K, Verma IM. Phosphorylation of SNAP-23 by IκB kinase 2 regulates mast cell degranulation. Cell 2008;134:485-95. https://doi.org/10.1016/j.cell.2008.05.050
27. Min A, Lee YA, Kim KA, El-Benna J, Shin MH. SNAP23-dependent surface translocation of leukotriene B4 (LTB4) receptor 1 is essential for NOX2-mediated exocytotic degranulation in human mast cells induced by *Trichomonas vaginalis*-secreted LTB4. Infect Immun 2016;85:e00526-16. https://doi.org/10.1128/IAI.00526-16
28. Hempel N, Trebak M. Crosstalk between calcium and reactive oxygen species signaling in cancer. Cell Calcium 2017;63:70-96. https://doi.org/10.1016/j.ceca.2017.01.007
29. Granfeldt D, Samuelsson M, Karlsson A. Capacitative Ca^{2+} influx and activation of the neutrophil respiratory burst: different regulation of plasma membrane- and granule-localized NADPH-oxidase. J Leukoc Biol 2002;71:611-7. https://doi.org/10.1189/jlb.71.4.611
30. Alsaleh NB, Persaud I, Brown JM. Silver nanoparticle-directed mast cell degranulation is mediated through calcium and PI3K signaling independent of the high affinity IgE receptor. PLoS One 2016;11:e0167366. https://doi.org/10.1371/journal.pone.0167366

Original Article

Parasites Hosts Dis 2026;64(1):52-61
https://doi.org/10.3347/PHD.25087

Parasites, Hosts and Diseases

pISSN 2982-5164 • eISSN 2982-6799

Genetic polymorphisms of merozoite surface protein-1 ICB 5–6 in Vietnamese *Plasmodium vivax* isolates

Thu Hằng Nguyễn[1,2,†], Đăng Thùy Dương Nguyễn[1,2,†], Hương Giang Lê[1,2], Tuấn Cường Võ[1,2], Nguyen Thi Minh Trinh[3], Minkyoung Cho[1,2], Chau Van Khanh[3], Huynh Hong Quang[3,*], Byoung-Kuk Na[1,2,*]

[1]Department of Parasitology and Tropical Medicine and Institute of Medical Science, Gyeongsang National University College of Medicine, Jinju, Korea; [2]Department of Convergence Medical Science, Gyeongsang National University, Jinju, Korea; [3]Tropical Diseases Clinical and Treatment Research Department, Institute of Malariology, Parasitology, and Entomology Quy Nhon, Gia Lai Province, Vietnam

Plasmodium vivax merozoite surface protein-1 (PvMSP-1) is one of the major polymorphic markers for molecular epidemiological purposes. In particular, the interspecies conserved block 5–6 (ICB 5–6) of PvMSP-1 is a region exhibiting extensive genetic polymorphism. In this study, we analyzed polymorphic characters of the *pvmsp-1* ICB 5–6 region from *P. vivax* isolates collected in 4 provinces of Vietnam (Dak Lak, Dak Nong, Gia Lai, and Khanh Hoa) between 2018 and 2022. A comparative analysis of *pvmsp-1* ICB 5–6 sequences was also conducted between Vietnam and other endemic regions. A total of 139 *pvmsp-1* ICB 5–6 sequences were obtained from 117 Vietnamese *P. vivax* isolates. Vietnam *pvmsp-1* ICB 5–6 were clustered into 34 distinct haplotypes at the amino acid level, with the recombinant types being predominant. The *pvmsp-1* ICB 5–6 from the Central Highlands, Dak Lak, Dak Nong, and Gia Lai, exhibited high genetic polymorphism, while the sequences from the South-Central region, Khanh Hoa, were less polymorphic. Highly diverse patterns of poly-glutamine (poly-Q) variants were identified in Vietnam *pvmsp-1* ICB 5–6. Comparable features of genetic polymorphism were also identified in the global *pvmsp-1* ICB 5–6 populations. Phylogenetic analysis of global *pvmsp-1* ICB 5–6 revealed no significant country-specific or region-specific clustering. This study suggests that Vietnam *pvmsp-1* ICB 5–6 exhibited a substantial genetic diversity with regional variations, implying the genetic heterogeneity of the Vietnamese *P. vivax* population. These findings emphasize the importance of continuous molecular surveillance to understand the genetic nature of the parasite in the country.

Keywords: *Plasmodium vivax*, PvMSP-1 ICB 5–6, genetic polymorphism, Vietnam

Introduction

Malaria is a life-threatening vector-borne disease caused by apicomplexan parasites belonging to the genus *Plasmodium*. Global efforts to combat malaria have continuously reduced the incidence and mortality of malaria worldwide since 2000. However, an estimated 263 million cases and about 600,000 deaths have been reported globally in 2023 [1], imposing a continuous substantial global health burden. Among the human-infecting *Plasmodium* species, *P. vivax* is the most widely distributed species worldwide, particularly prevalent in Asia and South America [1]. Vietnam is a country in the Greater Mekong Subregion (GMS), where malaria is endemic. Like the other countries in the GMS, Vietnam also aims to eliminate

Received: September 30, 2025 Accepted: December 1, 2025
*Correspondence: hhq, huynhquangimpe@yahoo.com; bkn, bkna@gnu.ac.kr

†These authors contributed equally to this work.

Citation
Nguyễn TH, Nguyễn DTD, Lê HG, Võ TC, Trinh NTM, Cho M, Khanh CV, Quang HH, Na BK. Genetic polymorphisms of merozoite surface protein-1 ICB 5–6 in Vietnamese *Plasmodium vivax* isolates. Parasites Hosts Dis 2026;64(1):52-61.

malaria by 2030, and has achieved significant malaria reduction over the past 2 decades [1]. However, the Central Highlands and the South-Central regions remain malaria hot spots. *P. falciparum* and *P. vivax* are the major species in the areas [2]. Although *P. falciparum* cases have remarkably declined, *P. vivax* is still prevalent, and severe cases are also identified [3]. A recent unprecedented large outbreak of *P. malariae*, antimalarial drug resistance, and asymptomatic submicroscopic *P. falciparum* and *P. vivax* are new challenges in eliminating malaria in Vietnam [4-6].

The persistent prevalence of vivax malaria is largely attributed to unique biological features of *P. vivax*, such as early gametocyte formation and dormant liver-stage hypnozoites, which may lead to relapses months or years after primary infection [7]. These underscore the urgent necessity of investigation on the genetic structure of the parasite population to understand the diversity, distribution, and dynamics of natural *P. vivax* populations, which could be supportive of developing effective vaccine strategies in combating the ongoing challenges posed by *P. vivax* [8].

Merozoite surface protein-1 (MSP-1) is a major surface protein of merozoites of *Plasmodium* species, playing a critical role in erythrocyte invasion [9,10]. *P. vivax* MSP-1 (PvMSP-1) is a 200-kDa protein encoded by the *pvmsp-1* gene and is regarded as a leading vaccine candidate targeting *P. vivax* [11-14]. Cross-species sequence analysis of *msp-1* from *P. vivax*, *P. falciparum*, and *P. yoelii* revealed 10 interspecies conserved blocks (ICBs) that include 8 major polymorphic regions among these *Plasmodium* parasites [15]. In particular, the ICB 5–6 region of the gene, encompassing highly polymorphic traits caused by insertions, deletions, intra-allelic recombination, and point mutations, has been identified as a reliable genetic polymorphic marker [16]. While genetic polymorphism studies of *pvmsp-1* ICB 5–6 have been undertaken in various endemic regions [17-24], information on the Vietnamese *P. vivax* population remains scarce.

This study aimed to characterize the genetic diversity of *pvmsp-1* ICB 5–6 in *P. vivax* isolates collected in Vietnam to understand the genetic nature of *P. vivax* population in the country.

Methods

Ethics statement

The study protocol was approved by the Ethical Review Committee of the Ministry of Health, Institute of Malariology, Parasitology and Entomology Quy Nhon, Vietnam (approval No. 386/VSR-LSDT, 45/VSR-NCDT, and 637/VSR-NCDT).

Blood samples

A total of 117 blood samples obtained from *P. vivax*-infected malaria patients in the Central Highlands (Gia Lai, Dak Nong, and Dak Lak provinces) and the South-Central region (Khanh Hoa province) of Vietnam in 2018–2022 were used in this study (Fig. 1). *P. vivax* infection was diagnosed by a rapid diagnostic test (SD-Bioline Malaria Pf/Pv HRP2/pLDH Ag) and microscopic examination of thick and thin blood smears. Before antimalarial drug administration, 2 or 3 drops of finger-prick blood were taken from each patient, spotted on Whatman 3 MM filter paper (GE Healthcare), and dried. Verbal informed consent was obtained from each participant before blood collection.

Amplification of *pvmsp-1* ICB 5–6

Genomic DNA of *P. vivax* was extracted from each dried blood spot using the QIAamp DNA Blood Kit (Qiagen) according to the manufacturer's protocols. Genomic DNA was eluted in 50 μl of the elution buffer in the kit, and DNA quality was assessed using a DS-11 spectrophotometer (DeNovix). The gene frag-

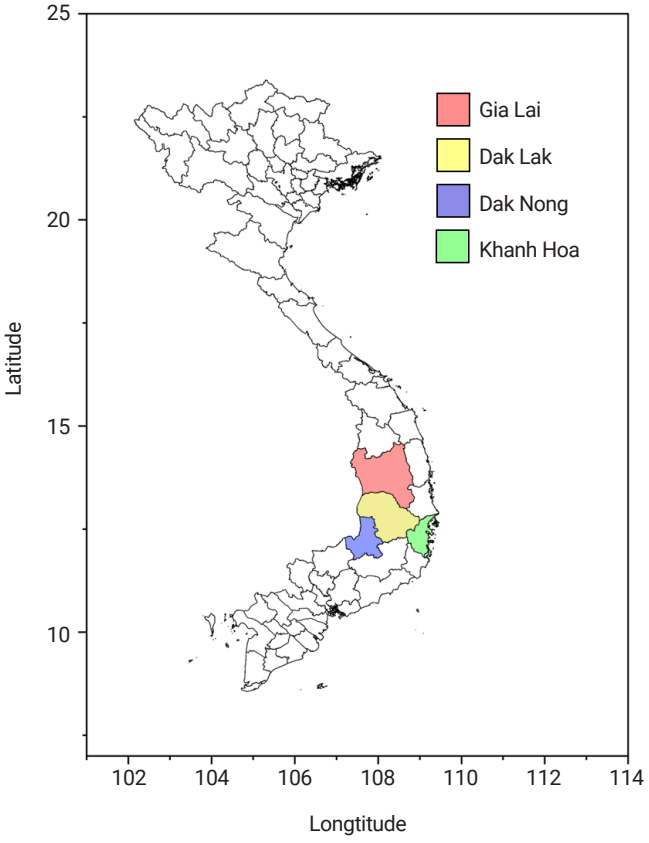

Fig. 1. Map of blood sample collection areas. Blood samples were collected from *Plasmodium vivax*-infected individuals in 4 provinces in Vietnam: Gia Lai, Dak Lak, Dak Nong, and Khanh Hoa.

ment covering *pvmsp-1* ICB 5–6 was amplified via a nested PCR using specific primer sets and thermal cycles described previously [19]. To enhance fidelity of amplification, Ex *Taq* DNA polymerase (Takara), possessing proofreading activity, was used in all amplification steps. Multiple amplicons with different sizes were identified in some samples, implying multiple infections. Each PCR product was cloned into the T&A cloning vector (Real Biotech Corporation) and transformed into *Escherichia coli* DH5α competent cells. The recombinant plasmids containing the insert of expected size were selected by colony PCR. Plasmids from selected clones were purified and subjected to bidirectional sequencing with M13 forward and reverse primers. To ensure sequence accuracy and minimize potential sequencing artifacts, plasmids isolated from at least 2 independent clones for each isolate were sequenced. Nucleotide sequences of *pvmsp-1* ICB 5–6 obtained in this study have been deposited in the GenBank database under the accession numbers PX388009–PX388147.

Polymorphism analysis of Vietnam *pvmsp-1* ICB 5–6

The nucleotide and deduced amino acid sequences of Vietnam *pvmsp-1* ICB 5–6 were analyzed using EditSeq and SeqMan programs in the DNSTAR package (DNASTAR) and MEGA7 [25]. The resulting sequences were further analyzed by comparing 2 reference sequences, Sal I (XM_001614792) and Belem (AF435594).

Comparative analysis of global *pvmsp-1* ICB 5–6

To assess the genetic polymorphisms and phylogenetic relationships between Vietnam and global *pvmsp-1* ICB 5–6 populations, publicly available nucleotide sequences of global *pvmsp-1* ICB 5–6 were extracted from GenBank databases: Myanmar (n=83, MW383137–MW383219), Thailand (n=170, GQ890872–GQ891041), Korea (n=255, KU893351–KU893605), Pakistan (n=75, OP313607–OP313681), Turkey (n=30, AB564559–AB564588), Azerbaijan (n=36, AY789657–AY789692), Kyrgyzstan (n=16, MH201430–MH201445), and Mexico (n=14, JX443532–JX443545). Phylogenetic tree of global *pvmsp-1* ICB 5–6 was constructed by using the Maximum Likelihood method in MEGA7 with 1,000 bootstrap replicates [25], and the final topology was visualized using the Interactive Tree of Life (iTOL) platform (https://itol.embl.de/). The analysis of molecular variance for global *pvmsp-1* ICB 5–6 sequences was performed with Arlequin 3.5, and the significance of variance levels was evaluated using 1,000 permutations [26].

Results

Genetic polymorphism of Vietnam *pvmsp-1* ICB 5–6

A total of 139 *pvmsp-1* ICB 5–6 sequences were obtained from 117 Vietnamese *P. vivax* isolates, suggesting an estimated multiplicity of infection value of 1.19. The *pvmsp-1* ICB 5–6 sizes were not equal, showing size polymorphisms ranging from 510 to 591 bp. Sequence analysis of the Vietnam *pvmsp-1* ICB 5–6 sequences at the amino acid level revealed that they were clustered into 34 distinct haplotypes, which were further classified into 3 different allele types: Sal I, recombinant, and Belem (Fig. 2). Nine haplotypes (H1–H9) were classified into Sal I types, while 24 haplotypes (H10–H33) were recombinant types. Only 1 haplotype (H34) was classified into the Belem type. Recombinant types exhibited the greatest polymorphisms and were prevalent, occupying 72.0% of the sequences (100/139), followed by Sal I types of 27.3% (38/139) and a Belem type of 0.7% (1/139). Haplotype 24 (H24) was the most prevalent, accounting for 25.9% (36/139). In Sal I types, H1 shared the identical amino acid sequence with Sal I reference (XM_001614792), while other haplotypes (H2–H9) had amino acid changes, such as P739Q, V744A, Q790R, I792T, A795S, T799N, E831Q, N873K, and T875N, caused by non-synonymous single nucleotide polymorphisms and an insertion of a glutamine (Gln, Q) residue between amino acid positions 737 and 738. Recombinant types were generated by potential recombination between Sal I and Belem types at 5 positions, and revealed highly diverse patterns of poly-Gln (poly-Q) repeats. Nine amino acid substitutions, including Q738H, V744A, I792T, T799D, E831Q, E868K, K871T, N873K, and T875N, were also found in recombinant haplotypes. H34 shared a highly conserved sequence with the Belem reference (AF435594), and had a different poly-Q pattern. The frequencies of *pvmsp-1* ICB 5–6 allelic types differed by province (Fig. 3). Three provinces in the Central Highlands, Dak Lak, Gia Lai, and Dak Nong, revealed mixed allelic types, in which recombinant types were prevalent. The Belem type was identified only in Dak Nong, while only recombinant types were identified in Khanh Hoa province. The *pvmsp-1* ICB 5–6 displayed pronounced genetic variability in the poly-Q repeat region due to unstructured tandem Q repeats, particularly in recombinant and Belem types. The number of Qs in poly-Q repeats differed in Vietnam *pvmsp-1* ICB 5–6, ranging from 15 to 26 (Fig. 4). The *pvmsp-1* ICB 5–6 from Khanh Hoa showed less polymorphic features than those from Gia Lai, Dak Lak, and Dak Nong: only 3 types of poly-Qs, 18, 19, and 20 Qs, were identified in Khanh Hoa, while more diverse types of poly-Qs were observed in Gia Lai (17, 18, 19, 20, and 21 Qs), Dak Lak (17, 18,

https://doi.org/10.3347/PHD.25087

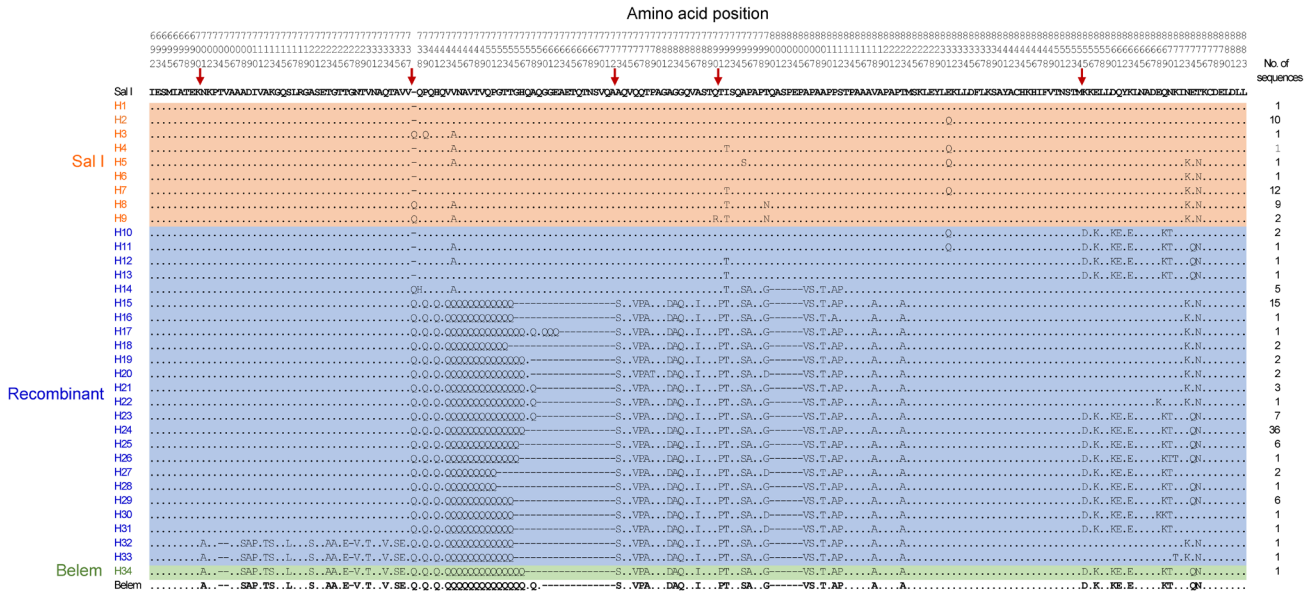

Fig. 2. Genetic polymorphisms of *pvmsp-1* ICB 5–6 in Vietnamese *Plasmodium vivax* isolates. Multiple sequence alignment of deduced amino acid sequences of 139 Vietnam *pvmsp-1* ICB 5–6 sequences revealed 34 different haplotypes, classifying into Sal I, recombinant, and Belem allelic types. Sal I (XM_001614792) and Belem (AF435594) were used as reference sequences. Amino acids identical to Sal I are represented by dots. The dashes represent alignment gaps. The red arrows mark the predicted recombination sites.

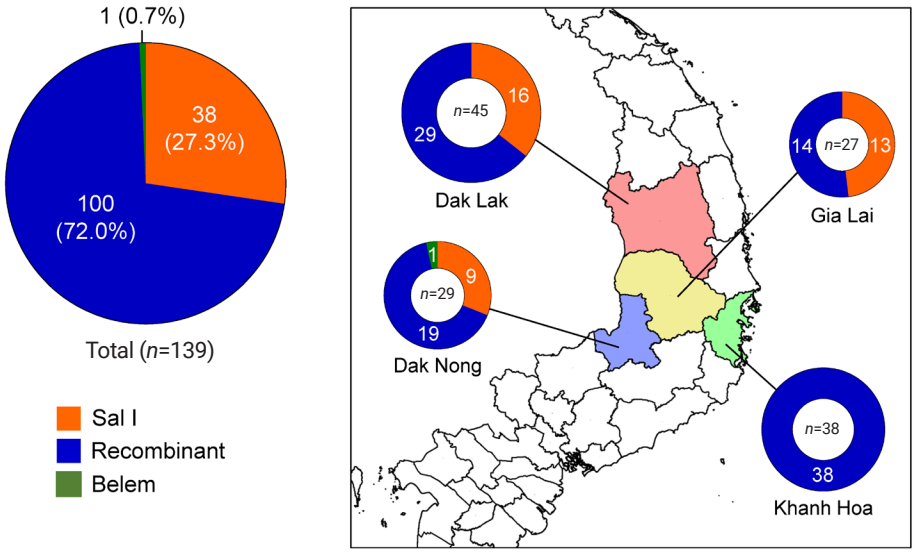

Fig. 3. Allelic distributions of *pvmsp-1* ICB 5–6 in the Vietnamese *Plasmodium vivax* population. Pie charts show the proportions of Sal I, recombinant, and Belem allelic types across the 4 provinces. Recombinant types were predominant in all provinces, while the Belem type was detected in only Dak Nong.

19, 20, 21, and 26 Qs), and Dak Nong (15, 17, 18, 20, and 22 Qs). Overall, 18 and 20 Qs were the most predominant poly-Q repeats in Vietnam *pvmsp-1* ICB 5–6.

Genetic polymorphisms of *pvmsp-1* ICB 5–6 in the global populations

Global *pvmsp-1* ICB 5–6 also showed great genetic polymorphisms, but the frequencies of 3 allelic types differed by country (Fig. 5). Recombinant types were the most prevalent allelic types in Vietnam, Myanmar, Thailand, Korea, Pakistan, Kyrgyzstan, and Mexico, while Belem types were significant in Turkey and Azerbaijan. Amino acid changes identified in the global *pvmsp-1* ICB 5–6 were also comparatively analyzed (Fig. 6). Overall profiles of amino acid changes in the global

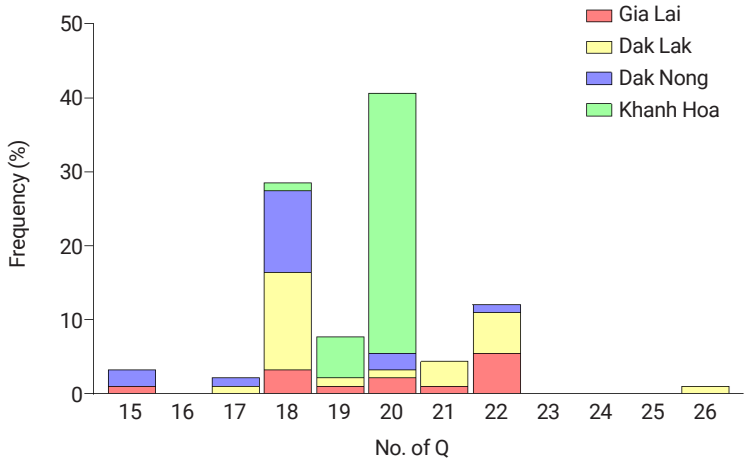

Fig. 4. Poly-Gln (Q) repeat variations in the Vietnam *pvmsp-1* ICB 5–6 population. Diverse types of poly-Q repeats, caused by different numbers of Qs ranging from 15 to 26, were identified in Vietnam *pvmsp-1* ICB 5–6. The frequencies of poly-Q patterns differed by province.

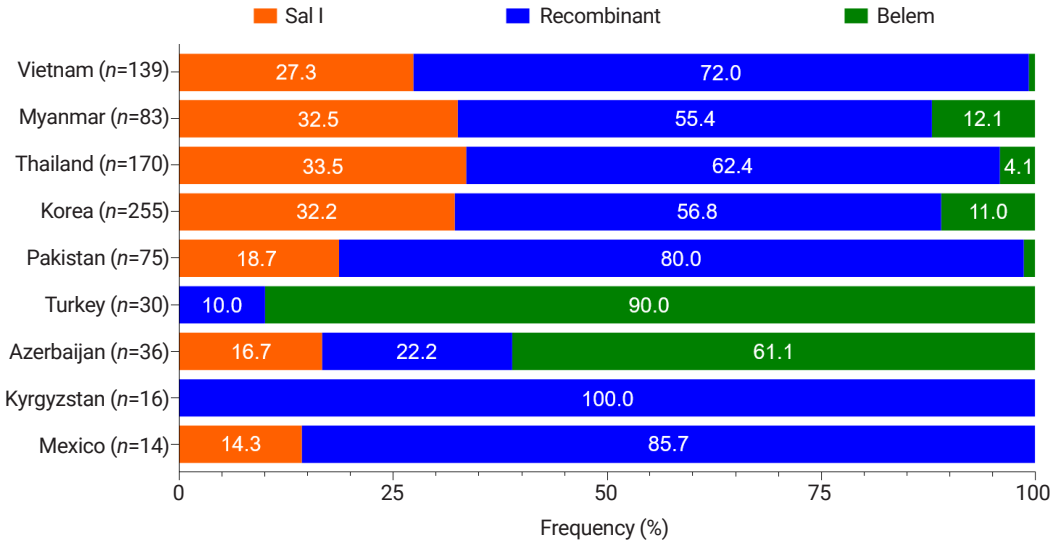

Fig. 5. Allelic distributions of *pvmsp-1* ICB 5–6 in the global *Plasmodium vivax* population. Bar graph shows the proportions of Sal I, recombinant, and Belem allelic types in the global *P. vivax* population. Recombinant types were the most prevalent except for Turkey and Azerbaijan.

populations differed by country. However, N873K was commonly detected in all countries analyzed in this study, with a frequency ranging from 10.0% (Turkey) to 85.7% (Mexico). I792T was also identified in *pvmsp-1* ICB 5–6 from countries except for Turkey. E693Q, S694A, A697T, Q738P, P739Q, V744A, T799D, A809V, and E831Q were also detected in *pvmsp-1* ICB 5–6 of more than 4 countries. A few amino acid changes with low frequencies were detected in country-specific manners, in which P779T, Q790R, A795S, E868K, and K871T were specific in Vietnam *pvmsp-1* ICB 5–6. Global *pvmsp-1* ICB 5–6 showed a high level of polymorphisms in the poly-Q repeats region. The Q count in poly-Q repeats exhibited great diversity in the global populations, from 9 to 30 (Fig. 7). The most common number of Q was 18, which was found in *pvmsp-1* ICB 5–6 from Vietnam, Myanmar, Thailand, Pakistan, Turkey, Azerbaijan, and Mexico. Interestingly, 17 Qs was highly prevalent (92.9%) in Kyrgyzstan, while 21 Qs was predominant (81.5%) in Azerbaijan. Meanwhile, 10 and 14 Qs were predominant in Korea, and 15 Qs was prevalent (63.3%) in Turkey. For Thailand, 27 Qs was predominant (53.9%). The most significant polymorphic patterns of poly-Qs were detected in Myanmar. A phylogenetic tree was constructed to determine the genetic lineages of the global *pvmsp-1* ICB 5–6 (Fig. 8). The phylogenetic tree branched into 3 major clusters, Sal I,

https://doi.org/10.3347/PHD.25087

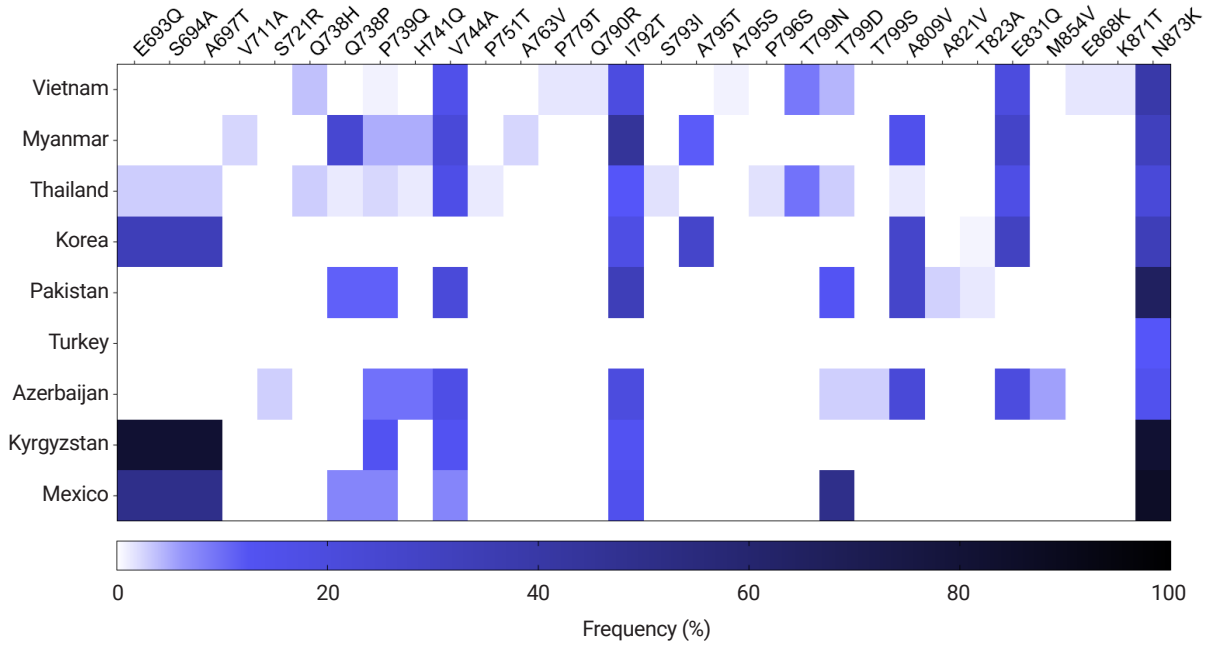

Fig. 6. Profiles of amino acid changes identified in the global *pvmsp-1* ICB 5–6 population. The heatmap illustrates the frequencies of amino acid changes identified in the global *pvmsp-1* ICB 5–6 populations compared to the Sal I reference sequence (XM_001614792).

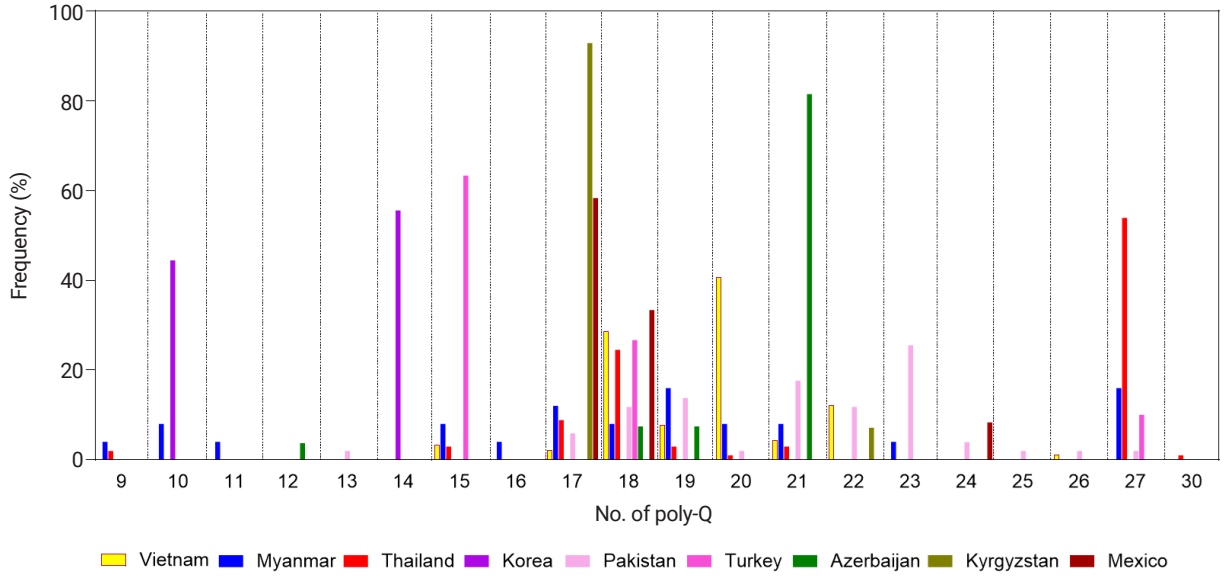

Fig. 7. Poly-Gln (Q) repeat variations in the global *pvmsp-1* ICB 5–6 population. Different patterns of poly-Q repeats were observed in the global *pvmsp-1* ICB 5–6 populations. Great polymorphic patterns were identified, but no significant country- or region-specific pattern was detected.

recombinant, and Belem types, but no significant country-specific or region-specific clustering was identified. This pattern was further supported quantitatively by analysis of molecular variance, suggesting that 46.6% of the total genetic variance was attributed to differences among populations.

Discussion

This is the first report on genetic characteristics of *pvmsp-1* ICB 5–6 in Vietnamese *P. vivax* isolates. Substantial genetic polymorphisms were identified in the Vietnam *pvmsp-1* ICB 5–6 population. All 3 allelic types, Sal I, recombinant, and

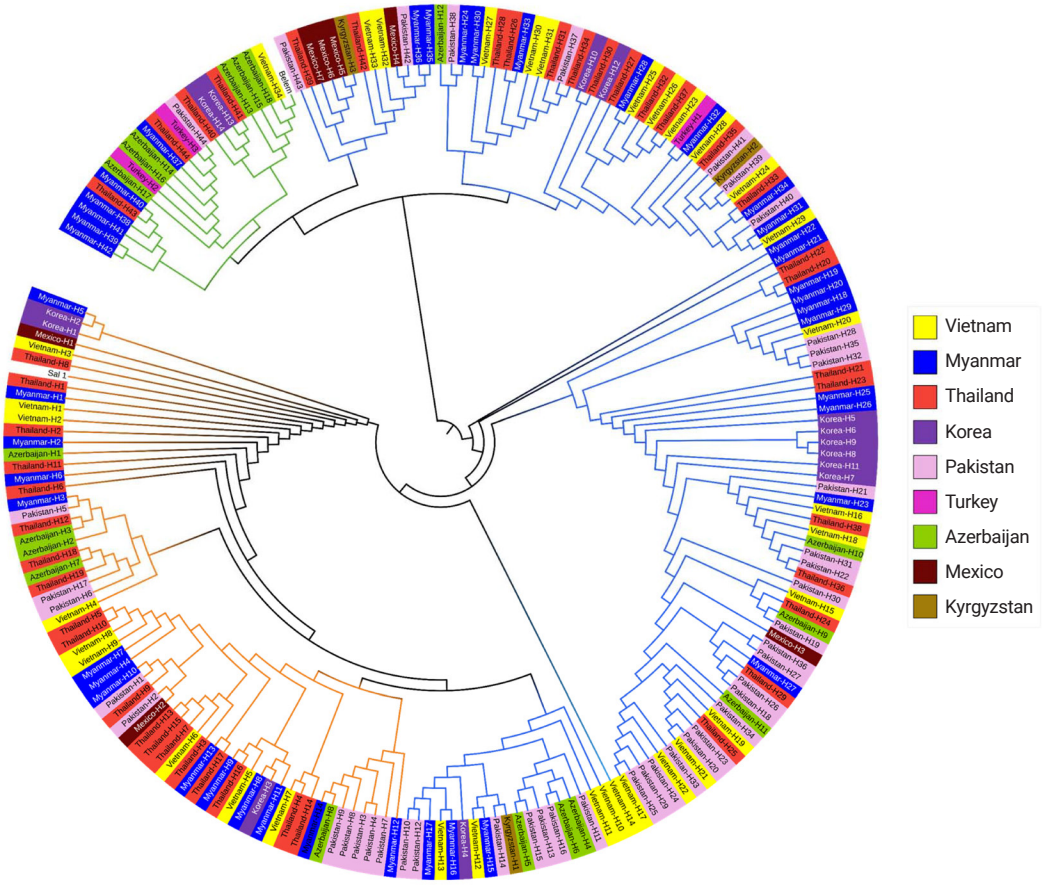

Fig. 8. Phylogenetic analysis of the global *pvmsp-1* ICB 5–6 population. A phylogenetic tree was constructed with the maximum likelihood method by the MEGA7 program, applying 209 global *pvmsp-1* ICB 5–6 sequences and 2 reference sequences of Sal I (XM_001614792) and Belem (AF435594).

Belem, were observed, but recombinant types were predominant. Similar patterns of predominance of recombinant allelic types were also identified in *pvmsp-1* ICB 5–6 populations from other countries, including neighboring Southeast Asian countries such as Myanmar and Thailand [20,27], except for *pvmsp-1* ICB 5–6 from Turkey and Azerbaijan, showing higher frequencies of Belem types. High prevalence of recombinant allelic types might be attributed to frequent recombination events between and among parasite populations with distinct genetic structures, which could be common in endemic areas where co-infection and/or super-infection allows active sexual recombination in the mosquito vector [28]. Interestingly, *pvmsp-1* ICB 5–6 from the South-Central province of Khanh Hoa displayed a different allelic distribution from those from the Central Highland provinces of Dak Lak, Dak Nong, and Gia Lai. The reason for this difference remains unclear, and further investigation is necessary.

Amino acid changes and size polymorphisms of poly-Q repeats were the major factors causing the genetic diversity of Vietnam and global *pvmsp-1* ICB 5–6 populations. The most significant amino acid changes were I792T and N873K, which were commonly identified in the global *pvmsp-1* ICB 5–6 populations, suggesting they may be under balancing selections or possible functional constraints. Polymorphisms in poly-Q repeats were significant in recombinant and Belem types. Various numbers of poly-Qs ranging from 9 to 30 were identified in the global *pvmsp-1* ICB 5–6 populations, and the patterns of poly-Qs differed by county. Generally, poly-Q heterogeneity was greater in Southeast Asian countries, including Myanmar, Thailand, and Vietnam, than in the other countries analyzed in this study. Interestingly, *pvmsp-1* ICB 5–6 from the Central Highlands of Dak Lak, Dak Nong, and Gia Lai provinces revealed higher levels of amino acid polymorphisms and greater poly-Q heterogeneity than those from Khanh Hoa province, the South-Central region. The *pvmsp-1* ICB 5–6 from Khanh Hoa exhibited limited genetic diversity, charac-

https://doi.org/10.3347/PHD.25087

terized by only an amino acid change and a predominant poly-Q lineage. This phenomenon could be due to the lower endemicity of malaria in Khanh Hoa than in the Central Highlands. High endemicity in the Central Highlands may maintain more diverse gene pools in the *P. vivax* population, enabling active recombination. While Khanh Hoa may harbor a less diverse parasite population, probably due to the low endemicity and restricted gene input, this drives the stable maintenance of genetic homogeneity. However, further comparative investigations for other polymorphic markers, such as circumsporozoite surface protein and apical membrane antigen-1, are necessary to understand the genetic differences of *P. vivax* populations between the 2 areas in Vietnam.

This study had several limitations. Only 4 malaria-endemic provinces in Vietnam were enrolled in this study, suggesting the results of this study could not provide the nationwide landscape of the genetic diversity in the Vietnam *pvmsp-1* ICB 5–6. Therefore, analysis of the gene from the other malaria-endemic provinces in Vietnam is necessary to understand and generalize the genetic nature of the gene in Vietnamese *P. vivax* population. Considering that malaria transmission and the genetic structure of malaria parasites can be influenced by diverse factors, such as human migration and vector species [29], further demographic analysis of the human population and distribution of mosquito vectors in the studied areas is necessary. Unequal numbers of global *pvmsp-1* ICB 5–6 sequences and limited numbers of countries due to the restricted availability of public genetic information about global *pvmsp-1* ICB 5–6 sequences are also limitations. The global *pvmsp-1* ICB 5–6 sequences that were gleaned from the previous studies also span a range of different chronological periods, suggesting that it is conceivable that the results of this study might not precisely depict the current genetic characteristics of the global *pvmsp-1* ICB 5–6 population. Interestingly, it was reported that Vietnamese *P. falciparum* and *P. vivax* populations exhibited different genetic structure and natural selection trends with other GMS countries, such as Myanmar and Thailand [30-34], emphasizing the necessity to investigate the *P. falciparum* and *P. vivax* populations in Lao PDR and Cambodia to unveil in-depth genetic lineages and evolutionary insights of the parasite population in the GMS.

In conclusion, this study demonstrated that Vietnam *pvmsp-1* ICB 5–6 displayed substantial genetic diversity within the *P. vivax* population, produced by amino acid changes and poly-Q repeat length polymorphisms. Recombination was also one of the driving forces contributing to the genetic diversity of Vietnam *pvmsp-1* ICB 5–6 by generating diverse recombinant types. Interestingly, different genetic profiles of Vietnam *pvmsp-1* ICB 5–6 were detected between the Central Highlands and South-Central regions, suggesting possible genetic differentiation between *P. vivax* population in the 2 malaria endemic regions. These findings provide valuable insights into the evolutionary dynamics of Vietnamese *P. vivax* and highlight the importance of continuous molecular surveillance of the parasite for Vietnam's malaria elimination goal.

Data availability

The data supporting the conclusions of this article are provided within the article. The original datasets analyzed in this study are available from the corresponding author upon request. All data generated or analyzed during this study are included in this published article. The sequence data obtained in this study are openly available in GenBank of NCBI at https://www.ncbi.nlm.nih.gov/ under the accession No. PX388009–PX388147.

Author contributions

Conceptualization: Na BK. Data curation: Nguyễn TH, Nguyễn DTD, Lê HG, Võ TC, Na BK. Formal analysis: Nguyễn TH, Nguyễn DTD, Lê HG, Võ TC, Cho M, Na BK. Funding acquisition: Na BK. Investigation: Nguyễn TH, Nguyễn DTD, Na BK. Methodology: Nguyễn TH, Nguyễn DTD, Trinh NTM, Khanh CV, Quang HH. Project administration: Quang HH, Na BK. Resources: Trinh NTM, Khanh CV, Quang HH. Software: Nguyễn TH, Nguyễn DTD. Supervision: Khanh CV, Quang HH, Na BK. Writing – original draft: Nguyễn TH, Na BK. Writing – review & editing: Nguyễn DTD, Lê HG, Võ TC, Trinh NTM, Cho M, Khanh CV, Quang HH.

Conflict of interest

The authors have no conflicts of interest to declare.

Funding

This work was supported by the National Research Foundation of Korea grant funded by the Korean government (MSIT) (RS-2025-02413635).

Acknowledgments

The authors thank the staff in the Tropical Diseases Clinical and Treatment Research Department, Institute of Malariology, Parasitology, and Entomology Quy Nhon, Vietnam for their contribution and technical support in field work.

ORCID

Thu Hằng Nguyễn, https://orcid.org/0009-0001-0300-853X
Đăng Thùy Dương Nguyễn, https://orcid.org/0009-0003-2446-7916
Hương Giang Lê, https://orcid.org/0000-0001-6294-9017
Tuấn Cường Võ, https://orcid.org/0000-0002-6604-4888
Nguyen Thi Minh Trinh, https://orcid.org/0009-0000-9547-4249
Minkyoung Cho, https://orcid.org/0000-0002-1776-7254
Chau Van Khanh, https://orcid.org/0009-0006-9787-2316
Huynh Hong Quang, https://orcid.org/0000-0003-3895-7142
Byoung-Kuk Na, https://orcid.org/0000-0002-6734-1673

References

1. World Health Organization. World malaria report 2024. The Organization; 2024.
2. Võ TC, Lê HG, Kang JM, et al. Molecular surveillance of malaria in the Central Highlands, Vie tnam. Parasitol Int 2021;83:102374. https://doi.org/10.1016/j.parint.2021.102374
3. Duong MC, Pham OKN, Thai TT, et al. Magnitude and patterns of severe *Plasmodium vivax* monoinfection in Vietnam: a 4-year single-center retrospective study. Front Med (Lausanne) 2023;10:1128981. https://doi.org/10.3389/fmed.2023.1128981
4. Quang HH, Chavchich M, Trinh NTM, et al. Multidrug-resistant *Plasmodium falciparum* parasites in the Central Highlands of Vietnam jeopardize malaria control and elimination strategies. Antimicrob Agents Chemother 2021;65:e01639-20. https://doi.org/10.1128/AAC.01639-20
5. Khanh CV, Lê HG, Võ TC, et al. Unprecedented large outbreak of *Plasmodium malariae* malaria in Vietnam: epidemiological and clinical perspectives. Emerg Microbes Infect 2025;14:2432359. https://doi.org/10.1080/22221751.2024.2432359
6. Lê HG, Võ TC, Kang JM, et al. Molecular profiles of antimalarial drug resistance in *Plasmodium* species from asymptomatic malaria carriers in Gia Lai province, Vietnam. Microorganisms 2025;13:2101. https://doi.org/10.3390/microorganisms13092101
7. Dayananda KK, Achur RN, Gowda DC. Epidemiology, drug resistance, and pathophysiology of *Plasmodium vivax* malaria. J Vector Borne Dis 2018;55:1-8. https://doi.org/10.4103/0972-9062.234620
8. Arnott A, Barry AE, Reeder JC. Understanding the population genetics of *Plasmodium vivax* is essential for malaria control and elimination. Malar J 2012;11:14. https://doi.org/10.1186/1475-2875-11-14
9. Holder AA, Blackman MJ, Burghaus PA, et al. A malaria merozoite surface protein (MSP-1) structure, processing and function. Mem Inst Oswaldo Cruz 1992;87 Suppl 3:37-42. https://doi.org/10.1590/s0074-02761992000700004
10. Beeson JG, Drew DR, Boyle MJ, et al. Merozoite surface proteins in red blood cell invasion, immunity and vaccines against malaria. FEMS Microbiol Rev 2016;40:343-72. https://doi.org/10.1093/femsre/fuw001
11. Valderrama-Aguirre A, Quintero G, Gómez A, et al. Antigenicity, immuogenicity, and protective efficacy of *Plasmodium vivax* MSP1 Pv200L: a potential malaria vaccine subunit. Am J Trop Med Hyg 2005;73:16-24. https://doi.org/10.4269/ajtmh.2005.73.16
12. Versiani FG, Almeida ME, Mariuba LA, Orlandi PP, Nogueira PA. N-terminal *Plasmodium vivax* merozoite surface protein-1, a potential subunit for malaria vivax vaccine. Clin Dev Immunol 2013;2013:965841. https://doi.org/10.1155/2013/965841
13. Herrera S, Corradin G, Arévalo-Herrera M. An update on the search for a *Plasmodium vivax* vaccine. Trends Parasitol 2007;23:122-8. https://doi.org/10.1016/j.pt.2007.01.008
14. Gibson HL, Tucker JE, Kaslow DC, et al. Structure and expression of the gene for Pv200, a major blood-stage surface antigen of *Plasmodium vivax*. Mol Biochem Parasitol 1992;50:325-33. https://doi.org/10.1016/0166-6851(92)90230-h
15. Portillo HAD, Longacre S, Khouri E, David PH. Primary structure of the merozoite surface antigen 1 of *Plasmodium vivax* reveals sequences conserved between different *Plasmodium* species. Proc Natl Acad Sci USA 1991;88:4030-4. https://doi.org/10.1073/pnas.88.9.4030
16. Putaporntip C, Jongwutiwes S, Sakihama N, et al. Mosaic organization and heterogeneity in frequency of allelic recombination of the *Plasmodium vivax* merozoite surface protein-1 locus. Proc Natl Acad Sci USA 2002;99:16348-53. https://doi.org/10.1073/pnas.252348999
17. Ruan W, Zhang LL, Feng Y, et al. Genetic diversity of *Plasmodium vivax* revealed by the merozoite surface protein-1 icb5-6 fragment. Infect Dis Poverty 2017;6:92. https://doi.org/10.1186/s40249-017-0302-6
18. Cerritos R, González-Cerón L, Nettel JA, Wegier A. Genetic structure of *Plasmodium vivax* using the merozoite surface protein 1 icb5-6 fragment reveals new hybrid haplotypes in southern Mexico. Malar J 2014;13:35. https://doi.org/10.1186/1475-2875-13-35
19. Naw H, Kang JM, Moe M, et al. Temporal changes in the genetic diversity of *Plasmodium vivax* merozoite surface protein-1 in Myanmar. Pathogens 2021;10:916. https://doi.org/10.3390/pathogens10080916
20. Putaporntip C, Jongwutiwes S, Tanabe K, Thaithong S. Interallelic recombination in the merozoite surface protein 1 (MSP-1) gene of *Plasmodium vivax* from Thai isolates. Mol Biochem Parasitol 1997;84:49-56. https://doi.org/10.1016/s0166-6851(96)02786-7
21. Zeyrek FY, Tachibana SI, Yuksel F, et al. Limited polymorphism of

https://doi.org/10.3347/PHD.25087

the *Plasmodium vivax* merozoite surface protein 1 gene in isolates from Turkey. Am J Trop Med Hyg 2010;83:1230-7. https://doi.org/10.4269/ajtmh.2010.10-0353

22. Goo YK, Moon JH, Ji SY, et al. The unique distribution of the *Plasmodium vivax* merozoite surface protein 1 in parasite isolates with short and long latent periods from the Republic of Korea. Malar J 2015;14:299. https://doi.org/10.1186/s12936-015-0803-3
23. Moon SU, Lee HW, Kim JY, et al. High frequency of genetic diversity of *Plasmodium vivax* field isolates in Myanmar. Acta Trop 2009;109:30-6. https://doi.org/10.1016/j.actatropica.2008.09.006
24. Kang JM, Lee J, Cho PY, et al. Dynamic changes of *Plasmodium vivax* population structure in South Korea. Infect Genet Evol 2016;45:90-4. https://doi.org/10.1016/j.meegid.2016.08.023
25. Kumar S, Stecher G, Tamura K. MEGA7: molecular evolutionary genetics analysis version 7.0 for bigger datasets. Mol Biol Evol 2016;33:1870-4. https://doi.org/10.1093/molbev/msw054
26. Excoffier L, Lischer HEL. Arlequin suite ver 3.5: a new series of programs to perform population genetics analyses under Linux and Windows. Mol Ecol Resour 2010;10:564-7. https://doi.org/10.1111/j.1755-0998.2010.02847.x
27. Na BK, Lee HW, Moon SU, et al. Genetic variations of the dihydrofolate reductase gene of *Plasmodium vivax* in Mandalay division, Myanmar. Parasitol Res 2005;96:321-5. https://doi.org/10.1007/s00436-005-1364-0
28. Camponovo F, Buckee CO, Taylor AR. Measurably recombining malaria parasites. Trends Parasitol 2023;39:17-25. https://doi.org/10.1016/j.pt.2022.11.002
29. Rougeron V, Elguero E, Arnathau C, et al. Human *Plasmodium vivax* diversity, population structure and evolutionary origin. PLoS Negl Trop Dis 2020;14:e0008072. https://doi.org/10.1371/journal.pntd.0008072
30. Kang JM, Lê HG, Võ TC, et al. Genetic polymorphism and natural selection of apical membrane antigen-1 in *Plasmodium falciparum* isolates from Vietnam. Genes (Basel) 2021;12:1903. https://doi.org/10.3390/genes12121903
31. Võ TC, Trinh NTM, Lê HG, et al. Genetic diversity of circumsporozoite surface protein of *Plasmodium vivax* from the Central Highlands, Vietnam. Pathogens 2022;11:1158. https://doi.org/10.3390/pathogens11101158
32. Võ TC, Lê HG, Kang JM, et al. Genetic polymorphism and natural selection of the erythrocyte binding antigen 175 region II in *Plasmodium falciparum* populations from Myanmar and Vietnam. Sci Rep 2023;13:20025. https://doi.org/10.1038/s41598-023-47275-6
33. Võ TC, Lê HG, Kang JM, et al. Genetic polymorphism of merozoite surface protein 1 and merozoite surface protein 2 in the Vietnam *Plasmodium falciparum* population. BMC Infect Dis 2024;24:1216. https://doi.org/10.1186/s12879-024-10116-6
34. Võ TC, Lê HG, Kang JM, et al. Genetic diversity and natural selection of circumsporozoite surface protein in Vietnam *Plasmodium falciparum* isolates. Malar J 2025;24:320. https://doi.org/10.1186/s12936-025-05585-2

Original Article

Parasites Hosts Dis 2026;64(1):62-69
https://doi.org/10.3347/PHD.25052

Parasites, Hosts and Diseases

pISSN 2982-5164 • eISSN 2982-6799

Genotyping of *Blastocystis* species in hemodialysis patients from Makkah, Saudi Arabia

Hattan S. Gattan[1,2], Ebtihal O. Bahwaireth[3], Majed H. Wakid[1,2,*], Muslimah N. Alsulami[4], Mohammed A. Al-Matary[5,6], Asmaa M. El-Kady[7]

[1]Department of Medical Laboratory Sciences, Faculty of Applied Medical Sciences, King Abdulaziz University, Jeddah, Saudi Arabia; [2]Special Infectious Agents Unit, King Fahd Medical Research Center, King Abdulaziz University, Jeddah, Saudi; [3]Microbiology Section, Department of Pathology and Laboratory Medicine, King Faisal Specialist Hospital & Research Centre, Jeddah, Saudi Arabia; [4]Department of Biological Sciences, College of Science, University of Jeddah, Jeddah, Saudi Arabia; [5]Department of Biological Sciences, Faculty of Science, King Abdulaziz University, Jeddah, Saudi Arabia; [6]Department of Animal Production, Faculty of Agriculture, Sana'a University, Sana'a, Yemen; [7]Department of Medical Parasitology, Faculty of Medicine, South Valley University, Qena, Egypt

The human gut is host to a diversity of microorganisms, including a parasite called *Blastocystis*. While there are increasing reports characterizing *Blastocystis* subtypes (STs) among healthy individuals, only a few studies have investigated the *Blastocystis* STs in renal or dialysis patients. This study investigates the *Blastocystis* prevalence and STs in hemodialysis patients. Fifty healthy controls and 100 chronic kidney disease patients undergoing dialysis participated in the study. *Blastocystis* infection was identified by using microscopic and molecular diagnosis using 18S rRNA-PCR. Then all positive samples were sent for sequencing to identify which ST they belong to. Phylogenetic and pairwise distance analyses were performed to confirm the validity of the STs. Thirty-four hemodialysis patients were infected with *Blastocystis* while 17 patients in the control were infected with the parasite. All positive samples were then confirmed using PCR. Genetic sequencing analysis subsequently revealed that 66% of *Blastocystis* infection belonged to ST1 and ST3 (33% each), followed by ST10 (20%), and ST6 (14%). The nucleotide sequence analysis of the 385 bp 18S rRNA gene revealed a >97% identity with previously identified *Blastocystis* isolates. The genetic analysis showed that the 8 identified isolates correspond to previously observed alleles. Six ST1 isolates produced a high frequency of *Blastocystis* isolates matching allele 4, with very low genetic divergence. ST3 isolates showed relatively increased genetic diversity and matching allele 34, which is the most common allele worldwide.

Keywords: *Blastocystis hominis*, parasites, genotype, hemodialysis

Introduction

Blastocystis is a protozoan parasite that could infect both humans and animals. It was first reported in 1912 from human stool samples and diagnosed as a yeast but now it is classified as an intestinal parasite. Most of the infection is believed to be asymptomatic; however, some of the infected cases shown symptoms [1]. It is believed that *Blastocystis* may contribute to bowel disorders such as irritable bowel syndrome and inflammatory bowel disease [2].

Significant genetic diversity has been observed among various *Blastocystis* sp. strains isolated from different hosts [3]. Thirty-eight subtypes (STs; ST1–ST38) have been obtained from humans and animals worldwide [4,5], while other STs have

Received: July 2, 2025 Accepted: October 27, 2025
*Correspondence: mwakid@kau.edu.sa

Citation
Gattan HS, Bahwaireth EO, Wakid MH, Alsulami MN, Al-Matary MA, El-Kady AM. Genotyping of *Blastocystis* species in hemodialysis patients from Makkah, Saudi Arabia. Parasites Hosts Dis 2026;64(1):62-69.

been found only in animals [6]. It appears that STs 1, 2, 3 and 4 are the most common in human while the other 10 STs are frequently detected in other various animal groups such as birds and hoofed animals [6,7]. Different epidemiological aspects have been investigated by molecular studies such as transmission route, host specificity, and chemotherapeutic drug resistance.

Hemodialysis (HD) patients are highly vulnerable to severe infections since there are immunosuppressed. These patients are immunocompromised for various reasons, including the impairment of granulocyte and lymphocyte functions due to uremic toxins and malnutrition.

Due to weakened immunity, HD patients are more susceptible to various parasitic infections that can negatively affect their quality of life [8]. Studies on the prevalence of parasitic infections among HD patients in Brazil, Turkey, Iran, and Saudi Arabia have revealed that *Blastocystis* sp. is among the most frequently identified microorganisms, in addition to *Cryptosporidium*, *Endolimax nana*, *Entamoeba coli*, *Entamoeba histolytica*, and *Entamoeba dispar*, and *Giardia lamblia* [9-12]. Despite the significant burden of *Blastocystis* sp. in humans, there is limited molecular research available that provides data on the prevalence and distribution of its STs in the Saudi population [13,14]. To date, no data are available on the prevalence and genotyping of *Blastocystis* in Saudi HD patients. Therefore, in this study, we aimed to investigate the *Blastocystis* prevalence and to identify the parasite STs in HD patients.

Methods

Ethics statement

The study was conducted after ethical approval (No.1439-280594) from the Medical Ethics Committee of the Saudi Ministry of Health, Makkah, Saudi Arabia, and informed consent form was signed by each participant.

Samples collections

The samples of the present study were collected from Saudi patients attending Al-Noor Specialist Hospital and King Faisal Hospital in Makkah, Saudi Arabia. Fifty healthy controls and 100 chronic kidney disease Saudi patients undergoing dialysis participated in the study. Each participant provided a stool sample in a clean dry container labelled with the patient's name, then each sample was subjected to microscopic and molecular examinations.

Microscopic examination

The first step was the microscopic examination to detect the presence of *Blastocystis* using direct smears, formol-ether concentration technique (Ritchie), and trichrome stating, as previously described [15].

Primer design

Different *Blastocystis hominis* 18S ribosomal RNA gene sequences were extracted from GenBank (https://www.ncbi.nlm.nih.gov/nucleotide/) and aligned using Clustal W to look for conserved regions for primer design. After the alignment was done, the best pair of primers were chosen and then checked using Primer blast to check the annealing temperature and the GC percentage (Table 1).

DNA extraction and PCR amplification

Samples tested for *Blastocystis* underwent DNA extraction, PCR, and sequencing. DNA was extracted from stool samples using the QIAamp Fast DNA Stool Mini Kit (Qiagen), following the manufacturer's instructions. PCR was done using specific primers for *Blastocystis* amplifying 18S rRNA gene. The PCR conditions were as follows: The standard protocols followed for amplification that was: denaturation (95°C) for 5 min, 40 cycles for 40 sec at 95°C, annealing at a temperature 52°C for 40 sec, elongation at 72°C for 1 min with final elongation at 72°C for 10 min. Then electrophoresis on 1.5% agarose gels was used to isolate PCR products which were then visualized using UV. A 385-bp band was produced by positive *Blastocystis* sp. samples.

Sequencing and phylogenetic analysis

Eight positive 18S rRNA-PCR samples (385 bp) were selected and purified using the QIAquick PCR Purification Kit (Qiagen). These purified samples were then subjected to Sanger DNA sequencing with an automated DNA sequencer (ABI 3730XL DNA Analyzer). The sequences were analyzed using DNA BaserV3 software (Heracle BioSoft SRL).

Table 1. PCR primers specific for 18S rRNA gene of *Blastocystis hominis*

Primer	Sequence (5'–3')	Target *Blastocystis* subtype	Specificity	Annealing temperature (°C)	Product size (bp)
18S rRNAF	ACTGCGAATGGCTCATTATAT	All	18S rRNA	54	385
18S rRNAR	GCATTGTGATTTATTGTCACTACC	All	18S rRNA	54	385

The sequence similarity was performed using BLASTN search in GenBank (http://www.ncbi.nlm.nih.gov/BLAST). Subtyping of *Blastocystis* sp. was done by uploading sequences data to PubMLST through the web interface (https://pubmlst.org).

The alignment of small subunit ribosomal RNA sequences was conducted using the ClustalW in the MEGA version 12 (https://megasoftware.net) and gaps and ambiguous sequences were removed by ocular inspection. Phylogenetic analyses using the neighbor-joining method and pairwise distances were performed. The phylogenetic tree for partial 18S rRNA sequences of *Blastocystis* sp. was constructed using the neighbor-joining method in MEGA. The Kimura 2-parameter model was applied, and bootstrap analysis with 1,000 replicates was performed to assess the reliability of the tree.

Statistical analysis

The collected data were analysed using IBM SPSS version 25 (IBM Corp.). Chi-square test was used to analyse categorical variables and *P*-value of <0.05 was considered significant. Kappa coefficient was used to measure reliability for different techniques used in the present study.

Results

A total of 150 stool samples were collected from 100 HD patients (mean ± SD, 51.57 ± 10.5 years) and 50 healthy controls (mean ± SD, 39.66 ± 11.9 years). Most of the HD patients and control were male (55 out of 100 HD patients and 34 out of 50 control). Some HD patients and control cases had gastrointestinal manifestations as abdominal pain, nausea, vomiting, and diarrhoea as shown in Table 2.

All stool samples were examined for the presence of *Blastocystis* by microscopy and conventional PCR. Microscopic examination showed that 34% (34/100) of the HD patients were infected with *B. hominis* in comparison to 34% (17/50) of the healthy control who were infected with the parasite (Table 3).

Among HD patients, using direct smear, *Blastocystis* was detected in 31 cases (31%), while Ritchie technique detected *Blastocystis* in 20 cases (20%). PCR diagnosed *Blastocystis* in 31 participants (31%). The total number of infected participants detected by all techniques was 34 (34%).

As shown in Table 4, when direct smears proposed to be the gold standard method for detection, substantial agreement (0.764) was found with Ritchie technique, and perfect agreement (0.831) with real-time PCR. However, when Ritchie technique assumed to be the gold standard, substantial agreement was found with direct smears and real-time PCR. Then, when real-time PCR was nominated to be the gold standard, fair agreement was found with direct smears, and substantial agreement with Ritchie technique.

Among the 34 HD patients infected with *Blastocystis*, males were at a higher percentage (21/55, 38.2%) compared to females (13/45, 29.9%). Table 5 shows the distribution of clinical characteristics (abdominal pain, nausea, vomiting, and diarrhoea) among HD patients. *Blastocystis* infection was more commonly associated with abdominal pain (64.7%) than other gastrointestinal symptoms. There were no statistically significant differences between the 2 groups in any of the variables studied, including gender ($P=0.329$), abdominal pain ($P=0.689$), nausea ($P=0.666$), vomiting ($P=0.948$), and diarrhoea ($P=0.758$).

DNA was extracted from all the positive samples, then PCR amplification of the 18S rRNA gene was successfully done for all samples (Fig. 1). Then, all the PCR products were sent to

Table 2. Demographic and gastrointestinal characteristics of the study group

Variable		Hemodialysis patients ($n=100$)	Normal control ($n=50$)	*P*-value
Age (yr)		51.57 ± 10.5	39.66+11.9	-
Sex	Male	55	34	0.127
	Female	45	16	
Abdominal pain	Yes	62	20	0.010
	No	38	30	
Nausea	Yes	47	17	0.130
	No	53	33	
Vomiting	Yes	29	4	0.003
	No	71	46	
Diarrhoea	Yes	42	11	0.016
	No	58	39	

Values are presented as mean±SD or number.

Table 3. *Blastocystis* infection among hemodialysis cases and healthy controls according to sex

	Hemodialysis patients			Normal control		
	Female ($n=45$)	Male ($n=55$)	Total ($n=100$)	Female ($n=16$)	Male ($n=34$)	Total ($n=50$)
Positive	13	21	34	7	10	17
Negative	32	34	66	9	24	33

https://doi.org/10.3347/PHD.25052

Table 4. Agreement between techniques used to detect *Blastocystis hominis*, in relation to direct smears, Ritchie technique, and real-time PCR

			N	P	κ	Agreement
Direct smears	Ritchie technique	N	$^{TN}103$	$^{FN}14$	0.764	Substantial
		P	$^{FP}0$	$^{TP}33$		
	Real-time PCR	N	$^{TN}97$	$^{FN}5$	0.831	Perfect
		P	$^{FP}6$	$^{TP}42$		
Ritchie technique	Direct smears	N	$^{TN}103$	$^{FN}0$	0.764	Substantial
		P	$^{FP}14$	$^{TP}33$		
	Real-time PCR	N	$^{TN}99$	$^{FN}3$	0.649	Substantial
		P	$^{FP}18$	$^{TP}30$		
Real-time PCR	Direct smears	N	$^{TN}97$	$^{FN}6$	0.831	Perfect
		P	$^{FP}5$	$^{TP}42$		
	Ritchie technique	N	$^{TN}99$	$^{FN}18$	0.649	Substantial
		P	$^{FP}3$	$^{TP}30$		

N, negative; P, positive; κ, kappa coefficient; TN, true negative; FN, false negative; FP, false positive; TP, true positive.

Table 5. Sex and clinical characters of hemodialysis patients

Variable		Positive ($n=34$)	Negative ($n=66$)	*P*-value
Sex	Male	21	34	0.329
	Female	13	32	
Abdominal pain	Yes	22	40	0.689
	No	12	26	
Nausea	Yes	17	30	0.666
	No	17	36	
Vomiting	Yes	10	19	0.948
	No	24	47	
Diarrhoea	Yes	15	27	0.758
	No	19	39	

Values are presented as number.

Macrogen for sequencing. Eight different sequences were obtained. The obtained sequences were analysed using BLASTN software for comparison with the 18S rRNA sequences deposited in the GenBank. The nucleotide sequence analysis of the 385 bp 18S rRNA gene revealed a >97% identity with previously identified *Blastocystis* isolates. Sequence analysis showed that the majority of *Blastocystis* isolated in the present study belong to *Blastocystis* sp. ST1 (33%) and ST3 (33%). ST10 was identified in 20% and ST6 in 14% of samples. The results of allele discrimination revealed the presence of alleles 4 in all ST1 samples. ST3 exhibited alleles 34, 38, and 59. ST6 represented alleles 122 only. The only ST10 was allele 152.

The phylogenetic analysis of *Blastocystis* sp. revealed that 6 different sequences were on the same clade as *Blastocystis* ST1 and 2 sequences were placed on the same clade as *Blastocystis* ST3 (Fig. 1). Two zoonotic STs, ST1 (6/8, 75%) and ST3 (2/8, 25%) were detected in this study. Among them, ST1 infection was the predominant and the related isolates were placed on 2 branches of the same clade as ST1b and ST1c with 37% nodal support (Fig. 2). Further, the phylogenetic tree revealed that *Blastocystis* isolates in the present study were most closely related to *Blastocystis* isolates from Thailand and grouped with isolates from the Middle East, Asia, North Africia, Ecuador, Spain, and the Dominican Republic.

As shown in Fig. 3, the pairwise distance of the *Blastocystis* sequences obtained in this study revealed that the overall mean distance is 0.25, and between them and the previous Saudi *Blastocystis* sequence (OL375688) retrieved from the GenBank database is 0.29. The 8 nucleotide sequences generated in this study have been deposited in GenBank under accession numbers OP901517 to OP901524. The sequence identity of OP901519 and OP901520 was 100% and ranged from 99.4%–99.9% among the remaining 6 sequences.

Discussion

In the current study, 22 out of 34 *Blastocystis* positive HD participants (64.7%) were complaining of abdominal pain. Regarding other symptoms including diarrhea, nausea and vomiting, *Blastocystis* infection was diagnosed more in asymptomatic cases. The pathogenic potential of *Blastocystis* remains controversial, as the parasite has been found in both symptomatic and asymptomatic cases in several investigations worldwide [13-20].

According to earlier findings, ST1 and ST3 are the STs that are most commonly seen in both humans and animals [21,22]. In Saudi Arabia, 4 STs (ST1, ST2, ST3, and ST5) have

Fig. 1. Electropherogram of the 1.5% agarose gel showing 385 bp PCR product of the 18S rRNA was successfully amplified for all the samples from hemodialysis patients. Arrow indicates band size. L, ladder.

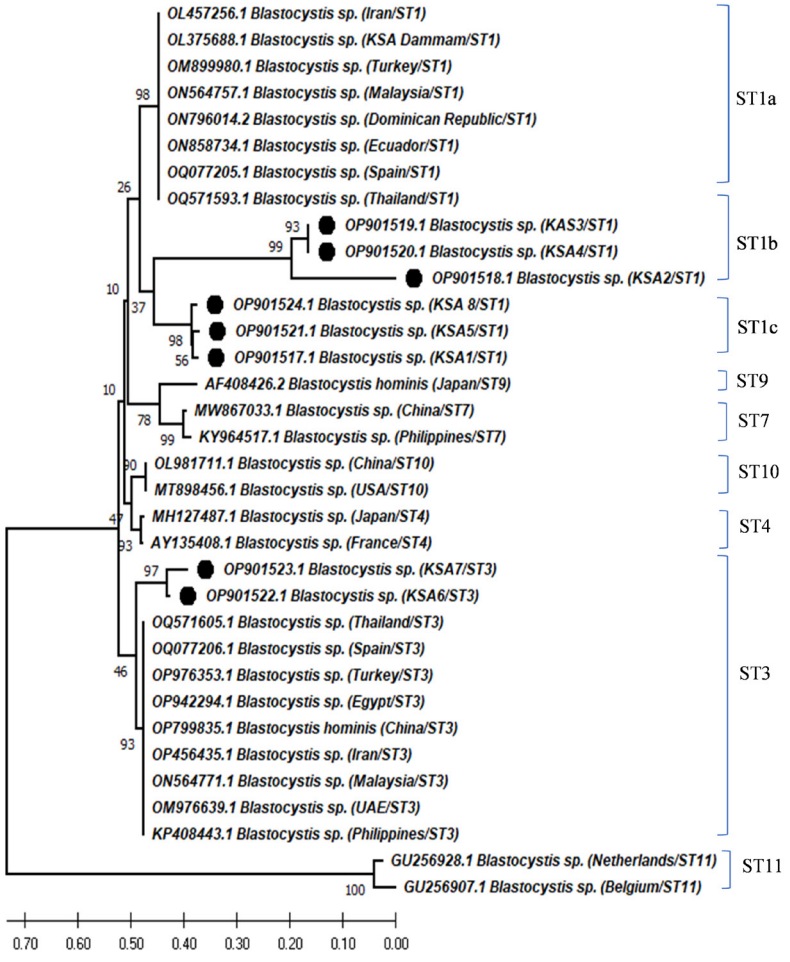

Fig. 2. Neighbor-joining tree of *Blastocystis* sp. based on the 18S rRNA nucleotide sequences showing the phylogenetic relationship of *Blastocystis* sp. collected in Saudi Arabia in the present study (black circles) with other *Blastocystis* isolates available in GenBank. The tree was constructed using the Kimura-2-parameter model. Bootstrap values are shown at the nodes of branches (1,000 replicates). Each sequence was identified by its GenBank accession number, country, and subtype (ST).

https://doi.org/10.3347/PHD.25052

		1	2	3	4	5	6	7	8	9
1	OL375688.1 *Blastocystis* sp. (KSA Dammam/ST1)		0.17	0.17	0.26	0.03	0.03	0.03	0.06	0.06
2	OP901519.1 *Blastocystis* sp. (KAS3/ST1)	0.41		0.00	0.09	0.16	0.16	0.16	0.17	0.16
3	OP901520.1 *Blastocystis* sp. (KSA4/ST1)	0.41	0.00		0.09	0.16	0.16	0.16	0.17	0.16
4	OP901518.1 *Blastocystis* sp. (KSA2/ST1)	0.58	0.23	0.23		0.24	0.24	0.24	0.24	0.24
5	OP901524.1 *Blastocystis* sp. (KSA8/ST1)	0.11	0.39	0.39	0.56		0.01	0.01	0.06	0.06
6	OP901521.1 *Blastocystis* sp. (KSA5/ST1)	0.11	0.40	0.40	0.56	0.02		0.01	0.06	0.06
7	OP901517.1 *Blastocystis* sp. (KSA1/ST1)	0.11	0.40	0.40	0.56	0.02	0.02		0.06	0.06
8	OP901523.1 *Blastocystis* sp. (KSA7/ST3)	0.23	0.37	0.37	0.51	0.23	0.21	0.22		0.01
9	OP901522.1 *Blastocystis* sp. (KSA6/ST3)	0.20	0.36	0.36	0.52	0.22	0.21	0.21	0.04	

Fig. 3. Pairwise distances between *Blastocystis* isolates of this study, and *Blastocystis* sp. (OL375688) partial-length 18S rRNA gene sequence showing the number of base substitutions per site from between sequences. Analyses were conducted using the maximum composite likelihood model and included 9 nucleotide sequences. Codon positions included were 1st+2nd+3rd+noncoding. All positions containing gaps and missing data were eliminated. There was a total of 257 positions in the final dataset.

been detected at varying frequencies using PCR and sequencing in some studies that investigated the occurrence and subtyping of *Blastocystis* sp., primarily in Makkah and Taif [13,14]. However, using genetic analysis of *Blastocystis* isolates, 2 STs of *Blastocystis* sp. were identified in this study: ST1 and ST3. Of these, ST1 was the most widely distributed (75%) and ST3 was the least (25%). Previous research in Saudi Arabia [13], Libya [21], Turkey [23], United Arab Emirates [24], Iran [25], and Syria [26], have shown similar results. In contrast, previous studies have reported that the most distributed ST was ST3 followed by ST1 or ST4 [27-32]. The high frequency of *Blastocystis* ST1 and ST3 infections in Saudi patients shows that the majority of infections are passed between persons. Several previous studies reported that ST1 and ST3 are associated to gastrointestinal symptoms, such as abdominal pain, diarrhoea, vomiting, and flatulence [3,20,26,29,33,34].

In the present study, the genetic analysis showed that the 8 identified isolates correspond to previously observed alleles. Six ST1 isolates produced a high frequency of *Blastocystis* isolates matching allele 4, with very low (0.04) genetic divergence. ST3 isolates ($n=2$) showed relatively increased genetic diversity (various nucleotide substitution ranged from 0.021 to 0.56) and matching allele 34 (the most common allele worldwide). In Egypt, ST1 and ST2 isolates were found with genetic diversity ranging from 1 to 11 nucleotide substitutions and ST3 isolates were found with low genetic divergence over 4 nucleotide substitutions [27]. Another study reported that among 11samples analysed, ST1 allele 4, ST2 alleles 9 and 12, and ST3 allele 34 were detected, with ST2 isolates showing low genetic diversity and numerous nucleotide changes [30].

Phylogenetic analysis of the 18S rRNA gene is useful for characterizing *Blastocystis* sp. Eight 18S rRNA sequences from Makkah were identified as *Blastocystis* sp. The phylogenetic tree based on 18S rRNA was beneficial in inferring the association between Saudi isolates from diverse regions, with a high bootstrap value. The Saudi isolates in this investigation and those received from GenBank were divided into 4 branches, and the collected isolates were divided into 3 haplotypes, ST1b, ST1c, and ST3. Furthermore, the examination of *Blastocystis* sp. 18S rRNA revealed genetic diversity within a single host, with at least 4 groups from different localities (this study and Dammam). This Saudi pattern illustrates how various *Blastocystis* genotypes have distinct geographic distributions in patients and exhibit diverse spreads in the Saudi Arabia. A previous study conducted in Egypt found that each *Blastocystis* sp. STs constituted a separate clade and that, based on phylogenetic analysis, the 11 *Blastocystis* sequences grouped into 3 STs (ST1, ST2, and ST3) with strong bootstrap value [30]. In another study, the same phylogenetic pattern was reported with ST1 and ST3 clusters in patients with irritable bowel syndrome [35]. The coevolution patterns between the parasite and its host are probably reflected in the phylogenetic analysis of genetically diverse *Blastocystis* isolates that differed in their ancestral and epidemiological characteristics.

The current study lacks information regarding environmental or animal contact. Future epidemiological studies are needed to evaluate the influence of environmental factors, animal interactions, and foreign travel history to determine the persistence of *Blastocystis*.

Author contributions

Conceptualization: Bahwaireth EO, Wakid MH, Alsulami MN, Al-Matary MA. Data curation: Gattan HS, Bahwaireth EO, Wakid MH, Al-Matary MA, El-Kady AM. Formal analysis: Gattan HS, Bahwaireth EO, Wakid MH, Alsulami MN, Al-Matary MA, El-Kady AM. Funding acquisition: Bahwaireth EO. Inves-

tigation: Gattan HS, Bahwaireth EO, Wakid MH, Alsulami MN, Al-Matary MA, El-Kady AM. Methodology: Bahwaireth EO, Wakid MH, Alsulami MN, Al-Matary MA. Project administration: Wakid MH. Software: Bahwaireth EO. Supervision: Wakid MH. Writing – original draft: Gattan HS, Bahwaireth EO, Alsulami MN, Al-Matary MA, El-Kady AM. Writing – review & editing: Wakid MH.

Conflict of interest

The authors have no conflicts of interest to declare.

Acknowledgments

The authors are very thankful to all the associated personnel for their beneficial help and cooperation.

ORCID

Hattan S. Gattan, https://orcid.org/0000-0003-3514-4912
Ebtihal O. Bahwaireth, https://orcid.org/0000-0001-5899-1351
Majed H. Wakid, https://orcid.org/0000-0003-4941-5373
Muslimah N. Alsulami, https://orcid.org/0000-0002-0447-8963
Mohammed A. Al-Matary, https://orcid.org/0009-0002-3129-1261
Asmaa M. El-Kady, https://orcid.org/0000-0002-9294-2630

References

1. Alqarni AS, Wakid MH, Gattan HS. Prevalence, type of infections and comparative analysis of detection techniques of intestinal parasites in the province of Belgarn, Saudi Arabia. PeerJ 2022;10:e13889. https://doi.org/10.7717/peerj.13889
2. Nagel R, Traub RJ, Allcock RJ, Kwan MM, Bielefeldt-Ohmann H. Comparison of faecal microbiota in *Blastocystis*-positive and *Blastocystis*-negative irritable bowel syndrome patients. Microbiome 2016;4:47. https://doi.org/10.1186/s40168-016-0191-0
3. Khademvatan S, Masjedizadeh R, Yousefi-Razin E, et al. PCR-based molecular characterization of *Blastocystis hominis* subtypes in southwest of Iran. J Infect Public Health 2018;11:43-7. https://doi.org/10.1016/j.jiph.2017.03.009
4. Stensvold CR, Tan KSW, Clark CG. Blastocystis. Trends Parasitol 2020;36:315-6. https://doi.org/10.1016/j.pt.2019.12.008
5. Maloney J, Jang Y, Molokin A, George N, Santin M. Wide genetic diversity of *Blastocystis* in white-tailed deer (*Odocoileus virginianus*) from Maryland, USA. Microorganisms 2021;9:1343. https://doi.org/10.3390/microorganisms9061343
6. Bahrami F, Babaei E, Badirzadeh A, Rezaeiriabi T, Abdoli A. *Blastocystis*, urticaria, and skin disorders: review of the current evidences. Eur J Clin Microbiol Infect Dis 2020;39:1027-42. https://doi.org/10.1007/s10096-019-03793-8
7. Parkar U, Traub RJ, Kumar S, et al. Direct characterization of *Blastocystis* from faeces by PCR and evidence of zoonotic potential. Parasitology 2007;134:359-67. https://doi.org/10.1017/S0031182006001582
8. Bahwaireth EO, Wakid MH. Molecular, microscopic, and immunochromatographic detection of enteroparasitic infections in hemodialysis patients and related risk factors. Foodborne Pathog Dis 2022;19:830-8. https://doi.org/10.1089/fpd.2022.0024
9. Karadag G, Tamer GS, Dervisoglu E. Investigation of intestinal parasites in dialysis patients. Saudi Med J 2013;34:714-8.
10. Omrani VF, Fallahi Sh, Rostami A, et al. Prevalence of intestinal parasite infections and associated clinical symptoms among patients with end-stage renal disease undergoing hemodialysis. Infection 2015;43:537-44. https://doi.org/10.1007/s15010-015-0778-6
11. Rasti S, Hassanzadeh M, Hooshyar H, et al. Intestinal parasitic infections in different groups of immunocompromised patients in Kashan and Qom cities, central Iran. Scand J Gastroenterol 2017;52:738-41. https://doi.org/10.1080/00365521.2017.1308547
12. Gama NA, Adami YL, Lugon JR. Assessment of *Blastocystis* spp. infection in hemodialysis patients in two centers of the metropolitan area of Rio de Janeiro. J Kidney Treat Diagn 2018;1:49-52.
13. Mohamed RT, El-Bali MA, Mohamed AA, et al. Subtyping of *Blastocystis* sp. isolated from symptomatic and asymptomatic individuals in Makkah, Saudi Arabia. Parasit Vectors 2017;10:174. https://doi.org/10.1186/s13071-017-2114-8
14. Wakid MH, Aldahhasi WT, Alsulami MN, El-Kady AM, Elshabrawy HA. Identification and genetic characterization of *Blastocystis* species in patients from Makkah, Saudi Arabia. Infect Drug Resist 2022;15:491-501. https://doi.org/10.2147/IDR.S347220
15. Aldahhasi WT, Toulah FH, Wakid MH. Evaluation of common microscopic techniques for detection of *Blastocystis hominis*. J Egypt Soc Parasitol 2020;50:33-40. https://doi.org/10.21608/JESP.2020.88748
16. Abdulsalam AM, Ithoi I, Al-Mekhlafi HM, et al. Prevalence, predictors and clinical significance of *Blastocystis* sp. in Sebha, Libya. Parasit Vectors 2013;6:86. https://doi.org/10.1186/1756-3305-6-86
17. Shehab A, El-Sayad M, Allam A, et al. Insights into the association between *Blastocystis* infection and colorectal cancer. Acta Parasitol 2025;70:156. https://doi.org/10.1007/s11686-025-01079-y
18. Ahmed HK, Mohamed KA, Sheishaa GAA, et al. *Blastocystis* SPP. infection prevalence and associated patient characteristics as predictors among a cohort of symptomatic and asymptomatic Egyptians. Int J Health Sci 2022;6:5839-52. https://doi.org/10.53730/ijhs.v6nS6.10918
19. Sylla K, Sow D, Lelo S, et al. *Blastocystis* sp. infection: prevalence and clinical aspects among patients attending to the laboratory of

parasitology-mycology of Fann University Hospital, Dakar, Senegal. Parasitologia 2022;2:292-301. https://doi.org/10.3390/parasitologia2040024

20. Kaneda Y, Horiki N, Cheng XJ, et al. Ribodemes of *Blastocystis hominis* isolated in Japan. Am J Trop Med Hyg 2001;65:393-6. https://doi.org/10.4269/ajtmh.2001.65.393. PMID: 11693890
21. Abdulsalam AM, Ithoi I, Al-Mekhlafi HM, et al. Subtype distribution of *Blastocystis* isolates in Sebha, Libya. PLoS One 2013;8:e84372. https://doi.org/10.1371/journal.pone.0084372
22. Stensvold CR, Clark CG. Current status of *Blastocystis*: a personal view. Parasitol Int 2016;65:763-71. https://doi.org/10.1016/j.parint.2016.05.015
23. Eroglu F, Genc A, Elgun G, Koltas IS. Identification of *Blastocystis hominis* isolates from asymptomatic and symptomatic patients by PCR. Parasitol Res 2009;105:1589-92. https://doi.org/10.1007/s00436-009-1595-6
24. AbuOdeh R, Ezzedine S, Samie A, Stensvold CR, ElBakri A. Prevalence and subtype distribution of *Blastocystis* in healthy individuals in Sharjah, United Arab Emirates. Infect Genet Evol 2016;37:158-62. https://doi.org/10.1016/j.meegid.2015.11.021
25. Taghipour A, Javanmard E, Mirjalali H, et al. *Blastocystis* subtype 1 (allele 4); predominant subtype among tuberculosis patients in Iran. Comp Immunol Microbiol Infect Dis 2019;65:201-6. https://doi.org/10.1016/j.cimid.2019.06.005
26. Darwish B, Aboualchamat G, Al Nahhas S. Molecular characterization of *Blastocystis* subtypes in symptomatic patients from the southern region of Syria. PLoS One 2023;18:e0283291. https://doi.org/10.1371/journal.pone.0283291
27. Souppart L, Moussa H, Cian A, et al. Subtype analysis of *Blastocystis* isolates from symptomatic patients in Egypt. Parasitol Res 2010;106:505-11. https://doi.org/10.1007/s00436-009-1693-5
28. Greige S, El Safadi D, Khaled S, et al. First report on the prevalence and subtype distribution of *Blastocystis* sp. in dairy cattle in Lebanon and assessment of zoonotic transmission. Acta Trop 2019;194:23-9. https://doi.org/10.1016/j.actatropica.2019.02.013
29. Gulhan B, Aydin M, Demirkazik M, et al. Subtype distribution and molecular characterization of *Blastocystis* from hemodialysis patients in Turkey. J Infect Dev Ctries 2020;14:1448-54. https://doi.org/10.3855/jidc.12650
30. Ahmed SA, El-Mahallawy HS, Mohamed SF, et al. Subtypes and phylogenetic analysis of *Blastocystis* sp. isolates from West Ismailia, Egypt. Sci Rep 2022;12:19084. https://doi.org/10.1038/s41598-022-23360-0
31. Hatalová E, Babinská I, Gočálová A, Urbančíková I. Molecular screening for enteric parasites and subtyping of *Blastocystis* sp. in haemodialysis patients in Slovakia. Ann Agric Environ Med 2024;31:193-7. https://doi.org/10.26444/aaem/185634
32. Abdellatif MZM, Abdel-Hafeez EH, Belal US, et al. Detection of *Blastocystis* species in immunocompromised patients (cancer, diabetes mellitus, and chronic renal diseases) by restriction fragment length polymorphism (RFLP). Beni-Suef Univ J Basic Appl Sci 2025;14:42. https://doi.org/10.1186/s43088-025-00631-z
33. El Safadi D, Meloni D, Poirier P, et al. Molecular epidemiology of *Blastocystis* in Lebanon and correlation between subtype 1 and gastrointestinal symptoms. Am J Trop Med Hyg 2013;88:1203-6. https://doi.org/10.4269/ajtmh.12-0777
34. Matovelle C, Quílez J, Tejedor MT, et al. Subtype distribution of *Blastocystis* spp. in patients with gastrointestinal symptoms in Northern Spain. Microorganisms 2024;12:1084. https://doi.org/10.3390/microorganisms12061084
35. El-Badry AA, Abd El Wahab WM, Hamdy DA, Aboud A. *Blastocystis* subtypes isolated from irritable bowel syndrome patients and co-infection with *Helicobacter pylori*. Parasitol Res 2018;117:127-37. https://doi.org/10.1007/s00436-017-5679-4

Original Article

Parasites Hosts Dis 2026;64(1):70-81
https://doi.org/10.3347/PHD.25083

Parasites, Hosts and Diseases

pISSN 2982-5164 • eISSN 2982-6799

Development and validation of a species-specific loop-mediated isothermal amplification assay for rapid detection of *Perkinsus marinus*

S.D.N.K. Bathige[1,2], Seung-Hyeon Kim[1], Donghyun Lee[1], Hyung-Bae Jeon[3], Yu Chen[1,2], Kyung-Il Park[1,2,*]

[1]*Department of Aquatic Life Medicine, College of Ocean and Biosciences, Kunsan National University, Gunsan, Korea*
[2]*Research Institute of Fisheries Science in Offshore Wind Farms (RIFSO), Kunsan National University, Gunsan, Korea*
[3]*National Institute of Biological Resources, Incheon, Korea*

Perkinsus marinus is a major protozoan pathogen of oysters, responsible for severe mortality events and substantial economic losses in the global aquaculture industry. Rapid, sensitive, and reliable detection of this parasite is therefore essential for effective monitoring and timely control of dermo disease outbreaks. In this study, we developed and optimized a novel loop-mediated isothermal amplification (LAMP) assay, designated Pm-LAMP, for the specific detection of *P. marinus* in oyster tissues. The optimized Pm-LAMP assay, employing 5 primers and performed at 67°C, demonstrated high analytical sensitivity, consistently detecting DNA concentrations as low as 40 fg/µl and enabling accurate quantification down to 0.4 pg/µl. The assay exhibited linear amplification across a wide template range from 4 ng/µl to 0.4 pg/µl, with a strong inverse correlation between template concentration and threshold time. Specificity testing confirmed exclusive amplification of *P. marinus*, with no cross-reactivity observed for *P. olseni*, *P. honshuensis*, or *P. chesapeaki*. This study represents the first LAMP assay specifically designed for the detection of *P. marinus*. The Pm-LAMP assay was validated using Pacific oyster tissues and cultured *P. marinus* isolates originating from the USA and Korea and was benchmarked against quantitative real-time PCR (qPCR). Although qPCR exhibited higher sensitivity for detecting trace DNA levels, the Pm-LAMP assay produced results within 20 min while maintaining reliable detection at low DNA concentrations. Diagnostic performance evaluation showed 100% sensitivity and 90.91% specificity, with substantial agreement with qPCR (Cohen's κ=0.811). Overall, the Pm-LAMP assay provides a rapid, robust, and field-deployable diagnostic tool for *P. marinus*, supporting improved disease surveillance and sustainable oyster aquaculture management.

Keywords: *Perkinsus marinus*, oysters, LAMP assay, quantitative real-time PCR

Introduction

Perkinsus marinus, a protistan parasite, is the causative agent of "dermo" disease (perkinsosis), which leads to chronic infections and significant mortality in oyster populations. It poses a major threat to oyster aquaculture, particularly in the Eastern oyster (*Crassostrea virginica*) along the Atlantic and Gulf coasts of the USA. Due to its high pathogenicity and economic impact, *P. marinus* has been listed as a notifiable pathogen by the World Organization for Animal Health (WOAH). *P. marinus* was first identified on the Gulf Coast of Mexico in the 1940s [1], and has since been reported in various bivalve species [2,3], Eastern oyster (*C. virginica*) is recognized as the primary host of *P. marinus* [4]. Notably, *P. marinus* has also caused high mor-

Received: September 24, 2025 Accepted: October 29, 2025
*Correspondence: kipark@kunsan.ac.kr

Citation
Bathige SDNK, Kim SH, Lee D, Jeon HB, Chen Y, Park KI. Development and validation of a species-specific loop-mediated isothermal amplification assay for rapid detection of *Perkinsus marinus*. Parasites Hosts Dis 2026;64(1):70-81.

tality in Pacific oysters (*C. gigas*) in the Gulf of California [5]. More recently, its presence was confirmed in *C. gigas* along the west coast of Korea, albeit at low infection intensity [6]. The severity of *P. marinus* infections typically increases during the warmer summer months, contributing to substantial economic losses in oyster-producing regions.

Traditional diagnostic methods for *P. marinus*, including Ray's fluid thioglycollate medium (RFTM) assay, histology, and conventional PCR, have been used for decades. Among these, the RFTM assay is regarded as the WOAH-recommended gold standard for *P. marinus* diagnosis. Molecular methods such as conventional PCR [7] and in situ hybridization [8] offer improved specificity but require specialized instrumentation and laboratory workflows; by contrast, microscopy-based diagnostics (e.g., RFTM/histology) are labor-intensive and can be highly operator-dependent.

To address these limitations, quantitative real-time PCR (qPCR) has emerged as a powerful tool for sensitive and specific detection of *P. marinus* DNA. It has been increasingly adopted for quantitative surveillance of this pathogen [9,10]. Recently, we developed an advanced qPCR assay using newly designed primers and a TaqMan-based probe with an internal quencher (i-EBQ), which significantly improves detection sensitivity and reliability [11]. Although qPCR is highly effective, its reliance on thermocyclers and controlled laboratory conditions limits its deployment in field settings or low-resource environments.

In recent years, loop-mediated isothermal amplification (LAMP) has emerged as a promising alternative for rapid, cost-effective, and sensitive pathogen detection [12]. Unlike PCR-based techniques, LAMP amplifies DNA at a constant temperature using a strand-displacing DNA polymerase derived from *Geobacillus stearothermophilus* [13,14]. The LAMP reaction utilizes 4 core primers targeting 6 distinct regions of the target gene, with 2 additional loop primers to further enhance the speed and efficiency of amplification [15,16]. Advantages of LAMP include rapid amplification, minimal equipment requirements, and adaptability to field conditions. Amplification products can be detected via turbidity, color changes, or fluorescence, with real-time monitoring enabling quantification [17].

LAMP assays have been successfully developed for a wide range of aquatic pathogens, including *Perkinsus* spp. [18]. Feng et al. [19] developed a LAMP assay capable of detecting both *P. marinus* and *P. olseni*. Other groups have introduced species-specific LAMP assays for *P. olseni* using 4 or 6 primers [20]. A duplex LAMP assay for the simultaneous detection of *Perkinsus* and *Bonamia* spp. has also been reported [21]. However, to date, no LAMP assay has been developed to exclusively detect *P. marinus*, without cross-amplifying other *Perkinsus* species.

Here, we report the development and validation of a Pm-LAMP, species-specific LAMP assay targeting a *P. marinus* hypothetical-protein locus. We describe primer design and in silico specificity screening, optimization of isothermal conditions and primer combinations, and analytical evaluations (limit of detection and exclusivity) alongside diagnostic performance benchmarking against qPCR using cultured strains and oyster tissues from Korea and the USA. Our goal was to establish a rapid, instrument-lean workflow suitable for routine surveillance of *P. marinus* in aquaculture settings.

Methods

Ethics statement

Not applicable.

Tissue samples, cells, and DNA extraction

Pacific oyster samples ($n = 16$), collected from the West Coast of Korea, were used as environmental samples in this study. Additionally, 6 *P. marinus* strains from different locations in the United States were obtained from the American Type Culture Collection (ATCC), with the following ATCC numbers: 50894, 50509, 50510, 50787, 50766, and 50849. Two other *Perkinsus* species, *P. honshuensis* (ATCC PRA-176) and *P. chesapeaki* (ATCC PRA-65), were also sourced from ATCC. *P. olseni*, originally isolated from Manila clams (*Ruditapes philippinarum*) in our laboratory [22], was also included in the experiments. All cells were maintained in standard DMEM/F-12 medium following previously established protocols [22,23]. Total DNA was extracted from approximately 25 mg of mantle tissue or cultured cells using a commercial DNA extraction kit (Qiagen) following the manufacturer's protocol. The extracted DNA was stored at -20°C until further use.

Conventional PCR and qPCR

The presence of *P. marinus* in the mantle tissues of Pacific oysters and the 6 strains obtained from ATCC was confirmed via conventional PCR using species-specific primers developed by Audemard et al. [7] and recommended by World Organization for Animal Health [24] (Table 1) [11,16,25]. The PCR reaction was carried out in a 50-µl mixture containing 0.4 µM of each primer (forward: PmarITS-70F and reverse: PmarITS600R), 0.2 mM dNTP mix, 10× Taq reaction Buffer (SolGent), 1.25 U of Solg Taq DNA polymerase (SolGent), 5 µl of template DNA, and

Table 1. Primers used in this study

Experiment	Primer name	Primer sequence (5'→3')	Target gene	Reference
PCR	PmarITS-70F	CTTTTGYTWGAGWGTTGCGAGATG	ITS	[11,25]
	PmarITS600R	CGAGTTTGCGAGTACCTCKAGAG		
qPCR	PmHP-F	CCCAGTTCACAGTGCCTGTC	Hypothetical protein	[16]
	PmHP-R	CATGGAATGCCGAGGGTACA		
	PmHP-P	[FAM]AGCGTCAT[i-EBQ]CGGACCTCGTGCA[Phosphate]		
LAMP	PmF3	GACAGATCGTGGCCCAAG	Hypothetical protein	This study
	PmB3	CAACGGCCAAGGTATCGTAT		
	PmFIP	GGCGTTCACCGGAAAACAGTTGACTACGCTGTCACTCTCGG		
	PmBIP	CTGTCTCTTGTGAGCTCAGCGCCAAGCCATGGCCTCTGATG		
	PmLF	GTGGGTCCAATGATGTCTACGTT		
	PmLB	TGTCAATAGGATCGTAATTGCAGCT		

qPCR, quantitative real-time PCR; LAMP, loop-mediated isothermal amplification; ITS, internal transcribed spacer.

nuclease-free water to final volume 50 μl. PCR amplification was performed using a SimpliAmp Thermal cycler (Thermo Fisher Scientific) under the following cycling conditions: initial denaturation at 95°C for 4 min; 40 cycles of denaturation at 94°C for 1 min; annealing at 57°C for 1 min; elongation at 65°C for 3 min; followed by a final elongation at 65°C for 10 min. PCR products were analyzed by electrophoresis on a 1.5% agarose gel.

The qPCR assay for *P. marinus* (Pm-qPCR) was conducted using a recently developed assay [11]. Briefly, the 25-μl reaction mixture included 0.6 μM of each primer and 0.4 μM of probes targeting the hypothetical protein gene of *P. marinus* and the movement protein gene of the tobacco mosaic virus (used as an internal control, IC). The mixture also included 15 μl of AccuPower Dual-HotStart RT-qPCR Master Mix (Bioneer), 5 μl of sample DNA, and 1 μl of IC template DNA. Because the template was genomic DNA, no reverse-transcription step was performed; reactions were run as DNA qPCR using the manufacturer's Dual-HotStart mix. Amplification was performed on a CFX Opus 96 Real-Time PCR System (Bio-Rad Laboratories) with the following cycling conditions: 95°C for 5 min, then 45 cycles of 95°C for 10 sec and 55°C for 20 sec. Fluorescence was acquired on the FAM channel for *P. marinus* and the Cy5 channel for the IC. Result interpretation followed our prior validation [11]: positive if Ct ≤35.8 with a sigmoidal curve and valid IC; Negative if Ct >35.8 or no amplification by 45 cycles with a valid IC.

Design and in silico validation of specific LAMP primers for *P. marinus*

LAMP primers were designed using the online primer design tool developed by New England Biolabs (NEB, https://lamp.neb.com) with default parameters. A genomic DNA sequence coding for a hypothetical protein was selected from the whole-genome sequence database of *P. marinus* (GenBank accession No. NW_003206658.1, ATCC 50983 genomic scaffold scf_1104296958712) as the target gene. A total of 6 primers, including 2 outer (forward outer and backward outer), 2 inner (forward inner and backward inner), and 2 loop primers (loop forward [LF] and loop backward [LB]), were designed to recognize 8 distinct regions on the target gene or its complementary sequence (Table 1; Fig. 1A). To verify primer specificity, multiple sequence alignment was performed against homologous gene sequences of *P. olseni* and *P. chesapeaki* retrieved from NCBI GenBank database. The alignments were conducted using the MUSCLE algorithm within the Geneious Prime software version 2023.1.2 (Geneious).

Construction of standard *P. marinus* template

A 504-bp genomic DNA fragment of the target gene, encompassing the regions recognized by the designed LAMP primers, was custom-synthesized by Macrogen. The synthetic DNA fragment was subsequently cloned into the pMG-Amp vector (Macrogen) to serve as a standard template for the Pm-LAMP assay.

Real-time fluorometric Pm-LAMP assay setup

The Pm-LAMP reactions were carried out using a WarmStart LAMP kit (E1700L, NEB) designed for real-time fluorescence detection. The Pm-LAMP was conducted in a 20-μl reaction mixture containing 10 μl of WarmStart LAMP 2× Master Mix (NEB), 1.6 μM of each inner primer, 0.2 μM each outer primer, 0.4 μM each loop primers, 0.5 μl of 50× fluorescence dye, and either 1 μl of standard plasmid DNA or 5 μl of sample template DNA. PCR-grade water was added to bring the final volume to

https://doi.org/10.3347/PHD.25083

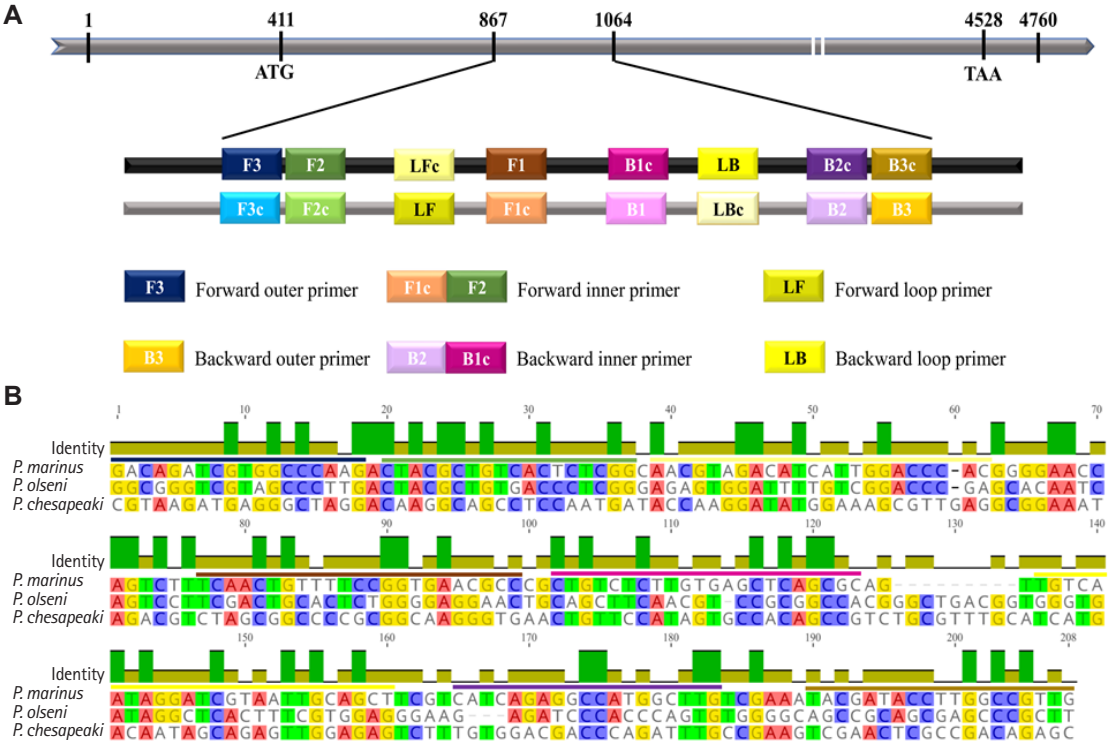

Fig. 1. Design of loop-mediated isothermal amplification (LAMP) primers specific for *Perkinsus marinus* based on the genomic sequence of a hypothetical protein. (A) Schematic representation of primers designed for the LAMP assay. Numbers in the grey bar represent the nucleotide positions. (B) Multiple sequence alignment performed using the MUSCLE algorithm, comparing with *P. marinus* and 2 related species, *P. olseni* and *P. chesapeaki*. Colored lines above the sequence indicate the designed primer regions, with sequence identity represented by a green bar.

20 μl. No-template controls (NTCs) included PCR-grade water instead of DNA to ensure the absence of non-specific amplification.

Amplification was performed isothermally at 65°C on a CFX Opus 96 Real-Time PCR detection system (Bio-Rad Laboratories) to record threshold-time (Tt) values and enable direct comparison with qPCR during assay optimization. Fluorescence was acquired every 30 sec on the FAM channel over a 30-min incubation at 65°C. For specificity confirmation, a post-amplification melting curve analysis was run from 65°C to 95°C in 0.5°C increments every 5 sec.

Pm-LAMP assay optimization

The optimal temperature for the Pm-LAMP assay was initially determined by conducting amplification reactions at temperatures ranging from 55°C to 70°C. Based on the results, 67°C was identified as optimal for subsequent experiments. To address non-specific amplification observed in the NTCs, additional optimization was conducted by modifying the standard Pm-LAMP protocol described in Section 2.5. Specifically, reactions were performed using 5 primers by excluding either the LF or the LB primers to assess their impact on non-specific amplification in NTCs. Amplification curves and melting peaks were analyzed, and Tt and melting temperature (Tm) values were recorded to evaluate the effectiveness and specificity of each reaction condition. After selecting the final configuration (5 primers, 67°C, LF omitted), we re-measured Tt and Tm; unless otherwise noted, all Tt and Tm values reported in the results refer to this finalized assay.

Sensitivity of Pm-LAMP assay

The sensitivity of the optimized Pm-LAMP assay, which uses a 5-primer system including the LB primer, was evaluated using 10-fold serial dilutions of standard *P. marinus* template DNA, with concentrations ranging from 4 ng/μl to 0.4 fg/μl. All reactions were conducted at 67°C using a real-time PCR system, and melting curve analysis was performed to confirm amplification specificity. Tt values obtained from each dilution were used to generate a standard curve, allowing the quantification of assay performance and determination of the detection limit.

Specificity of Pm-LAMP assay

The specificity of the optimized Pm-LAMP assay was tested using total DNA (approximately 50 ng/μl) extracted from *P. honshuensis* (ATCC PRA-176), *P. chesapeaki* (ATCC PRA-65), and *P. olseni*. This assay ensured that the Pm-LAMP assay exclusively detected *P. marinus* without cross-reactivity with other *Perkinsus* species.

Validation of Pm-LAMP assay

The Pm-LAMP assay was validated using tissue samples from 16 Pacific oysters collected from the West Coast of Korea, as well as 6 *P. marinus* strains obtained from ATCC. Additionally, a Korean *P. marinus* strain isolated from Pacific oysters [6] was included in the validation process. A 10-fold dilution series of the Korean *P. marinus* sample (56 ng/μl) was tested using both Pm-LAMP and qPCR assays. The optimized Pm-LAMP assay was employed to determine the Tt for each sample by measuring the fluorescence intensities of the amplified targets. Specific amplification was confirmed by evaluating the melting peaks. The results from the Pm-LAMP assay were then compared with those obtained from conventional PCR and/or qPCR to assess performance and reliability.

Data analysis

To validate the results, both amplification plots and melting peaks were thoroughly examined. Standard curve for the test was generated using Excel 2019 (Microsoft), and the coefficient of determination (R^2) was calculated to assess the quantification capability of the Pm-LAMP assay. For the optimized Pm-LAMP assay, clinical diagnostic sensitivity and specificity were estimated using a confusion matrix (2×2 contingency table) [26]. These metrics were compared against results from a recently developed qPCR assay [11]. In this analysis, samples that tested positive by both qPCR and LAMP were classified as true positives, while those that tested negative by both methods were classified as true negatives. Samples that were positive by LAMP but negative by qPCR were considered as false positives.

Cohen's kappa test was performed to assess the reliability of the optimized Pm-LAMP assay. Cohen's kappa coefficient (κ) was calculated using the GraphPad online statistical tool (https://www.graphpad.com/quickcalcs/kappa1/) with a 95% confidence interval. The κ-value ranges from 0 (indicating no agreement) to 1 (indicating perfect agreement). The κ-values were interpreted as follows: perfect agreement (0.81–1.00), substantial agreement (0.61–0.80), moderate agreement (0.41–0.60), and fair agreement (0.21–0.40).

Results

Development of specific LAMP primers for *P. marinus*

Multiple sequence alignment of the genomic DNA sequence of a hypothetical protein of *P. marinus* with corresponding regions of *P. olseni* and *P. chesapeaki* revealed a 198-bp region with high interspecific variations. Six specific LAMP primers were designed within this region, as depicted in Fig. 1B.

Optimization of Pm-LAMP assay

Temperature

The initial LAMP assay was performed at various temperatures ranging from 55°C to 70°C using 6 primers. The results revealed that the lowest Tt value was observed at 67.5°C (Fig. 2). Therefore, 67°C was selected as the optimal reaction temperature for the LAMP primers designed in this study, and all subsequent reactions were conducted at this temperature.

Five primers

During optimization at 67°C, the LAMP assay exhibited non-specific amplification in the NTC, as shown in Fig. 3A. To further refine the assay, 5-primer reactions were tested by excluding either the LF or LB primer. These reactions also produced non-specific amplification in the NTCs. Notably, when the LB primer was used (i.e., LF excluded), amplification in the NTCs was observed occasionally only after 50 cycles (Fig. 3B, C), suggesting improved specificity compared to other conditions. Further, distinct melting peaks were observed in the specific and non-specific amplifications. The Tm values for standards ranged from 86.5°C to 87.0°C, while those for the NTCs ranged from 88.5°C to 89.0°C, particularly when the LF primer was excluded (Fig. 3C). Based on these observations, the LAMP assay using the LB (without LF) was selected as the optimized method for detecting *P. marinus*. This optimized assay showed linear amplification across template concentrations from 4 ng/μl to 0.4 pg/μl (Fig. 4A), with a strong correlation between template concentration and Tt values (R^2 = 0.9987) (Fig. 4B). According to Fig. 4A, 0.4 pg/μl—the lowest concentration that could be accurately quantified—was amplified in under 34 cycles, which corresponds to approximately 17 min. This indicates that the LAMP assay is not only sensitive and quantitative but also rapid, making it suitable for timely detection of *P. marinus*.

Analytical specificity of the Pm-LAMP assay

Three species, *P. olseni*, *P. honshuensis*, and *P. chesapeaki*,

https://doi.org/10.3347/PHD.25083

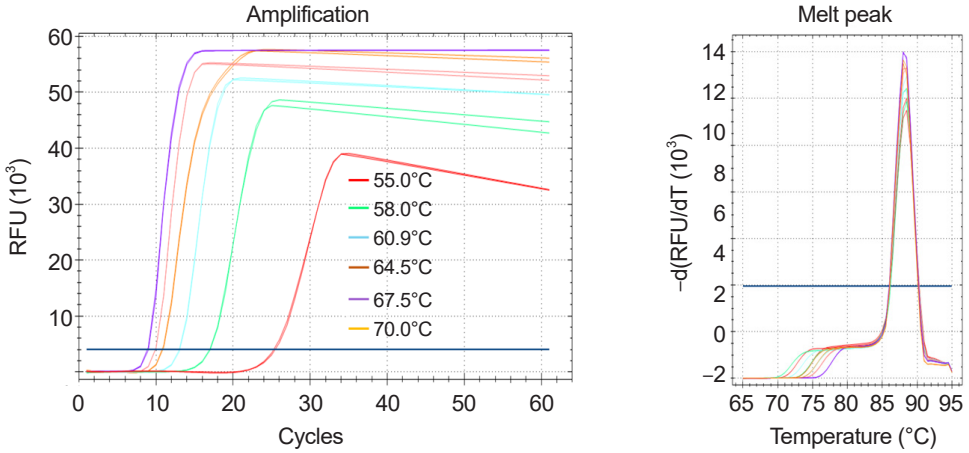

Fig. 2. Evaluation of optimum temperature for the Pm-LAMP (species-specific loop-mediated isothermal amplification assay targeting a *Perkinsus marinus* hypothetical-protein locus) assay. Amplification plots and melting peaks at different temperatures from 55°C to 70°C were assessed using temperature gradient. RFU, relative fluorescence units.

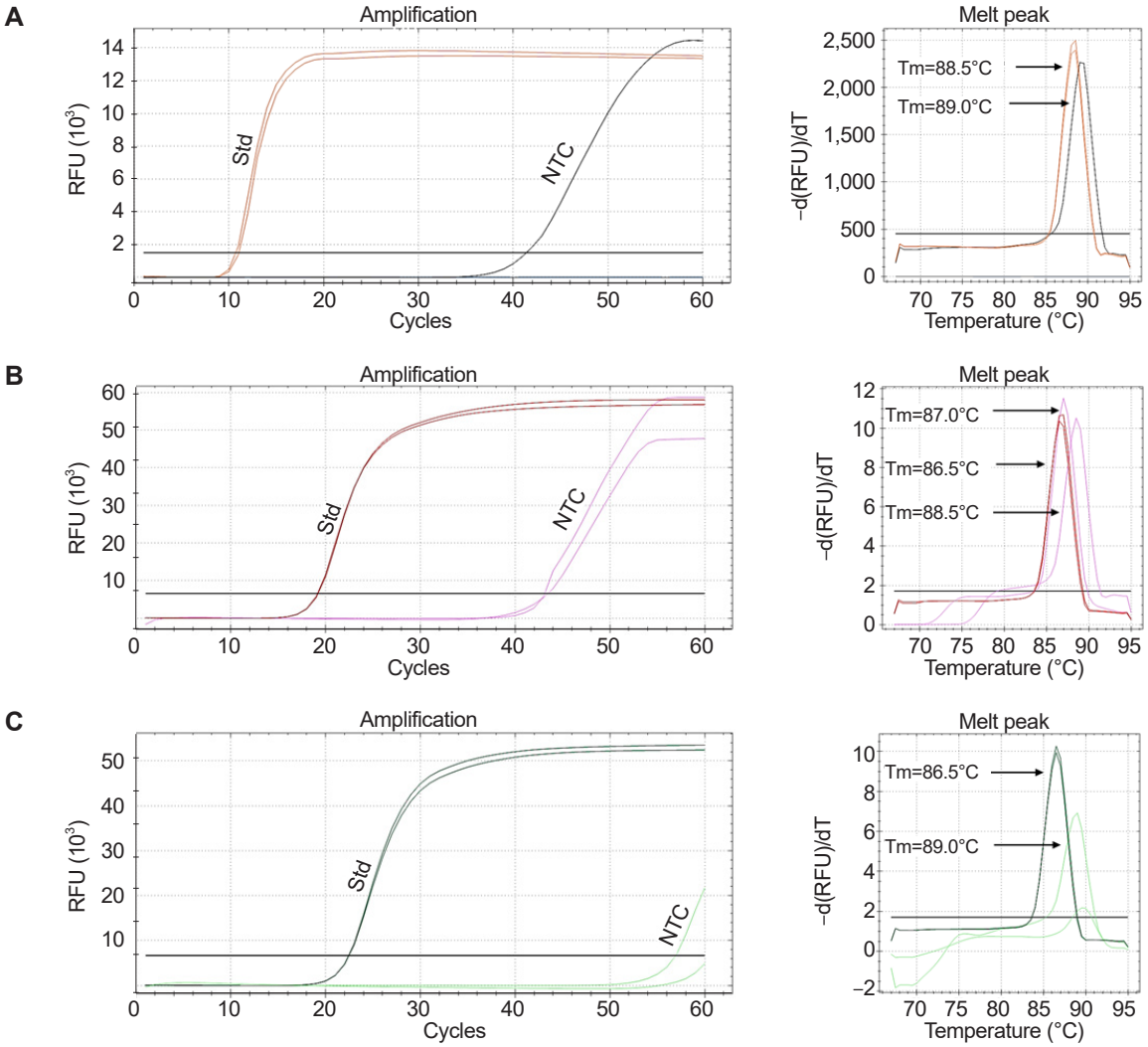

Fig. 3. Evaluation of Pm-LAMP (species-specific loop-mediated isothermal amplification [LAMP] assay targeting a *Perkinsus marinus* hypothetical-protein locus) with a combination of LAMP primers. Amplification plots and melting peaks for reaction with (A) 6 primers, (B) 5 primers (without loop backward) and (C) 5 primers (without loop forward). Amplification plots for the *P. marinus* standard (Std) and no template control (NTC) were marked. The melting temperature (Tm) of each melting peak of the standard and NTC is displayed. RFU, relative fluorescence units.

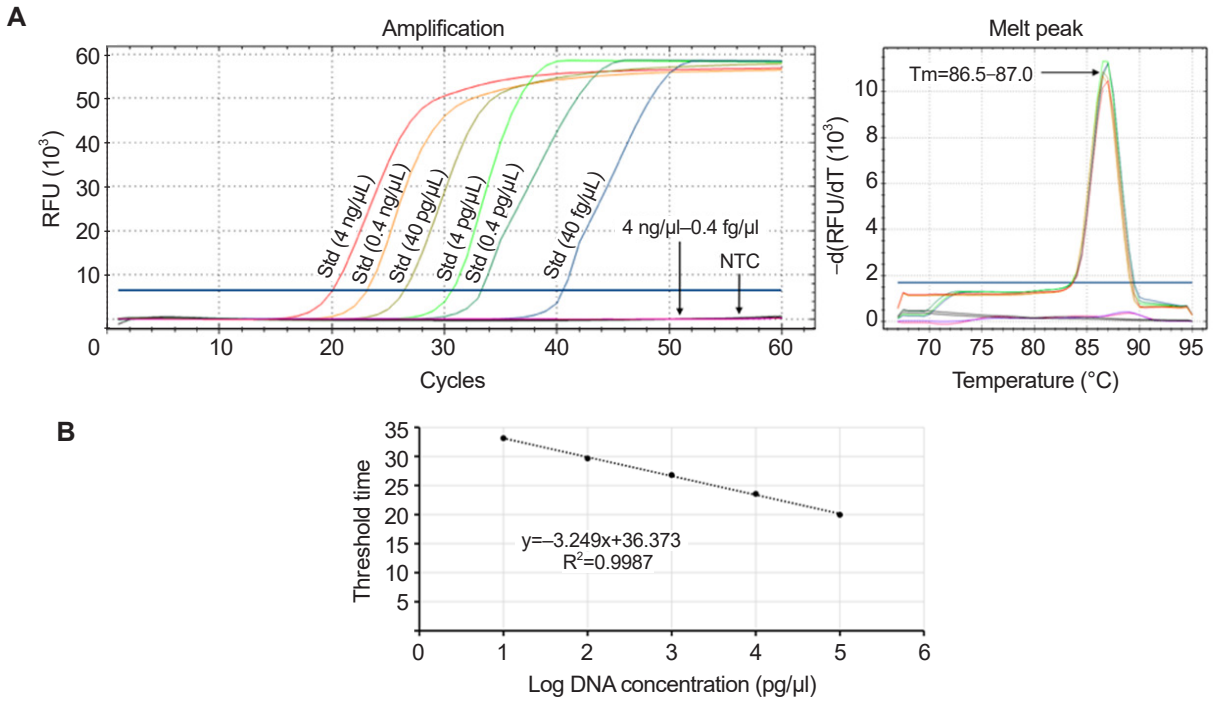

Fig. 4. Evaluation of limit of detection. (A) Amplification plots for a 10-fold dilution series of standards (4 ng/μl–0.4 fg/μl) without the loop forward primer. (B) Standard curve generated based on the threshold time and log value of corresponding template concentrations. RFU, relative fluorescence units; Std, standard; NTC, no template control.

were tested to assess the analytical specificity of the Pm-LAMP assay developed herein. No specific amplification was observed for any of these species, confirming the high specificity of the assay for *P. marinus* (Fig. 5; Table 2).

Evaluation of Pm-LAMP assay for *P. marinus* detection

The Pm-LAMP assay was successfully applied to 6 *P. marinus* strains and cultured cells isolated from the West Coast of Korea. Amplification was observed in all cases, and the specific product exhibited a single melting curve within 86.5°C–87.0°C (Table 2). Among 16 environmental oyster tissue samples, 5 tested positive for *P. marinus* using conventional PCR, as confirmed by agarose gel electrophoresis (data not shown). Using the validated cutoff from a previous study [11], Pm-qPCR calls were positive if Ct ≤ 35.8 and negative if Ct >35.8 (with valid IC and appropriate curve shape). By Pm-qPCR, 7 samples were positive (high Ct values) and 9 were negative. The optimized Pm-LAMP detected 6 positives that met the melting curve criterion above, while 8 samples tested negative. Two additional samples produced amplification with a single peak in the 86.5°C–87.0°C window but were classified as false positives for diagnostic analysis because both conventional PCR and Pm-qPCR were negative (Table 3). Sample No. 7 was positive by qPCR (Ct ≤35.8) but negative by Pm-LAMP owing to a very late Tt and a Tm of 88.5°C, which falls outside the 86.5°C–87.0°C acceptance window; thus, it was adjudicated as discordant. Analysis of DNA extracted from *P. marinus* cells indicated that both the Pm-qPCR and Pm-LAMP assays could detect *P. marinus* at concentrations as low as 56 pg/μl (Table 4). The clinical diagnostic sensitivity and diagnostic specificity of the Pm-LAMP assay for detecting *P. marinus* were 100% and 80.0%, respectively. Cohen's kappa analysis confirmed substantial agreement between the Pm-LAMP and Pm-qPCR assays, with a κ-value of 0.750.

Discussion

P. marinus poses a significant threat to oyster populations, causing substantial mortality and economic losses in the aquaculture industry [5,27]. Rapid detection of *P. marinus* is essential for effectively managing and controlling dermo disease outbreaks in oyster farms. Molecular techniques, such as conventional PCR [7] and qPCR [9,10], are widely used; indeed, we recently developed a highly specific and sensitive qPCR assay for *P. marinus* [11]. However, these approaches require specialized instruments and longer turnaround times. LAMP assay offers a valuable alternative by enabling rapid and specific DNA amplification under isothermal conditions.

https://doi.org/10.3347/PHD.25083

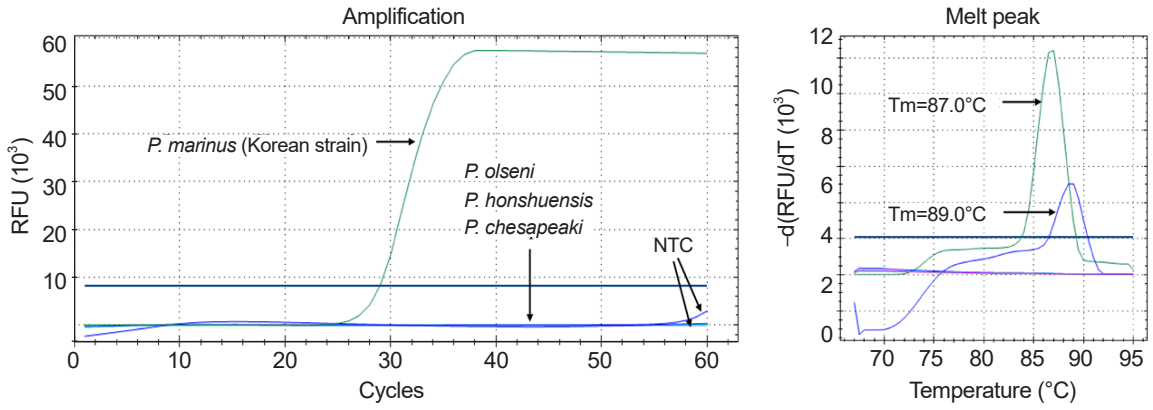

Fig. 5. Evaluation of the analytical specificity of Pm-LAMP (species-specific loop-mediated isothermal amplification assay targeting a *Perkinsus marinus* hypothetical-protein locus) assay. Amplification plots and melting peaks for *P. marinus* and 3 other species: *P. olseni*, *P. honshuensis*, and *P. chesapeaki*. Two distinct melting peaks were observed for the *P. marinus* standard and no template control (NTC), each with different melting temperature (Tm) values. RFU, relative fluorescence units.

Table 2. Pm-LAMP performance on cultured isolates and non-target species

Species	Source	Pm-LAMP		Results
		Tt	Tm	
P. marinus	ATCC 50894	33.0	86.5	Positive
P. marinus	ATCC 50509	34.5	86.5	Positive
P. marinus	ATCC 50510	32.6	87.0	Positive
P. marinus	ATCC 50787	27.7	87.0	Positive
P. marinus	ATCC 50766	28.0	87.0	Positive
P. marinus	ATCC 50849	32.1	87.0	Positive
P. marinus	Korea	28.6	87.0	Positive
P. olseni	Korea	ND	None	Negative
P. honshuensis	ATCC PRA-176	ND	None	Negative
P. chesapeaki	ATCC PRA-65	ND	None	Negative

All entries are cultured cells at 67°C using 5-primer assay with the loop forward primer omitted.
Pm-LAMP, species-specific loop-mediated isothermal amplification assay targeting a *Perkinsus marinus* hypothetical-protein locus; Tt, threshold time; Tm, melting temperature; ND, not detected.

Table 3. Summary of environmental oyster tissue samples analyzed by the Pm-LAMP assay with comparison to conventional PCR and Pm-qPCR results

Sample No.	PCR	qPCR		LAMP		
		Ct	Interpretation	Tt	Tm	Interpretation
1	P	35.2	P	38.3	86.5	P
2	P	31.5	P	37.4	87.0	P
3	P	33.2	P	40.5	86.5	P
4	P	31.7	P	47.2	87.0	P
5	P	34.8	P	43.5	87.0	P
6	ND	35.2	P	42.4	87.0	P
7	ND	34.1	P	50.9	88.5	ND
8	ND	36.3	ND	32.0[a]	87.0[a]	P[a]
9	ND	36.2	ND	41.8[a]	87.0[a]	P[a]
10	ND	36.8	ND	46.3	88.5	ND
11	ND	36.7	ND	46.8	88.5	ND
12	ND	36.8	ND	ND	None	ND
13	ND	36.0	ND	49.7	88.5	ND
14	ND	36.0	ND	ND	None	ND
15	ND	37.0	ND	42.2	89.0	ND
16	ND	36.2	ND	42.7	89.0	ND

Pm-LAMP, species-specific loop-mediated isothermal amplification (LAMP) assay targeting a *Perkinsus marinus* hypothetical-protein locus; Pm-qPCR, quantitative real-time PCR assay for *P. marinus*; Ct, threshold cycles; Tt, threshold time; Tm, melting temperature; P, positive; ND, not detected.
[a]False-positive samples—defined as LAMP-positive with both PCR and Pm-qPCR negative—have their Tt and Tm values indicated.

In this study, we developed and validated a *P. marinus*-specific LAMP assay for rapid, quantitative detection of the parasite, and we benchmarked its performance against our previously established Pm-qPCR [11]. The results demonstrate the assay's potential as a robust diagnostic tool for *P. marinus*.

For analytical benchmarking, LAMP Tt were recorded on a laboratory real-time platform to standardize optimization and allow head-to-head comparison with qPCR. This choice does not constrain deployment: the same primers and chemistry are compatible with simple constant-temperature heaters and endpoint visual/fluorometric readouts suitable for field or low-resource settings.

We selected a species-specific target, an uncharacterized (hypothetical-protein) locus from the *P. marinus* whole-genome sequence database available in the NCBI. Homology analysis confirmed low sequence conservation between this

Table 4. Summary of 10-fold dilution series analysis of a Perkinsus marinus Korean strain using the Pm-LAMP assay and comparison with the results Pm-qPCR method

Sample dilution	DNA concentration	qPCR		LAMP		
		Ct	Interpretation	Tt	Tm	Interpretation
1	56 ng/μl	22.6	P	27.7	86.5	P
1/10	5.6 ng/μl	26.0	P	29.1	87.0	P
1/100	0.56 ng/μl	29.3	P	32.3	87.0	P
1/1000	56 pg/μl	32.9	P	42.5	87.0	P
1/10000	5.6 pg/μl	36.6	ND	ND	None	ND
NTC	NTC	ND	ND	ND	None	ND

Pm-LAMP, species-specific loop-mediated isothermal amplification (LAMP) assay targeting a *Perkinsus marinus* hypothetical-protein locus; Pm-qPCR, quantitative real-time PCR assay for *P. marinus*; Ct, threshold cycles; Tt, threshold time; Tm, melting temperature; P, positive; ND, not detected; NTC, no template control.

target sequence and the corresponding regions in *P. olseni* and *P. chesapeaki*, supporting the high specificity of the designed primers. Previous LAMP assays for *Perkinsus* spp. primarily targeted the ITS region, which is not species-specific for *P. marinus* [19,21]. In contrast, the target used here preserved species-level exclusivity without major loss of analytical sensitivity: Pm-LAMP detected cultured *P. marinus* DNA down to 56 pg/μl and yielded faster time-to-result than qPCR. Two LAMP-positive/qPCR-negative environmental samples exhibited late Tt yet a single melting curve within the acceptance window; we classified these as false positives for diagnostic analysis because neither conventional PCR nor Pm-qPCR confirmed them. Such borderline, late-appearing signals can occur at very low template input; conservative Tt cutoffs, carryover-prevention chemistry (UDG/dUTP), and—where available—portable melting curve checks help minimize their occurrence.

Optimization of the LAMP protocol revealed that non-specific amplification occurred in NTCs at the initial temperature of 65°C. We evaluated higher reaction temperatures (up to 70°C), since previous studies noted that elevated temperatures can improve specificity and reduce non-specific amplification [28,29]. At 67°C, the assay yielded the lowest Tt value and a marked reduction in non-specific amplification, identifying 67°C as the optimal amplification temperature. In addition, to further minimize background amplification, the LF primer was removed, based on recent reports of similar LAMP optimization [30]. This modification significantly reduced non-specific amplification. The fully optimized Pm-LAMP assay (employing 5 primers at 67°C) exhibited high sensitivity, consistently detecting as little as 40 fg/μl of *P. marinus* DNA and accurately quantifying down to 0.4 pg/μl.

The analytical specificity of the assay was confirmed using genomic DNA from *P. olseni*, *P. honshuensis*, and *P. chesapeaki*—none of these non-target species yielded amplification, whereas amplification was observed exclusively for *P. marinus*. In environmental oyster tissue samples, Pm-LAMP showed high analytical specificity (single melting curve within 86.5°C–87.0°C) and good diagnostic agreement with qPCR (diagnostic sensitivity = 100%, diagnostic specificity = 80.0%, $\kappa = 0.750$). While qPCR was more sensitive for trace DNA, Pm-LAMP delivered substantially faster results, supporting its use as a practical alternative with appropriate confirmatory safeguards.

Given that the primary host of *P. marinus* is the Eastern oyster (*C. virginica*) [4], the Pm-LAMP assay could be especially beneficial in regions where *C. virginica* is cultured by enabling rapid on-site detection of *P. marinus*. Notably, in our study, the Pm-LAMP assay could detect as little as 40 fg/μl of target DNA with a Tt of approximately 20 min. In contrast, a 0.4 pg/μl template produced a positive LAMP result in about 17 min. These rapid detection times, even at very low DNA concentrations, underscore the assay's efficiency for quick diagnostics in the field.

Operationally, most non-specific LAMP products were filtered by melting curve analysis: true positives exhibited a single peak within 86.5°C–87.0°C, whereas non-specific signals showed higher Tm values (≈88.5°C–89.0°C). To prioritize specificity, we apply a conservative Tt cutoff, scoring late signals as indeterminate and retesting; in our cohort, 2 LAMP-positive/qPCR-negative samples met the Tm window but had late Tt and were classified as false positives for diagnostic analysis. Melting curve analysis is widely used to differentiate LAMP products among parasite species or gene targets [31,32]. For field use, portable fluorescence LAMP analyzers can run a brief post-amplification melting curve analysis step to verify the expected Tm (≈86.5°C–87.0°C); where such devices are unavailable, instrument-free strategies are

https://doi.org/10.3347/PHD.25083

viable, including closed-tube colorimetric LAMP, lateral-flow dipstick confirmation, and procedural safeguards (conservative Tt cutoffs and UDG/dUTP carryover prevention).

Field applicability is further supported by portable isothermal fluorescence devices (e.g., Genie-class instruments such as Genie II, OptiGene) that provide real-time detection without conventional thermal cycling and can optionally run a brief melting curve check [25]. In this study, all oyster tissue DNAs were purified using a commercial kit; to fully enable field deployment, future work will evaluate simplified extraction (e.g., heat treatment or alkaline lysis) and perform head-to-head Pm-LAMP vs. qPCR comparisons on crude extracts for low-burden samples, building on field-deployable LAMP workflows [33-35]. Integrating such extraction-light methods with portable platforms should allow on-site testing by non-experts, reducing cost and infrastructure needs while facilitating real-time surveillance of *P. marinus* in aquaculture settings.

In summary, the Pm-LAMP assay developed here is a robust, efficient method for *P. marinus* detection that complements existing qPCR workflows. Optimized at 67°C in a 5-primer configuration (LF omitted), the assay showed high analytical specificity and good diagnostic agreement with qPCR. Ongoing work will focus on enhancing sensitivity for low-burden samples, extending the assay to environmental DNA monitoring, and validating extraction-light, field-friendly confirmation options (e.g., portable anneal/melt checks or lateral-flow dipsticks), thereby broadening the assay's impact across diagnostic and ecological settings.

Author contributions

Conceptualization: Bathige SDNK. Funding acquisition: Park KI. Methodology: Bathige SDNK, Kim SH, Lee D, Jeon HB. Project administration: Park KI. Resources: Chen Y. Supervision: Park KI. Writing – original draft: Bathige SDNK. Writing – review & editing: Bathige SDNK, Jeon HB, Chen Y, Park KI.

Conflict of interest

The authors have no conflicts of interest to declare.

Funding

This study was supported by the Korea Institute of Marine Science & Technology Promotion (KIMST), funded by the Ministry of Oceans and Fisheries, Korea (grant No. RS-2022-KS221679) and the National Research Foundation of Korea (grant No. RS-2022-NR069484).

ORCID

S.D.N.K. Bathige, https://orcid.org/0000-0003-3118-7704
Seung-Hyeon Kim, https://orcid.org/0009-0000-9010-6092
Donghyun Lee, https://orcid.org/0009-0005-0371-5460
Hyung-Bae Jeon, https://orcid.org/0000-0002-0819-5004
Yu Chen, https://orcid.org/0009-0008-5510-7143
Kyung-Il Park, https://orcid.org/0000-0001-8667-3908

References

1. Ray SM. Biological studies of *Dermocystidium marinum*, a fungus parasite of oysters. Rice University; 1954.
2. Cáceres-Martínez J, Vásquez-Yeomans R, Padilla-Lardizábal G. Parasites of the pleasure oyster *Crassostrea corteziensis* cultured in Nayarit, Mexico. J Aquat Anim Health 2010;22:141-51. https://doi.org/10.1577/H09-052.1
3. Cáceres-Martínez J, Vásquez-Yeomans R, Padilla-Lardizábal G, del Río Portilla MA. *Perkinsus marinus* in pleasure oyster *Crassostrea corteziensis* from Nayarit, Pacific coast of México. J Invertebr Pathol 2008;99:66-73. https://doi.org/10.1016/j.jip.2008.03.005
4. Andrews JD. Epizootiology of the disease caused by the oyster pathogen *Perkinsus marinus* and its effects on the oyster industry. Am Fish Soc Spec Publ 1988;18:47-63.
5. Enríquez-Espinoza TL, Grijalva-Chon JM, Castro-Longoria R, Ramos-Paredes J. *Perkinsus marinus* in *Crassostrea gigas* in the Gulf of California. Dis Aquat Organ 2010;89:269-73. https://doi.org/10.3354/dao02199
6. Kim SH, Bathige SDNK, Jeon HB, et al. First report of *Perkinsus marinus* occurrence associated with wild Pacific oysters *Crassostrea gigas* from the west coast of Korea. J Invertebr Pathol 2024;204:108119. https://doi.org/10.1016/j.jip.2024.108119
7. Audemard C, Reece KS, Burreson EM. Real-time PCR for detection and quantification of the protistan parasite *Perkinsus marinus* in environmental waters. Appl Environ Microbiol 2004;70:6611-8. https://doi.org/10.1128/AEM.70.11.6611-6618.2004
8. Moss JA, Burreson EM, Reece KS. Advanced *Perkinsus marinus* infections in *Crassostrea ariakensis* maintained under laboratory conditions. J Shellfish Res 2006;25:65-72. https://doi.org/10.2983/0730-8000(2006)25[65:APMIIC]2.0.CO;2
9. Gauthier JD, Miller CR, Wilbur AE. TaqMan® MGB real-time PCR approach to quantification of *Perkinsus marinus* and *Perkinsus* spp. in oysters. J Shellfish Res 2006;25:619-24. https://doi.org/10.2983/0730-8000(2006)25[619:TMRPAT]2.0.CO;2
10. Rocha CSD, Sabry RC, Rocha RDS, et al. First record of *Perkinsus marinus* infecting *Crassostrea* sp. in Rio Grande do Norte, Brazil, using real-time PCR. J Invertebr Pathol 2023;198:107917. https://

doi.org/10.1016/j.jip.2023.107917

11. Kim SH, Bathige SDNK, Kim HJ, et al. A highly sensitive and specific real-time quantitative polymerase chain reaction assay for *Perkinsus marinus* detection in oysters. Sci Rep 2024;14:25475. https://doi.org/10.1038/s41598-024-76822-y
12. Mori Y, Notomi T. Loop-mediated isothermal amplification (LAMP): a rapid, accurate, and cost-effective diagnostic method for infectious diseases. J Infect Chemother 2009;15:62-9. https://doi.org/10.1007/s10156-009-0669-9
13. Aliotta JM, Pelletier JJ, Ware JL, et al. Thermostable Bst DNA polymerase I lacks a 3′→5′ proofreading exonuclease activity. Genet Anal 1996;12:185-95. https://doi.org/10.1016/S1050-3862(96)80005-2
14. Nazina TN, Tourova TP, Poltaraus AB, et al. Taxonomic study of aerobic thermophilic bacilli: descriptions of *Geobacillus subterraneus* gen. nov., sp. nov. and *Geobacillus uzenensis* sp. nov. from petroleum reservoirs and transfer of *Bacillus stearothermophilus*, *Bacillus thermocatenulatus*, *Bacillus thermoleovorans*, *Bacillus kaustophilus*, *Bacillus thermodenitrificans* to *Geobacillus* as the new combinations *G. stearothermophilus*, G. th. Int J Syst Evol Microbiol 2001;51:433-46. https://doi.org/10.1099/00207713-51-2-433
15. Notomi T, Okayama H, Masubuchi H, et al. Loop-mediated isothermal amplification of DNA. Nucleic Acids Res 2000;28:E63. https://doi.org/10.1093/nar/28.12.e63
16. Nagamine K, Hase T, Notomi T. Accelerated reaction by loop-mediated isothermal amplification using loop primers. Mol Cell Probes 2002;16:223-9. https://doi.org/10.1006/mcpr.2002.0415
17. Pumford EA, Lu J, Spaczai I, et al. Developments in integrating nucleic acid isothermal amplification and detection systems for point-of-care diagnostics. Biosens Bioelectron 2020;170:112674. https://doi.org/10.1016/j.bios.2020.112674
18. Biswas G, Sakai M. Loop-mediated isothermal amplification (LAMP) assays for detection and identification of aquaculture pathogens: current state and perspectives. Appl Microbiol Biotechnol 2014;98:2881-95. https://doi.org/10.1007/s00253-014-5531-z
19. Feng C, Wang C, Lin X, et al. Development of a loop-mediated isothermal amplification method for detection of *Perkinsus* spp. in mollusks. Dis Aquat Organ 2013;104:141-8. https://doi.org/10.3354/dao02591
20. Qu P, Wang CM, Ren WC, et al. Establishment and application of a loop-mediated isothermal amplification (LAMP) method for *Perkinsus olseni* detection. J Fish China 2012;36:1281-9.
21. Wang C, Feng CY, Wang QL, et al. Establishment of duplex loop-mediated isothermal application method for simultaneous detection of shellfish infected with *Perkinsus* and *Bonamia*. China Anim Husb Vet Med 2015;42:1935-42.
22. Gajamange D, Kim SH, Choi KS, Azevedo C, Park KI. Scanning electron microscopic observation of the in vitro cultured protozoan, *Perkinsus olseni*, isolated from the Manila clam, *Ruditapes philippinarum*. BMC Microbiol 2020;20:238. https://doi.org/10.1186/s12866-020-01926-0
23. Zhao B, Kim SH, Koh DW, et al. Molecular phylogeny, distribution, and pathogenicity of a novel thraustochytrid protist in the Manila clam, *Ruditapes philippinarum*, on the west and south coasts of Korea. Aquaculture 2023;575:739779. https://doi.org/10.1016/j.aquaculture.2023.739779
24. World Organization for Animal Health. Infection with *Perkinsus marinus*. In: World Organization for Animal Health. Manual of diagnostic tests for aquatic animals. The Organization; 2022.
25. Yang Q, Domesle KJ, Ge B. Loop-mediated isothermal amplification for *Salmonella* detection in food and feed: current applications and future directions. Foodborne Pathog Dis 2018;15:309-31. https://doi.org/10.1089/fpd.2018.2445
26. Zararsiz G, Akyildiz HY, Göksülük D, Korkmaz S, Öztürk A. Statistical learning approaches in diagnosing patients with nontraumatic acute abdomen. Turk J Electr Eng Comput Sci 2016;24:3685-97. https://doi.org/10.3906/elk-1501-181
27. Villalba A, Reece KS, Ordás MC, Casas SM, Figueras A. Perkinsosis in molluscs: a review. Aquat Living Resour 2004;17:411-32. https://doi.org/10.1051/alr:2004050
28. Ferrara M, Logrieco AF, Moretti A, Susca A. A loop-mediated isothermal amplification (LAMP) assay for rapid detection of fumonisin producing *Aspergillus* species. Food Microbiol 2020;90:103469. https://doi.org/10.1016/j.fm.2020.103469
29. Rakhmat P, Saepuloh U, Darusman HS. Development of phenol red colorimetric RT-LAMP assay in high-buffered SARS-CoV-2 sample. Hayati J Biosci 2023;30:621-31. https://doi.org/10.4308/hjb.30.4.621-631
30. Alhamid G, Tombuloglu H, Al-Suhaimi E. Development of loop-mediated isothermal amplification (LAMP) assays using five primers reduces the false-positive rate in COVID-19 diagnosis. Sci Rep 2023;13:5066. https://doi.org/10.1038/s41598-023-31760-z
31. Kreitlow A, Becker A, Ahmed MFE, et al. Combined loop-mediated isothermal amplification assays for rapid detection and one-step differentiation of *Campylobacter jejuni* and *Campylobacter coli* in meat products. Front Microbiol 2021;12:668824. https://doi.org/10.3389/fmicb.2021.668824
32. Tone K, Fujisaki R, Yamazaki T, Makimura K. Enhancing melting curve analysis for the discrimination of loop-mediated isothermal amplification products from four pathogenic molds: Use of inorganic pyrophosphatase and its effect in reducing the variance in melting temperature values. J Microbiol Methods 2017;132:41-5. https://doi.org/10.1016/j.mimet.2016.10.020
33. Hodgetts J. Rapid sample preparation and LAMP for phytoplasma detection. Methods Mol Biol 2019;1875:187-201. https://doi.

org/10.1007/978-1-4939-8837-2_15

34. Boza JM, Erickson DC. Comparison and optimization of simple DNA extraction methods for LAMP-based point-of-care applications employing submillimeter skin biopsies. ACS Omega 2024;9:38855-63. https://doi.org/10.1021/acsomega.4c05025

35. Goudoudaki S, Kambouris ME, Manoussopoulou M, et al. Fast and sustainable thermo-osmotic DNA extraction protocol for trans-spectrum contingency and field use. Bio Protoc 2023;13:e4796. https://doi.org/10.21769/BioProtoc.4796

Brief Communication

Parasites Hosts Dis 2026;64(1):82-86
https://doi.org/10.3347/PHD.25078

Parasites, Hosts and Diseases

pISSN 2982-5164 • eISSN 2982-6799

Identification of maternal antibodies targeting a cystatin-like protein of *Trichinella spiralis* in offspring

Minkyoung Cho[1,2], Hak Sun Yu[3,4,*]

[1]Department of Parasitology and Tropical Medicine and Institute of Medical Science, Gyeongsang National University College of Medicine, Jinju, Korea; [2]Department of Convergence Medical Science, Gyeongsang National University, Jinju, Korea; [3]Department of Parasitology and Tropical Medicine, School of Medicine, Pusan National University, Yangsan, Korea; [4]Research Institute for Convergence of Biomedical Science and Technology, Pusan National University Yangsan Hospital, Yangsan, Korea

Vertical transfer of maternal antibodies can provide passive protection to offspring against specific pathogens. In this study, we detected antibodies in the sera of uninfected offspring born to chronically *Trichinella spiralis*-infected female mice. Immunoblotting consistently revealed a distinct band at ~38 kDa in both *T. spiralis* excretory-secretory products and total somatic extracts. This band was identified by MALDI-TOF/TOF mass spectrometry as a cystatin-like protein of *T. spiralis* (Ts-CLP). Structural modeling and domain analysis indicated a typical cystatin-like fold comprising a central α-helix and an antiparallel β-sheet core. To confirm antigen identity, recombinant Ts-CLP protein was expressed and used to generate a polyclonal anti-recombinant Ts-CLP protein antibody. This antibody specifically recognized a ~38 kDa band in *T. spiralis* excretory-secretory products and total somatic extracts, consistent with that detected by offspring sera. Collectively, these findings demonstrate that maternal antibodies specific to Ts-CLP are vertically transferred and detectable in uninfected offspring. Although the functional significance remains to be determined, this observation provides a basis for future studies on passive immunity and host-parasite interactions.

Keywords: Cystatin-like protein, maternal antibodiesm, *Trichinella spiralis*, vertical transfer

Trichinella spiralis is a parasitic nematode that employs various immunoevasive strategies to establish chronic infection within its host. Among these strategies, the secretion of immunomodulatory proteins as part of the parasite's excretory-secretory products (ESPs) plays a critical role in modulating host immune responses[1-4]. One such molecule, a cystatin protein, has been reported to suppress host cysteine protease activity, potentially interfering with antigen processing and presentation, as well as inflammatory signaling [5-9]. However, little is known about host antibody responses to this molecule, or whether such responses can be vertically transmitted to offspring.

In the present study, we investigated the possibility of maternal antibody transfer in a murine model chronically infected with *T. spiralis*, and identified a parasite-derived antigen recognized by these antibodies in uninfected offspring delivered by infected female mice. Female C57BL/6 mice (6 weeks old) were orally infected with 250 *T. spiralis* muscle larvae. All animal experiments were conducted in accordance with institutional guidelines and were approved by the Institutional Animal Care and Use Committee of Pusan National University (No. PNU-2013-0293). After 4 weeks of infection, the female mice were mated with uninfected males to produce offspring. To confirm

Received: September 3, 2025 Accepted: September 17, 2025
*Correspondence: hsyu@pusan.ac.kr

Citation
Cho M, Yu HS. Identification of maternal antibodies targeting a cystatin-like protein of *Trichinella spiralis* in offspring. Parasites Hosts Dis 2026; 64(1):82-86.

that the offspring were uninfected, muscle tissue samples were examined by direct microscopic observation of compressed tissue preparations, and no parasites were detected. Sera were collected from the offspring at 5 weeks of age and used as primary antibody sources in Western blot analyses against *T. spiralis* ESPs and total somatic extracts (TSEs). Immunoblotting consistently revealed a band migrating at approximately 38 kDa (gray arrowhead) in both ESPs and TSEs. In addition, bands at around 80 kDa in ESPs (black arrowhead) and 30 kDa in TSEs (black arrowhead) were also observed. (Fig. 1A, B). To identify the common band at ~38 kDa, this band was excised and subjected to MALDI-TOF/TOF mass spectrometry, which identified it as a cystatin-like protein of *T. spiralis* (Ts-CLP) (Fig. 1C).

Biotechnology Information for cystatin-like protein (accession No. ABY59464.1; previously, GI: 164504316), consistent with the GI number identified in the MALDI-TOF/TOF analysis. The nucleotide sequence comprised 714 bp, encoding an amino acid sequence of 237 residues, with a predicted molecular weight of 27.5 kDa. Signal peptide analysis using InterPro (https://www.ebi.ac.uk/interpro) predicted a 20-residue signal peptide at the N-terminus, with residues 1–7 corresponding to the N-terminal signal region, residues 8–15 forming a hydrophobic core, and residues 16–20 representing the C-terminal signal peptide region (Fig. 2A). In addition, the amino acid sequence of Ts-CLP was analyzed using the AlphaFold Protein Structure Database (AFDB) (https://alphafold.ebi.ac.uk). The predicted model was further segmented into structural domains using the Encyclopedia of Domains, which defines consensus domain boundaries across AFDB entries by integrating multiple structure-based methods [10]. The AFDB model reproduced the characteristic cystatin-like fold, in which a central α-helix is packed against a 5-stranded antiparallel β-sheet, consistent with previously described cystatin family structures [11-13]. The model displayed an average predicted Local Distance Difference Test (pLDDT) of 75.12, indicating generally reliable prediction quality (Fig. 2B). The Encyclopedia of Domains analysis identified 2 structural domains comprising 106 and 98 residues, respectively, while the remaining 33 residues were not assigned to either domain and correspond mainly to terminal and linker regions. Domain 1 (residues 9–114) exhibited an α–

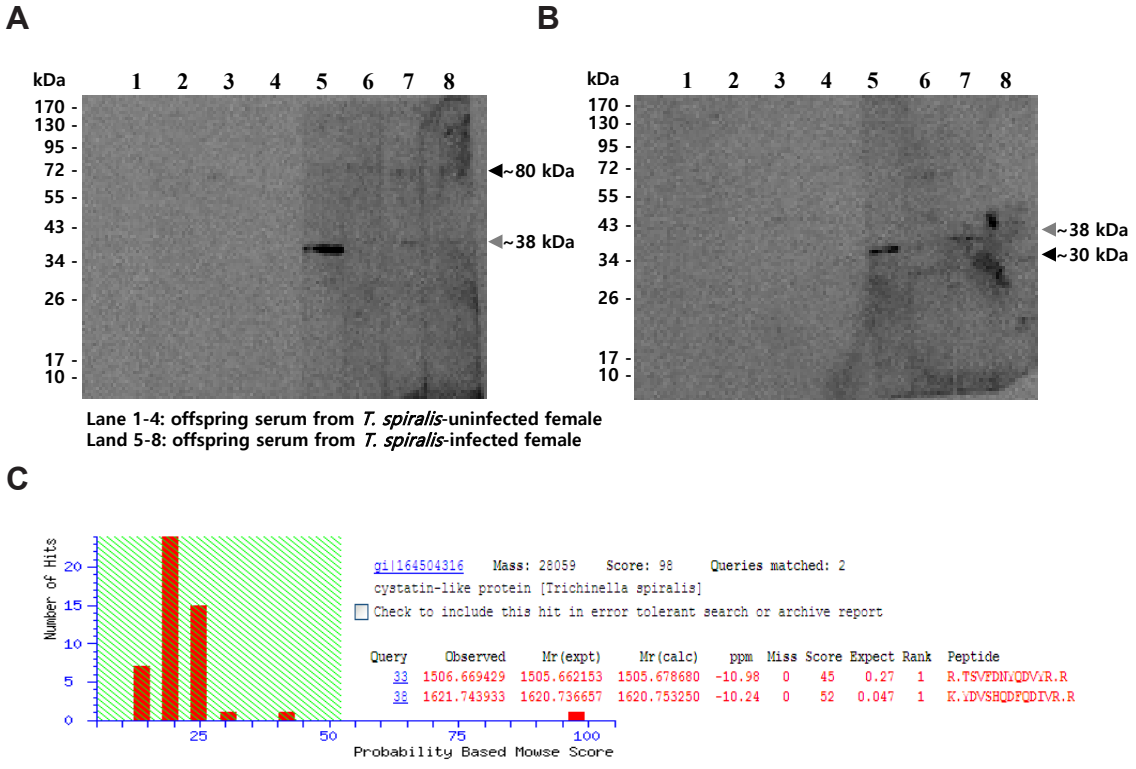

Fig. 1. Identification of a *Trichinella spiralis* cystatin-like protein (Ts-CLP) recognized by maternal antibodies in offspring sera. (A, B) Immunoblot of *T. spiralis* excretory-secretory products (A) or total somatic extracts (B) probed with sera collected from 5-week-old uninfected offspring. Lane 1–4: offspring of normal females; Lane 5–8: offspring of chronically infected females. (C) The common immunoreactive band of approximately 38 kDa (gray arrowheads) was excised from SDS-PAGE and identified by MALDI-TOF/TOF mass spectrometry. Additional immunoreactive bands of different molecular weights are indicated by black arrowheads.

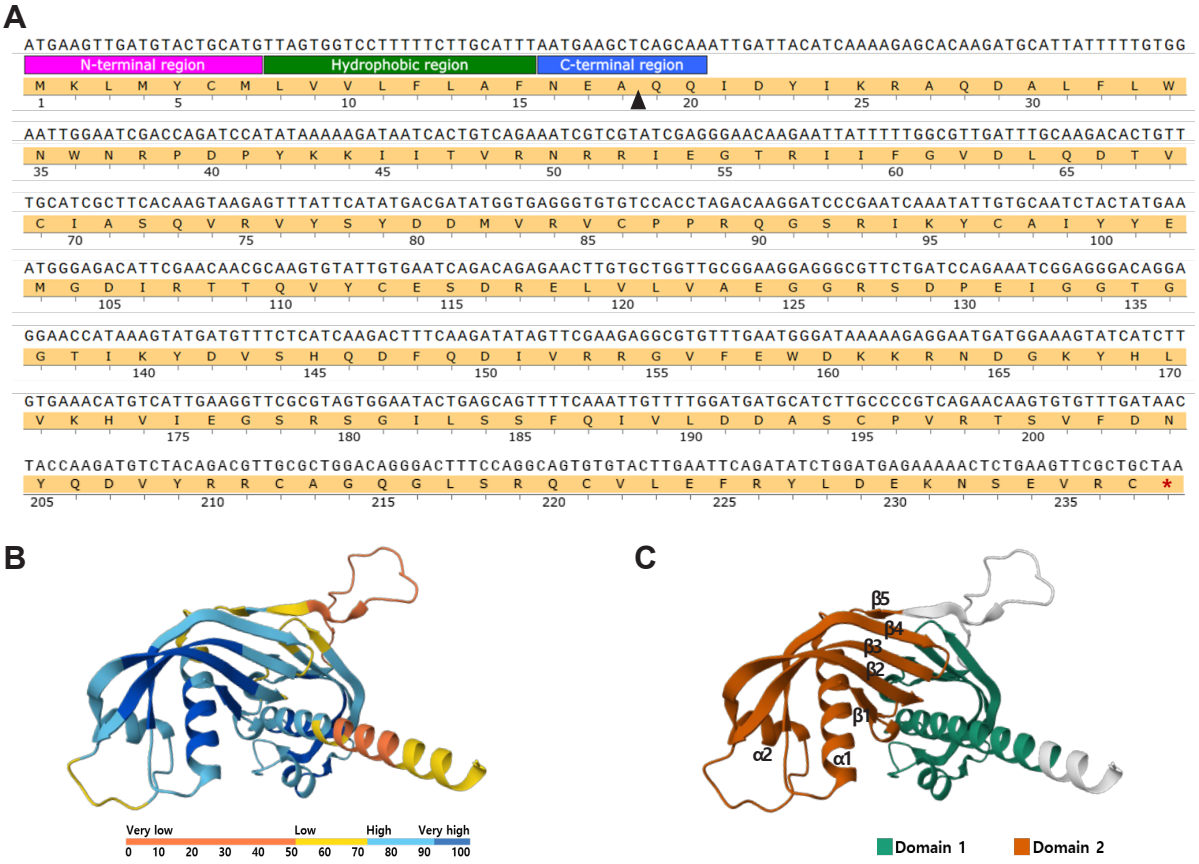

Fig. 2. Sequence features and structural modeling of *Trichinella spiralis* cystatin-like protein (Ts-CLP). (A) Nucleotide and deduced amino acid sequence of Ts-CLP. The predicted N-terminal signal peptide is subdivided into 3 regions: the N-terminal signal region (pink), hydrophobic core (green), and C-terminal signal peptide region (blue). The arrowhead indicates the predicted signal peptide cleavage site. The stop codon is marked with an asterisk. (B) Predicted tertiary structure of Ts-CLP generated using the AlphaFold Protein Structure Database. Structural prediction confidence is indicated by the color gradient from blue (high) to orange (low). (C) Predicted tertiary structure of Ts-CLP with domain segmentation based on The Encyclopedia of Domains. Domain 1 and Domain 2 are represented in distinct colors.

β–β–α topology with a central α-helix and short β-strands. Domain 2 (residues 140–237) displayed a β–α–β–β–α–β–β arrangement, in which 5 β-strands assembled into an antiparallel β-sheet core interleaved with 2 α-helices. This organization corresponds to the canonical cystatin architecture described above (Fig. 2C).

Having established its structural characteristics, we next examined the developmental gene expression of Ts-CLP. Total RNA was extracted from newborn larvae, muscle larvae, and adult worms of *T. spiralis*, followed by RT-PCR analysis. Newborn larvae were obtained from adult worm delivery, muscle larvae were collected from infected muscle tissue, and adult worms were recovered from the intestines of infected mice. For each preparation, multiple worms were pooled, and each biological replicate ($n=3$) represented an independently prepared pool of parasites obtained from separate infected mice. The Ts-CLP transcript was detected at all life stages, with the highest expression in muscle larvae. This pattern indicates a constitutive expression with stage-specific enhancement, suggesting that Ts-CLP may be particularly important for establishing chronic infection within host tissue (Fig. 3A). To further validate the identity of the antigen recognized by offspring sera, the Ts-CLP gene was amplified from *T. spiralis* cDNA, cloned into the pTNT vector (Promega), and expressed ex vivo using TNT T7 Quick Coupled Transcription/Translation System (Promega). The recombinant Ts-CLP protein (rTs-CLP) was separated on a 10% SDS-PAGE gel and visualized by Coomassie blue staining solution (Fig. 3B). A polyclonal anti–rTs-CLP antibody was generated by immunization with rTs-CLP and Freund's adjuvant, and subsequently used as the primary antibody for immunoblotting. This anti–rTs-CLP antibody specifically recognized approximately ~38 kDa band in both *T. spiralis* ESPs and TSEs, consistent with the band detected by offspring sera (Fig. 3C).

Although the predicted molecular weight of Ts-CLP is 27.5

https://doi.org/10.3347/PHD.25078

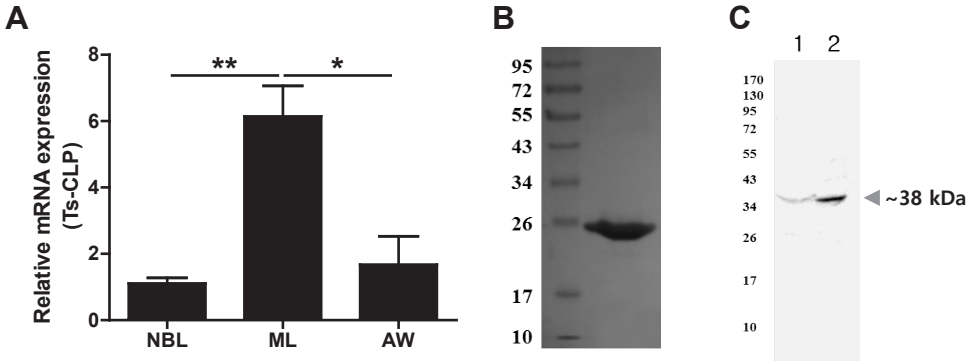

Fig. 3. Gene expression and immunological validation of *Trichinella spiralis* cystatin-like protein (Ts-CLP). (A) Relative transcript levels of Ts-CLP in 3 developmental stages of *T. spiralis*: newborn larvae (NBL), muscle larvae (ML), and adult worms (AW), analysed by RT-PCR. Data are presented as mean±SEM from 3 independent biological replicated (n=3), and statistical significance was assessed by Tukey's test ($^{*}P$<0.05, $^{**}P$<0.01). (B) Recombinant Ts-CLP expressed in an ex vivo system, separated by SDS-PAGE, and visualized by Coomassie blue staining. (C) Immunoblot of Ts–excretory-secretory products (lane 1) or Ts–total somatic extracts (lane 2) probed with polyclonal anti–recombinant Ts-CLP antibody.

kDa, the naive protein migrated around ~38 kDa in both ESPs and TSEs. This upward shift is plausibly attributable to post-translational modifications (e.g., glycosylation) and/or the presence of unprocessed peptide regions [14,15]. Notably, apparent molecular weight differences between native and recombinant forms are common when the latter are produced in cell-free systems lacking such modifications [16]. To address the discrepancy between the predicted molecular weight of Ts-CLP (~27.5 kDa) and the larger size observed in native parasite extracts (~38 kDa), we performed in silico glycosylation site prediction using multiple tools (NetNGlyc, NetOGlyc, GlycoEP, and ISOGlyP). These analyses did not identify any strong canonical N-linked sites, although residues 204 (NYQ) and 232 (NSE) showed weak potential signals, with the latter approaching the threshold value (0.5). In addition, several serine/threonine residues (128, 135, 138, 144, 200, and 233) were suggested as potential O-linked glycosylation sites, but all with scores below the confidence cutoff. However, it should be noted that most currently available prediction tools were developed primarily on mammalian protein datasets, and their applicability to helminth proteins may therefore be limited. Taken together, these bioinformatic analyses cannot provide definitive evidence. They nevertheless suggest that partial or helminth-specific O-glycosylation may contribute to the observed size discrepancy. This underscores the need for experimental validation, including enzymatic deglycosylation or mass spectrometry. Together, these findings support the conclusion that the antigen recognized by maternally transferred antibodies in offspring is Ts-CLP, and further indicate that Ts-CLP is present in both secreted and somatic fractions of the *T. spiralis*.

Collectively, these findings demonstrate the presence of antibodies reactive to Ts-CLP in the sera of offspring born to chronically infected mothers, despite the offspring themselves being uninfected. While the precise mechanism of transfer remains to be elucidated, and the possibility of passive transmission of parasite antigens cannot be excluded, the detection of IgG-class antibodies strongly suggests that maternal transfer of IgG is the most plausible explanation. Although our findings strongly suggest maternal IgG transfer, the precise route of antibody passage (placental versus lactational) remains unresolved. In the present study, we did not include IgG subclass-specific analyses, and while preliminary experiments confirmed the presence of total IgG in maternal milk, no distinct Ts-CLP–specific band was detected. The lack of subclass characterization and absence of definitive evidence for antigen-specific antibodies in milk, therefore, represent a limitation of this work. Future studies are required to determine whether IgG subclass distribution or milk-derived antibodies contribute to the vertical transfer of maternal immunity, thereby clarifying the mechanism of vertical antibody passage.

The functional relevance of these maternally derived antibodies also remains to be determined. It is not yet clear whether they confer protective immunity against *T. spiralis* or instead exert immunomodulatory effects. Future investigations should include functional validation of maternally transferred Ts-CLP antibodies, such as in vivo challenge experiments to assess protection and in vitro neutralization assays to evaluate potential immunomodulatory roles. Such approaches will be essential to establish the biological significance of these antibodies in host-parasite interactions.

Nevertheless, this study provides an initial basis for further investigation into passive immunity against helminths and the

host recognition of parasite-derived immunoregulatory molecules.

Author contributions

Conceptualization: Yu HS. Data curation: Cho MK, Yu HS. Formal analysis: Cho MK. Funding acquisition: Cho MK. Methodology: Yu HS. Software: Cho MK, Yu HS. Supervision: Yu HS. Validation: Cho MK, Yu HS. Visualization: Cho MK, Yu HS. Writing – original draft: Cho MK. Writing – review & editing: Yu HS.

Conflict of interest

Hak Sun Yu serves as an editor of Parasites, Hosts and Diseases but had no involvement in the decision to publish this article. No other potential conflicts of interest relevant to this study were reported.

Funding

This work was supported by the research grant of the new professor of the Gyeongsang National University in 2024 (GNU-2024-240612).

ORCID

Minkyoung Cho, https://orcid.org/0000-0002-1776-7254
Hak Sun Yu, https://orcid.org/0000-0002-6696-7981

References

1. Cho M, Yu HS. Therapeutic potentials of *Trichinella spiralis* in immune disorders: from allergy to autoimmunity. Parasites Hosts Dis 2025;63:123-34. https://doi.org/10.3347/PHD.24086
2. Ilic N, Bojic-Trbojevic Z, Lundström-Stadelmann B, et al. Immunomodulatory components of *Trichinella spiralis* excretory-secretory products with lactose-binding specificity. EXCLI J 2022;21:793-813. https://doi.org/10.17179/excli2022-4954
3. Wang J, Tang B, You X, et al. *Trichinella spiralis* excretory/secretory products from adult worms inhibit NETosis and regulate the production of cytokines from neutrophils. Parasit Vectors 2023;16:374. https://doi.org/10.1186/s13071-023-05979-8
4. Kang SA, Yu HS. Proteome identification of common immunological proteins of two nematode parasites. Parasites Hosts Dis 2024;62:342-50. https://doi.org/10.3347/PHD.24027
5. Yuthithum T, Phuphisut O, Reamtong O, et al. Identification of the protease inhibitory domain of *Trichinella spiralis* novel cystatin (TsCstN). Parasites Hosts Dis 2024;62:330-41. https://doi.org/10.3347/PHD.24026
6. Li H, Qiu D, Yuan Y, et al. *Trichinella spiralis* cystatin alleviates polymicrobial sepsis through activating regulatory macrophages. Int Immunopharmacol 2022;109:108907. https://doi.org/10.1016/j.intimp.2022
7. Acevedo N, Lozano A, Zakzuk J, et al. Cystatin from the helminth *Ascaris lumbricoides* upregulates mevalonate and cholesterol biosynthesis pathways and immunomodulatory genes in human monocyte-derived dendritic cells. Front Immunol 2024;15:1328401. https://doi.org/10.3389/fimmu.2024.1328401
8. Alghanmi M, Minshawi F, Altorki TA, et al. Helminth-derived proteins as immune system regulators: a systematic review of their promise in alleviating colitis. BMC Immunol 2024;25:21. https://doi.org/10.1186/s12865-024-00614-2
9. Khatri V, Chauhan N, Kalyanasundaram R. Parasite cystatin: immunomodulatory molecule with therapeutic activity against immune mediated disorders. Pathogens 2020;9:431. https://doi.org/10.3390/pathogens9060431
10. Lau AM, Bordin N, Kandathil SM, et al. Exploring structural diversity across the protein universe with The Encyclopedia of Domains. Science 2024;386:eadq4946. https://doi.org/10.1126/science.adq4946
11. Dall E, Hollerweger JC, Dahms SO, et al. Structural and functional analysis of cystatin E reveals enzymologically relevant dimer and amyloid fibril states. J Biol Chem 2018;293:13151-65. https://doi.org/10.1074/jbc.RA118.002154
12. Zalar M, Indrakumar S, Levy CW, et al. Studies of the oligomerisation mechanism of a cystatin-based engineered protein scaffold. Sci Rep 2019;9:9067. https://doi.org/10.1038/s41598-019-45565-6
13. Ochieng J, Chaudhuri G. Cystatin superfamily. J Health Care Poor Underserved 2010;21:51-70. https://doi.org/10.1353/hpu.0.0257
14. Wang G, de Jong RN, van den Bremer ETJ, Parren PWHI, Heck AJR. Enhancing accuracy in molecular weight determination of highly heterogeneously glycosylated proteins by native tandem mass spectrometry. Anal Chem 2017;89:4793-7. https://doi.org/10.1021/acs.analchem.6b05129
15. Salazar VA, Rubin J, Moussaoui M, et al. Protein post-translational modification in host defense: the antimicrobial mechanism of action of human eosinophil cationic protein native forms. FEBS J 2014;281:5432-46. https://doi.org/10.1111/febs.13082
16. Fogeron ML, Lecoq L, Cole L, Harbers M, Böckmann A. Easy synthesis of complex biomolecular assemblies: wheat germ cell-free protein expression in structural biology. Front Mol Biosci 2021;8:639587. https://doi.org/10.3389/fmolb.2021.639587

Brief Communication

Parasites Hosts Dis 2026;64(1):87-91
https://doi.org/10.3347/PHD.25070

Parasites, Hosts and Diseases

pISSN 2982-5164 • eISSN 2982-6799

First record of 3 chewing louse species from the Oriental stork (*Ciconia boyciana*) in Korea: Insights into conservation of co-associated species

Jeong Hun Shim[1,2], Seongjun Choe[1], Sukyung Kim[3], Dongsoo Ha[3], Soo Hyung Eo[2,*]

[1]Department of Parasitology, School of Medicine, Chungbuk National University, Cheongju, Korea; [2]Department of Forest Science, Kongju National University, Yesan, Korea; [3]Eco-Institute for Oriental Stork, Korea National University of Education, Cheongju, Korea

The Oriental stork (*Ciconia boyciana* Swinhoe, 1873) is an endangered species, with active restoration efforts ongoing in Korea. Despite the ecological importance of host-specific parasites, such as chewing lice (Phthiraptera), information on the chewing lice fauna associated with *C. boyciana* in Korea remains unclear. Previous records of 2 chewing louse species from the host have been questioned due to potential misidentification. To clarify the chewing lice fauna of the host, we conducted a survey of captive *C. boyciana* at Yesan Oriental Stork Park, Korea, in October 2022. Morphological identification of collected louse specimens revealed 3 species: *Neophilopterus incompletes* (Denny, 1842), *Ardeicola ciconiae* (Linnaeus, 1758) and *Colpocephalum zebra* Burmeister, 1838. These species are typical ectoparasites of Ciconiiform birds and represent the first verified louse records of chewing lice from *C. boyciana* in Korea. Unlike with a previous report, *Cuclotogaster heterographus* (Nitzsch, 1866) and *Anaticola anseris* (Linnaeus, 1758) were not detected. Our findings provide an updated checklist of chewing louse species for *C. boyciana* in Korea, contributing to a more accurate understanding of host-parasite associations and supporting future conservation efforts for both the host and its associated parasite fauna.

Keywords: Bird lice, conservation, co-associated species, ectoparasites, Menoponidae, Philopteridae

Chewing lice (Phthiraptera: Ischnocera and Amblycera) are permanent ectoparasites that primarily feed on the feathers, dead skin, blood, and secretions of birds and mammals. These ectoparasite species interact with their hosts and exhibit high host specificity [1-3]. Due to these characteristics, lice living on endangered hosts may face a higher risk of extinction, sometimes even greater than that of their hosts [2]. A notable example is the extinction of the endemic chewing louse species *Colpocephalum californici* Price & Beer, 1963, due to antiparasitic treatment as part of the breeding program for the California condor, *Gymnogyps californianus* (Shaw, 1797) [2]. Thus, it is necessary to pay attention to not only the hosts but also their associated species, including ectoparasites living on endangered hosts, to prevent unintended extinctions.

In Korea, the breeding population of the Oriental stork, *Ciconia boyciana* Swinhoe, 1873, was extirpated in the 1970s due to habitat destruction, overhunting, and food shortages. Consequently, the stork was designated as an "Endangered Species Level I" by the Korean Ministry of Environment [4,5]. Efforts to restore the breeding population of *C. boyciana* in Korea began in 1996, with storks being imported from Germa-

Received: August 26, 2025 Accepted: October 14, 2025
*Correspondence: eosh@kongju.ac.kr

Citation
Shim JH, Choe S, Kim S, Ha D, Eo SH. First record of 3 chewing louse species from the Oriental stork (*Ciconia boyciana*) in Korea: insights into conservation of co-associated species. Parasites Hosts Dis 2026;64(1):87-91.

ny, Russia, and Japan. In 2007, 2 storks were released on a trial basis, and continuous releases have been conducted since 2015 [4].

Although the breeding of *C. boyciana* has stabilized, various research fields need to be explored to effectively conserve the storks [4,6]. However, most studies published in international journals on storks in Korea are almost related to genetics, implying that research in other fields is limited [6]. Despite the fact that ectoparasites such as chewing lice can interact with their hosts and influence each other, only 2 articles on the ectoparasites of *C. boyciana* in Korea exist [7,8], with only one article specifically addressing chewing lice [7].

In Korea, the 2 chewing louse species of *C. boyciana* were first studied in 1984 from a moribund migrant captured in Jeju-do [7]. However, because this study predated the reintroduction of *C. boyciana* in Korea, and given the host specificity of the 2 louse species identified, it remains uncertain whether these same species actually occur on *C. boyciana*. Therefore, we aimed to clarify the chewing lice fauna of *C. boyciana* in Korea and to discuss the conservation of co-associated species, such as chewing lice, in relation to their endangered host

In October 2022, we conducted a survey on 3 captive *C. boyciana* at the Yesan Oriental Stork Park in Korea. Chewing lice were collected using a tweezer from the body, crissum, head, and wings of the storks (Fig. 1) and preserved in a 95% ethanol solution. To minimize stress on the storks during the survey, the storks were blindfolded and immobilized by keepers, and the survey was conducted with permission from the Korea Heritage Service (B0030104016624) [8]. Some of the collected lice were cleared in 10% potassium hydroxide, mounted on slides using polyvinyl alcohol mounting medium, and examined using a Olympus DP28 camera and a Olympus BX53 microscope. The identification of chewing lice was performed using morphological keys provided in previous studies [9,10].

Fig. 1. Chewing lice on *Ciconia boyciana*. The photo shows *Neophilopterus incompletus*.

Three chewing louse species were collected from 3 captive *C. boyciana* at the Yesan Oriental Stork Park and identified as *Neophilopterus incompletus* (Denny, 1842), *Ardeicola ciconiae* (Linnaeus, 1758), and *Colpocephalum zebra* Burmeister, 1838 (Fig. 2). *N. incompletus* (Ischnocera: Philopteridae) was identified by morphological features such as a triangular head with a rounded anterior end, a distinct nodus on the marginal carina anterior to the dorsal preantennal suture, a dorsal anterior plate with sublateral triangular extensions, and a short elliptical abdomen with highly sclerotized lateral tergal plates (Figs. 2A, B, 3A) [9,10], and was collected from the body and head of *C. boyciana*. *A. ciconiae* (Ischnocera: Philopteridae) was identified by morphological features such as an elongated and conical head, a largely brown dorsal anterior plate with short striations ornamentation, and an elongated abdomen with thickened tergal plates (Figs. 2C, 3B) [9,10], and was collected from the wings. *C. zebra* (Amblycera: Menoponidae) was identified by morphological features such as a large head, slightly rounded anterior margin, elongated abdomen, and sternal plates III with 2 ctenidia (Figs. 2D-E, 3C) [9,10], and was collected from the crissum.

This study discovered *N. incompletus*, *A. ciconiae*, and *C. zebra* on captive *C. boyciana* in Korea. These 3 chewing louse species were previously reported in 1977 from *C. boyciana* in Japan [9] and are also known to be found on the white stork, *Ciconia ciconia* (Linnaeus, 1758) [9,10]. In Korea, this is the first record of these 3 species. While the presence of these 3 ectoparasites on *C. boyciana* released into the wild in Korea has not yet been officially confirmed, storks exposed to chewing lice at the Yesan Oriental Stork Park are continually being released. Therefore, we believe that these co-associated species may also inhabit *C. boyciana* released into the wild in Korea.

In 1984, 2 chewing louse species, *Cuclotogaster heterographus* (Nitzsch, 1866) and *Anaticola anseris* (Linnaeus, 1758), were reported to have been found on *C. boyciana* in Korea [7]. But among the lice collected from *C. boyciana* in the present study, we did not find any individuals related to these 2 species. In fact, considering that *C. heterographus* and *A. anseris* are primarily associated with the families Phasianidae and Anatidae, respectively [1], the possibility of misidentification cannot be excluded for the records previously discovered in Korea [7].

While conducted with a small number of samples, our study is significant as it provides the first insight into the relation-

https://doi.org/10.3347/PHD.25070

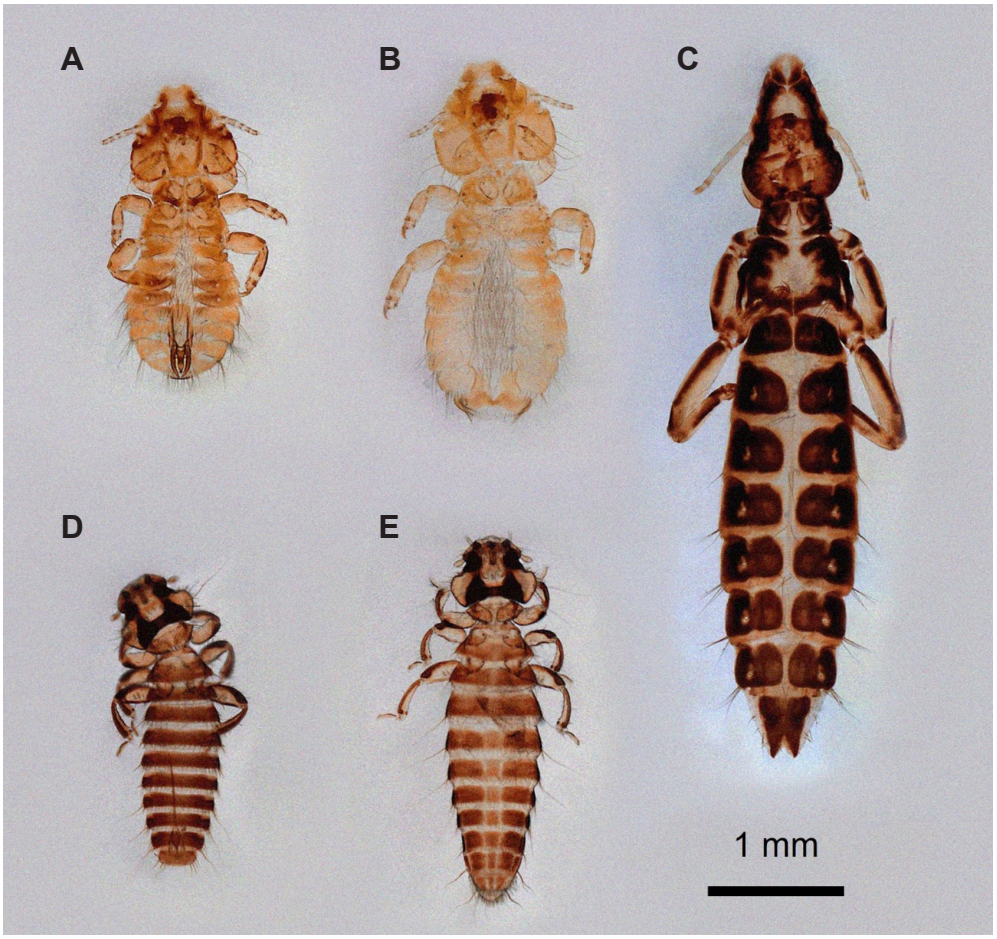

Fig. 2. Dorsal view of 3 chewing lice species from captive *Ciconia boyciana* in Korea. (A) Male *Neophilopterus incompletus*. (B) Female *Neophilopterus incompletus*. (C) Female *Ardeicola ciconiae*. (D) Male *Colpocephalum zebra*. (E) Female *Colpocephalum zebra*.

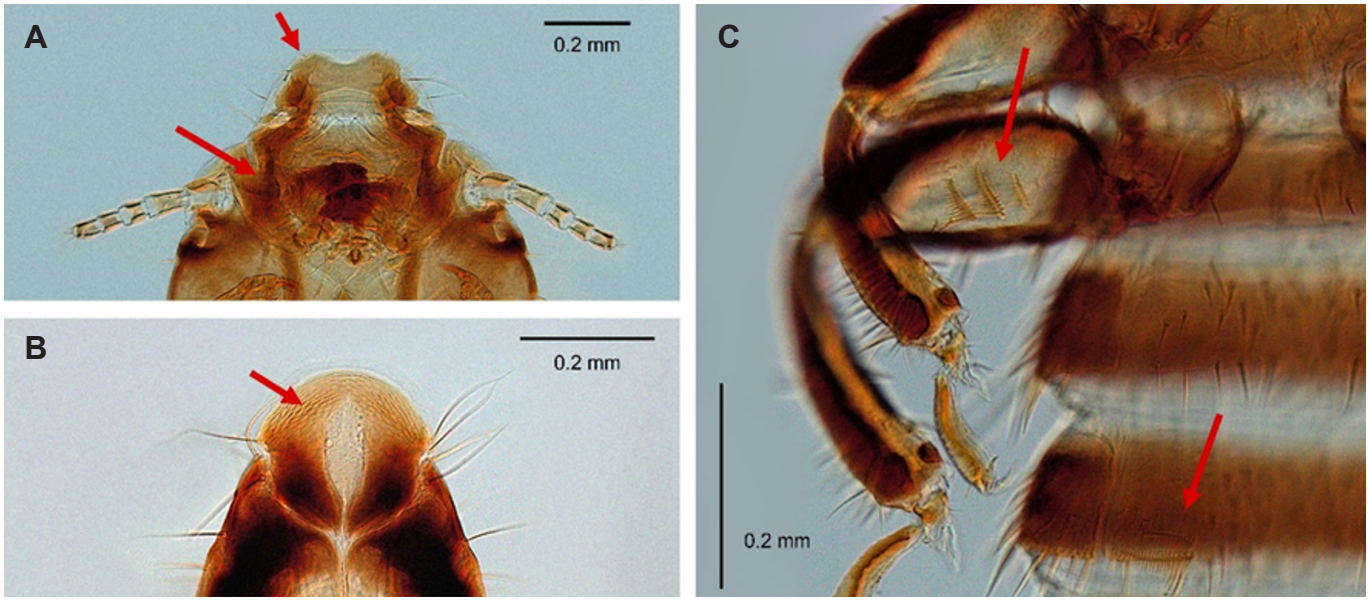

Fig. 3. Identification keys of 3 chewing lice species. (A) Dorsal view of nodus and dorsal anterior plate of *Neophilopterus incompletus*. (B) Dorsal view of dorsal anterior plate of *Ardeicola ciconiae*. (C) Ventral view of ctenidia of *Colpocephalum zebra*.

ship between chewing lice and *C. boyciana* in captivity in Korea, promising to guide future management strategies for these storks. However, this study only identified the species composition of chewing lice parasitizing *C. boyciana* and did not evaluate their impact on the storks, which represents a limitation. Therefore, future research should focus on studying the impact of the chewing lice identified in this study on *C. boyciana*.

Finally, we would like to discuss the conservation issues of the 3 chewing louse species found on captive *C. boyciana* in Korea. These co-associated species have the potential to cause various adverse effects on their hosts [1,3], but they also constitute a significant part of biodiversity, play important ecological roles, serve as indicators of ecosystem quality, and have unique evolutionary value [11]. Therefore, despite being considered pests, they need to be conserved [11]. In Spain, efforts have been made to assess the extinction risk status of lice based on the extinction risk of Spanish birds and mammals to conserve endangered lice species [12]. Although the 3 chewing louse species we found are not exclusive to the *C. boyciana* and are also found on *C. ciconia* [9,10], making their global extinction risk low, the absence of the *C. ciconia* in Korea means that these lice could unintentionally disappear from Korea during the reintroduction process of *C. boyciana*, similar to the case of *C. californici* in *G. californianus* [2]. Considering the ecological importance of these chewing louse species, efforts to conserve them alongside their host, *C. boyciana*, should be taken into account to enhance Korea's biodiversity and support ecosystem health. The present study provides a basis for further investigations into lice and other co-associated species associated with endangered bird species in Korea, for example, the crested ibis, *Nipponia nippon* (Temminck, 1835) and the black-faced spoonbill, *Platalea minor* Temminck & Schlegel, 1850, both of which are under similar conservation concerns.

Author contributions

Data curation: Shim JH. Formal analysis: Shim JH, Choe S. Funding acquisition: Kim S, Ha D, Eo SH. Investigation: Shim JH, Kim S, Ha D, Eo SH. Methodology: Shim JH, Choe S. Project administration: Shim JH, Kim S, Ha D, Eo SH. Resources: Kim S, Ha D, Eo SH. Supervision: Eo SH. Validation: Choe S, Kim S, Ha D, Eo SH. Visualization: Shim JH, Eo SH. Writing – original draft: Shim JH. Writing – review & editing: Choe S, Kim S, Ha D, Eo SH.

Conflict of interest

The authors have no conflicts of interest to declare.

Funding

This research was supported by the reintroduction project of Oriental stork funded by the Cultural Heritage Administration and Yesan county, Republic of Korea, in 2025 (grant No. 2025 0326000003378354).

ORCID

Jeong Hun Shim, https://orcid.org/0009-0000-1858-7725
Seongjun Choe, https://orcid.org/0000-0002-9204-2173
Sukyung Kim, https://orcid.org/0000-0003-3545-0282
Dongsoo Ha, https://orcid.org/0000-0002-1943-9190
Soo Hyung Eo, https://orcid.org/0000-0001-6719-1612

References

1. Price RD, Hellenthal RA, Palma RL, Johnson KP, Clayton DH. The chewing lice: world checklist and biological overview. Illinois Natural History Survey; 2003.
2. Pizzi R. Veterinarians and taxonomic chauvinism: the dilemma of parasite conservation. J Exot Pet Med 2009;18:279-82. https://doi.org/10.1053/j.jepm.2009.09.005
3. Clayton DH, Adams RJ, Bush SE. Phthiraptera, the chewing lice. In: Atkinson CT, Thomas NJ, Hunter DB, editors. Parasitic diseases of wild birds. John Wiley & Sons; 2008. p. 513-26.
4. History of Oriental Stork Restoration. History of the Oriental stork restoration [Internet]. [cited 2025 Mar 24]. Available from: https://www.stork.or.kr/index.php?pg_idx=58
5. Sung HC, Cheong SW, Kim JH, Kim SK, Park SR. A case study of foraging time budget and habitat selection of oriental white storks (*Ciconia boyciana*) in natural state. Korean J Environ Biol 2008;26:121-7.
6. Shim JH, Eo SH. Research trends of the genus *Ciconia* (Aves, Ciconiidae) using text-mining and co-occurrence word analysis: focus on the Oriental Stork conservation. Korean J Ornithol 2024;31:77-84. https://doi.org/10.30980/kjo.2024.12.31.2.77
7. Kang YB, Byun SY. *Cuclotogaster heterographus* and *Anaticola anseris* (Mallophagh; Ischnocera): collection from *Ciconia boyciana*, description and observation with scanning electron microscopy. Korean J Vet Res 1984;24:227-36.
8. Shim JH, Han YD, Kim S, et al. A new feather mite species of the genus *Mycterialges* Gaud & Atyeo, 1981 (Acari, Xolalgidae) from the Oriental Stork, *Ciconiaboyciana* (Ciconiiformes, Ciconiidae) in Korea. ZooKeys 2024;1192:179-96. https://doi.org/10.3897/zookeys.1192.115749
9. Kaneko K, Kadosaka T. Notes on three species of biting lice (Mallo-

https://doi.org/10.3347/PHD.25070

phaga) found on Japanese White Stork *Ciconia ciconia boyciana* in Japan. J Yamashina Inst Ornithol 1977;9:259-63.
10. Gustafsson DR, Diblasi E, Olsson U, et al. Checklist and key to the lice (Insecta: Phthiraptera) of Sweden. Entomol Tidskr 2018;139:205-394.
11. Pérez JM. How many threatened lice are there? An approximation to the red list of the Spanish Phthiraptera. Int J Parasitol Parasites Wildl 2023;23:100903. https://doi.org/10.1016/j.ijppaw.2023.100903
12. Rózsa L, Vas Z. Co-extinct and critically co-endangered species of parasitic lice, and conservation-induced extinction: should lice be re-introduced to their hosts? Oryx 2015;49:107-10. https://doi.org/10.1017/S0030605313000628

Case Report

Parasites Hosts Dis 2026;64(1):92-97
https://doi.org/10.3347/PHD.25076

Parasites, Hosts and Diseases

pISSN 2982-5164 • eISSN 2982-6799

Feline heartworm (*Dirofilaria immitis*) infection in stray cats in Ulsan, Korea

Jihyun Kim[1,2], Miryeng Kim[1], Seungjin Lee[1], Youngmin Yun[2,*]

[1]Lee Seungjin Animal Medical Center, Ulsan, Korea; [2]College of Veterinary Medicine and Veterinary Medical Research Institute, Jeju National University, Jeju, Korea

Feline heartworm (*Dirofilaria immitis*) infection is an uncommon but clinically significant disease in Korea. A retrospective review of electronic medical records from a secondary referral animal hospital in Ulsan, Korea, identified 2 antigen-positive (1.5%) cases among 130 stray cats tested between 2019 and 2023, while no infections were detected in 298 client-owned cats. As antigen testing may yield false-negative results in cats with male-only infections, the true prevalence is likely underestimated. This report describes the clinical and echocardiographic findings of 2 infected stray cats. Case 1 involved successful long-term management of heartworm-associated respiratory disease, with the cat remaining healthy for 4 years following diagnosis. Case 2 demonstrated persistent evidence of adult heartworms and sudden death after an asymptomatic period of 1 year. Echocardiography in Case 2 revealed multiple hyperechoic double lines within the pulmonary arteries, consistent with intraluminal adult worms. These cases illustrate the diagnostic challenges and variable clinical outcomes of feline heartworm infection, emphasizing the need for increased awareness in Korea.

Keywords: Feline heartworm, *Dirofilaria immitis*, echocardiography, heartworm-associated respiratory disease, Ulsan

Introduction

Heartworm (*Dirofilaria immitis*) is a parasitic disease that occurs worldwide, and its prevalence has been reported among stray cats in Korea [1,2]. With climate change and growing pet populations, the risk of infection is increasing, highlighting the importance of heartworm prevention in domestic pets [3,4]. Although cats are susceptible hosts, they are more resistant to adult *D. immitis* infection than dogs [5,6]. Most adult heartworm infections in cats are comparatively mild, typically involving fewer than 6 worms [7,8]. The true prevalence of heartworm infection in cats is likely underestimated because of diagnostic limitations, transient clinical signs, and sudden death without diagnostic confirmation [9,10].

In Korea, limited epidemiological data are available, particularly in cats. In a retrospective review of electronic medical records from a secondary referral animal hospital in Ulsan, Korea, we identified 428 cats that underwent heartworm antigen testing using a commercial ELISA kit (SNAP Feline Triple Test, IDEXX Laboratories) between January 2019 and December 2023. Testing was performed randomly and was not limited to cats with specific clinical conditions. Of the cats tested, 130 were strays and 298 were client-owned pets. Two stray cats (1.5%) tested positive, whereas no infections were detected in the client-owned population.

The present case report describes 2 clinical cases of heartworm infection in stray cats in Korea: one involving successful long-term management of heartworm-associated respiratory

Received: August 31, 2025 Accepted: November 11, 2025
*Correspondence: dvmyun@jejunu.ac.kr

Citation
Kim J, Kim M, Lee S, Yun Y. Feline heartworm (*Dirofilaria immitis*) infection in stray cats in Ulsan, Korea. Parasites Hosts Dis 2026;64(1):92-97.

disease (HARD) with complete clinical recovery, and the other demonstrating echocardiographic visualization of multiple adult heartworms. This finding is exceptionally rare and, to our knowledge, has not been previously documented in cats in Korea.

The authors declare that no institutional animal care and use committee or other ethical approval was required, as this study was a retrospective analysis of electronic medical records.

Case Report

Case 1

A 2-year-old female stray cat presented with cough, vomiting, and diarrhea in April 2021. Physical examination revealed tachypnea, crackling lung sounds, and ear mites. Complete blood count (CBC), serum chemistry, electrolyte analysis, probrain natriuretic peptide (proBNP) measurement, feline leukemia virus (FeLV) testing, feline immunodeficiency virus (FIV) testing, heartworm antigen testing using an ELISA kit (SNAP Feline Triple test, IDEXX Laboratories), antibody testing (Heska Corporation, an Antech company), thoracic and abdominal radiography, and abdominal ultrasonography were performed. Results for CBC, serum chemistry, electrolyte levels, proBNP, FeLV testing, and FIV testing were all within reference ranges; however, the heartworm antigen and antibody tests were both positive. Thoracic radiography revealed pulmonary artery enlargement extending to the right caudal lung lobe, interstitial infiltration of the pulmonary field, and multiple fissure lines. Abdominal ultrasonography revealed a mild increase in mucosal echogenicity in specific small intestinal segments, as well as a small amount of fluid stasis, indicating mild enteritis and localized hypomotility. Cardiac ultrasonography could not be performed because of severe respiratory distress, representing a limitation in confirming the presence of adult worms. The diagnosis of HARD was therefore based on compatible clinical signs, thoracic radiographic findings, and concurrent antigen and antibody positivity.

The cat was treated with oxygen supplementation, maintenance fluid therapy, prednisone [1 mg/kg orally (PO) twice daily (BID)], doxycycline (5 mg/kg PO BID), acetylcysteine (10 mg/kg PO BID), pheniramine (1 mg/kg PO BID), and metronidazole (10 mg/kg intravenously BID). Daily thoracic radiographs were obtained to monitor lung condition (Fig. 1). On hospitalization day 5, thoracic radiographs showed normalization of pulmonary fields. At discharge, prednisone (1 mg/kg PO BID), doxycycline (5 mg/kg PO BID), acetylcysteine (10 mg/kg PO BID), and pheniramine (1 mg/kg PO BID) were prescribed for an additional week to manage HARD [11]. Revolution (selamectin, Zoetis) was applied topically once a month as a preventive macrocyclic lactone to avoid reinfection and target potential immature stages [12]. Thoracic radiographs showed no significant changes upon reevaluation after 1 week. The same medications were continued, except prednisone, which was tapered to 0.5 mg/kg PO every other day for 2 weeks. Subsequent follow-up radiographs revealed no significant changes, and a medication-free period was initiated.

On day 56 of the medication-free period, the cat developed coughing, and thoracic radiographs revealed progression of interstitial infiltration in the pulmonary fields. The cat was readministered prednisone at 1 mg/kg PO BID. After 2 weeks of clinical improvement, the dose was tapered to 0.5 mg/kg PO every other day for another 2 weeks before discontinuation.

At 6, 12, and 18 months after the initial diagnosis, both heartworm antigen and antibody tests yielded negative results, indicating serologic conversion and the likely resolution of infection. No recurrent antigen or antibody positivity was detected during subsequent follow-up assessments. Currently, 4 years after the initial diagnosis, the cat remains asymptomatic and in good health, suggesting successful long-term management.

Case 2

A 5-year-old rescued female stray cat presented with generalized skin ulcers, maggot infestation, and cachexia in August 2019. CBC, serum chemistry, electrolyte analysis, proBNP, FeLV and FIV tests, heartworm antigen and antibody kit tests, thoracic and abdominal radiographs, and abdominal ultrasound were performed. Test results were positive for heartworm antigen and antibody tests, anemia, dehydration, and azotemia. Thoracic radiographs revealed marked dilation and tortuosity of pulmonary arteries coursing through both caudal lung lobes. B-mode echocardiography revealed multiple hyperechoic, parallel double lines within the main pulmonary artery bifurcation and right pulmonary artery branches, consistent with adult heartworms. Standard short-axis, M-mode, and Doppler echocardiography demonstrated a normal left atrium-to-aorta ratio (1.36), preserved systolic function (fractional shortening: 56.3%), and no evidence of severe pulmonary hypertension. These findings confirmed the presence of multiple adult heartworms (Fig. 2).

Ultrasonographic examination indicated jejunojejunal intussusception. After blood transfusion for anemia, surgery was performed to resect the intussuscepted segment, and an intestinal anastomosis was performed. After 1 month of hospitaliza-

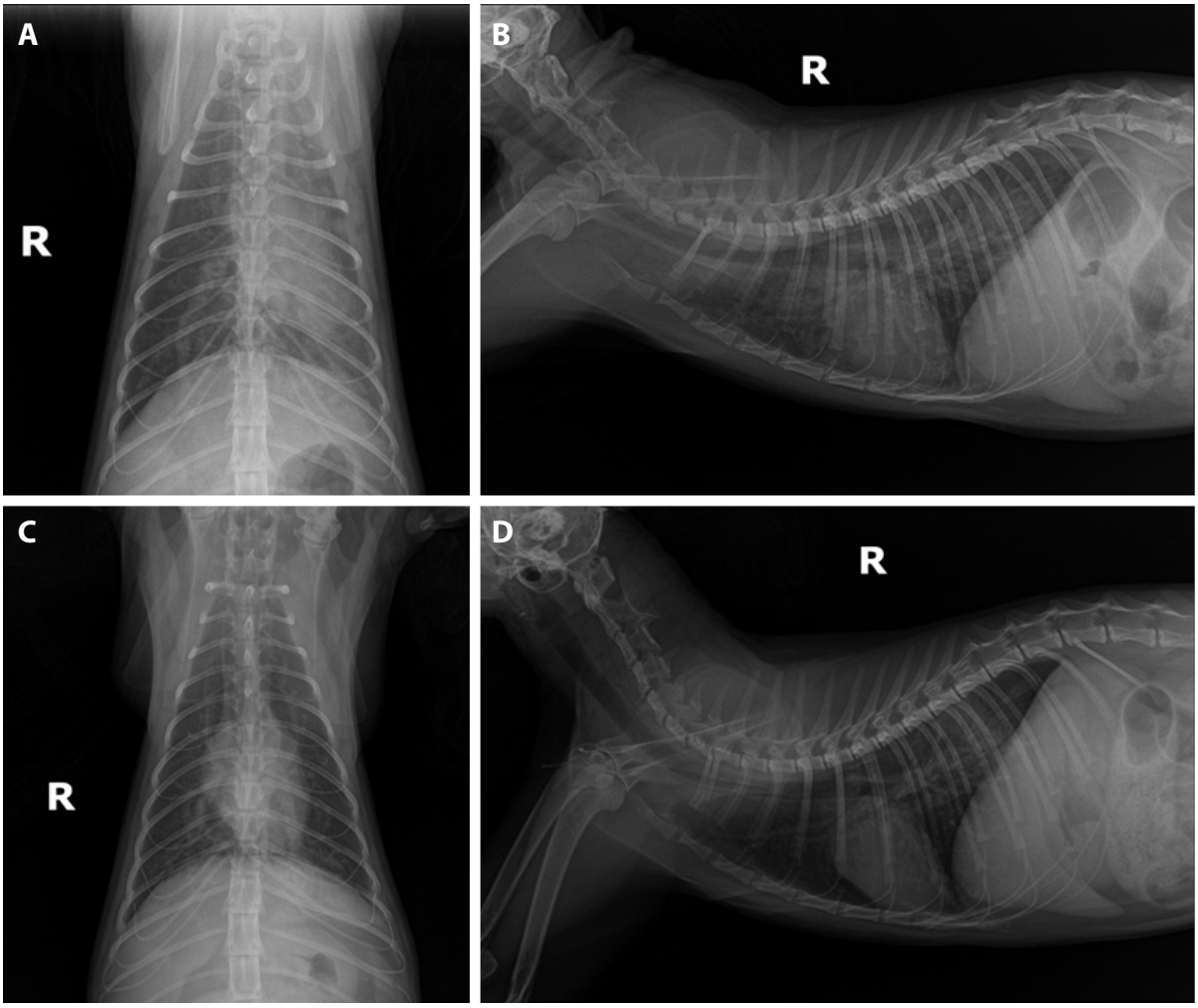

Fig. 1. Thoracic radiographs of Case 1. Day 1: (A) ventrodorsal view and (B) right lateral view. Pulmonary artery enlargement extending to the right caudal lung lobe is evident in the dorsoventral projection. Additionally, interstitial infiltration is present in the lung field, with multiple fissure lines observed. Day 5: (C) ventrodorsal view and (D) right lateral view. Compared with the findings on Day 1, pulmonary infiltration decreased over the 5-day period.

tion with assisted feeding, nutritional support, and regular wound care, the skin ulcers and maggot infestation had completely resolved. The cat was discharged with a body condition score of approximately 4/9 and showed no evidence of gastrointestinal or respiratory clinical signs. Revolution (selamectin, Zoetis) was applied topically once a month. Follow-up monitoring involved thoracic radiography, abdominal ultrasound, and serologic testing every 3 months. Follow-up thoracic radiographs revealed persistent, marked dilation and tortuosity of the pulmonary arteries coursing through both caudal lung lobes. Both antigen and antibody tests remained positive 1 year after infection. Despite apparent clinical stability, the cat died suddenly 1 year after infection was confirmed. As a necropsy was not performed, the cause of death could not be definitively determined; however, heartworm-associated complications, such as pulmonary embolism or cardiovascular compromise, were considered possible contributing factors.

Discussion

A 2005 study involving 155 stray cats in Gyoenggi-do province, Korea, reported that 2.6% (4 cats) tested positive for *D. immitis* [1]. Another study investigating 235 stray cats in Korea (Daejeon, Seoul, and Gyeonggi-do province) in 2014 identified heartworm infection in 14 cats (6%) [2]. In this retrospective review of 428 cats tested over a 5-year period in Ulsan, Korea, antigen positivity was confirmed in 2 of 130 stray cats (1.5%), whereas none of the 298 client-owned cats tested positive. Al-

https://doi.org/10.3347/PHD.25076

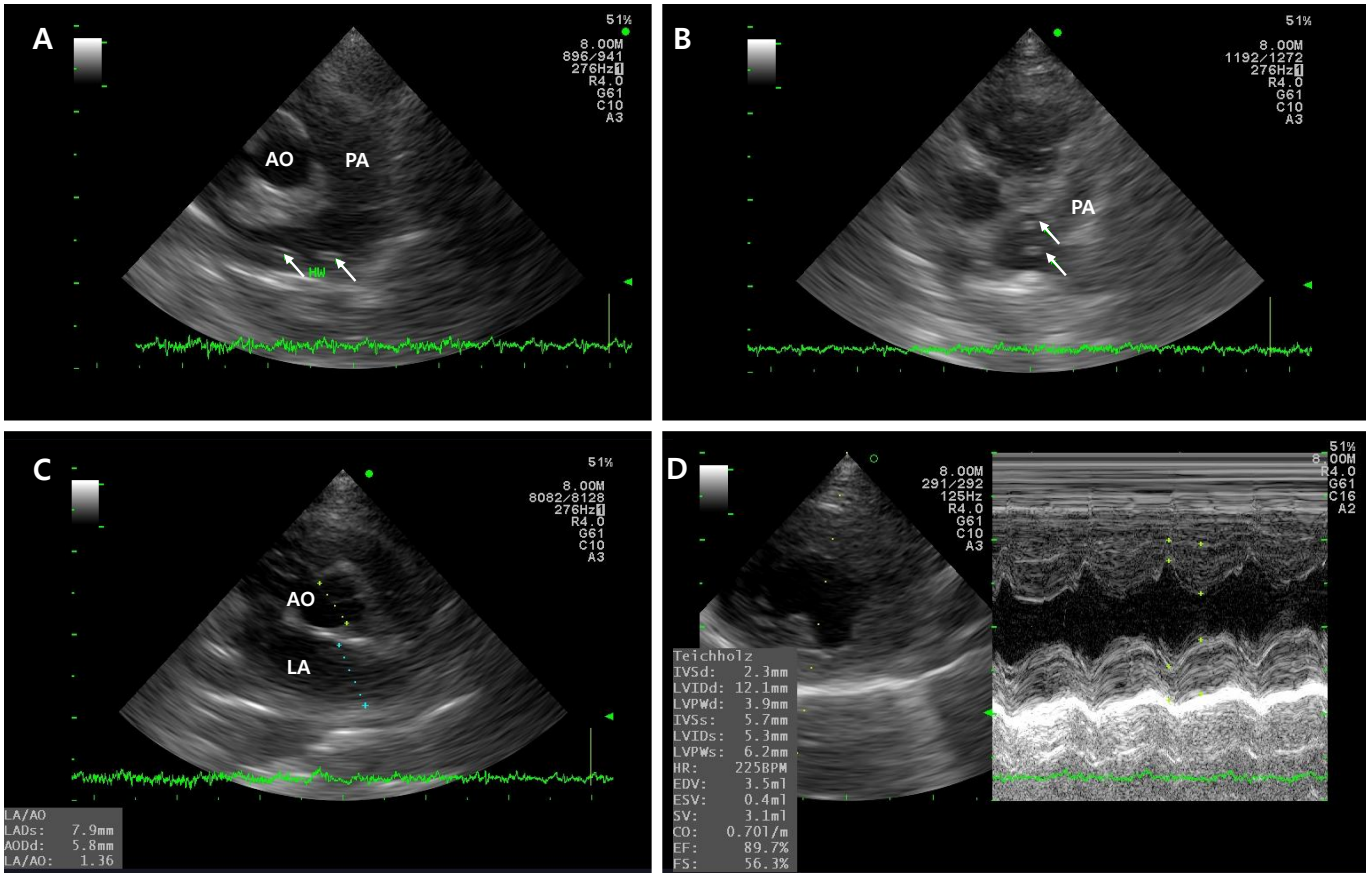

Fig. 2. Echocardiographic findings in Case 2. (A, B) B-mode image showing multiple hyperechoic, parallel double lines (white arrows) within the bifurcation of the main pulmonary artery (PA) and branches of the right PA, consistent with intraluminal adult heartworms. (C) Right parasternal short-axis view at the level of the aortic root showing a left atrium (LA)-to-aorta (AO) ratio of 1.36, indicating no overt left atrial enlargement. (D) M-mode echocardiography demonstrating normal left ventricular wall motion and systolic function (fractional shortening: 56.3%).

though the overall prevalence was low, these findings align with those of previous reports, suggesting that stray cats are at a higher risk of infection due to greater mosquito exposure.

According to the American Heartworm Society, approximately 75% of heartworm-infected cats are stray cats, whereas 25% are indoor cats [13,14]. However, to date, no cases of heartworm infections in indoor cats have been documented in Korea. This may be attributed to differences in residential environments, as apartments are predominant in Korea, which may reduce the risk of mosquito exposure and the potential use of preventive medications. Additionally, asymptomatic cases or sudden deaths may be undiagnosed [15,16].

In dogs, antigen testing is considered the "gold standard" for diagnosing heartworm infections. Commercially available antigen tests target antigens in the reproductive tract of adult females; however, their reliability in cats is limited because unisex infections involving only male worms or symptomatic immature infections are more common in cats [5,17]. In contrast, antibody testing can detect infections caused by larvae of either sex as early as 2 months post-infection. Combining serum antigen and antibody tests provides higher sensitivity and specificity than using either test alone. Previous studies have reported sensitivities of up to 100% and specificities of up to 99.4% when both tests were combined compared with a maximum sensitivity of 89.5% and specificity of 92.9% when these tests were used alone [18]. Although echocardiography could not be performed, Case 1 demonstrated concurrent positivity for both antigen and antibody tests at diagnosis, indicating the high sensitivity of combined serologic testing for detecting feline heartworm infection. During follow-up, serial negative conversion of both markers further supported successful resolution of the infection.

Case 1 highlights the potential for favorable outcomes with timely and appropriate treatment. Medications considered for feline heartworm disease include prednisolone to relieve coughing and other respiratory signs, doxycycline to eliminate *Wolbachia* organisms from heartworms that contribute to disease pathogenesis, and supportive therapy such as bronchodi-

lators, oxygen, and fluids to alleviate respiratory distress [6,11,19,20]. With appropriate management, the cat has survived for 4 years following diagnosis and has remained asymptomatic to date. In Case 2, echocardiography played a pivotal role in confirming heartworm infection in this cat, demonstrating characteristic imaging findings. B-mode imaging revealed multiple hyperechoic, parallel double lines in the main and right pulmonary arteries, a pathognomonic sign of adult heartworms. Echocardiography showed normal chamber sizes, preserved systolic function, and no severe pulmonary hypertension, underscoring its value for detecting early or asymptomatic infections and complementing antigen testing.

This case report has several limitations, including the small number of cases, absence of necropsy in Case 2, and potential selection bias from a single secondary referral hospital, where a large proportion of client-owned cats routinely receive preventive care. Moreover, this report was confined to a single geographic region (Ulsan). Nevertheless, our cases provide valuable clinical insights into feline heartworm infection in Korea, reporting the prevalence of infection in stray cats in Ulsan and describing 2 cases that highlight both the potential for long-term survival with appropriate treatment and the risk of sudden death in asymptomatic cats.

To the best of our knowledge, this report provides one of the few documented descriptions of the prevalence, clinical manifestations, detailed echocardiographic findings, and long-term management of heartworm infection in stray cats in Korea. Timely and appropriate treatment, including supportive therapies and medications, can improve HARD, although sudden death remains a possible outcome in some cases.

Author contributions

Conceptualization: Kim J, Yun Y. Data curation: Kim J, Kim M. Formal analysis: Kim J. Funding acquisition: Yun Y. Investigation: Kim J. Resources: Kim J. Supervision: Lee S, Yun Y. Writing – original draft: Kim J.

Conflict of interest

The authors have no conflicts of interest to declare.

Funding

This research was supported by the Regional Innovation System & Education (RISE) program through the Jeju RISE center, funded by the Ministry of Education (MOE) and the Jeju Special Self-Governing Province, Republic of Korea (2025-RISE-17-001).

ORCID

Jihyun Kim, https://orcid.org/0009-0003-9133-9228
Miryeng Kim, https://orcid.org/0009-0005-1478-3856
Seungjin Lee, https://orcid.org/0009-0007-3036-7777
Youngmin Yun, https://orcid.org/0000-0003-0695-0843

References

1. Liu J, Song KH, Lee SE, et al. Serological and molecular survey of *Dirofilaria immitis* infection in stray cats in Gyunggi province, South Korea. Vet Parasitol 2005;130:125-9. https://doi.org/10.1016/j.vetpar.2005.03.026
2. Park HJ, Lee SE, Lee WJ, et al. Prevalence of *Dirofilaria immitis* infection in stray cats by nested PCR in Korea. Korean J Parasitol 2014;52:691-4. https://doi.org/10.3347/kjp.2014.52.6.691
3. Ledesma N, Harrington L. Fine-scale temperature fluctuation and modulation of *Dirofilaria immitis* larval development in *Aedes aegypti*. Vet Parasitol 2015;209:93-100. https://doi.org/10.1016/j.vetpar.2015.02.003
4. Morchón R, Carretón E, González Miguel J, Mellado Hernández I. Heartworm disease (*Dirofilaria immitis*) and their vectors in Europe: new distribution trends. Front Physiol 2012;3:196. https://doi.org/10.3389/fphys.2012.00196
5. Lee AC, Atkins CE. Understanding feline heartworm infection: disease, diagnosis, and treatment. Top Companion Anim Med 2010;25:224-30. https://doi.org/10.1053/j.tcam.2010.09.003
6. Nelson CT. *Dirofilaria immitis* in cats: anatomy of a disease. Compend Contin Educ Vet 2008;30:382-9.
7. Nelson CT, McCall JW, Rubin SB, et al. 2005 Guidelines for the diagnosis, prevention and management of heartworm (*Dirofilaria immitis*) infection in cats. Vet Parasitol 2005;133:267-75. https://doi.org/10.1016/j.vetpar.2005.07.009
8. Genchi C, Guerrero J, Di Sacco B, Formaggini L. Prevalence of *Dirofilaria immitis* infection in Italian cats. In: American Heartworm Society. Proceedings of Heartworm Symposium '92; 1992; Austin, TX, USA. p. 97-102.
9. Carleton RE, Tolbert MK. Prevalence of *Dirofilaria immitis* and gastrointestinal helminths in cats euthanized at animal control agencies in northwest Georgia. Vet Parasitol 2004;119:319-26. https://doi.org/10.1016/j.vetpar.2003.10.019
10. Levy JK, Snyder PS, Taveres LM, et al. Prevalence and risk factors for heartworm infection in cats from northern Florida. J Am Anim Hosp Assoc 2003;39:533-7. https://doi.org/10.5326/0390533
11. Nelson CT. Heartworm and related nematodes. In: Sykes J, editors. Greene's infectious diseases of the dog and cat. 5th ed. Saunders; 2021. p. 1399-417.
12. McTier TL, Shanks DJ, Watson P, et al. Prevention of experimentally

induced heartworm (*Dirofilaria immitis*) infections in dogs and cats with a single topical application of selamectin. Vet Parasitol 2000;91:259-68. https://doi.org/10.1016/s0304-4017(00)00297-1

13. Atkins CE, DeFrancesco TC, Coats JR, Sidley JA, Keene BW. Heartworm infection in cats: 50 cases (1985–1997). J Am Vet Med Assoc 2000;217:355-8. https://doi.org/10.2460/javma.2000.217.355
14. Genchi C, Venco L, Ferrari N, Mortarino M, Genchi M. Feline heartworm (*Dirofilaria immitis*) infection: a statistical elaboration of the duration of the infection and life expectancy in asymptomatic cats. Vet Parasitol 2008;158:177-82. https://doi.org/10.1016/j.vetpar.2008.09.005
15. Dillon R. Feline dirofilariasis. Vet Clin North Am Small Anim Pract 1984;14:1185-99. https://doi.org/10.1016/s0195-5616(84)50153-3
16. Evans EA, Litster AL, Gunew MNM, Menrath VH. Forty-five cases of feline heartworm in Australia (1990-1998). Aust Vet Pract 2000;30:11-6.
17. Berdoulay P, Levy JK, Snyder PS, et al. Comparison of serological tests for the detection of natural heartworm infection in cats. J Am Anim Hosp Assoc 2004;40:376-84. https://doi.org/10.5326/0400376
18. Snyder PS, Levy JK, Salute ME, et al. Performance of serologic tests used to detect heartworm infection in cats. J Am Vet Med Assoc 2000;216:693-700. https://doi.org/10.2460/javma.2000.216.693
19. Taylor MJ, Bandi C, Hoerauf A. *Wolbachia* bacterial endosymbionts of filarial nematodes. Adv Parasitol 2005;60:245-84. https://doi.org/10.1016/S0065-308X(05)60004-8
20. Bouchery T, Lefoulon E, Karadjian G, Nieguitsila A, Martin C. The symbiotic role of *Wolbachia* in Onchocercidae and its impact on filariasis. Clin Microbiol Infect 2013;19:131-40. https://doi.org/10.1111/1469-0691.12069

Case Report

Parasites Hosts Dis 2026;64(1):98-103
https://doi.org/10.3347/PHD.25022

Parasites, Hosts and Diseases

pISSN 2982-5164 • eISSN 2982-6799

A fatal case of complex hepatic alveolar echinococcosis

Li Xin[1,†], Li Mengmeng[2,†], Yu Huixia[2], Zan Runna[2], Li Guojun[2], Shang Rongjian[3], Yu Jia[4,*]

[1]Department of Hepatobiliary Surgery, Chifeng Multiple Hospital, Chifeng, China; [2]Chifeng Center for Disease Control and Prevention, Chifeng, China; [3]Balin Left Banner Center for Disease Control and Prevention, Chifeng, China; [4]School of Basic Medicine, Chifeng University, Chifeng, China

Hepatic alveolar echinococcosis (HAE), a life-threatening zoonosis, poses formidable surgical challenges when involving critical vasculature. Herein, we reported the periprocedural management dilemmas in radical resection for advanced HAE. A 58-year-old female visited the outpatient department presented with HAE. Imaging examination revealed extensive invasion of the hilum, bile duct, and several hepatic vessels, as well as left adrenal metastasis. The patient underwent right trisegmentectomy with left hepatic vein reconstruction, auto-transplantation, and adrenalectomy, with intraoperative Doppler demonstrating patent portal flow before abdominal closure. However, emergency thrombectomy and transcatheter thrombolysis were performed due to the abrupt occurrence of portal vein thrombosis 3 h after surgery. Despite intervention, the residual liver volume remained insufficient (approximately 28% of the standard liver volume), leading to progressive liver failure. The patient expired from multiorgan failure 9 days after operation. This case underscores not only the critical balance between radical resection and preservation of residual liver function in the surgical management of complex HAE, but also the imperative need to establish a comprehensive postoperative thromboprophylaxis.

Keywords: Echinococcosis, liver transplantation, portal vein thrombosis

Introduction

Hepatic alveolar echinococcosis (HAE), caused by the larval stage of *Echinococcus multilocularis*, poses a significant zoonotic burden in endemic regions such as the Mediterranean, Central Asia, and East Africa [1-3]. Although the majority of hydatid cysts localize to the liver (50%–75%) or lungs (25%), invasive forms involving critical vasculobiliary structures remain formidably challenging in relevant therapies [4,5]. Notably, 2%–10% of hepatic cases exhibit intrahepatic vascular invasion, yet concurrent infiltration of portal veins, hepatic veins, and bile ducts—termed "complex echinococcosis"—constitutes a distinct clinical entity with a post-resection mortality exceeding 40% [6].

The current consensus defines complex echinococcosis by the necessity for vascular/biliary reconstruction due to invasion of ≥2 major hepatic structures (Glissonian pedicles or hepatic venous confluences) [7]. This advanced stage of disease correlates with catastrophic complications: 31% of patients develop vascular thrombosis, while 58% of patients progress to liver failure despite undergoing macroscopic radical resection [8]. Pathophysiologically, parasitic-induced perivascular fibrosis disrupts endothelial integrity, creating a prothrombotic milieu exacerbated by surgical manipulation [9].

This case report describes a 58-year-old female with complex HAE. Intraoperative findings revealed extensive invasion of the

Received: April 23, 2025 Accepted: September 15, 2025
*Correspondence: 15124905188@163.com

[†]These authors contributed equally to this work.

Citation
Xin L, Mengmeng L, Huixia Y, Runna Z, Guojun L, Rongjian S, Jia Y. A fatal case of complex hepatic alveolar echinococcosis. Parasites Hosts Dis 2026; 64(1):98-103.

first and second hepatic hila, encasement of the right and middle hepatic veins, and involvement of the right hepatic duct, right portal vein branch, and right hepatic artery, accompanied by concurrent left adrenal metastasis. The patient underwent ex vivo right trisegmentectomy combined with left hepatic vein reconstruction, autologous liver transplantation, and adrenalectomy. Despite emergency thrombectomy and interventional thrombolysis for early postoperative portal vein trunk thrombosis, acute liver failure secondary to insufficient residual hepatic functional reserve ensued, culminating in fatal multiorgan failure on the postoperative day 9. Therefore, we present a fatal case of complex HAE with critical vascular invasion, managed through radical resection and auto-transplantation yet complicated by fulminant portal thrombosis, aiming to emphasize the critical importance of preoperative hemodynamic mapping and protocolized anticoagulation in mitigating catastrophic outcomes for such advanced cases.

This study was approved by the Ethics Committee of Chifeng Center for Disease Control and Prevention (approval No. 20250001). Informed consent was obtained from the legal guardian of patient whom consented to the publication of this case report.

Case Report

A 58-year-old female from a pastoral area in Chifeng, Inner Mongolia, presented with unexplained abdominal pain persisting for 1 month. She had a history of close contact with cattle, sheep, and foxes, without prior treatment-related history. Physical examination revealed no abdominal tenderness, and the liver and spleen were not palpable, but liver percussion pain was positive.

To investigate the potential source of exposure, metagenomic sequencing was performed on blood samples from livestock (dog, sheep, and rat) within the patient's household. The analysis revealed sequences aligning with *E. multilocularis*, indicating environmental contamination and underscoring the risk of zoonotic transmission (Table 1).

Laboratory examination showed alpha-fetoprotein at 2.37 ng/ml (normal <7.0), carcinoembryonic antigen at1.39 μg/L (normal <5.0) and negative echinococcus IgG antibody (ELISA) (optical density value 0.12, cut-off 0.35). It is noteworthy that up to 10% of diagnosed patients with confirmed alveolar echinococcosis may present with false-negative serological results, potentially due to immune exhaustion, sequestration of antigens within cysts, or technical limitations of the assay. Therefore, negative serology cannot unequivocally exclude the diagnosis, particularly in the context of highly suggestive imaging and histopathological findings.

Ultrasound showed a heterogeneous hyperechoic mass (7.8 × 5.5 cm) with unclear borders in liver segments S4, S7, and S8 (Fig. 1). Computed tomography suggested a large, poorly defined mass with mixed density and patchy calcifications (maximum cross-sectional area 15.11 × 11.29 cm) in the liver. No enhancement was observed in dynamic contrast imaging. A low-density lesion in the left adrenal gland showed no enhancement (Fig. 2A). The right portal vein was narrowed. The right and middle hepatic veins were partially obscured in the portal venous phase (Fig. 2B). The presence of a large, infiltrative mass with heterogeneous density and irregular calcifications is a recognized, though not universal, imaging presentation of advanced alveolar echinococcosis, which can mimic

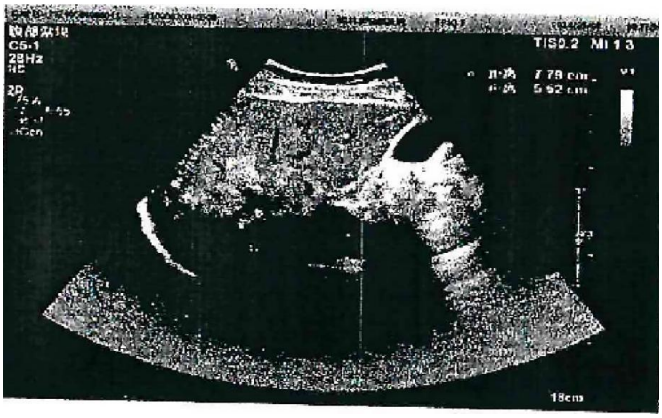

Fig. 1. Abdominal color doppler ultrasound showed a heterogeneous.

Table 1. Metagenomic-based screening for *Echinococcus multilocularis* infection in domestic animals of alveolar echinococcosis patient's household

Sample ID	Species	Target	Query sequence	Matched species	Accession	Identity (%)	E-value	Matched gene/region
D-01	Dog	Serum antibody metagenomics	0001_31224071500758_CF-CDC01_F-COI	*E. multilocularis*	Query_635351	90%	5E-123	cox1 gene
R-01	Sheep	Serum antibody metagenomics	0005_31224071500760_CF-CDC45_F-COI	*E. multilocularis*	Query_9585824	87%	1E-122	cox1 gene
P-01	Rat	Serum antibody metagenomics	0007_31224071500761_CF-CDC61_F-COI	*E. multilocularis*	Query_9233003	87%	2E-122	cox1 gene

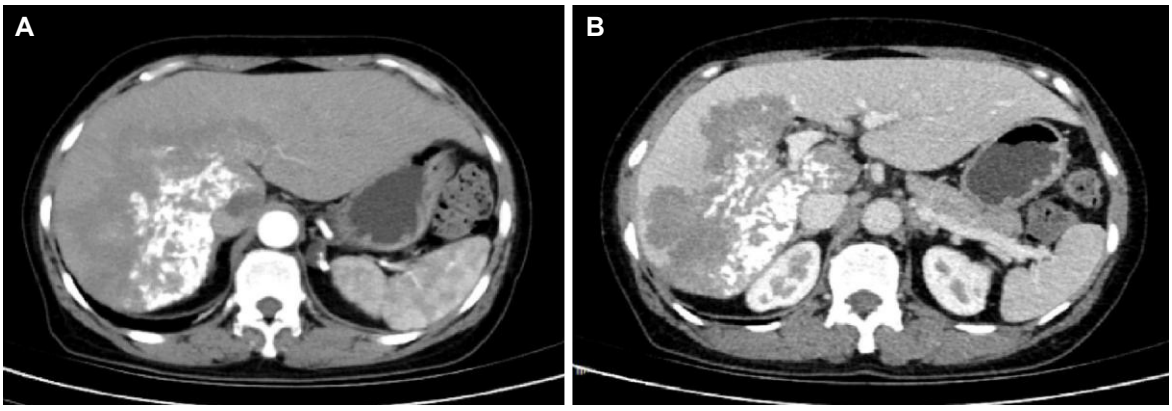

Fig. 2. Abdominal computed tomography (CT) of the liver. (A) Arterial phase CT demonstrates a large hypodense occupying lesion in the liver with patchy hyperdense areas, showing no enhancement. A non-enhancing hypodense lesion is observed in the left adrenal region. (B) Portal venous phase CT reveals stenosis of the right portal vein branch within the lesion area, with partial obscuration of the right and middle hepatic veins.

malignancy.

Magnetic resonance imaging showed irregular, slightly hyperintense T1 signals in the right lobe and caudate lobe (14.5×9.6×11.5 cm) without enhancement. The capsule showed enhancement, with inferior vena cava locally compressed. Diffusion-weighted imaging revealed slightly high signals (Fig. 3). T2-weighted imaging showed irregular, slightly hyperintense T2 signals in the right lobe and caudate lobe, with high diffusion-weighted imaging signals. A round, hyperintense T2 lesion (1.6×1.3 cm) was seen in the left adrenal gland (Fig. 4A, B). The absence of typical multilocular cystic structures cannot rule out HAE, as the disease may present as a solid, pseudotumoral mass with central necrosis and peripheral fibrosis, especially in endemic areas.

Child-Pugh score was classified as Class A (5 points), with the 15-min indocyanine green retention rate of 8.2% (normal <10.0%) and residual liver volume of 45.6% (520/1,140 g), meeting the criteria for autologous liver transplantation (>30.0%).

Intraoperative exploration revealed invasion of the left hepatic vein root. The patient underwent right trisegmentectomy with left hepatic vein reconstruction (using the portal vein), autologous liver transplantation, portocaval shunt, and left adrenalectomy. Intraoperative ultrasound confirmed patent blood flow in all vessels. The surgery lasted 12 h and 19 min, with 400 ml of blood loss and no transfusion. Postoperative hepatic vascular ultrasound suggested portal vein thrombosis (PVT), prompting re-exploration within 3 h. The liver appeared dark and swollen. Intraoperative ultrasound confirmed weak portal vein flow with thrombosis. Thrombectomy and portal vein reconstruction (using the umbilical vein) were therefore performed. Postoperative ultrasound and flowmetry confirmed normal portal vein flow.

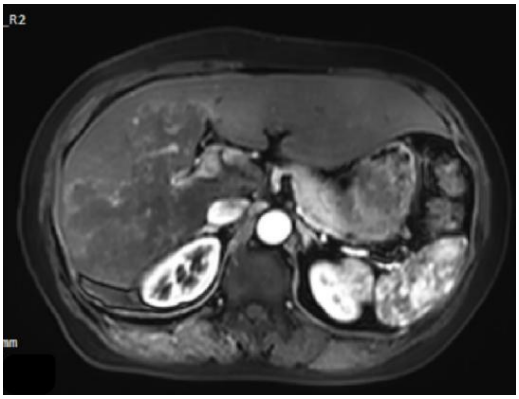

Fig. 3. Magnetic resonance imaging demonstrates a large area of mildly prolonged T1 signal within the liver parenchyma, showing no enhancement post-contrast, with slightly hyperintense signal on diffusion-weighted imaging.

PVT was detected 3 h postoperatively (flow velocity <5 cm/sec). Emergency thrombectomy revealed a mixed thrombus of 3.2 cm. By postoperative day 5, total bilirubin increased to 15.6 mg/dl (direct bilirubin >70%), and the international normalized ratio exceeded 3.0, meeting the criteria for acute-on-chronic liver failure (chronic liver failure consortium organ failure score: 11). On postoperative day 9, PVT recurred with left hepatic vein stenosis (narrowing >80%). Despite the operation of thrombolysis (recombinant tissue plasminogen activator 20 mg local infusion), the patient progressed to multiorgan dysfunction syndrome (sequential organ failure assessment score: 14) and died.

Postoperative pathology revealed features of alveolar echinococcosis, including extensive necrotic debris and peripheral palisading granulomatous inflammation with fibrosis (Fig. 5). The presence of a characteristic laminated layer was observed.

https://doi.org/10.3347/PHD.25022

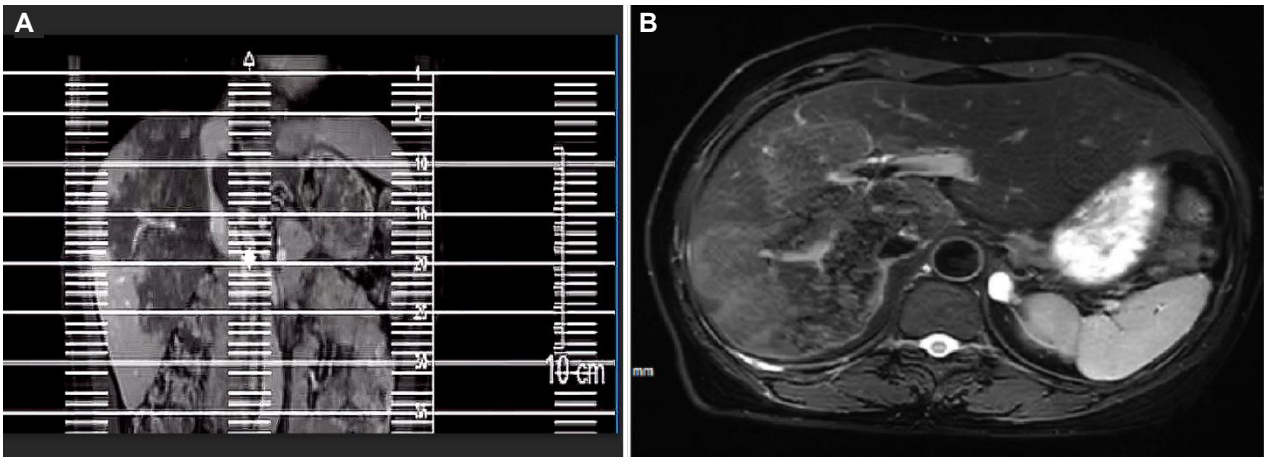

Fig. 4. (A) Magnetic resonance imaging T2-weighted imaging demonstrates mildly prolonged T2 signal in the right hepatic lobe and caudate lobe. (B) A round-shaped, hyperintense T2 signal lesion is observed in the left adrenal gland, which also shows high signal intensity on diffusion-weighted imaging.

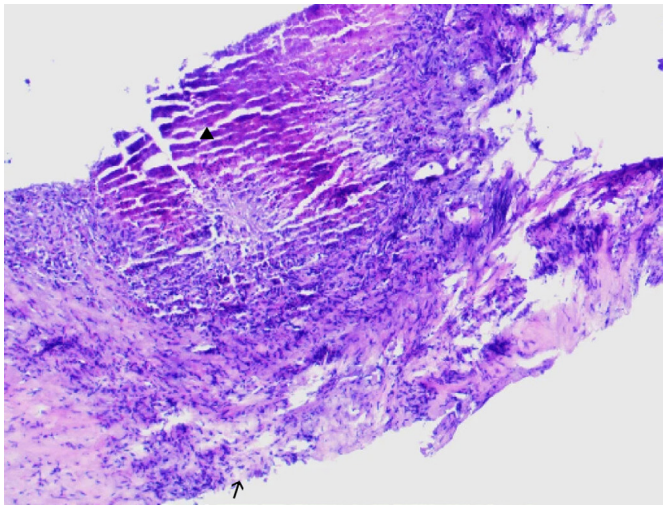

Fig. 5. The histopathological examination reveals a characteristic laminated layer (▲), displaying a wavy eosinophilic structure. The germinal layer (→) shows hyperchromatic nuclei. Surrounding hepatic tissue exhibits inflammatory cell infiltration. H&E staining, ×400.

The overall histopathological architecture, in conjunction with the clinical and radiological presentation, was highly consistent with HAE despite the absence of protoscoleces.

Discussion

The definitive histological diagnosis of alveolar echinococcosis typically relies on the identification of parasitic structures, such as the laminated layer and protoscoleces within the lesion. In the present case, the pathological findings were highly suggestive of HAE, demonstrating the characteristic laminated layer and surrounding fibro-inflammatory response. However, the absence of observable protoscoleces on histopathology remains common, particularly in advanced cases where extensive necrosis and calcification may obscure parasitic elements, making it important to integrate pathological findings with serological, molecular, and imaging data for a conclusive diagnosis.

The imaging findings in this case, while not displaying the classic 'hive-like' multilocular cysts often associated with HAE, were consistent with an advanced and infiltrative pseudotumoral form of the disease. Key features such as the lack of enhancement, internal calcifications, and invasion of vascular structures have been well-documented in the literature on atypical HAE presentations. The radiological differential diagnosis primarily include infiltrative hepatocellular carcinoma or intrahepatic cholangiocarcinoma; However, the diagnosis towards HAE is guided by the patient's epidemiological background, the stability of the lesion's characteristics across multiple imaging modalities, and ultimately the histopathological results.

HAE, caused by *E. multilocularis*, is a zoonotic parasitic infection with a malignant clinical course. Inoperable or advanced HAE requires a long-term primary treatment of albendazole chemotherapy, which is typically lifelong. Radical resection is only feasible in a minority of patients with localized disease [10-12].

Due to the asymptomatic feature of the early-stage, many patients present at advanced stages of the disease. For advanced cases, liver reserve function and residual liver volume must be carefully assessed [9]. Resection and reconstruction are necessary under the condition of involved major vessels, with autologous or synthetic grafts considered for extensive vascular de-

fects [10].

In this case, PVT developed within 3 h postoperatively. Although thrombectomy was performed, liver failure ensued, and PVT recurred on day 9, ultimately leading to death. PVT is a rare but severe complication of autologous liver transplantation. According to Yerdel's classification, this case was classified as Grade I, indicating surgical feasibility. However, despite early intervention, liver failure and recurrent thrombosis occurred, highlighting the high risk of PVT.

The development of postoperative PVT in this case stemmed from a multifactorial interplay of Virchow's triad components. Hemorheological abnormalities arose from hydatid cyst invasion at the left hepatic vein root, necessitating reconstruction after right trisegmentectomy. Postoperative angiography revealed a stenosis that can impair venous outflow and cause hepatic congestion, elevated portal pressure, and stasis, requiring balloon angioplasty. Vascular endothelial injury occurred due to cyst invasion into portal venous branches, mandating vascular reconstruction during autologous transplantation. This disrupted thromboresistance via increased platelet-activating factor (HMDB HMDB0009435)-mediated platelet aggregation, elevated endothelin-1 (encoded by gene EDN1, gene ID 1906, UniProt P05305), and reduced prostacyclin (synthesized by PTGIS, gene ID 5740, UniProt Q16647), thereby promoting vasospasm and thrombosis. Hypercoagulability emerged from a prolonged surgery lasting 12 h and 19 min, anesthesia-induced hemodynamic instability, anhepatic phase coagulopath caused by clotting factor consumption and delayed post-reperfusion synthesis. Concurrently, reduced fibrinolysis, hyperlactatemia, and hypocalcemia exacerbated coagulative dysregulation. Ischemia-reperfusion injury further destabilized the coordinated recovery of pro-/anticoagulant mechanisms, while left adrenalectomy extended operative trauma and fluid loss, indirectly amplifying the risks of PVT. Collectively, these factors precipitated a lethal cascade: PVT-triggered portal flow obstruction reduced hepatic perfusion by 60%–70%, inducing ischemic necrosis, failed regeneration, and fatal multiorgan failure although thrombectomy has been performed.

Postoperatively, there was an unstable equilibrium between the hemodynamic and coagulation systems of the patient, compounded by immature hepatic collateral circulation. Rapid PVT progression acutely obstructed portal flow, reduced hepatic perfusion by 60%–70%, and precipitated hepatocellular hypoxia, ischemic necrosis, and fulminant hepatic failure. Although thrombectomy was performed, ischemia-reperfusion injury and delayed hepatocyte apoptosis further compromised hepatic regeneration. Recurrent PVT precipitated irreversible liver failure, culminating in multiorgan dysfunction and mortality.

This case highlights the challenges in managing HAE with vascular invasion. Early diagnosis and multidisciplinary intervention are critical for prognosis. Postoperative complications such as PVT and hepatic failure remain formidable despite the therapeutic option provided by right trisegmentectomy combined with portal vein reconstruction. In endemic regions, heightened suspicion for parasitic infections and proactive screening are essential to mitigate disease progression.

Author contributions

Data curation: Huixia Y. Formal analysis: Huixia Y, Rongjian S. Investigation: Guojun L. Methodology: Guojun L. Resources: Rongjian S. Supervision: Jia Y. Validation: Runna Z. Visualization: Runna Z. Writing – original draft: Xin L, Mengmeng L. Writing – review & editing: Jia Y.

Conflict of interest

The authors have no conflicts of interest to declare.

Acknowledgments

We would like to express our gratitude to Hongmei Bao for her invaluable technical assistance throughout this study. We also extend our thanks to Ping Huang for his helpful discussion and critical review of the manuscript.

ORCID

Li Xin, https://orcid.org/0009-0006-7791-2800
Li Mengmeng, https://orcid.org/0009-0001-5542-3858
Yu Huixia, https://orcid.org/0009-0003-0067-9009
Zan Runna, https://orcid.org/0000-0001-9711-5549
Li Guojun, https://orcid.org/0009-0009-4409-7610
Shang Rongjian, https://orcid.org/0009-0006-9536-0384
Yu Jia, https://orcid.org/0000-0002-6027-1334

References

1. Autier B, Gottstein B, Millon L, et al. Alveolar echinococcosis in immunocompromised hosts. Clin Microbiol Infect 2023;29:593-9. https://doi.org/10.1016/j.cmi.2022.12.010
2. Bhutani N, Kajal P. Hepatic echinococcosis: a review. Ann Med Surg (Lond) 2018;36:99-105. https://doi.org/10.1016/j.amsu.2018.10.032
3. Rostami A, Lundström-Stadelmann B, Frey CF, et al. Human alveolar echinococcosis: a neglected zoonotic disease requiring urgent attention. Int J Mol Sci 2025;26:2784. https://doi.org/10.3390/ijms26062784

4. Hillenbrand A, Beck A, Kratzer W, et al. Impact of affected lymph nodes on long-term outcome after surgical therapy of alveolar echinococcosis. Langenbecks Arch Surg 2018;403:655-62. https://doi.org/10.1007/s00423-018-1687-9
5. Marquis B, Demonmerot F, Richou C, et al. Alveolar echinococcosis in solid organ transplant recipients: a case series from two national cohorts. Parasite 2023;30:9. https://doi.org/10.1051/parasite/2023008
6. Casulli A, Siles-Lucas M, Tamarozzi F. Echinococcus granulosus sensu lato. Trends Parasitol 2019;35:663-4. https://doi.org/10.1016/j.pt.2019.05.006
7. Zhaxi YD, Ping C, Zhuang ZN. Surgical management of complex hepatic echinococcosis. Chin J Curr Adv Gen Surg 2024;27:412-4. https://doi.org/10.3969/j.issn.1009-9905.2024.05.019
8. Sączek A, Batko K, Krzanowska K, et al. Multicellular echinococcosis (alvococcosis) in a kidney transplant patient. Pol Arch Intern Med 2024;134:16705. https://doi.org/10.20452/pamw.16705
9. Woolsey ID, Miller AL. *Echinococcus granulosus sensu lato* and *Echinococcus multilocularis*: a review. Res Vet Sci 2021;135:517-22. https://doi.org/10.1016/j.rvsc.2020.11.010
10. Aji T, Dong JH, Shao YM, et al. Ex vivo liver resection and autotransplantation as alternative to allotransplantation for end-stage hepatic alveolar echinococcosis. J Hepatol 2018;69:1037-46. https://doi.org/10.1016/j.jhep.2018.07.006
11. Beldi G, Vuitton D, Lachenmayer A, et al. Is ex vivo liver resection and autotransplantation a valid alternative treatment for end-stage hepatic alveolar echinococcosis in Europe? J Hepatol 2019;70:1030-1. https://doi.org/10.1016/j.jhep.2018.12.011
12. Shen S, Kong J, Qiu Y, et al. Ex vivo liver resection and autotransplantation versus allotransplantation for end-stage hepatic alveolar echinococcosis. Int J Infect Dis 2019;79:87-93. https://doi.org/10.1016/j.ijid.2018.11.016

Instructions for authors

Parasites, Hosts and Diseases

Enacted: June 1963
Revised: February 2023
Last revision: January 1, 2026

Parasites, Hosts and Diseases (PHD) is an open access, peer-reviewed, online journal published quarterly on the last day of January, April, July, and October. As the official journal of The Korean Society for Parasitology and Tropical Medicine, PHD aims to generate new knowledge on parasites infecting humans and animals, disease vectors, host-parasite relationships, zoonotic diseases, and tropical medicine.

Manuscripts should adhere to the Recommendations for the Conduct, Reporting, Editing, and Publication of Scholarly Work in Medical Journals, issued by the International Committee of Medical Journal Editors (ICMJE; http://www.icmje.org/recommendations/), unless otherwise specified.

1. Article Processing Charge

Accepted manuscripts are published with the understanding that the author(s) will cover the associated publication costs, including page charges. The standard page charge is 700,000 KRW for Korean authors and 700 USD for others, covering up to 10 pages. An additional 100,000 KRW (for Korean authors) or 100 USD per page applies from the 11th page onward. The page charge for Letters to the Editor is 350 USD.

2. Research and Publication Ethics

It is available at: https://parahostdis.org/policy/ethics.php

3. Submission and Peer Review Process

A. Submission

Authors should submit their manuscripts online through the PHD submission system at https://submit.parahostdis.org/. Once logged in, the system will guide you through the submission process step-by-step. Detailed submission instructions are available on the website, and all manuscripts must comply with these guidelines. Failure to do so may result in the return of the manuscript and potential delays in publication.

B. Peer review process

PHD reviews all submitted manuscripts. Each manuscript is first assessed for format and relevance to the journal's aims and scope. If it meets these criteria, it is sent to two experts in the relevant field for review. PHD uses a single-blind process, where reviewer identities are concealed from the author, but both are visible to the decision-making editor. Reviewers make one of four recommendations: accept, minor revision, major revision, or reject. A first decision is typically made within an average of 4 weeks after the reviewers have agreed to evaluate the manuscript. In cases of review discrepancies, the editorial board will conduct an additional review to make a final determination. Authors are expected to revise their manuscripts based on reviewer feedback and provide explanations for any feedback they choose not to implement. The editorial board makes the final publication decision and may request further changes.

C. Cover Letter

The cover letter should confirm that the submitted material, in whole or in part, has neither been published previously nor is under consideration for publication elsewhere. Additionally, it should disclose any potential conflicts of interest that could influence the authors' interpretation of the data, such as financial support, affiliations with pharmaceutical companies, political pressures from interest groups, or academically related conflicts. The cover letter should also specify that all authors have approved the manuscript for submission and confirm that the manuscript complies with ethical guidelines, including IRB approval and informed consent where applicable.

4. Manuscript Preparation

A. Article types

- Original articles: Original articles present results of research investigations on parasites, parasitic diseases, host-parasite relationships and tropical medicine. They should be organized in the following sequence: Title page, Abstract (≤250 words) and Keywords, Main text (Introduction, Methods, Results, and Discussion), References, Tables, Figure legends, and Figures. Original articles should not include more than a total of 35 references.
- Reviews or mini reviews: Reviews provide a comprehensive analysis of specific topics. The text should be organized in the following sequence: Title page, Abstract (≤250 words) and Keywords, Main text (Introduction, Body text, and Conclusion), References, Tables, Figure legends, and Figures. Unsolicited reviews are also welcome. A mini-re-

view is a shorter version of a full review article. Systematic reviews and meta-analyses should be submitted as review articles but require a structured abstract and should follow the PRISMA guidelines (http://www.prisma-statement.org/).

- Case reports: Case reports are accepted only when they present clinically important information about unique cases. Reports should describe cases not previously observed or reported. If a case involves a common condition but is deemed significant, the editorial board will review it to determine acceptance. They should be organized in the following sequence: Title page, Abstract (≤250 words) and Keywords, Introduction, Case Report, Discussion, References, Tables, Figure legends, and Figures. The number of references should not exceed 20.
- Brief communications: Brief communication is a short article detailing clinically or experimentally significant findings or major advancements. It should adhere to the guidelines for original articles, but the text should be formatted as a single section without headings or section divisions. Additionally, the number of references should be no more than 20.
- Letters to the editor: Letters offer rapid publication of new findings of unique clinical importance, recent perspectives on articles, or topics of interest published in the journal. They may also include opinions on specific topics of academic relevance. The text should be organized in the following sequence: Title page, Main text, References, Tables, Figure legends, and Figures (if applicable). The text should be formatted as a single section without headings or section divisions with no more than 10 references.
- Book reviews: Invited book reviews are eligible for publication. Submissions should provide a critical evaluation of the book's arguments and content. The text should include the title of the book reviewed, the author(s) and editor(s), and publisher, the total number of pages, and the ISBN number, followed by the main text, with no more than 10 references.

B. General requirements

- Manuscripts should be prepared using Microsoft Word (doc or docx format). They should be formatted on A4 (21.0×29.7 cm), with margins of at least 2.54 cm on all sides.
- Texts should be double-spaced with the same normal, plain font throughout, preferably 11-point Times New Roman.
- Genera and species names of parasites and living organisms should be written in italic.
- Other Latin origin words, such as "et al.", "in situ", "in vitro", and "in vivo" should not be italicized.
- Provide the names of manufacturers.
- When quoting from other sources, give a reference number after the author's surname or at the end of the quotation.
- Authors should express all measurements in conventional units, using International System of Units (SI units).
- Authors should follow International Rules for Nomenclature and, if new names are introduced, the International Code for Zoological Nomenclature. All strains and sources of hosts and parasites should be stated.
- Abbreviations should be used sparingly and unambiguously.

C. Key features

Key features and limits of articles are summarized in Table 1 below. However, the limits are negotiable with the editor.

Table 1. Key features and limits of articles

Type of article	Abstract	Text structure	References
Original Article	≤250 words	Introduction, Methods, Results, Discussion	35
Review and Mini Review	≤250 words	Introduction, Body text, Conclusion	No limit
Case Report	≤250 words	Introduction, Case report, Discussion	20
Brief Communication	≤250 words	Single section with no headings	20
Letters to the Editor	Not required	Single section with no headings	10
Book reviews	Not required	Free-form style	10

D. Reporting guidelines

For specific study designs, such as randomized controlled trials, diagnostic accuracy studies, meta-analyses, observational studies, and non-randomized studies, authors should follow the relevant reporting guidelines. Recommended sources include the EQUATOR Network (https://www.equator-network.org/) and the National Library of Medicine (https://www.nlm.nih.gov/services/research_report_guide.html).

E. Manuscript structure and format

Organize your manuscript file as follows:

Manuscript file: (1) Title page (2) Abstract & keywords, (3) Body text, (4) References list, (5) Notes (author contributions, conflict of interest, funding, acknowledgments) (6) Tables (each beginning on a new page), (7) Figure legends (upload figures in separate files)

Supplementary materials (upload separately)

• **Title page**

The title page should include the following items:

- **Title:** The article title should be concise and precise. The title should also indicate the study design. If the study involved human participants, the country where the study was conducted should be included.
- **Running title:** Less than 50 characters
- **Authors and affiliations:** Each author's given name and surname should be provided. For authors with different affiliations, use superscripted Arabic numerals (e.g., [1], [2], [3]) placed at the top-right of each author's name and before each corresponding affiliation. If an author is associated with multiple departments or institutions, arrange affiliations in the order of the authors and indicate them with superscript numbers. The corresponding author should be marked with an asterisk (*) as a superscript.
- **ORCID:** All authors are required to provide their ORCIDs. If an author does not have an ORCID, they can register for one at the ORCID website (https://orcid.org/). Registration is free to all researchers.
- **Corresponding author:** The corresponding author's email address should be provided. If no corresponding author is specified, the editorial board will assume the first author holds this role.

• **Abstract and keywords**

- **Abstract:** For original articles, reviews and mini reviews, case reports, and brief communications, provide an unstructured abstract of less than 350 words. Ensure all data in the abstract appear in the manuscript text or tables.
- **Keywords:** Up to 6 keywords should be listed at the bottom of the abstract to be used as index terms. PHD strongly recommends using Medical Subject Headings (MeSH; https://meshb.nlm.nih.gov/) keywords.

• **Main text**

The main text of an original article must be prepared under the following subheadings: Introduction, Methods, Results, and Discussion. Case report should be organized with Introduction, Case Report, and Discussion. In addition to these types, manuscripts that fall under specific reporting guidelines must be prepared accordingly.

- **Introduction:** Provide the background and purpose of the article, emphasizing its significance. Summarize the rationale with only relevant references, avoiding diffuse listing of related topics. Do not include data or conclusions from the study itself.
- **Methods:** Authors must provide sufficient details to enable an independent researcher to reproduce the work. Previously published methods should be summarized and cited appropriately, without unnecessary repetition. If directly quoting a published method, cite the source. Any major modifications to existing methods must be clearly described. The number of experiments, replicates, and statistical tests used should be specified. An ethics statement must be included when studies involve clinical samples, human data, or animals. This statement should appear as the first subheading in the Methods section. Examples are shown in the following: "We conducted this study in compliance with the principles of the Declaration of Helsinki. The study's protocol was reviewed and approved by the Institutional Review Board of OO (No. OO). Written informed consents were obtained from the patients. The requirement for informed consent was waived."
- **Results:** Present the results in a logical sequence across the text, tables, and figures. Avoid repeating data in the text that is already provided in tables or figures; instead, highlight and summarize key findings and insights.
- **Discussion:** Emphasize the novel and important aspects of the study, along with the conclusions drawn from them. Avoid detailed repetition of data or material already presented in the Introduction or Results sections. Discuss the implications and limitations of the findings, including potential impacts on future research. Connect the conclusions to the study's objectives by comparing and discussing relevant findings from other research. Avoid unqualified statements and conclusions not fully supported by the data. Where applicable, propose new hypotheses and include recommendations as appropriate.

• **References**

In the text, references should be cited with Arabic numerals in square brackets, numbered in the order of appearance. In the References, the references should be numbered and listed in the order of appearance in the text. List all authors when there are 5 or fewer. For sources with 6 or more authors, list the first 3 authors followed by "et al." If an article has been published online, but not yet assigned an issue or page numbers, the DOI should be supplied. journals should be abbreviated according to the style used in the list of journals indexed in the NLM Journal Catalog (https://www.ncbi.nlm.nih.gov/nlmcatalog/journals). For journal titles not listed in the Catalog, they should follow the ISO abbreviation as described in "ISO 4:1997 Information and documentation—Rules for the abbreviation of title words and titles of publica-

tions" (https://www.iso.org/iso/home/store/catalogue_tc/catalogue_detail.htm?csnumber=3569).

Journal articles:

1. Aung JM, Joo SY, Na BK, et al. Establishing a Cre/loxP-based genetic manipulation system for *Acanthamoeba*: targeted genome editing and stable reporter expression. Parasites Hosts Dis 2025;63:25-36. https://doi.org/10.3347/PHD.24078
2. Kim MJ, Moon EK, Jo HJ, Quan FS, Kong HH. Identifying the function of genes involved in excreted vesicle formation in *Acanthamoeba castellanii* containing *Legionella pneumophila*. Parasit Vectors 2023;16:215. https://doi.org/10.1186/s13071-023-05824-y
3. Poncet AF, Blanchard N, Marion S. Toxoplasma and dendritic cells: an intimate relationship that deserves further scrutiny. Trends Parasitol 2019;35:870-86. https://doi.org/10.1016/j.pt.2019.08.001

Book & book chapter:

4. Khan NA. *Acanthamoeba*: biology and pathogenesis. 2nd ed. Caister Academic Press; 2015.
5. Nesheim MC. Ascariasis and human nutrition. In: Crompton DW, Nesheim MC, Pawlowski ZS, editors. Ascariasis and its prevention and control. Taylor and Francis; 1989. p. 87-100.

• **Notes**

- **Conflict of interest:** Authors should disclose any potential conflict of interest. If there are no conflicts of interest to declare, authors should include the following sentence: "The authors have no conflicts of interest to declare."
- **Author contributions:** Describe contributions using the Contributor Roles Taxonomy (CRediT; https://credit.niso.org/). Contributors must meet at least one core role (conceptualization, data curation, formal analysis, investigation, methodology, software, and validation) and one writing role (original draft preparation, review, and editing). Authors who do not meet these requirements will not qualify for authorship.
- **Funding:** Funding for the research should be detailed here. Provision of a FundRef ID is recommended, including the name of the funding agency, country, and (if available) the number of the grant provided by the funding agency. If the funding agency lacks a FundRef ID, please ask that agency to contact the FundRef registry (e-mail: fundref.registry@crossref.org).
- **Data availability:** Include a statement indicating where the data supporting the article's results can be found, with hyperlinks to publicly archived datasets if applicable.
- **Acknowledgments:** All persons who have made substantial contributions, but do not meet the criteria for authorship, should be acknowledged here.

• **Tables**

Table titles and content should be concise, clear, and self-explanatory, so readers do not need to refer to the main text. The table title should be placed at the top-left corner, formatted as "Table [Arabic numeral]." Tables should not contain vertical lines.

Include abbreviations or necessary descriptions in footnotes below the table, using superscript letters (a, b, c) to indicate each footnote, ensuring each note has a corresponding marker. List abbreviations in the footnote section, explaining any empty cells. Where possible, place units directly within the table, avoiding separate listing, and use lowercase symbols for units. In the main text, the term "Table" should appear as "Table" followed by an Arabic numeral.

• **Figures**

Number figures in the order they are cited in the text, using Arabic numerals. Upload each figure as a single image file with a resolution of at least 300 dpi. For figures depicting averages or proportions, use bar or line graphs. Specify the statistical methods used in a footnote for each figure. For multiple panels within the same figure number, use English letters after the numeral to indicate order (e.g., Fig. 1A, Fig. 2B, C).

• **Permission**

If any tables or figures are taken or modified from other papers, authors should obtain permission through the Copyright Clearance Center (https://www.copyright.com/) or from the individual publisher, unless the materials are from an open access journal under the Creative Commons license. For open access journal materials, simply verify the source in the accompanying footnote. Note the distinction between free-access and open access journals: permission from the publisher is required for using tables or figures from free-access journals.

Examples:

Reprinted (Modified) from Tanaka et al. [48], with permission of Elsevier.

Reprinted (Modified) from Weiss et al. [2], according to the Creative Commons License.

• **Supplementary materials**

Supplemental material includes files provided by the authors to accompany their article, typically featuring additional content not included in the print version, such as appendices or extra tables. All supplemental materials will be pub-

lished online with the full-text article. List the supplemental materials at the end of the manuscript file, and ensure they are cited consecutively within the manuscript text.

5. Processing After Acceptance

Once a paper is accepted for publication, the corresponding author must submit a signed copyright transfer agreement form via email to the editorial office. The paper will not be published until the copyright transfer is complete. Around this time, the invoice for the article processing charge (APC) will also be issued. Please note that publication will proceed only after the APC has been paid in full. Failure to complete payment may result in a delay in publication or, in some cases, withdrawal of the manuscript.

After the APC has been confirmed, the manuscript editor will format the paper to meet the journal's publication standards. Authors are required to respond within 3 working days to any revision requests from the manuscript editor. Please note that delays in response may result in the publication being postponed to the next issue.

A. Galley proofs

Once all corrections have been completed, the corresponding author will receive the final version of the manuscript in PDF format.

Within 5 working days of receipt, authors must reply to the printing office of any errors found in the file. The proof may be revised more than once by the corresponding author, if needed. Authors should double-check for corrections in the content, title, affiliation, capitalization, locations of figures, and references.

6. Post-Publication Corrections

To correct errors in published articles, the corresponding author should contact the journal's editorial office with a detailed description of the proposed correction. Corrections that profoundly affect the interpretation or conclusions of the article will be reviewed by the editors. Corrections will be published as author correction or publisher correction in a later issue of the journal.

Minor errors will be corrected directly in the online version of the article. An indication of the correction, along with the date it was made, will be added to the article information in both the HTML and PDF versions. A separate correction note will not be published.

Contact Us

Editor-in-Chief: Myeong Heon Shin, MD, PhD
Email: myeong@yuhs.ac

Editorial Office

Department of Tropical Medicine, Yonsei University College of Medicine, Yonsei-ro 50-1, Seodaemun-gu, Seoul 03722 Korea
Tel: +82-2-2228-1844 Email: support@parahostdis.org

NOTICE: These instructions to authors will be effective from the January 2026 issue.